**The Dissertation Committee for Thomas Edward Macrini Certifies that this is the approved version of the following dissertation:**

# The Evolution of Endocranial Space in Mammals and Non-mammalian Cynodonts

**Committee:**

Timothy Rowe, Supervisor

Christopher Bell

David Cannatella

Zhe-Xi Luo

James Sprinkle

# The Evolution of Endocranial Space in Mammals and Non-mammalian Cynodonts

**by**

**Thomas Edward Macrini, A. B.; M.S.**

**Dissertation**

Presented to the Faculty of the Graduate School of

The University of Texas at Austin

in Partial Fulfillment

of the Requirements

for the Degree of

**Doctor of Philosophy**

**The University of Texas at Austin**

**May 2006**

# Dedication

To my parents, Thomas Gene and Nancy Jean Macrini whose love and support made this possible.

## Acknowledgments

I first want to thank my advisor, Tim Rowe, who provided integral guidance and encouragement during my graduate career at UT. Second, I want to acknowledge Chris Bell who in many ways was an unofficial co-advisor for both of my graduate degrees at UT. Chris was especially helpful in making me aware of appropriate literature and for motivating me to work harder. Zhe-Xi Luo was a late addition to my dissertation committee but has made a big impact on my research as I have gotten to know him better over the past year. Dave Cannatella and Jim Sprinkle were important committee members and I value their input on my research. I had the privilege of taking classes from both Cannatella and Sprinkle and I also worked with both of them as a teaching assistant.

I also thank Walt Wilczynski who served on my dissertation committee for three years but had to be replaced because he moved on to a new job away from UT. Although Wilczynski was on my committee for a relatively short period of time, I appreciated his input and perspective as a neurobiologist. Matt Colbert was in many regards an unofficial dissertation committee member. I am grateful for Matt's assistance with image processing and his willingness to share his knowledge of morphology and paleontology.

I thank Mike Archer, Rich Cifelli, Zhe-Xi Luo, Christian de Muizon, Mike Novacek, and Guillermo Rougier for allowing me to work with CT scans from unique and important fossil specimens. My dissertation would not be possible without inclusion of these key specimens. I am also indebted to John VandeBerg of the Southwest Foundation for Biomedical Research in San Antonio, TX for providing the data in Table 4.2.

The extant mammal specimens used in my research came from a number of institutions, most notably the Vertebrate Paleontology Laboratory collections of the Texas Natural Science Center in Austin, TX, the American Museum of Natural History (AMNH) in New York, NY, and the Field Museum (FMNH) in Chicago, IL. I thank the a number of people for loans of specimens, including Lyn Murray (TMM), Pamela Owen (TMM), Bruce Patterson (FMNH), John Phelps (FMNH), Tim Rowe (TMM), Nancy Simmons (AMNH), and Jean Spence (AMNH). The *Monodelphis domestica* specimens were all obtained from the Southwest Foundation for Biomedical Research in San Antonio, TX. I thank Janice MacRossin and John VandeBerg for arranging the sale of these specimens.

The specimens used for my research were scanned at The University of Texas High-Resolution X-ray CT Facility (UTCT) by Matt Colbert, Bill Carlson, Cambria Denison, Rich Ketcham, Tim Rowe, and Philip Watson. I thank the employees of the UTCT for use of the facility, for image processing, and for data collection. In particular I thank Amy Balanoff, Matt Colbert, Julian Humphries, Rich Ketcham, Jessie Maisano, and Alison Mote of the UTCT for processing the raw CT imagery, helping me with image processing, and implementing the specimens on the DigiMorph website.

I visited the American Museum of Natural History (AMNH) in New York on two occasions to examine specimens in the Division of Paleontology and Department of Mammalogy and collect data for my dissertation. I thank Denny Diveley, Carl Mehling, Jin Meng, Chris Norris, and Mike Novacek in Paleontology, and Darrin Lunde, Teresa Pacheco, Nancy Simmons, Jean Spence, and Robert Voss in Mammalogy for access to the AMNH collections.

My dissertation research was funded by a National Science Foundation (NSF) Dissertation Improvement Grant (to Rowe and Macrini), an NSF Digital Libraries

Initiative Grant (to Rowe), scholarships and professional development funds from the UT Geology Foundation, and an American Federation of Mineralogical Societies Scholarship.

The quality of my research was improved by conversations and comments with many graduate students, past and present, of the Jackson School of Geosciences at UT. In particular I would like to thank Amy Balanoff, Gabe Bever, Anjan Bhullar, Lance Christian, Kerin Claeson, Dave Dufeau, Eric Ekdale, Ryan Ewing, Jon Franzosa, Christian George, Chris Jass, Murat Maga, Lyn Murray, Holly Nance, Jen Olori, Jeri Rodgers, Dennis Ruez, Nina Triche, Ron Tykoski, Jon Wagner, Farrah Welch, Patrick Wheatley, and Bryan Wilbur. Many others at UT were influential in my graduate training, especially Matt Colbert, Wann Langston, Ernie Lundelius, Pamela Owen, Bob Rainey, and Jack Wilson. My research also benefited from interactions and conversations with many others from outside UT, most notably Rich Cifelli, Grant Hurlburt, Zhe-Xi Luo, Christian de Muizon, Guillermo Rougier, Mark Springer, John VandeBerg, Robert Voss, Larry Witmer, and Mike Woodburne. Last but certainly not least I would like to acknowledge the love, support, and encouragement of my family.

# The Evolution of Endocranial Space in Mammals and Non-mammalian Cynodonts

Publication No._____

Thomas Edward Macrini, Ph.D.

The University of Texas at Austin, 2006

Supervisor: Timothy Rowe

I examined cranial endocasts of extinct and extant mammals and non-mammalian cynodonts in order to study the evolution of endocranial space in Mammalia. A cranial endocast represents the three-dimensional space within the braincase (= endocranial space). During life, the endocranial space of mammals is largely filled by the brain but also contains associated nerves, blood vessels, and meninges. Therefore, cranial endocasts provide a proxy for studying the brains of extinct mammals.

To study the evolution of endocranial space in mammals, I described new digital endocast data from four fossil mammals and a non-mammalian mammaliaform. The non-destructive nature of computed tomography allowed me to examine the cranial endocasts of these rare and unique specimens. I produced anatomical descriptions of the new cranial endocast material, and determined encephalization quotients for all of the taxa examined in this dissertation. Encephalization quotients (or EQs) are measures of the size of endocranial volume relative to body size for a particular taxon. EQs are determined from allometric comparisons of a number of closely related taxa.

Based on new endocast data combined with data obtained from the literature, I scored 39 endocast characters by incorporating data from 23 taxa. I examined these characters across a hypothesis of phylogenetic relationships for Mammalia and non-mammalian cynodonts. Examination of the distribution of these 39 endocast characters across mammal phylogeny revealed synapomorphies for the following clades: Mammalia, Monotremata, Theria, Marsupialia, and Placentalia.

The 39 endocast characters examined across mammal phylogeny were also examined in a sample of endocasts from a single mammalian species, *Monodelphis domestica*. The purpose of this analysis was to begin exploring the extent to which ontogenetic and individual variation of these 39 characters affects how the characters might be scored for a phylogenetic analysis. Results indicate that although there is detectable ontogenetic and individual variation among these characters when the entire *M. domestica* endocast sample is examined, if only qualitative characters are examined on adult specimens of *Monodelphis*, none of the characters are variable. Additional studies are required to determine the taxonomic extent of individual and ontogenetic variation of these characters.

# Table of Contents

# List of Tables

## List of Figures

# Chapter 1: Introduction

## CRANIAL ENDOCASTS AND BRAINS

This dissertation deals with cranial endocasts of mammals and their closest extinct relatives, the non-mammalian cynodonts. An endocast is the three-dimensional representation of the space within a cavity. Cranial endocasts are representations of the space within the cranial cavity (= endocranial space), which is filled in life to some degree by the brain. Soft tissue structures, such as organs, only fossilize under extraordinary conditions, as is the case with frozen Pleistocene mammals from northern Russia and Alaska (Farrand, 1961; Guthrie, 1990). Because of the extreme rarity of this type of soft tissue preservation, paleontologists rely heavily on cranial endocasts to study the brain and central nervous system in extinct animals. This branch of paleontology dealing with the fossil record of the nervous system is known as paleoneurology.

Cranial endocasts provide better approximations of the brains of some vertebrates than others based on the degree to which the brain fills the endocranial space (Jerison, 1973). The brains of mammals largely fill the endocranial space leaving an impression on the internal surfaces of skull bones. Because of this, the importance of cranial endocasts for studying the evolution of the brain in fossil mammals has long been recognized (e.g., Simpson, 1927, 1937; Edinger, 1942, 1948, 1949, 1955, 1964, 1975; Radinsky, 1968a, b, 1973a, b, 1976, 1977; Jerison, 1973, 1991; Kielan-Jaworowska, 1983, 1984, 1986; Rowe, 1996a, b).

It is imperative to point out that besides the brain, the cranial cavity also houses other soft tissue structures such as the meninges, blood vessels, and nerves, and therefore, cranial endocasts only provide approximations of external features of the brain. Even so, the general shapes and volumes of some external features of the brain can be inferred from endocasts. However, cranial endocasts do not provide any direct or absolute information about the internal structure of the brain such as morphology of the neurons, number of neurons, neuron density, or neuron connectivity (Deacon, 1990). These absolute data can only be obtained from the brains themselves.

The endocasts used to study endocranial space may either be naturally occurring or artificially generated. A natural endocast or Steinkern is formed when sediment fills the cranial cavity of a skull and then lithifies. Natural endocasts are often exposed as the skull breaks and weathers away. Artificial endocasts are often made to visualize the endocranial space of skulls that lack a natural endocast. Artificial endocasts can be generated using conventional techniques by, for example, constructing a latex internal mold of the endocranial cavity, extracting the mold through the foramen magnum, and then using the mold to make a plaster cast (e.g., Radinsky, 1968a).

For many fossil specimens, it is not possible to generate artificial endocasts from latex molds because the cranial cavity is filled with matrix. In the past, the endocranial space of these skulls was studied using destructive techniques. This usually involved either serial sectioning of the skull (e.g., Sollas, 1904) or physical removal of surrounding bones of the braincase to reveal the natural endocast (e.g., Hofer and Wilson, 1967). These methods are obviously unfavorable for studying rare or unique specimens.

An alternative and non-destructive approach to studying these specimens is to generate digital artificial endocasts. Digital artificial endocasts are generated by first digitizing a skull via magnetic resonance imaging (MRI) or computed tomography (CT), and then digitally isolating the space within the endocranial cavity. Digitally generated endocasts are often referred to as 'virtual endocasts.' This dissertation mainly deals with data obtained from digital endocasts.

## WHY STUDY ENDOCASTS?

Comparisons of the relative sizes of gross structures of the brains of extant animals are used to infer the degree of evolution of different sensory systems associated with the brain (Jerison, 1973; Butler and Hodos, 1996). This is based on the 'principle of proper mass' which states that the mass of the neural tissue of a particular segment of the brain is correlated with the amount of information processing involved in performing that particular function (Jerison, 1973:8). A related assumption, based on observations on extant mammals, is that gross structures of cranial endocasts of mammals provide reasonable proxies for the size of the corresponding brain feature (Edinger, 1948; Jerison, 1973). Therefore, comparative studies of different portions of endocasts of extinct mammals provide information about the evolution of different sensory systems (e.g., Radinsky, 1968a, b, 1973a, b, 1976, 1977). For example, an endocast with relatively large superior colliculus casts suggests that this individual and presumably its species had large superior colliculi and more acute eyesight in comparison to an endocast with

smaller superior colliculus casts. Studies based on these types of comparisons between regions of the cranial cavity are crude, but endocasts are the best available information about the central nervous system and sensory systems of extinct taxa.

Study of the sensory systems of organisms is important for understanding behavior of those organisms. Behavior is response to stimuli and the brain is the organ in which sensory information and motor functions are coordinated. The evolution of behavior is tied to the evolution of the brain, and therefore cranial endocasts are useful for studying the behavior of extinct animals.

In addition, cranial endocasts represent a potentially large amount of unexplored phylogenetic data. The majority of morphological data for mammal and cynodont phylogenetic analyses comes from the exterior of the skull, including the dentition. Internal cranial morphology is poorly represented in phylogenetic analyses because of the difficulty in visualizing and studying this anatomy. The advent of computed tomography (CT) technology has revolutionized the collection of data on the internal cranial morphology of vertebrate skulls (e.g., Rowe et al., 1995, 1999, 2005; Brochu, 2000; Larsson et al., 2000; Tykoski et al., 2002; Witmer et al., 2003; Maisey, 2004, 2005; Van Valkenburgh et al., 2004; Colbert et al., 2005; Franzosa and Rowe, 2005), and therefore provides the potential to incorporate these new data into phylogenetic analyses.

## PHYLOGENETIC DEFINITIONS USED

Before proceeding, some phylogenetic definitions are presented to be explicit about the taxa discussed in this dissertation. Crown-groups comprise the most recent common ancestor of all extant taxa of a particular group, and all descendants of that ancestor. Stem taxa lie along the branch leading to a crown group, but are excluded from the crown group.

Synapsida is defined here as a stem-based monophyletic group consisting of crown-group Mammalia and all amniotes more closely related to mammals than to extant reptiles. The term 'cynodont' refers to members of the taxon Cynodontia which is a monophyletic group if it includes crown-group Mammalia. Cynodontia is a less inclusive group than Synapsida and was defined by Hopson and Kitching (2001:6) as the stem group taxon that consists of "the most inclusive clade including Mammalia and excluding *Bauria*." The definition of Mammaliaformes (sensu Rowe, 1988) is the most recent common ancestor between *Morganucodon* and Mammalia and all descendants of that ancestor. Crown-group Mammalia is defined by Rowe (1988) as comprising the most recent common ancestor of monotremes and therians and all descendants of that ancestor. Crown-group Monotremata comprises the most recent common ancestor of crown Ornithorhynchidae and crown Tachyglossidae and all descendants of that ancestor. The names Marsupialia and Placentalia refer to crown clades. Theria comprises the most recent common ancestor of Marsupialia and Placentalia and all descendants of that ancestor. Metatherian is a stem-based monophyletic group that includes Marsupialia and all therians more closely related to crown marsupials than crown placentals. Eutheria is a

stem-based monophyletic group that includes Placentalia and all therians more closely related to crown placentals than crown marsupials.

## PREVIOUS ENDOCAST WORK

This is not an exhaustive review of previous endocast work, but merely an overview of the more important studies and ideas, especially in regard to the study of cranial endocasts of mammals and non-mammalian cynodonts. The early history of the study of cranial endocasts was summarized by Jerison (1973) and an extensive bibliography of endocast literature was provided in Edinger (1975).

At the end of the 19th century, 'laws' of brain evolution were proposed by Marsh (1884) based on the study of natural endocast material. These 'laws' as defined by Marsh (1884:58) are listed below.

> 1) All Tertiary mammals had small brains.
> 2) There was a gradual increase in the size of the brain during this period.
> 3) This increase was confined mainly to the cerebral hemispheres, or higher portion of the brain.
> 4) In some groups, the convolutions of the brain have gradually become more complex.
> 5) In some, the cerebellum and the olfactory lobes have even diminished in size.
> 6) There is some evidence that the same general law of brain growth holds good for birds and reptiles from the Cretaceous to the present time.

These 'laws' of brain evolution dominated the science of paleoneurology through the early part of the 20th century until they were mostly rejected by the work of Edinger (1951) and later Jerison (1973).

During the first half of the 20th century, a number of significant descriptions of natural endocasts from non-mammalian cynodonts and basally-diverging fossil mammals were published. These include the non-mammalian cynodonts *Thrinaxodon liorhinus* (= *Nythosaurus larvatus*; discussed and figured by Watson, 1913, and by Simpson, 1927) and *Diademodon* (Watson, 1913). From these descriptions, a picture of the brain of basally-diverging cynodonts began to emerge. The endocasts of these cynodonts and presumably the corresponding brains were tube-shaped without much lateral expansion in the cerebral region. Subsequent descriptions of additional non-mammalian cynodont natural endocast material confirmed this basic design (e.g., *Exaeretodon* [Bonaparte, 1966], *Trirachodon* [Hopson, 1979]). In contrast, natural cranial endocasts of Mesozoic and early Tertiary mammals such as the Jurassic triconodontid *Triconodon* (Simpson, 1927, 1928), and the early Paleocene multituberculate *Ptilodus* (Simpson, 1937) show some lateral expansion in the cerebral region.

Also in the first half of the 20th century, artificial endocasts were widely incorporated in paleoneurological studies for the first time, following the work of Tilly Edinger (Buchholtz and Seyfarth, 1999). Largely due to the efforts of Edinger, comparative studies of the paleoneuroanatomy within different mammalian lineages were published for the first time (e.g., Edinger, 1941, 1948, 1955). One of the most prominent of these studies was on horses (Edinger, 1948).

In the period ranging from the 1950's to the early 1970's, two measures of relative brain size in mammals were presented; one based on relative body size (i.e., encephalization; Jerison, 1955, 1973) and a second relating the endocranial cavity volume to foramen magnum area (Radinsky, 1967). The former of these two comparisons, which is still in common use today, utilizes encephalization quotients or EQs (Jerison, 1955, 1973). An EQ is the ratio of actual to expected brain sizes for a particular taxon. These ratios are determined using plots of body size versus brain size among a number of closely related taxa. On these plots, EQs are equivalent to the residuals derived from the regression line of all the species examined in the study.

Encephalization quotients are widely utilized in the literature but also frequently criticized (e.g., Deacon, 1990; Striedter, 2005). Some of the criticism of EQ analyses revolves around their biological significance, but methodological issues associated with these analyses also raise concern. A discussion of these criticisms is presented in the next section of this chapter.

Despite the criticisms, EQ analyses are significant because they show that brain size is allometrically related to body size among mammals and other groups of vertebrates (Jerison, 1973). Encephalization quotients provide quantitative estimates of relative brain sizes in extinct mammals, and can be correlated with the evolution of different sensory systems and behavior (Jerison, 1955, 1961, 1973). Overall brain size is useful for estimating sizes of many constitute parts of the brain, cortical volume, neuron density, and neuronal connectivity (Jerison, 1973). In addition, relatively large brain size in mammals appears to correlate with ecologically important variables such as foraging capabilities and the amount of social interaction for a particular taxon (Eisenberg and

Wilson, 1978, 1981; Dunbar, 1995; Striedter, 2005). This being said, the biological significance of increase in relative brain size is still not well understood.

Beginning in the late 1960's, trends in brain size and the evolution of specific neuroanatomical features, such as differences in cerebral sulcus patterns and expansion of the isocortex, were examined in a number of groups of mammals including carnivorans, ungulates, and primates (Radinsky, 1968a, b, 1973a, b, 1975, 1977, 1978, 1981; Jerison, 1973, 1991). The isocortex (or neocortex) is the six-layered portion of the dorsal pallial cortex that forms the majority of the cerebral hemispheres in mammals (Butler and Hodos, 1996). The amount of isocortex on endocasts is often inferred as the portion of the cerebral hemispheres above the rhinal fissure, a structure that may or may not always be visible on endocasts (Jerison, 1991).

Since the publication of Jerison's book in 1973, there has been a dramatic increase in the diversity of known endocast material for non-mammalian cynodonts and extinct mammals. Natural cranial endocast material known from non-mammalian synapsids was summarized by Hopson (1979). Subsequent to this, a number of cranial endocasts from Mesozoic mammals particularly those from Mongolia (Kielan-Jaworowska, 1983, 1984, 1986; Kielan-Jaworowska et al., 1986; Krause and Kielan-Jaworowska, 1993; Kielan-Jaworowska and Lancaster, 2004) and non-mammalian cynodonts from South America (Quiroga, 1979, 1980a, 1980b, 1984) were described for the first time. A summary of current knowledge about cranial endocasts of Mesozoic mammals was provided by Zielan-Jaworowska et al. (2004).

Despite this increase in taxonomic sampling of cynodont endocasts, there are relatively few studies to date comparing brain evolution or examining brain character

evolution in Cynodontia. Summaries of evolutionary changes of the brain in the synapsid lineage as inferred from endocasts were provided by Hopson (1979).

Beginning in the 1980's, a series of analyses employed central nervous system (CNS) characters to build phylogenies of extant mammals (Johnson et al., 1982a, b; Kirsch, 1983; Kirsch and Johnson, 1983; Kirsch et al., 1983; Johnson et al., 1994). Fifteen characters in 147 extant mammals and many extant non-mammalian tetrapods were used to build phylogenies using Wagner tree algorithms (Johnson et al., 1982a, b; Kirsch, 1983). Unfortunately, many of these characters are not visible on the exterior of the brain and most likely would not be visible on endocasts. Of the characters examined, all but one is related to the isocortex, suggesting they might be correlated. Later the same group of researchers examined the same 15 characters across 133 taxa using 154 specimens (Kirsch and Johnson, 1983). Different analyses using subsets of the characters and taxa recovered some of the major clades of mammals as supported by a variety of other data (Kirsch and Johnson, 1983; Kirsch et al., 1983). However, the brain characters did not provide much resolution to mammal phylogeny, because too few characters were examined relative to the number of taxa in the analysis. In a later study by the same group (Johnson et al., 1994), nine new characters were added, only one of which might be visible on endocasts.

A different study mechanistically tied the separation of the postdentary elements from the mandible in cynodont evolution and development with the expansion of the isocortex in Mammalia (Rowe, 1996a, b). In that study, isocortex expansion was mapped across a cladogram depicting the relationships of seven cynodonts including two extant mammals. More recently, a study comparing cranial vault width in mammaliaformes

associated with the discovery of a new taxon suggested that neocortical expansion may be a synapomorphy for a group more inclusive than Mammalia (Luo et al., 2001b).

## NEW APPROACHES TO PREVIOUS ENDOCAST STUDIES

The lack of natural cranial endocast material for a number of fossil mammals and non-mammalian cynodonts is a great impediment to endocast studies. Furthermore, it is impossible to non-destructively generate artificial endocasts from many fossil skulls using conventional techniques. Computed tomography (CT) technology was successfully employed to digitize skulls for non-destructive extraction of digital endocasts from fossil skulls (e.g., Brochu, 2000; Larsson et al., 2000; Marino et al., 2000, 2003; Witmer et al., 2003; Franzosa, 2004). High-resolution X-ray CT is used to this end in this dissertation (Chapter 2).

Many of the natural cranial endocast specimens that are available for study are incomplete or cannot be studied in all views (e.g., the basicranial bones often obscure the ventral surface of endocasts). Because of this, it is difficult to take accurate linear and volumetric measurements from natural endocast material. CT technology can remedy this problem. Volume measurements from CT data in some cases are more accurate than volumes taken from natural endocast material (Chapter 2).

One limitation of most studies of natural cranial endocasts to date is that individual and ontogenetic variation is not examined. Only a few studies have examined multiple individuals of a particular taxon to understand variation (Edinger, 1948;

Radinsky, 1968b, 1973a; Novacek, 1982, 1986), but I am unaware of any studies that have examined ontogenetic variation of endocasts for a particular taxon. However, some opportunities do exist for future studies of individual variation of natural endocasts from a single taxon. For example, a large collection of natural endocasts of the early Oligocene oreodont *Bathygenys reevesi* is in the Texas Natural Science Center collections housed at the Vertebrate Paleontology Laboratory (Wilson, 1971; Macrini, in preparation).

As mentioned earlier in this chapter, concerns about the biological significance and methodology for determining encephalization quotients are presented in the literature (e.g., Deacon, 1990; Striedter, 2005). A discussion of some of the criticisms of EQ analyses is warranted because of the amount of literature devoted to this subject.

A controversial idea is that EQ is correlated with relative biological intelligence (Jerison, 1973). Following the 'principle of proper mass', a larger ratio of brain mass-to-body-size suggests a greater capacity for an organism to process stimuli from its environment (Jerison, 1973). Taxa that are better equipped in this manner are generally considered more intelligent (Jerison, 1955, 1973, 2001). Biological intelligence was defined by Jerison (1973) as the difference between species in their ability to integrate different sensory data to shape a realistic perception of the environment. Another term for this is cognitive ability (Striedter, 2005).

The idea that a mammal species with a relatively larger brain is more intelligent or has greater cognitive ability than those mammals with relatively smaller brains is controversial for multiple reasons. First, the use of EQs in this capacity assumes that intelligence can be measured by a single scalar variable. One argument is that there is no

basis for this assumption when the results of comparative intelligence tests are considered (Deacon, 1990). Designing laboratory intelligence tests that are comparable for different species is a difficult task (Striedter, 2005). One idea is that intelligence is not a biological property, but a value of judgment on the part of the observer based on the merits of observed behavior (Butler and Hodos, 1996).

Second, larger brains have decreased neuronal connectivity, and are more compartmentalized than smaller brains (Jerison, 1973; Deacon, 1990). The overall number of neurons increases with brain size, but the number of neurons per unit volume decreases. This inverse relationship between brain size and neuron density results from a combination of reasons, mainly because axons and dendrites are larger in neurons of larger brains, thus occupying more space than in smaller brains (Striedter, 2005). Longer axons allow neuronal connectivity between increasingly distant portions of larger brains. However, the number of possible neuronal connections increases as the square of the number of neurons (Striedter, 2005). This makes it physically impossible for neurons to be completely connected with all other neurons in a large brain. Furthermore, large brains cannot maintain an amount of neuronal connectivity that is proportional to that of smaller brains because of the increase in neuron number associated with increased brain size. Therefore, relative neuronal connectivity decreases with increasing brain size but absolute connectivity is maintained for the most part (Striedter, 2005). As a result of decreased neural connectivity, larger brains become more compartmentalized and functions are shared among different centers (Deacon, 1990; Striedter, 2005). This results in reduced integration of distributed functions and increased transmission and processing times (Deacon, 1990). Therefore, larger brains are not necessarily more

efficient and more powerful than smaller brains. It is unclear how increasing capacity to process and store information is balanced by reduced efficiency and integration as brain size increases (Deacon, 1990). Based on this it is not clear how increases in EQ relate to relative intelligence, however one might chose to define intelligence (Deacon, 1990).

Another criticism of brain allometry studies is that selective pressures are different for body size and brain size (Butler and Hodos, 1996). For body mass for example, aquatic animals can achieve larger body masses than terrestrial animals because they live in a buoyant environment (Butler and Hodos, 1996). This contributes to reduced EQs in some aquatic animals. Alternatively, selective pressures for brain development also vary for different parts (Butler and Hodos, 1996). For example, there are different selective pressures for the autonomic nervous system than the visual system in mammals (Butler and Hodos, 1996).

In addition to philosophical disagreements about the biological significance of EQs, there are also methodological difficulties associated with EQs. First, there are errors associated with measuring both endocranial volume and body mass in fossil specimens. Although estimates of endocranial volume are sometimes difficult to obtain from natural endocasts, accurate volume measurements can be obtained from digital endocasts (see Chapter 2). Body mass estimation from fossil specimens is a more difficult issue. Because osteological and dental material is all that is available for most mammal fossils, a number of proxies for body mass based on these elements are used. These proxies include skull length, skull width, postcanine tooth measurements, lengths of long bones, mid-shaft circumferences of long bones, cross-sectional area of vertebral

elements, and scaling elements from fossils with those of closely related extant mammals (Romer and Price, 1940; Damuth and MacFadden, 1990).

A second methodological difficulty with EQs is that the equations derived from brain size versus body size plots are not determined using the same techniques in different analyses (Pagel and Harvey, 1988; Striedter, 2005). One difference is whether or not the volume of the olfactory bulbs is included in determination of endocranial or brain volume. Olfactory bulb volume was excluded from an early analysis for two reasons (Jerison, 1973). First, the olfactory bulb casts are confluent with the nasal cavity in some fossil specimens, especially those that lacked a cribriform plate (e.g., non-mammalian cynodonts) or for those specimens in which the ethmoid was damaged postmortem. This makes it difficult to determine the anterior edge of the olfactory bulbs in some natural endocasts; therefore, the anterior border of endocranial space was defined by the circular fissure, the posterior border of the olfactory bulbs. Second, olfactory bulb casts do not scale with brain size unlike other parts of the brain associated with sensory and motor integration (Jerison, 1973). Furthermore, it was argued that because olfactory bulbs are associated with receiving and transmitting sensory data rather than analyzing and storing sensory information, the olfactory bulbs are not directly associated with cognitive ability (Jerison, 1973). However, some level of analysis of odorant molecules does occur in the glomeruli of the olfactory bulbs (summarized by Rowe et al., 2005).

The equations used to derive EQs vary depending on the data included in the study and basic assumptions in analyses (Striedter, 2005). For example, the exponent determined from analyses including general sampling across Mammalia varies between 0.67 and 0.76 (Hurlburt, 1996). The exponent of 0.67 was fit for the plot of brain and

body size data for mammals based on the idea that brain size scales to body surface by the same exponential factor (Jerison, 1973). Subsequent analyses were based on different statistical techniques applied to double log plots of brain size versus body size of a sample of multiple groups of mammals. Most of these determined the exponent to be around 0.74 or 0.75 (e.g., Eisenberg and Wilson, 1978, 1981; Eisenberg, 1981; Hurlburt, 1996).

The equations for EQ for different groups of mammals can also vary. Exponents vary between 0.46 for cetaceans (Harvey and Krebs, 1990; Harvey and Pagel, 1991), 0.70 for marsupials (Harvey and Krebs, 1990; Harvey and Pagel, 1991), 0.72 for a combined analysis of cetaceans and primates (Marino, 1998), 0.74 for didelphid marsupials (Eisenberg and Wilson, 1981), and 0.92 for primates (Harvey and Krebs, 1990; Harvey and Pagel, 1991). In addition, the EQ exponent varies with taxonomic level, such that the exponent is higher for higher taxa (e.g., 0.75 for Mammalia but 0.2-0.5 among closely related species; Jerison, 1973; Lande, 1979; Riska and Atchley, 1985; Pagel and Harvey, 1988, 1989). This discrepancy may result from artifacts associated with use of improper statistical methods (e.g., using inappropriate models of regression; Pagel and Harvey, 1988).

Another methodological difficulty with EQs is that the data points are not statistically independent. The phylogenetic relationships of the taxa being compared must be taken into account to assure that similarity in closely related species is not a result of shared ancestry (Felsenstein, 1985). This can be accomplished by the method of independent contrasts (Harvey and Pagel, 1991). A sample of brain and body mass data for 917 species of mammals was analyzed using independent contrasts, resulting in a line

with a slope of 0.69 (Harvey and Krebs, 1990; Harvey and Pagel, 1991). This suggests that brain size shows a strong allometric relationship across mammals, even when the phylogenetic effects are taken into account. Furthermore, the brain allometry slope determined from independent contrasts (0.69) differs from the slopes (0.75) obtained from analyses that did not use independent contrasts by 8%, a difference that may not be statistically significant. Even so, independent contrasts have not been applied to smaller taxonomic groups within Mammalia to see if the same relationship holds true.

## GOALS OF THIS DISSERTATION

The overall purpose of this dissertation is to cast new light on the study of endocranial space of mammals and non-mammalian cynodonts. This is accomplished through the incorporation of new cranial endocast data with previously published data and examination of these data in a phylogenetic context. There are three main goals of this dissertation and each goal is addressed in a separate chapter.

The first goal is to generate and describe new digital endocast material from fossil mammals and non-mammalian mammaliaforms, contributing to a denser sample of taxa. This includes taxa from which the endocranial space was previously undescribed, because natural endocast material is unknown or cranial material is rare for these taxa. Computed tomography allows for the endocranial space of these rare and unique specimens to be non-destructively studied. Those data are presented in Chapter 2.

The second goal is to study the evolution of mammalian endocranial space through examination of endocast characters in the context of a phylogeny. I generated a matrix of endocast characters using data from digital endocasts I generated and descriptions of fossil endocasts in the literature. Optimizing endocast characters on a hypothesis of mammalian evolutionary relationships is useful for determining which major external brain features evolved multiple times and which features are diagnostic of major clades of mammals. The distribution of the major features of the mammalian brain has not been rigorously examined in such a way. This character distribution provides a framework for examining the phylogenetic and temporal history of different sensory systems associated with the brain. These data have implications for study of the evolution of behavior. A different aspect of this work was to combine the endocranial characters with a larger matrix of independent osteological and dental characters, to determine if endocranial characters significantly affected tree topology. Those analyses are presented in Chapter 3.

The third goal is to examine individual and ontogenetic variation for endocasts from a single mammalian species (*Monodelphis domestica*). The purpose of this work is to begin documenting the amount of individual and onotogenetic variation associated with the endocranial characters listed in Chapter 3. This work has implications on the utility of these characters in future phylogenetic studies. Those results are presented in Chapter 4.

Finally, additional contributions of the data presented in this dissertation are explored in Chapter 5. In particular, the evolution of relative brain size within Mammalia is examined by combining data from the literature with new data presented in this

dissertation. These relative brain size data combined with the discrete endocranial character data presented in Chapter 3 were examined in the context of mammal phylogeny to provide an emerging picture of the evolution of the mammalian brain. These data have implications for the study of evolution of sensory systems, physiology, and behavior in mammals.

# Chapter 2: Description of Fossil Cranial Endocasts

## INTRODUCTION

The opportunities for further study of the cranial cavity of non-mammalian cynodonts and basal mammals and the need for incorporation of these data into phylogenetic analyses were noted by several researchers (e.g., Kermack and Kermack, 1984; Kielan-Jaworowska, 1997). As a first step, the cranial endocasts of a number of key taxa need to be described in their entirety and that is the goal of this chapter.

Skulls of many Mesozoic and early Cenozoic mammals are rare, and destructive disassembly or sectioning to better expose their cranial cavities is not justified. Therefore, much of what is currently known about the evolution of endocranial space in Mesozoic mammals is based on fragmentary skulls with exposed partial natural cranial endocasts (Simpson, 1927, 1937; Jerison, 1973; Kielan-Jaworowska, 1983, 1984, 1986, 1997; Kielan-Jaworowska and Lancaster, 2004). Portions of these endocasts, in particular the ventral surfaces, are often not visible. This makes it difficult to reconstruct the entire endocranial space for these taxa.

One solution to this problem is to study the endocranial space of complete skulls via non-destructive methods. High-resolution X-ray CT (HRXCT) is a proven technique for studying cranial endocasts of fossil or unique specimens (e.g., Rowe et al., 1995; Brochu, 2000; Larsson et al., 2000; Witmer et al., 2003; Franzosa and Rowe, 2005).

Digital endocasts can be extracted from the CT images and linear and volumetric measurements can be taken relatively easily.

Here, I describe digital cranial endocasts of five key taxa representing the early radiation of mammals. These taxa are *Hadrocodium wui*, *Obdurodon dicksoni*, *Kryptobaatar dashzevegi*, *Vincelestes neuquenianus*, and *Pucadelphys andinus*. The context for the significance of these taxa is described below. Natural endocast material is unknown for *Hadrocodium*, *Obdurodon*, *Pucadelphys*, and *Vincelestes*. Furthermore, two of these taxa (*Obdurodon* and *Hadrocodium*) are known from only a single individual (Archer et al., 1992; Luo et al., 2001b). Natural cranial endocast material was described for *Kryptobaatar dashzevegi* (Kielan-Jaworowska and Lancaster, 2004), but the ventral endocranial surface is not visible in that material. A digital endocast of *Kryptobaatar* is described here to provide a more complete picture of the endocranial space in this taxon. In addition, endocast measurements for *Kryptobaatar* obtained from natural material are compared to those obtained from the virtual endocast described here.

**Institution Abbreviations—AMNH**, American Museum of Natural History, New York, New York, U.S.A.; **FMNH**, Field Museum, Chicago, Illinois, U.S.A.; **GI PST**, Paleontological and Stratigraphic Section of the Geological Institute, Mongolian Academy of Sciences, Ulaan Baatar, Mongolia; **IVPP,** Institute of Vertebrate Paleontology and Paleoanthropology, Chinese Academy of Sciences, Beijing, China; **MACN,** Museo Argentino de Ciencias Naturales, Buenos Aires, Argentina; **MAE**, Mongolian-American Museum Expedition; **MHNC**, Museo de Historia natural de Cochabamba, Cochabamba, Bolivia; **PSS**, Paleontological and Stratigraphic Section of the Geological Institute, Mongolian Academy of Sciences, Ulaan Baatar, Mongolia; **QM**

**F**, fossil collection of Queensland Museum, Brisbane, Australia; **TMM M**, extant mammal collections of the Texas Memorial Museum/ Texas Natural Science Center housed at the Vertebrate Paleontology Laboratory, Austin, Texas, U.S.A.; **UTCT**, University of Texas High-Resolution X-ray Computed Tomography Facility, Austin, Texas, U.S.A.

## MATERIALS AND METHODS

### Specimens examined

***Hadrocodium wui***. A digital endocast was extracted from the skull of the only known specimen of *Hadrocodium wui* (IVPP 8275), a non-mammalian mammaliaform and the closest outgroup to crown Mammalia (Luo et al., 2001b, 2002, 2003). The specimen was collected from the lower Lufeng Formation (lower Jurassic) of Yunnan, China. The skull is mostly complete but there is damage to the medial and posterior portions of the braincase roof and the basicranium in several places. I calculated volumes for the endocranial cavity of *Hadrocodium* both before ('raw volume') and after reconstructing the endocast ('reconstructed volume') in the damaged region of the skull. This specimen is either an adult or an old subadult based on dental and mandibular characters (Luo et al., 2001b). Endocast and skull measurements are provided in Appendix 1.

***Obdurodon dicksoni***. The only known skull of *Obdurodon dicksoni* (QM F20568), a fossil platypus, was collected from the Middle Miocene Ringtail Site on the

Riversleigh World Heritage property in Queensland, Australia (Musser and Archer, 1998). This specimen of *Obdurodon dicksoni* represents the oldest, nearly complete skull of a monotreme from which an endocast can be extracted. This skull was collected from freshwater carbonate deposits at sites well known for aquatic vertebrates including crocodiles, turtles, and lungfish (Archer et al., 1992). Based on this, it is assumed that *O. dicksoni* was aquatic similar to its extant relative *Ornithorhynchus anatinus*.

The skull of *Obdurodon dicksoni* is nearly complete but is missing a large, oblique section of the cranial roof that extends from the lambdoidal crest on the right dorsum of the skull to anterior of the orbit on the left side (Musser and Archer, 1998). The *Obdurodon* skull is presumed to belong to an adult, because it is about 30% larger than skulls of adult *Ornithorhynchus* (Appendix 1; Archer et al., 1992). When the *Obdurodon* skull was first discovered, the endocranial cavity was filled with a natural limestone endocast that was only partially exposed through breaks in the skull. The skull was subsequently acid-prepared resulting in the destruction of this natural endocast (Figure 1).

***Kryptobaatar dashzevegi***. A digital endocast was extracted from a single skull of *Kryptobaatar dashzevegi* (PSS-MAE 101), a multituberculate mammal. The skull was collected from the upper Cretaceous Djadokhta Formation near Ukhaa Tolgod, Mongolia by a joint Mongolian Academy of Sciences-American Museum of Natural History Expedition. The skull is nearly complete with relatively little distortion. However, a large circular portion of the skull roof including most of the parietals and the posterior portion of the frontals is missing from this specimen. The endocranial cavity of this specimen is filled with a natural endocast, providing a surface along the damaged skull

roof to reconstruct the dorsal edge of the endocast. Endocast and skull measurements are provided in Appendix 1.

***Vincelestes neuquenianus***. A digital endocast was extracted from a skull of *Vincelestes neuquenianus* (MACN-N 04), a stem therian. This skull was collected from the lower Cretaceous La Amarga Formation of the southern Neuquén Province, Argentina. The skull is mostly complete but the snout and right side of the braincase, particularly the petrosal, are damaged (Figure 2). However, there does not appear to be much distortion to the braincase and therefore the corresponding endocast is relatively undistorted.

The *Vincelestes* skull examined here is from an old adult based on tooth wear and fusion of braincase sutures. There is sexual dimorphism among the known adult *Vincelestes* skulls, and this specimen belongs to the smaller of the two size classes and is presumably a female (Rougier, 1993). The maximum body size for *Vincelestes* is estimated based on isolated humeri and femora and using the formulae of Alexander et al. (1979). Endocast and skull measurements are provided in Appendix 1.

***Pucadelphys andinus***. A digital endocast was extracted from a skull of *Pucadelphys andinus* (MHNC 8266), a stem marsupial (= non-marsupial metatherian). This skull was collected from a site called "the Quarry" in the lower Paleocene Santa Lucía Formation at Tiupampa, Mizque Province, Department of Cochabamba, south-central Bolivia (Marshall and Muizon, 1988; Marshall et al., 1995). The skull is essentially complete with minor damage to the palate, the right zygomatic portion of the squamosal, and the nasals and surrounding bones of the roof of the snout (Figure 3). There is very little distortion to the skull. This specimen is an adult individual, based on

its full set of dentition. Body mass was estimated by taking an average for masses of several specimens of 90-day old *Monodelphis domestica*, the gray short-tailed opossum (Marsupialia: Didelphidae), which have nearly identical skull lengths with that of this specimen of *Pucadelphys*. The *Pucadelphys* endocast was compared to digital endocasts extracted from skulls of *Monodelphis domestica*. Endocast and skull measurements are provided in Appendix 1.

**Extant mammals**. In addition to the five fossil taxa discussed above, I extracted digital cranial endocasts from skulls of extant mammals for comparative purposes and to provide extant phylogenetic bracketing of soft tissue structures. This sample includes digital endocasts extracted from four skulls of extant monotremes (two of *Ornithorhynchus anatinus*, one of *Tachyglossus aculeatus*, and one of *Zaglossus bruijni*). The platypus sample includes one skull from a juvenile (AMNH 252512) retaining all of its deciduous dentition and one adult skull (AMNH 200255); both echidna skulls are from adults. A complete list of the digital endocasts I extracted from extant mammals is provided in Appendix 1.

## About CT scanning

All skulls were CT scanned at UTCT. HRXCT utilizes differential attenuation of X-rays passed through a specimen to differentiate between bone and other material to produce two-dimensional images (i.e., slices) that reveal internal details of specimens (for a detailed description of CT see Denison et al., 1997 and <www.ctlab.geo.utexas.edu>). Consecutive equidistant 2-D slices provide a three-dimensional digital map of the

specimen that can be manipulated using a variety of image processing techniques and software. All skulls were scanned in their entirety in the coronal (= transverse of some authors) slice plane. Scan parameters for these specimens are provided in Appendix 2.

**Extraction of endocasts**

The digital endocasts were generated using the program VGStudioMax© (version 1.2; Volume Graphics GmbH, 2004). VGStudioMax© is a program designed for the analysis and visualization of voxel data that allows the user to digitally individuate or segment (in the jargon of informatics) portions of volumetric datasets. I loaded the entire dataset of each specimen into VGStudioMax©, but I only manipulated one slice at a time. Even so, VGStudioMax© allows the user to simultaneously view all three slice planes and a volumetric rendering of a dataset. In order to select the endocranial space, I utilized the 'segmentation' menu of VGStudioMax©. I used the magic wand tool of the segmentation menu to select the endocranial space in each coronal slice that intersects the endocranial cavity of a skull. I used the lasso tool and 'expand' functions of the segmentation menu to fine-tune the endocranial selections. Endocranial selections were transfered between consecutive slices by enabling the '2-D selection propagate' function in the segementation menu. A selection is initially saved by clicking the 'accept' button in the segmentation menu. This creates an 'endocast segment' that is separate from the original scan data (e.g., the skull). I saved changes to the endocast selection by clicking the 'add' button in the segmentation menu.

I used the lasso tool to draw lines to seal off openings in the braincase (e.g., foramen magnum, foramina for passage of nerves and vessels) in each coronal slice where it was necessary. For the most part lines were drawn through the center of openings in order to match the contours of the inner sufaces of the surrounding bone.

I saved the lines to a segment that is separate from the endocast selection. Subsequently, I was able to go back into the 'endocast segment' and add selections from slices that previously had cranial openings. The lines established boundaries of the endocranial cavity and served as a guide for selecting the endocranial space.

I used the same procedure to segment portions of the endocranial space with bony landmarks representing distinctive structures such as the olfactory bulb casts, paraflocculars casts, hypophyseal fossa casts, and cavum epiptericum casts. The geometric shapes of these endocast features do not precisely reflect the histological boundaries of soft tissue structures but rather serve as reasonable proxies.

The cribriform plate serves as the anterior boundary of the olfactory bulb space in mammals. *Ornithorhynchus* (Zeller, 1988) and *Obdurodon* have a partially ossified cribriform plate, with the anterodorsal portion remaining unossified in adults. In these two taxa, the anterior end of the olfactory bulbs casts was determined by the curvature of the bones surrounding the ethmoidal fossa (e.g., frontal, lamina obturans). The posterior end of the olfactory bulb casts for all specimens was determined by the medial inflection of the endocast at the anterior edge of the circular fissure (sensu Loo, 1930; Rowe 1996a, b; = transverse fissure of Krause and Kielan-Jaworowska, 1993), as viewed dorsally. This surface was treated as a coronal plane. However, the cribriform plate of *Tachyglossus* (Figure 4) and *Zaglossus* extends posterior to the circular fissure as do the

corresponding olfactory nerve fibers. The olfactory bulb surface area and volume are correlated with the surface area of the cribriform plate (Rowe et al., 2005) and, therefore, the olfactory bulb casts of echidnas extend beyond the circular fissure. There are no distinctive bony markers to segregate the posterior portion of the olfactory bulb space from the rest of the endocranial cavity and, therefore, the volumes of the olfactory bulb casts in the two species of echidnas are underestimated.

The medial end of each parafloccular lobe cast was treated as an oblique sagitto-coronal cut plane. Its location was determined as the point of constriction of the parafloccular casts into a neck but prior to the connection with the main body of the cerebellum. The dorsal cut plane of the hypophyseal fossa was determined by the dorsalmost horizontal slice in which the lateral walls, dorsum sella, and clinoid processes of the sella turcica are all visible. The cavum epiptericum was determined as the space posterior of the sphenorbital fissure to the posterior end of the foramen ovale. A horizontal line was drawn across the top of this space in each coronal slice as an arbitary boundary for cast of the cavum epiptericum.

The relative proportions of different regions of the endocasts are expressed as percentages of the total endocranial volume (e.g., percent of endocranial space composed by the olfactory bulb casts). Although proportions and ratios are often criticized in the literature, their use is appropriate in this situation because the intention is to determine the relationship between two variables (e.g., olfactory bulb cast volume and endocranial volume) to express proportionality and not to provide statistical control for the variance of one factor in relation to another (Smith, 2005).

Endocast flexure was measured in lateral view by taking the acute angle between two lines, both of which pass through the hypophyseal cast (Figure 5). The first line passes through the middle of the olfactory bulb casts to the middle of the hypophyseal cast. The second line passes from the middle of the hypophyseal cast to the middle of the foramen magnum.

I also used VGStudioMax© to calculate volumes and partial volumes, to take linear measurements of the extracted endocast segments, and to generate movie frames of the rotating endocasts. VGStudioMax© provides measurements with accuracy to the third decimal place (i.e., 0.001). The movie frames were exported to National Institutes of Health ImageJ and/or Adobe Photoshop® where they were cropped and rotated as necessary. The frames were then exported to QuickTime™ and compiled into self-contained movies. The movies of the endocasts along with CT slices of the skulls of these specimens are available on the Digimorph website (Appendix 3). Isosurface models of the endocasts were generated using VGStudioMax© and then exported to Amira 3.1™ (Zuse Institute Berlin, 2004) where the surfaces of the endocasts were smoothed. Images of the smoothed endocasts are used here for aesthetic purposes only. I obtained all linear and volume measurements prior to smoothing the specimens.

**Encephalization quotients**

Encephalization quotients (EQ) were calculated based on endocranial volumes of the fossil endocasts described in this chapter. For comparative purposes, EQs were

calculated for additional taxa examined in this dissertation and for other taxa with endocranial volumes and body masses reported in the literature.

Brain volume in milliliters is equivalent to brain mass in grams if the specific gravity of brains is assumed to be 1.0 g/cm$^3$, following the work of others (e.g., Jerison, 1973). I determined body mass using a number of techniques. I used actual body masses of museum specimens if the collector recorded these data. The techniques to record these data were usually unspecified. I measured body masses from frozen and pickled specimens of *Monodelphis domestica*, the gray short-tailed opossum (Chapter 4). I used published body mass averages for skeletonized extant specimens (with the exception of *M. domestica*) for which mass data were not recorded. The techniques employed for estimating body mass for skeletonized *M. domestica* are described in Chapter 4. I used previously published body mass estimates for fossil taxa. For fossil taxa without published mass estimates, I used body mass averages from extant mammals with comparable skeletal measurements (e.g., skull length or total skeleton length). Endocranial volumes, body masses, and techniques for estimating body mass, when appropriate, are presented in Appendix 1.

Encephalization quotients were calculated using the equations provided by three different studies (Jerison, 1973; Eisenberg, 1981; Hurlburt, 1996). These three studies provide different equations from analyses that employ different techniques and samples of mammals. For each taxon, EQs were calculated using two sets of endocranial volumes: one that includes the olfactory bulbs and one that excludes the volume comprising the olfactory bulbs. The three equations and the EQ values are provided in Appendix 4.

## ANATOMICAL DESCRIPTIONS

***Hadrocodium wui***. In dorsal view, the overall shape of the *Hadrocodium* endocast is of an asymmetrical hexagon (Figure 6). The occipital edge of the endocast is transversely wider than the cribriform edge. In between are the anterolateral and posterolateral edges. The anterolateral edges of the olfactory bulb casts and the cerebral hemisphere casts extend posterolaterally from the cribriform edge of the endocast. These two anterolateral edges together form the longest sides of the hexagon. The posterolateral edges of the endocast extend posteromedially from the widest transverse width of the endocast (at the posterior end of the anterolateral endocast edges) to the occipital edge of the endocast. Each posterolateral edge is roughly the same length as the occipital edge of the endocast.

In lateral view, the endocast is tallest in the hindbrain region and shows almost no flexion from horizontal (Figure 6A). A rhinal fissure is not visible on the lateral surface or anywhere else on the endocast.

The *Hadrocodium* endocast width/length aspect ratio is 0.77, the height/length ratio is 0.47, and the height/width ratio is 0.60. The endocast has a raw volume of 45.075 $mm^3$ (= 0.0045075 milliliters). The volume of the endocast with the damaged portions of the basicranium reconstructed is 48.695 $mm^3$. There are no differences in linear dimensions between the raw and reconstructed endocasts.

The olfactory bulb casts are relatively large and combined they compose 14.22% of the entire endocranial space. The olfactory bulb casts are anteroposteriorly oval in shape and are separated from the rest of the cerebral cast by a poorly developed circular fissure.

The cerebral hemisphere casts are elongate, extending over half of the anteroposterior length of the endocast. The two hemisphere casts are separated by a wide, shallow furrow near their anterior end but the casts splay laterally at their posterior end (Figure 6B). This furrow represents the median sulcus that is laterally expanded because of damage to the skull roof. A partial cast of the superior sagittal sinus lies within the median sulcus (Figure 6B). The skull roof covering the dorsal midbrain and hindbrain is also damaged on this skull and, consequently, very little detail is discernable in this portion of the endocast. It is not clear if the midbrain is exposed on the dorsal surface of the endocast. The size and anterior extent of the cast of the vermis of the cerebellum is also not discernable from this skull. The transverse and sigmoid sinuses are not visible on this specimen. The parafloccular casts of the cerebellum are present and relatively small on the endocast of *Hadrocodium*; the parafloccular casts compose 0.28% of the total endocranial space. The cerebellum appears to be laterally expanded in *Hadrocodium*, but there is no other indication of distinctive cerebellar hemispheres on the endocast.

Little anatomical detail is visible on the ventral surface of the *Hadrocodium* endocast, a result of damage to the basicranium of the skull. The hypophyseal cast, however, is visible on this endocast (Figure 6C). The hypophyseal cast is fairly shallow and constitutes 0.22% of the total endocranial space. The paired canal casts for cranial

nerves II, III, IV, $V_1$, and VI lie anterior and lateral to the hypophyseal cast. These canals are widely separated by a deep indentation on the ventral surface of the endocast such that the right and left sphenorbital fissures are separate.

The casts of the cava epipterica are relatively large, composing 0.72% of the total endocranial space. A large, circular opening perforates the floor of the cavum epiptericum (Luo et al., 2001b). The internal carotid artery presumably passed through the ventral opening of the cavum epiptericum in many non-mammalian cynodonts because these taxa lack a separate internal carotid foramen (Kielan-Jaworowska et al., 2004). The cavum epiptericum for the trigeminal ganglion and cavum supracochleare for the geniculate ganglion were confluent in *Hadrocodium*. The foramen for the mandibular branch of the trigeminal nerve ($V_3$) is on the ventrolateral surface of the skull and anterolateral to the ventral opening of the cavum epiptericum (Luo et al., 2001b).

***Obdurodon dicksoni***. The cranial endocast of *Obdurodon dicksoni* (Figure 7) is similar in overall morphology to that of the extant platypus, *Ornithorhynchus anatinus*, but size is a major difference. The *Obdurodon* endocast is significantly larger than that of the adult *Ornithorhynchus* (Figure 8), and aspect ratios of endocast width/length and height/length vary between the two taxa. The height/width aspect ratio is well conserved among the three specimens examined here. The width/length aspect ratio of the *Obdurodon* endocast is 0.77, the height/length ratio is 0.57, and the height/width ratio is 0.74. In contrast, the adult *Ornithorhynchus* endocast has a width/length ratio of 0.93, a height/length ratio of 0.69, and a height/width ratio of 0.74. The juvenile *Ornithorhynchus* endocast has a width/length ratio of 0.97, a height/length ratio of 0.73,

and a height/width ratio of 0.75. The endocast volumes presented here compare favorably with published brain volumes and partial volumes for extant monotremes (Pirlot and Nelson, 1978; Ross et al., 2004).

The endocast of *Obdurodon* is dominated by massive, lissencephalic (= smooth) cerebral hemisphere casts that are separated dorsally by a deep median sulcus (Figure 9). A prominent ossified falx cerebri (Figure 10), an ossification of a portion of the dura mater of the meninges, sits in the median sulcus. Damage to the dorsal surface of the skull of *Obdurodon* prevents an accurate reconstruction of the shape of the anterodorsal surface of the olfactory bulb casts, giving the appearance that the cerebral hemisphere and olfactory bulb casts are not separated by a deep circular fissure (Figures 1, 7). Both *Ornithorhynchus* endocasts have massive, lissencephalic hemisphere casts and a prominent median sulcus resulting from a conspicuous ossified falx cerebri (Figure 10 shows the ossified falx cerebri in the adult skull).

The anterodorsal portion of the lamina cribrosa is unossified in the adult *Ornithorhynchus*, such that the foramen olfactorium advehens remains open (Zeller, 1988). However, the posterior portion of the cribriform plate of *Ornithorhynchus* is ossified. This ossified portion of the cribriform plate is formed by the coalescence of endoturbinals I, II, and III of the ethmoid bone as in other mammals (see CT movies on the web, Appendix 3; Rowe et al., 2005). A hint of the ossified posterior cribriform plate of *Obdurodon* is also visible on the CT slices (see CT movies on the web, Appendix 3). The cribriform plate of *Obdurodon* also appears to be formed by coalescence of the ossified turbinal elements of the ethmoid bone.

The olfactory bulbs of *Obdurodon* are relatively small, together composing about 1.90% of the endocast volume. The olfactory bulb casts of the extant platypus specimens are even smaller. In the adult *Ornithorhynchus*, the olfactory bulb casts together constitute 0.95% of the total endocranial space and are about half the relative size of the corresponding structures in *Obdurodon*. In the juvenile *Ornithorhynchus*, the olfactory bulb casts together compose 1.80% of its endocranial space.

The mesencephalon is not visible on the dorsal surface of the *Obdurodon* endocast or on the exterior of extant monotreme brains (Griffiths, 1978) or endocasts (Macrini and Rowe, 2004). A cast of the vermis of the cerebellum of *Obdurodon* and all the extant monotremes is well developed on the dorsal surface of the endocasts (Macrini and Rowe, 2004; Figures 4, 7, 8, 9). Casts of the cerebellar hemisphere and paraflocculi of the cerebellum are also conspicuous on the *Obdurodon* and *Ornithorhynchus* endocasts (Figures 7, 8, 9). The parafloccular casts are small and spherical but distinct, similar to those of *Ornithorhynchus*. The parafloccular casts compose about 0.57%, 0.71%, and 0.58% of the endocranial volume in *Obdurodon*, the juvenile *Ornithorhynchus*, and the adult *Ornithorhynchus*, respectively.

On the ventral surface of the *Obdurodon* endocast, the cast of the hypophyseal fossa is prominent (Figure 7C). The hypophyseal cast of *Obdurodon* is more pronounced than that of the adult *Ornithorhynchus* endocast, which is much narrower transversely (Figure 8C). The hypophyseal fossa of the adult *Ornithorhynchus* is confluent anteriorly with a long, narrow groove in the basisphenoid. At least some of this groove is occupied by the pituitary gland (Zeller, 1989a). The hypophyseal fossa in *Obdurodon* composes 0.17% of the endocast volume, while in *Ornithorhynchus* this hypophyseal fossa

composes 0.10% and 0.08% of the total endocranial space for the adult and juvenile endocasts, respectively.

The maxillary branch of the trigeminal nerve ($V_2$) passes through the foramen rotundum of the skull of *Ornithorhynchus*; large casts of the canals transmitting these nerves are visible on the endocast immediately anterior and lateral to the hypophyseal cast. Cranial nerves II, III, IV, $V_1$, and VI pass through the sphenorbital fissure of the skull of *Ornithorhynchus* (Zeller, 1989a, b); casts of the canals transmitting these nerves are smaller and anterior to the maxillary branch casts. The cast of the canal that transmitted $V_2$ is much thinner transversely in the adult *Ornithorhynchus* compared to *Obdurodon*. The paired canal casts for cranial nerves II, III, IV, $V_1$, and VI are confluent in the adult *Ornithorhynchus* endocast (Figure 8C), but not in *Obdurodon* (Figure 7C). That is, there is no bony septum between the paired sphenorbital fissures in *Ornithorhynchus* (figure 53 in Zeller, 1989a), but a bony division is clearly visible in *Obdurodon*.

Casts of massive trigeminal nuclei sit posterior to the hypophyseal cast of *Obdurodon* (Figure 7C). The trigeminal nucleus casts of *Obdurodon* are flatter and less pronounced than those of *Ornithorhynchus*. Neither echidna endocast shows any indication of a trigeminal nucleus cast. The large jugular foramen lies posterior and lateral to the trigeminal nucleus cast in *Obdurodon* and *Ornithorhynchus*. Cranial nerves IX, X, XI, and XII pass through this opening in *Ornithorhynchus* (Zeller, 1989a, b).

The cavum epiptericum is quite large in *Obdurodon* (composing 1.34% of endocranial space) as well as in *Ornithorhynchus* (constituting 1.24% of endocranial space in the juvenile and 1.09% in the adult). The cavum epiptericum in both taxa

extends from just posterior of the foramen rotundum to just posterior to the foramen ovale, therefore including the cast of the canal that transmits $V_2$ (Figures 7, 8; Zeller, 1989a). There is no clear separation between the cavum epiptericum and the cavum supracochleare space in *Obdurodon* or *Ornithorhynchus*; therefore, the geniculate ganglion was likely incorporated within the space of the cavum epiptericum. In addition to the geniculate ganglion, the trigeminal ganglion, the rostral portion of the otic ganglion, and portions of several cranial nerves transverse the cavum epiptericum of *Ornithorhynchus* (Zeller, 1989b).

The pons and medulla oblongata do not leave distinctive marks on the ventral surface of the endocasts of *Obdurodon* or *Ornithorhynchus*. The rhinal fissure is poorly represented on the ventral surface of the endocasts of *Obdurodon* and *Ornithorhynchus*. It is most visible on the juvenile platypus endocast. Lateral to the anterior portion of the trigeminal nucleus is the cast of the internal auditory meatus for cranial nerves VII and VIII (Archer et al., 1992). In posterior view, the foramen magnum appears relatively taller in the adult *Ornithorhynchus* compared to *Obdurodon* (Figure 9).

***Tachyglossus aculeatus***. The cranial endocasts of *Tachyglossus aculeatus* and *Zaglossus bruijni* are nearly identical except for differences in size (the volume of the *Zaglossus* endocast is nearly twice that of the *Tachyglossus* endocast; Appendix 1), hence only the *Tachyglossus* endocast is described and figured here (Figure 4). However, the echidna endocasts look very different from the endocasts of *Obdurodon* and *Ornithorhynchus*. The surface of the cerebral hemisphere casts of the echidna endocasts are very gyrencephalic (= convoluted) in contrast to the lissencephalic condition of the

platypus endocasts. Several sulci are visible on the surface of the *Tachyglossus* endocast including the sylvian fissure, sulcus antesylvius rostralis, sulcus antesylvius caudalis, sulcus postsylvius rostralis, sulcus postsylvius caudalis, and the rhinal fissure medialis (Figure 4).

The olfactory bulb casts of the tachyglossids are relatively larger than the corresponding structures in the *Obdurodon* and *Ornithorhynchus* endocasts. The olfactory bulb casts compose 2.28% of the total endocranial volume (EV) of *Tachyglossus* and 3.08% of the EV of *Zaglossus*. In actuality the discrepancy between relative olfactory bulb cast size in tachyglossids and ornithorhynchids is even greater because the volumes of these casts are underestimated in echidnas, as discussed previously. In addition to reduced olfactory bulb casts, both *Ornithorhynchus* and *Obdurodon* have three endoturbinals but *Tachyglossus* has seven (Paulli, 1900). A preliminary survey of multiple mammalian species suggests that endoturbinal surface area corresponds to olfactory acuity and olfactory bulb size (summarized in Rowe et al., 2005).

The mesencephalon does not leave a cast on the dorsal surface of the echidna endocasts similar to the condition seen in other monotreme and mammalian endocasts. However, the cerebellar cast is prominent on the *Tachyglossus* endocast and casts of the vermis and cerebellar hemispheres are clearly discernable. *Tachyglossus* and *Zaglossus* skulls lack the subarcuate fossa of the petrosal bone, and therefore, parafloccular casts are absent on the corresponding endocasts.

The hypophyseal cast lies in the center of the ventral surface of the *Tachyglossus* endocast (Figure 4C). The hypophyseal fossa is more circular in tachyglossids than in

ornithorhynchids; the width/length aspect ratio of the hypophyseal cast is 0.56 in *Tachyglossus* and 0.73 in *Zaglossus*. The hypophyseal cast makes up 0.16% of the volume of the *Tachyglossus* endocast and 0.04% of the volume of the *Zaglossus* endocast.

A cast of the optic chiasm for transmitting the optic nerve (cranial nerve I) is immediately anterior to the hypophyseal cast in *Tachyglossus* (Figure 4C). The large, circular foramen ovale lies directly lateral to the hypophyseal cast in *Tachyglossus*. This opening transmitted the mandibular branch of the trigeminal nerve ($V_3$; Kuhn, 1971). The sphenorbital fissure lies anterior and lateral to the hypophyseal cast (Figure 4C). The right and left openings of the sphenorbital fissure are widely separated by a deep fossa that lies immediately anterior to the cast of the optic chiasm. This fossa on ventral surface of the endocast is a result of the posterior extension of the sphenethmoid recess of the nasal cavity in echidnas.

The cavum epiptericum and corresponding trigeminal ganglion are large in echidnas (constituting 1.30% of the total endocranial space in *Tachyglossus* and 1.11% of endocranial space of *Zaglossus*; Abbie, 1934; Figure 4C) but, unlike in the platypus, this space does not encompass the geniculate ganglion in *Tachyglossus* (Kuhn, 1971; Zeller, 1989a). The trigeminal sensory nucleus of the hindbrain is enlarged in *Tachyglossus* (Abbie, 1934; Brauer and Schober, 1970), but not to the extent seen in the extant platypus. The trigeminal nucleus does not leave a noticeable impression on the endocast of either species of echidna unlike the condition seen in the *Ornithorhynchus* and *Obdurodon* endocasts. The pons and medulla oblongata do not leave distinguishable impressions on the echidna endocasts.

***Kryptobaatar dashzevegi***. The cranial endocast of *Kryptobaatar* is roughly oval in shape when viewed dorsally with the exception of the large, oval-shaped posterolaterally directed parafloccular casts (Figure 11). The width/length aspect ratio of the endocast is 0.75, the height/length ratio is 0.59, and the height/width ratio is 0.80.

The olfactory bulb casts are prominent on the dorsal surface of the endocast. They are large and anteroposteriorly elongate, together composing 5.85% of the total endocranial space. The circular fissure separating the olfactory bulb casts from the lissencephalic cerebral hemisphere casts is not deep on the digital endocast. The median sulcus dividing the cerebral hemispheres is also not deep on this specimen. However, both the circular fissure and median sulcus are well developed on other *Kryptobaatar* endocasts (GI PST 8-2; Kielan-Jaworowska and Lancaster, 2004). It is unclear if the differences in the development of the circular fissure and median sulcus between the natural and digital endocasts of *Kryptobaatar* represent polymorphism (individual variation) or are an artifact of preservational differences.

The natural endocast has a small triangular-shaped convex structure located between the anterior portion of the cerebral hemispheres and just posterior to the circular fissure (Kielan-Jaworowska and Lancaster, 2004). This unnamed structure (possibly part of the superior sagittal sinus system) is not visible on the digital endocast. There is no midbrain exposure on the dorsal surface of any of the endocasts of *Kryptobaatar*. A large bulge on the posterior dorsal surface of the endocast covers the midbrain and the middle, dorsal portion of the cerebellum. This structure is referred to elsewhere as a cast of the superior cistern sinus (Kielan-Jaworowska and Lancaster, 2004); however, I interpret this

structure to be the cast of the vermis of the cerebellum. The vermis cast extends anterior to the parafloccular casts in *Kryptobaatar*. The transverse and sigmoid sinuses are not clearly demarked on the surface of the digital endocast but are visible on the natural one (Kielan-Jaworowska and Lancaster, 2004).

Cerebellar hemisphere casts are absent on the digital endocast as in other multituberculate specimens (Kielan-Jaworowska, 1983, 1986). Lateral to the vermis cast the parafloccular casts of the cerebellum diverge from the main portion of the cerebellum. The parafloccular casts are large and ventrolaterally directed, together composing 4.04% of the total endocranial space.

The ventral surface of the digital endocast is well-preserved overall. The hypophyseal cast is prominent and semi-spherical in shape because of some damage to the basicranium of the specimen. The anterior portion of the sella turcica including the dorsum sellae is damaged. The hypophyseal fossa constitutes 0.77% of the total endocranial space.

The optic foramen is located anterior to the sella turcica and transmitted the optic nerve (cranial nerve II) and the ophthalmic branch of the internal carotid artery (Wible and Rougier, 2000). The exact location of this opening is difficult to determine because of damage to the skull just posterior to the orbitosphenoid bone and consequently, the optic foramen is not reflected on the endocast.

Casts for the voluminous cava epipterica lie immediately lateral to the hypophyseal cast. The cavum epiptericum is confluent with the cavum supracochleare in *Kryptobaatar*. This space presumably housed the trigeminal and facial ganglia as well as portions of the oculomotor (III), trochlear (IV), ophthalmic ($V_1$), maxillary ($V_2$),

mandibular ($V_3$) and abducent (VI) nerves (Kielan-Jaworowska et al., 1986; Wible and Rougier, 2000). The two cava together compose 1.36% of the total endocranial space.

A cast of the prootic canal for transmitting the prootic sinus (Wible and Rougier, 2000) lies lateral to the posterior portion of the cavum epiptericum cast. The cast for the internal auditory meatus lies immediately posterior to the cavum epiptericum cast. The auditory nerve (VIII) and a branch of the facial nerve (VII) presumably occupied this space. The pons and medulla oblongata do not leave distinctive impressions on the floor of the cast of the hindbrain, as in many other mammal cranial endocasts. The rhinal fissure does not leave a distinctive mark on the *Kryptobaatar* endocast. Casts of the olfactory tracts leading from the bulbs to the cortex are also not visible on the ventral surface of the endocast.

A broken cribriform plate is clearly visible on the CT images of *Kryptobaatar* (PSS-MAE 101) in the sagittal and coronal planes (Figures 12, 13). In *Monodelphis domestica*, the gray short-tailed opossum, the bases of the endoturbinals and ectoturbinals coalesce to form the cribriform plate (Rowe et al., 2005). Similarly, the cribriform plate of *Kryptobaatar* is constructed from the bases of several turbinal elements of the ethmoid bone; however, the exact number and assignments of these elements are unclear at this point. The mesethmoid is present but not well preserved in this specimen, and therefore it is unclear if a crista galli that extended into the ethmoidal fossa was also present.

The cribriform plate forms the anterior and lateral walls of the ethmoidal fossa, which house the olfactory bulbs. It also forms the roof of the posterior portion of the sphenethmoid recess, the space into which the caudal most endoturbinal projects (Rowe et al., 2005).

***Vincelestes neuquenianus***. The overall shape of the endocast in dorsal view approximates that of two pairs of cylinders: a small pair of cylinders comprising the olfactory bulb casts and a larger, posterior pair of cylinders comprising the rest of the endocast (Figures 14, 15). In lateral view, the endocast shows some moderate flexure (23º) around the hypophyseal cast. A rhinal fissure is not visible on the lateral surface or anywhere else on the endocast. The width/length aspect ratio of the entire *Vincelestes* endocast is 0.55, the height/length ratio is 0.34, and the height/width ratio is 0.61.

The olfactory bulb casts are relatively large, together constituting approximately 10.81% of the total endocranial space. The casts have the shape of anteroposteriorly long, narrow ovals. The circular fissure separating the olfactory bulb casts from the rest of the cerebral hemisphere casts is well-developed (Figures 14B, 15B). In addition to the main olfactory bulbs, casts of the accessory olfactory bulbs are also discernable on the dorsal surface of the *Vincelestes* endocast. Accessory olfactory bulbs of extant mammals receive projections from the vomeronasal organ (discussed in Rowe et al., 2005). The olfactory tracts leading from the bulbs to the cortex do not leave an impression on the ventral surface of the endocast; the tracts are obscured by meninges.

The cerebral hemisphere casts are enlarged and lissencephalic; they are divided by a deep median sulcus. When viewed dorsally, the cerebral hemisphere casts are antero-posterior elongated ovals that diverge from each other posteriorly (Figures 14B, 15B). At least a partial ossified falx cerebri sits in the median sulcus (Figure 16). There is a large, continuous bulbous structure just posterior to this that covers the midbrain and the dorsal portion of the cerebellum. I interpret this as the cast of the vermis of the

cerebellum. The vermis cast extends anterior to the position of the paraflocculus cast. Dural venous structures such as the superior (dorsal) sagittal, transverse, and sigmoid sinuses are not clearly visible on the endocast due to damage of this skull. However, the blood vessels that leave impressions on the petrosal bone are reconstructed elsewhere (Rougier et al., 1992) based on an isolated petrosal and other skulls of *Vincelestes*.

The cerebellar hemisphere casts of the hindbrain are present in *Vincelestes*. A deep, narrow subarcuate fossa is visible on the left side of the skull of MACN-N 04, but the corresponding structure on the right side is damaged. The cast of the left paraflocculus of the cerebellum composes 0.23% of the total endocranial space.

On the ventral surface of the *Vincelestes* endocast, a wide, circular, deep hypophyseal cast is the most conspicuous structure, located in the center (Figures 14C, 15C). The hypophyseal cast constitutes about 0.71% of the entire endocranial space. Casts of the canals that presumably transmitted the internal carotid arteries insert into the anterolateral portions of the hypophyseal cast. The foramina for the entrance of the carotid arteries are oriented nearly vertical and are located ventrolateral to the anterior portion of the hypophyseal cast.

Casts of confluent canals that end at the sphenorbital fissure are located anterior to the hypophyseal cast. These openings transmitted cranial nerves II, III, IV, $V_1$, and VI (Hopson and Rougier, 1993). The cavum epiptericum is large and the two cava together constitute 0.82% of the total endocranial space. The cast of the canal that transmitted the mandibular branch of the trigeminal nerve, which exited the skull through the foramen ovale, is visible on each side of the endocast (Figures 14C, 15C). Based on comparative anatomy and extant phylogenetic bracketing of soft tissue structures, the cavum

epiptericum housed the trigeminal ganglion in *Vincelestes*, but the geniculate ganglion was located in the separate cavum supracochleare located within the petrosal (Rougier et al., 1992). The fenestra semilunaris and hiatus Fallopii, the opening for the facial nerve, of the petrosal are clearly visible on the CT images (C260-262; Rougier et al., 1992).

The ventrum of the hindbrain cast is unremarkable in *Vincelestes*; the medulla oblongata and pons do not leave distinctive impressions on the endocast (Figures 14C, 15C). These structures are obscured by meninges and associated cistern sinuses.

***Pucadelphys andinus***. The overall gestalt of the *Pucadelphys* endocast (Figures 17, 18) is similar to that of the didelphid marsupial *Monodelphis domestica* (Figures 19, 20). In dorsal view, the endocast is wedge-shaped with large, circular olfactory bulb casts on its anterior terminus (Figure 17). In lateral view, the endocast is low and shows moderate flexure around the hypophyseal cast (26º; Figure 17A). A rhinal fissure is not visible on the lateral surface or anywhere else on the endocast. The width/length endocast aspect ratio is 0.58, the height/length ratio is 0.44, and the height/width ratio is 0.75.

The olfactory bulb casts are relatively large, together constituting about 11.69% of the total endocranial space. The casts are oval in shape with a width/length aspect ratio of 0.62. The circular fissure separating the olfactory bulb casts from the rest of the cerebral hemisphere casts is well developed (Figure 18B). The olfactory tracts from the bulbs and leading to the hippocampus do not leave an impression on the ventral surface of the endocast.

The cerebral hemisphere casts are lissencephalic and are divided by a deep median sulcus. It is noteworthy that the sulcus is deeper in *Pucadelphys* than in *Monodelphis*. The two cerebral hemispheres are triangular in shape, being narrow anteriorly and expanding laterally toward their posterior ends. The cerebral hemisphere casts of *Pucadelphys* do not expand as far laterally as in *Monodelphis*, whose casts extend beyond the lateral extent of the parafloccular casts of the cerebellum (compare Figures 17, 18, 19, 20). The height/length aspect ratio of the cerebral hemisphere casts of *Pucadelphys* is 0.62 (Table 2.1). This ratio is much larger in the *Monodelphis* endocasts examined (range=0.74–0.86; mean=0.79; n=3; Table 2.1). However, the combined width/length aspect ratio for the cerebral hemisphere casts of *Pucadelphys* is 1.12, which is significantly different from the ratio in *Monodelphis* (range=1.24–1.38; mean=1.29; n=3; Table 2.1). The cerebral hemisphere cast length/total endocast length ratios are quite similar between *Pucadelphys* (0.51) and *Monodelphis* (range=0.42–0.50; mean=0.47; n=3; Table 2.1).

A large bulge on the posterior surface of the endocast covers the midbrain (Figure 18B); this structure is interpreted as the cast of the vermis of the cerebellum. The vermis cast of *Pucadelphys* extends anterior to the casts of the paraflocculi and has a width/length ratio of 0.81 (Table 2.1), indicating that the structure has a somewhat anteroposteriorly elongate oval shape. Cerebellar hemisphere casts are also visible on the endocast, but distinctive superior (dorsal) sagittal, transverse, and sigmoid sinuses are not visible. The parafloccular casts of the cerebellum are prominent, together composing 0.95% of the endocranial space.

A conspicuous, wide, circular, shallow hypophyseal cast is present in the center of the ventral surface of the *Pucadelphys* endocast (Figure 18C). The hypophyseal cast constitutes about 0.54% of the entire endocranial space. The hypophyseal fossa is wider than long, with a width/length aspect ratio of 1.10.

The right and left casts of the canals that transmitted the maxillary branches of the trigeminal nerve ($V_2$) are widely separated and are located just anterolateral to the hypophyseal cast (Marshall and Muizon, 1995). The foramen rotundum is the opening in the skull through which this nerve presumably passed. The sphenorbital fissure (= optic-orbital foramen), which presumably transmitted cranial nerves II, III, IV, $V_1$, VI, the ophthalmic artery, and a vein (Marshall and Muizon, 1995), is located anteromedial to the foramen rotundum (Figure 18C). The right and left casts of those fissures in the endocast are in close proximity to each other but are not confluent.

The foramen ovale lies anteromedial to the parafloccular cast and posterolateral to the hypophyseal cast. This opening presumably transmitted the mandibular branch of the trigeminal nerve ($V_3$; Marshall and Muizon, 1995). The cavum epiptericum, which presumably housed the trigeminal ganglion, is not confluent with the cavum supracochleare for the geniculate ganglion in *Pucadelphys*. The cava epipterica of *Pucadelphys* together composed 0.17% of the total endocranial space. The cast of the internal auditory meatus for passage of cranial nerves VII and VIII is visible on the right side of the endocast (Figure 18C). The rectangular cast for the ventral surface of the hindbrain is located posterior to the foramen ovale. The hindbrain cast is unremarkable in *Pucadelphys*; the medulla oblongata and pons do not leave distinctive impressions on the endocast.

## DISCUSSION

### *Hadrocodium wui*

The digital endocast of *Hadrocodium* described above represents the only cranial endocast from a non-mammalian mammaliaform. Because *Hadrocodium* is the sister taxon to Mammalia (Luo et al., 2001b, 2002, 2003), it possesses a number of mammalian characters that will be useful for polarizing endocast characters for the study of the evolution of endocranial space in mammals. The distribution of these characters is discussed in Chapter 3.

The EQ range calculated for *Hadrocodium* using the Eisenberg (1981) equation and a range of body size estimates is 0.32-0.49 (Appendix 4). The EQ range of *Hadrocodium* is larger than those of other non-mammalian cynodonts (*Thrinaxodon*, *Diademodon*, *Probelesodon*, *Probainognathus*, *Massetognathus*, *Exaeretodon*; Appendix 4) suggesting that an increase in overall brain size occurred in the least inclusive clade containing *Hadrocodium* and crown Mammalia (Luo et al., 2001b).

### *Vincelestes neuquenianus*

The cranial endocast of *Vincelestes* described above is important because of the phylogenetic position of this taxon. Some previous phylogenetic analyses place *Vincelestes* as the sister taxon to Theria and within the larger clade Theriiformes that also contains multituberculates (Rowe, 1993; Rougier et al., 1996a). More recent analyses

that include additional taxa of varying completeness suggest that *Vincelestes* is slightly more removed from crown Theria based on dentral characters (Luo et al., 2002, 2003). Given the lack of cranial and postcranial evidence for the phylogenetic position of many of these incomplete stem therians, *Vincelestes* is the *de facto* outgroup for studies that focus on cranial and postcranial character systems, or simply analyses restricted to the consideration of relatively complete forms (Rowe, 1993; Rougier et al., 1996a, 1998; Novacek et al., 1997; Horovitz and Sánchez-Villagra, 2003).

Regardless of its exact phylogenetic position, *Vincelestes* is one the most completely known stem therians, being represented by six nearly complete skulls, 17 lower jaws, and a number of postcranial elements, all from a single locality (Rougier et al., 1992). Although the exterior of the skull of *Vincelestes* is described in the literature, the internal cranial osteology and cavities within the skull are virtually unknown with the exception of the petrosal and cranial vascular reconstructions (Rougier et al., 1992; Hopson and Rougier, 1993). The *Vincelestes* endocast described above represents the first cranial endocast from a close extinct relative of crown Theria and therefore it is important for understanding the evolution of endocranial space in this diverse clade of mammals. The distribution of these characters is discussed in Chapter 3.

The EQ value calculated for *Vincelestes* using the Eisenberg (1981) equation is 0.25 (Appendix 4). The EQ values of all of the members of crown Theria examined here (Appendix 4) are higher than that of *Vincelestes* suggesting that overall brain size increased in Theria.

***Pucadelphys andinus***

The cranial endocast of *Pucadelphys* described above is also important because of the phylogenetic position of this taxon. *Pucadelphys andinus* is arguably the best preserved stem-marsupial, represented by multiple, nearly complete, three-dimensional skulls and skeletons. Recent phylogenetic analyses place *Pucadelphys* in a polytomy with other stem-marsupials and crown Marsupialia (Rougier et al., 1998; Luo et al., 2003). Other stem-marsupials, such as *Asiatherium reshetovi* from the Late Cretaceous of Mongolia (Szalay and Trofimov, 1996) and *Sinodelphys szalayi* from the Early Cretaceous of China (Luo et al., 2003), are fairly complete but are not known from three-dimensional specimens. *Deltatheridium* is represented by specimens that only preserve the rostral portion of the skull, dentition, and incomplete tarsals (Luo et al., 2002).

The extracranial anatomy and postcranial osteology of *Pucadelphys andinus* are well documented in the literature (Marshall and Muizon, 1995; Marshall and Sigogneau-Russell, 1995; Muizon, 1998), but the internal cavities of its skull, including the endocranial cavity, are undescribed. In fact, no cranial endocast (natural or artificial) has yet been described for any stem-marsupial. *Pucadelphys* represents the oldest and most basally diverging taxon within the metatherian lineage for which a cranial endocast can be acquired. Therefore, the digital endocast described above is useful for polarizing characters for study of the evolution of endocranial space and brain evolution in marsupials. The distribution of these characters is discussed in Chapter 3.

***Obdurodon dicksoni***

The *Obdurodon* digital endocast described above is important because it represents the oldest cranial endocast from an unequivocal member of either extant monotreme lineage (Ornithorhynchidae and Tachyglossidae) and is therefore important for inferring character support for Monotremata, a clade that is not well-diagnosed. Monotremes are generally held to comprise two extant clades, Ornithorhynchidae represented by the duckbill platypus (*Ornithorhynchus anatinus*) and Tachyglossidae with two extant species of echidnas (*Tachyglossus aculeatus* and *Zaglossus bruijni*). These three taxa are different morphologically and ecologically, and were initially united based on plesiomorphic characters (e.g., presence of a cloaca, ovipary, presence of an interclavicle and a procoracoid in the shoulder girdle; Griffiths, 1978). *Ornithorhynchus anatinus* is aquatic, has webbed feet, and a bill-shaped snout. Echidnas are terrestrial and have rounded and dorsoventrally compressed bodies that are mostly covered by hollow spines that are essentially modified hairs. The most prominent feature on the echidna head is the elongated, hairless snout.

Whereas monotreme monophyly is virtually unquestioned, there are relatively few unequivocal morphological synapomorphies for Monotremata described in the literature; most of these are osteological (as summarized by Gregory, 1947 and Rowe, 1986). However, some of these were subsequently shown to be equivocal. For instance presence of a tarsal spur, found in all three extant species of monotremes, was a suggested synapomorphy for the group (Ax, 1987). A tarsal spur is now known from a number of fossil mammals including *Gobiconodon*, some multituberculates, *Zhangheotherium*, and

*Henkelotherium* and therefore is plesiomorphic for Monotremata (Luo et al., 2002, 2003; Hurum et al., 2006; Ji et al., 2006).

Moreover, the differences between the platypus and echidnas are profound and the fossil record suggests both had diverged from a common ancestor with therian mammals by the mid-Jurassic (Rowe, 1986, 1988, 1993; Messer et al., 1998; Luo et al., 2001b, 2002; Rauhut et al., 2002). The pre-Pleistocene fossil record for crown Monotremata is represented by only a handful of fossils (Archer et al., 1985; Pascual et al., 1992; Rich et al., 1999, 2001; Musser, 2003). This raises the possibility that monotreme monophyly could be a manifestation of long-branch attraction. A nearly complete skull of a fossil platypus, *Obdurodon dicksoni*, from Miocene deposits of Riversleigh, Australia represents the oldest record of an unequivocal member of either monotreme clade and is therefore significant for monotreme systematics (Archer et al., 1992, 1993; Musser and Archer, 1998).

I explore the question of monotreme monophyly by examining the nervous system, an anatomical system that is poorly represented in phylogenetic analyses (but notable exceptions include Johnson et al., 1982a, b, 1994; Kirsch, 1983; Kirsch and Johnson, 1983; Kirsch et al., 1983; Northcutt, 1984, 1985). Because soft tissue anatomy such as the brain almost never fossilizes, cranial endocasts are often the only material that paleontologists have to study the central nervous system of fossil mammals (Jerison, 1973). Endocast characters that diagnose Monotremata are discussed in Chapter 3.

The average adult monotreme encephalization quotient (EQ) calculated using the Eisenberg (1981) equation is 0.87 (range: 0.75-1.00; Appendix 4), which is fairly close to the average for mammals (1.00). Comparing adult monotremes only, Ornithorhynchidae

has a higher average EQ than Tachyglossidae (0.92 versus 0.82; Appendix 4). The EQ of *Obdurodon* is 1.00 which is higher than the adult extant platypus (0.84; Appendix 4). The juvenile platypus has an EQ that is nearly half that of the adult sampled, suggesting that endocranial volume shows positive allometry with body size from the stage when all teeth are present throughout adulthood.

***Kryptobaatar dashzevegi***

Following is a discussion of some differences between the digital cranial endocast of *Kryptobaatar* described in this chapter and a natural endocast of the same taxon described by Kielan-Jaworowska and Lancaster (2004). In addition, the implications of an unequivocal cribriform plate being present in *Kryptobaatar* are discussed. All of these data have implications for the study of endocranial space in multituberculates as well as Mammalia.

**Endocranial Volume and Encephalization Quotient.** To access the accuracy of VGStudioMax© in measuring endocranial volume (EV), the EVs of two echidnas (one *Tachyglossus* and one *Zaglossus*; Macrini and Rowe, 2004) were compared with published brain volumes for the two taxa (Ross et al., 2004). The EVs measured from VGStudioMax are quite similar to their respective brain volumes taken from two different specimens. The EVs of the *Zaglossus* and *Tachyglossus* are about 1% and 3.5% larger than the respective published brain volumes for the two taxa. These values are well within the range of measurement error. Furthermore, the fact that there are differences is unsurprising because endocranial volumes should be larger than brain volumes for a particular taxon because of other features that occupy the endocranial

space such as meninges and blood vessels. In addition, individual variation likely accounts for some of the discrepancy in volume because the brain volume and EV were not measured on the same individuals.

I also estimated the endocranial volume from the endocasts of the two echidnas by treating the olfactory bulbs and the remainder of the endocast as separate cylinders; the sum of the two volumes is the estimated EV (following the methodology of Kielan-Jaworowska and Lancaster, 2004). The estimated EVs were then compared to their respective measured EVs. The estimated EV for *Tachyglossus* is approximately 74% greater than the measured EV. For *Zaglossus*, the estimated EV is about 70% greater than the measured EV. Based on these results it seems that estimating EV with cylinders is considerably less accurate than the measured EV values obtained digitally.

The measured endocranial volume (EV) of the digital endocast of *Kryptobaatar* ('the AMNH specimen') differs dramatically from an estimate of the EV from a natural endocast of *Kryptobaatar* ('the Polish specimen'; GI PST 8-2; Kielan-Jaworowska and Lancaster, 2004). The skulls of the two specimens are not identical; the AMNH specimen is about 76% the length of the skull of the Polish specimen (26 mm versus 34 mm, respectively; Wible and Rougier, 2000; Kielan-Jaworowska and Lancaster, 2004).

The volume of the Polish endocast was estimated using the cylinder approach (Kielan-Jaworowska and Lancaster, 2004). The estimated EV of the Polish endocast including the olfactory bulbs is 0.84 mL and the estimated EV of the AMNH endocast is about 0.95 mL, using the same procedure. The EV of the AMNH endocast (0.34 mL) measured using VGStudioMax© is nearly three times smaller than that of the estimated EV for the same specimen. Taking into account the difference in size of the two

specimens, the measured EV for the AMNH specimen is about half the estimated EV for the Polish endocast. This great a difference is not likely a result of individual variation.

Discrepancies in estimated vs. measured EV have important implications for calculation of the encephalization quotient (EQ) of *Kryptobaatar*. Body weight for *Kryptobaatar* was approximated at 28.12 g based on the following equations: L = 4(S); Wt = 0.025($L^3$) (L = body length in cm; S = skull length in cm; Wt = body weight in grams; Kielan-Jaworowska and Lancaster, 2004). Using the measured EV of the digital endocast and the above mentioned estimated body weight, the EQ of *Kryptobaatar* ranges from 0.29 to 0.53 (Appendix 4). An EQ of 0.71 is obtained from using the equation of Eisenberg (1981) and the EV estimate of the Polish specimen from Kielan-Jaworowska and Lancaster (2004).

An EQ of 0.53 is within the range estimated for two other multituberculates: *Ptilodus* (EQ = 0.62) and *Chulsanbaatar* (EQ = 0.54-0.56) (Kielan-Jaworowska, 1983; Krause and Kielan-Jaworowska, 1993; Kielan-Jaworowska and Lancaster, 2004). However, it is likely that the EQs of these taxa would differ if their EVs were determined using a different method, such as via measurement from CT data.

The method in which EVs are determined should be standardized. Endocranial volumes should be measured using programs such as VGStudioMax© if a specimen is digitized through techniques such as CT. Accurate volume measures can also be obtained from isolated natural endocasts by volumetric displacement of specimens in water. The technique of estimating endocast volume via the cylindrical method is inaccurate and should be abandoned.

**Anatomical Interpretation of *Kryptobaatar* Endocranial Space.** The overall structure and relative proportions of parts of the digitally constructed *Kryptobaatar* endocast are similar to those of other multituberculate endocasts. The olfactory bulb casts are relatively large in *Kryptobaatar* (Kielan-Jaworowska and Lancaster, 2004) as they are in *Ptilodus* (Simpson, 1937; Krause and Kielan-Jaworowska, 1993), *Chulsanbaatar* (Kielan-Jaworowska, 1983, 1986; Kielan-Jaworowska et al., 1986), and *Nemegtbaatar* (Kielan-Jaworowska, 1986; Kielan-Jaworowska et al., 1986). All of these taxa have large cerebral hemisphere casts that diverge from the midline posteriorly (Simpson, 1937; Kielan-Jaworowska, 1983, 1986; Kielan-Jaworowska et al., 1986; Krause and Kielan-Jaworowska, 1993; Kielan-Jaworowska and Lancaster, 2004). The cerebellum of all of these taxa is represented on the endocasts with large casts of what I interpret to be the vermis and large parafloccular casts that are elongated laterally (Simpson, 1937; Kielan-Jaworowska, 1983, 1986; Kielan-Jaworowska et al., 1986; Krause and Kielan-Jaworowska, 1993; Kielan-Jaworowska and Lancaster, 2004).

However, the representation of a cast of the vermis on multituberculate endocasts was recently disputed (Kielan-Jaworowska and Lancaster, 2004). A bulge covering the midbrain and extending to cover the middle, dorsal portion of the cerebellum of *Kryptobaatar* is the structure that I interpret to be the vermis as it was originally described in multituberculates (e.g., Simpson, 1937; Kielan-Jaworowska, 1983, 1986; Krause and Kielan-Jaworowska, 1993). This bulge was recently referred to in the literature as a cast of the superior cistern sinus; however, convincing evidence was not presented to support this claim (Kielan-Jaworowska and Lancaster, 2004). Support for the cistern sinus cast idea comes from the claim that *Phascolarctos cinereus* (the koala)

possesses an enlarged cistern sinus cast that leaves an impression on the inner surface of the skull (Kielan-Jaworowska and Lancaster, 2004). To examine this claim, a skull of *Phascolarctos* was CT scanned and I built a digital cranial endocast from these CT data. The bulge on the posterior dorsal surface of the koala endocast does not appear to be continuous with the structure covering the midbrain, but rather sits atop the cerebellum (Figure 21). Therefore, I interpret this bulge to be a cast of the vermis in *Phascolarctos*. Following this line of evidence, there is no reason to discount the idea that the bulge on the *Kryptobaatar* endocast could also be a cast of the vermis. The superior cistern sinus of the subarachnoid space likely covered the midbrain and possibly the vermis in *Kryptobaatar*, but the bulge on the endocast is probably partially if not nearly entirely a contribution of the underlying vermis, especially given the great lateral expansion of the cerebellum. In other words, there is no evidence that the superior cistern sinus is unusually thick in *Kryptobaatar* in comparison to other mammals such that it would bulge out and leave an impression on the skull.

A rhinal fissure was not positively identified on the digital endocast of *Kryptobaatar* described in this paper or on any other multituberculate endocast studied to date (Kielan-Jaworowska, 1983, 1986; Krause and Kielan-Jaworowska, 1993; Kielan-Jaworowska and Lancaster, 2004). The rhinal fissure is typically used as an indication of the ventral boundary of isocortex (= neocortex) in mammals and thus can be used to record the expansion of the isocortex in extinct taxa (Jerison, 1991). However, lack of a rhinal fissure on a cranial endocast is not an indication of absence of isocortex. The rhinal fissure does not always leave an impression on cranial endocasts (Jerison, 1991); for example, it is not seen on multiple endocasts of the extant marsupial *Monodelphis*

*domestica* even though this structure is clearly visible on the exterior of corresponding brains (Macrini and Rowe, 2002, 2005). Presence or absence of the rhinal fissure on an endocast is a function of the meninges overlying that structure on the brain.

The trigeminal nerve reportedly enters the hindbrain anterior to the pons in an endocast of the multituberculates *Chulsanbaatar* and *Nemegtbaatar* (Kielan-Jaworowska, 1986). However, the casts of the pons are not prominent on these specimens (based on the description and illustrations presented by Kielan-Jaworowska [1986]) and their exact positions are open to interpretation. Regardless, the pons does not leave a distinct impression on the endocast of *Kryptobaatar* described here and therefore this character cannot be evaluated for this taxon. The trigeminal nerve is known to insert in the hindbrain anterior to the pons only in monotremes among extant mammals (Griffiths, 1968, 1978).

The HRXCT data (Figures 12, 13) from *Kryptobaatar* provide the first definitive evidence that at least some multituberculates possessed an ossified cribriform plate. Because the cribriform plate is constructed from the bases of turbinals, *Kryptobaatar* also had ossified turbinals. Previous anatomical studies (Miao, 1988; Wible and Rougier, 2000) and phylogenetic analyses (Wible, 1991; Luo et al., 2002, 2003) questioned the presence of an ossified cribriform plate and ossified turbinals in multituberculates and in particular cimolodontans. These characters need to be re-evaluated in future phylogenetic analyses.

In summary, differences between the digital and natural endocasts of *Kryptobaatar* are apparent. Some differences such as discrepancies in EV are artifacts of the methods. Other differences such as the relative depth of the circular fissure and

median sulcus, and presence of a small triangular-shaped convex structure seen only the dorsal surface of the natural endocast are not as easily explained. It is unclear at this point whether these result from individual variation or from differences in the quality of preservation of the specimens. In the future, more endocasts (digital or natural) should be examined to clarify the reconstruction of endocranial space in *Kryptobaatar*.

Additional studies of digital endocasts of multituberculates generated from CT data will allow quantification of relative sizes of portions of endoc asts. The relative sizes of the olfactory bulb casts in *Kryptobaatar*, *Chulsanbaatar*, *Nemegtbaatar*, and *Ptilodus*, for instance, can be quantified for better comparison among multituberculates and with non-multituberculate taxa.

## CONCLUSIONS

The descriptions of the cranial endocasts of the fossils presented above were made possible by the non-destructive nature of CT technology. Data from the endocranial cavity of many fossils cannot be obtained otherwise without destructively sampling the specimens. Destructive sampling of any fossil is unfavorable, particularly if the taxon is known from a single individual (e.g., *Hadrocodium*, and *Obdurodon*). Therefore, CT technology has the potential to increase the taxonomic sampling of data from the internal cranial morphology of fossil mammals. Digital techniques can also add to the knowledge of endocranial space for taxa previously known from natural endocast material (e.g., *Kryptobaatar*). Isolated natural endocast material is rare, especially multiple specimens

of a particular taxon (but some exceptions are described by Wilson [1971] and Lewy et al. [1992]). Furthermore, many natural endocasts only provide partial representations of endocranial space, because the endocasts are broken or because portions of endocasts are partially obscured by attached skull elements. CT technology can increase the number of known, whole cranial endocasts by sampling from complete skulls of fossils. However, CT is expensive and potentially cost prohibitive for studies requiring large taxonomic or intraspecific samples of endocasts. In addition, the process of isolating digital endocasts from a skull is labor-intensive, particularly for fossil specimens. It can be much more cost and time effective to study natural endocasts if these samples are available.

In addition to making it easier to study discrete anatomical features of the endocranial space of some fossils, CT allows for the relatively easy acquisition of accurate volume and linear measurements from endocasts. The measurements reported in Appendix 1 may prove valuable in future comparative studies of mammalian endocasts. The phylogenetic variation of these endocast measurements are explored in Chapter 3 and the variation of these measurements within a single species (e.g., *Monodelphis*) are explored in Chapter 4.

Endocranial volumes are already known to be valuable for studies of encephalization quotients (EQs; Jerison, 1973). Because of EQ studies, future endocast studies should strive for obtaining accurate endocranial volumes. Endocranial volume measurements from digitized endocasts can be considerably more accurate than volume estimates obtained by treating endocasts as a set of cylinders. This was demonstrated with specimens of the two extant taxa of echidnas (*Tachyglossus* and *Zaglossus*).

Accurate endocranial columes can be obtained from fossil specimens either through the techniques described in this chapter or by measuring the volumetric displacement of isolated, whole natural endocasts. CT technology provides accurate endocranial volume measurements of fossil taxa for which complete, isolated natural endocasts are not available. But again, measurements of endocranial volumes from digital endocasts obtained using CT can be expensive and time consuming.

TABLE 2.1. Linear measurements from metatherian endocasts used in this study. All measurements given in mm. Abbreviations: [a] = specimen # TMM M-7599; [b] = specimen # TMM M-8271; [c] = specimen # TMM M-8273; * = combined cerebral hemisphere cast width.

| Taxon | Vermis cast length, width | Cerebral hemisphere cast length, width*, height |
|---|---|---|
| *Pucadelphys andinus* | 3.498, 2.816 | 8.107, 9.056, 5.025 |
| *Dasyurus hallucatus* | 4.059, 4.115 | 17.799, 19.185, 13.773 |
| *Didelphis virginiana* | 5.399, 3.926 | 23.015, 18.821, 16.320 |
| *Dromiciops australis* | 4.947, 3.543 | 11.028, 12.537, 9.000 |
| *Monodelphis domestica*[a] | 2.417, 3.367 | 10.466, 13.056, 8.090 |
| *Monodelphis domestica*[b] | 2.191, 3.021 | 10.283, 12.709, 7.657 |
| *Monodelphis domestica*[c] | 2.752, 3.068 | 9.490, 13.091, 8.130 |
| *Phascolarctos cinereus* | 7.208, 6.816 | 35.284, 34.275, 25.718 |
| *Vombatus ursinus* | 12.175, 8.317 | 46.087, 50.483, 33.905 |

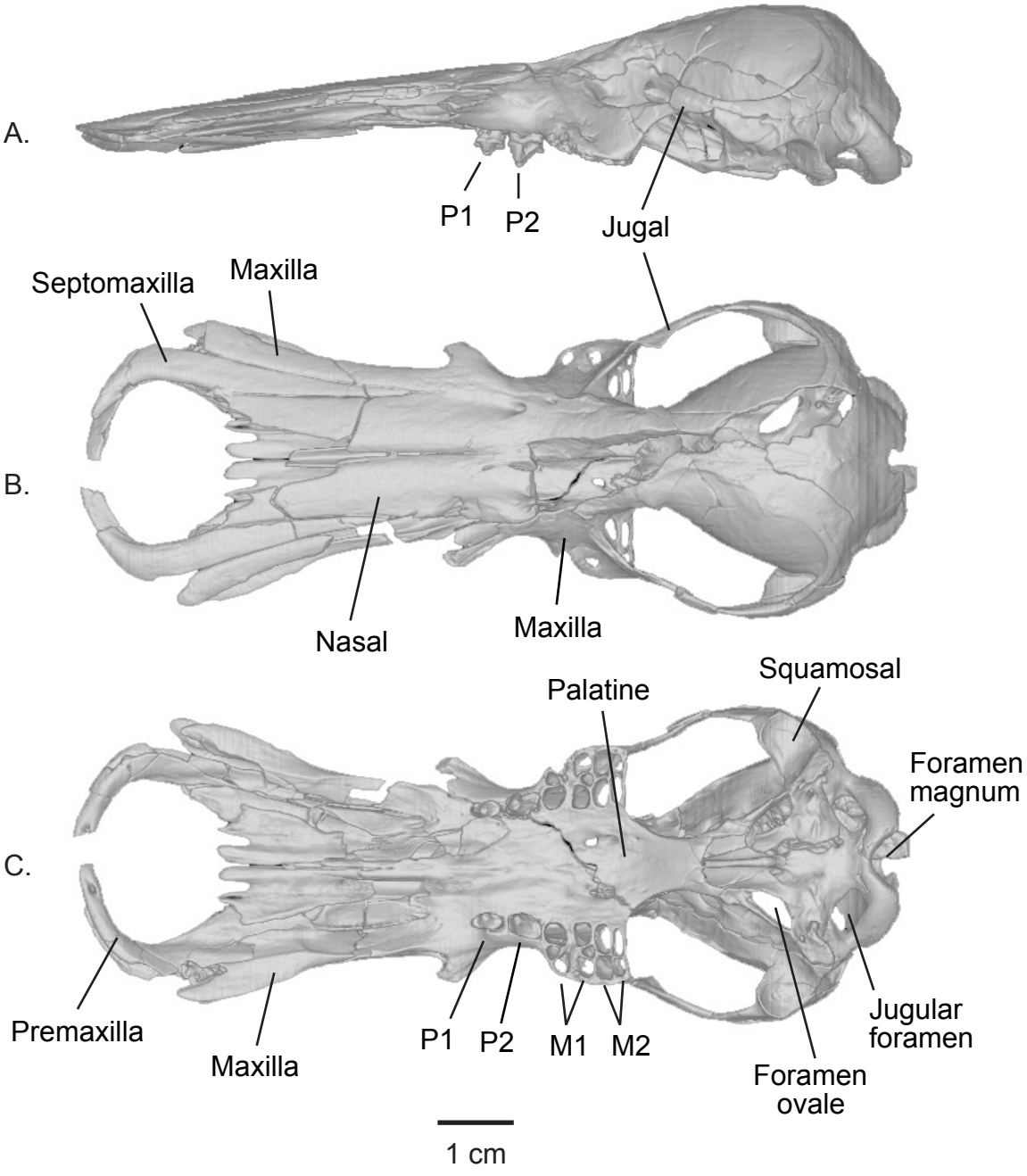


Figure 1. Digital rendering constructed from CT images of the acid prepared skull of *Obdurodon dicksoni* (QM F20568) shown in (A) left lateral, (B) dorsal, and (C) ventral views.

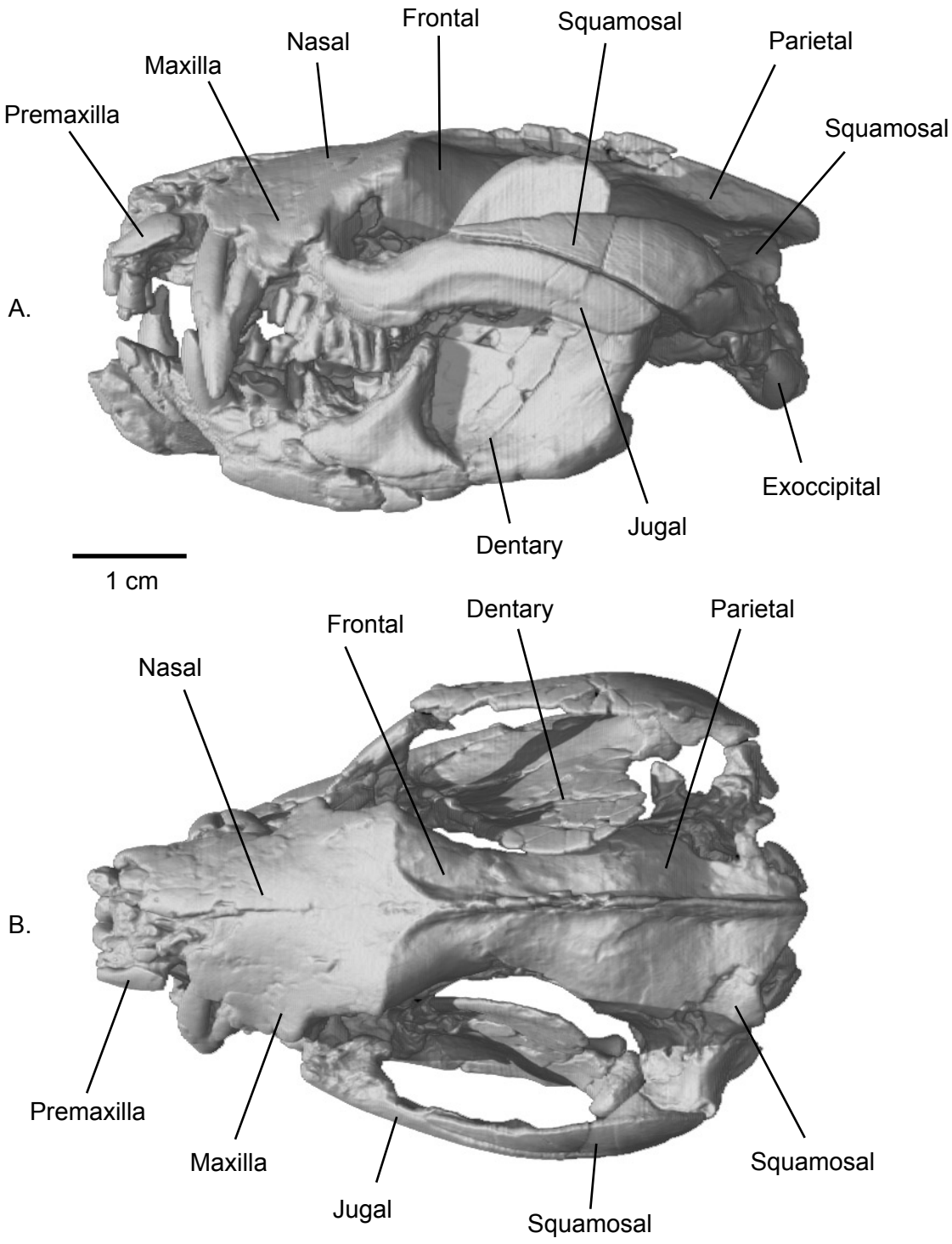


Figure 2. Digital rendering of the skull of *Vincelestes neuquenianus* (MACN-N 04) shown in (A) left lateral, and (B) dorsal views.

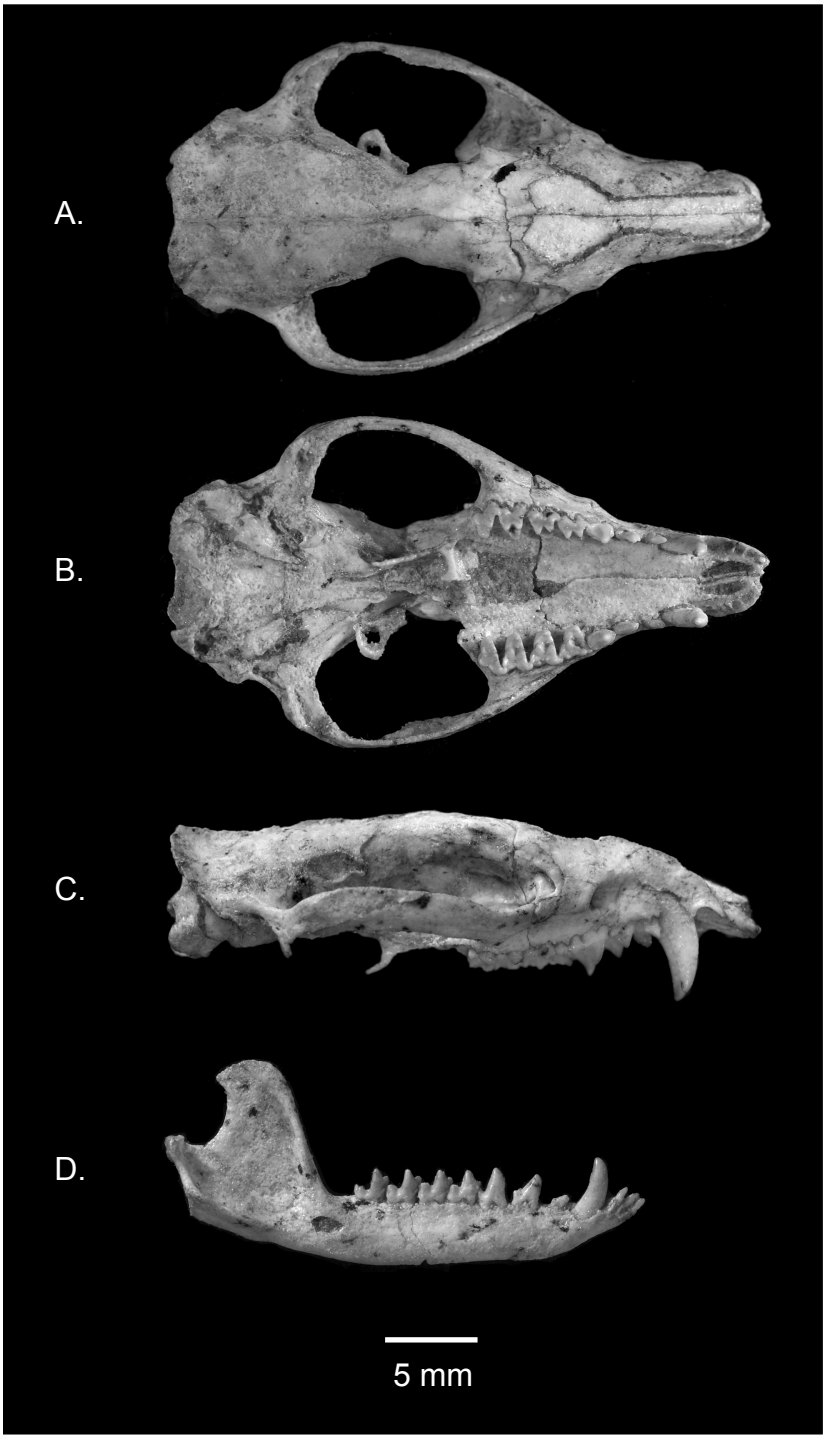


Figure 3. (A) Dorsal, (B) ventral, and (C) right lateral, views of a skull of *Pucadelphys andinus* (MHNC 8266). (D) Right lateral view of the mandible. Photographs courtesy of Christian de Muizon.

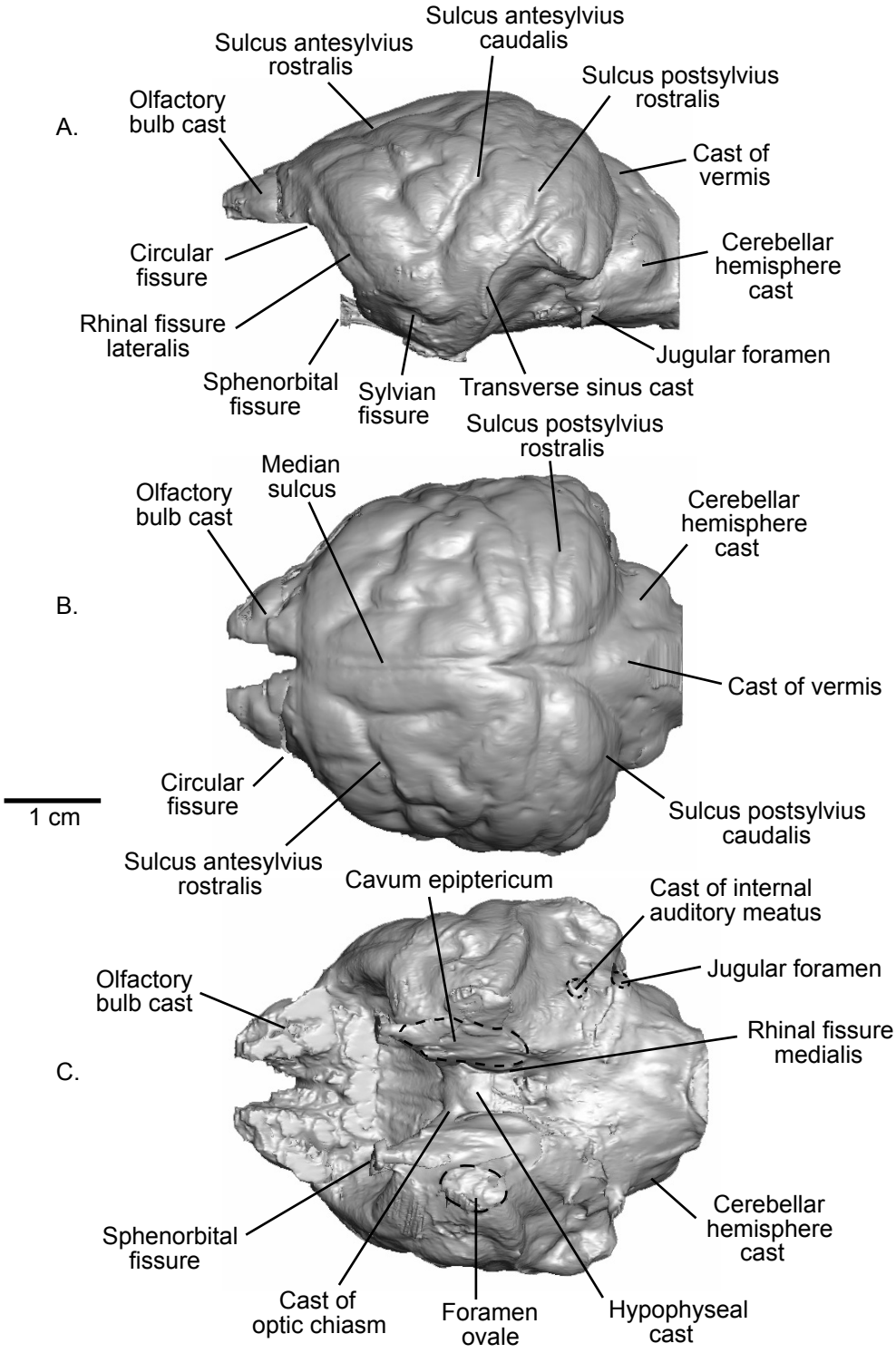


Figure 4. Digital rendering of the cranial endocast from a *Tachyglossus aculeatus* (AMNH 154457) shown in (A) left lateral, (B) dorsal, and (C) ventral views.

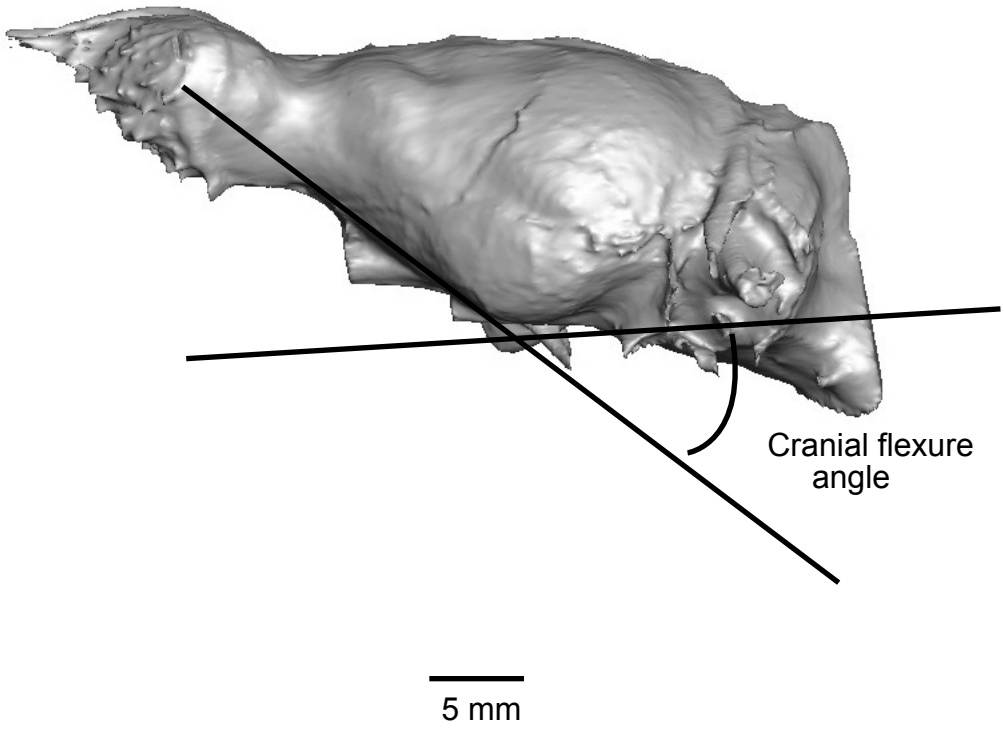


Figure 5. Digital endocast of *Didelphis virginiana*, the Virginia opossum, (TMM M-2517) shown in left lateral view and illustrating how cranial flexure was measured.

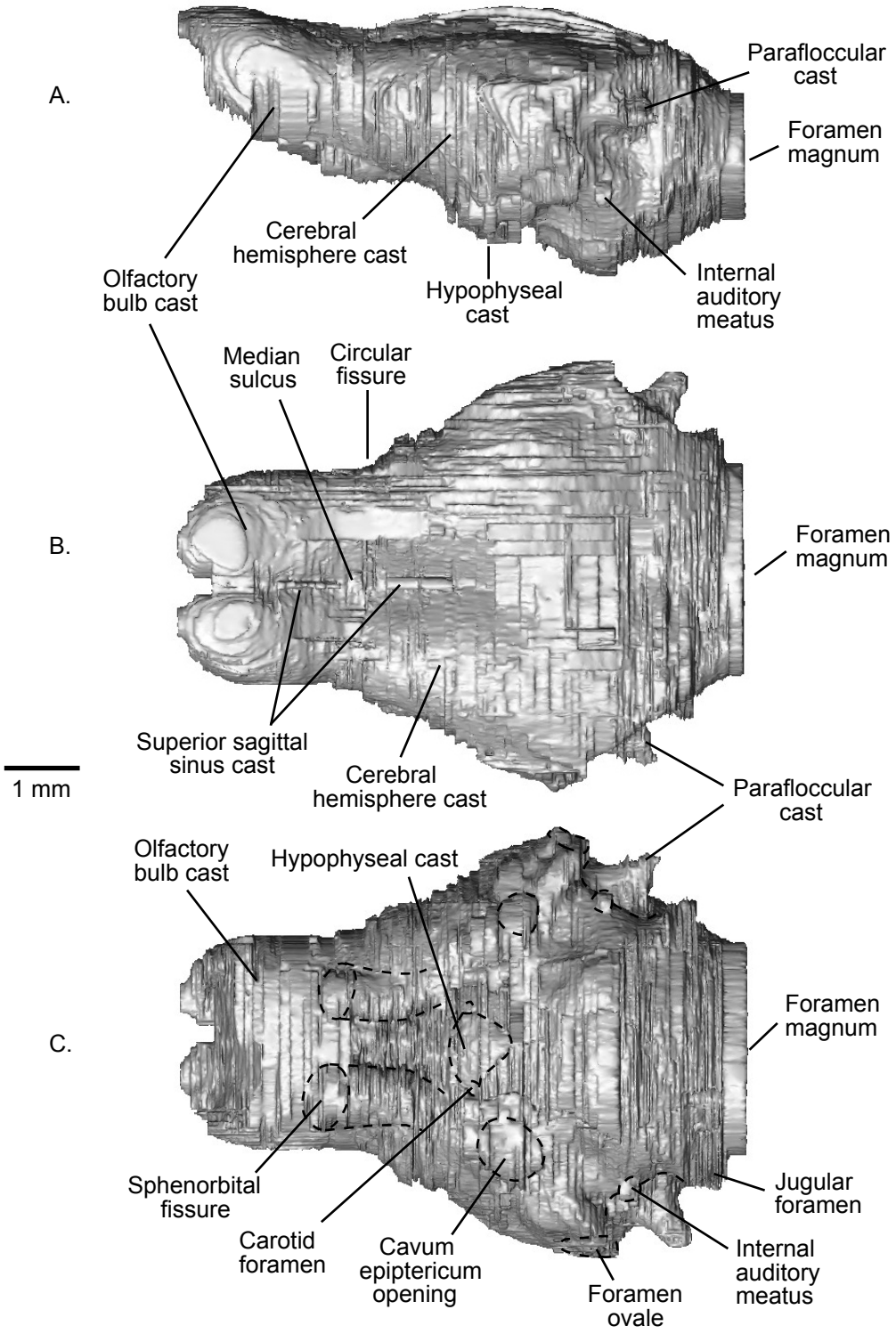


Figure 6. Digital rendering of the cranial endocast of *Hadrocodium wui* (IVPP 8275) shown in (A) left lateral, (B) dorsal, and (C) ventral views.

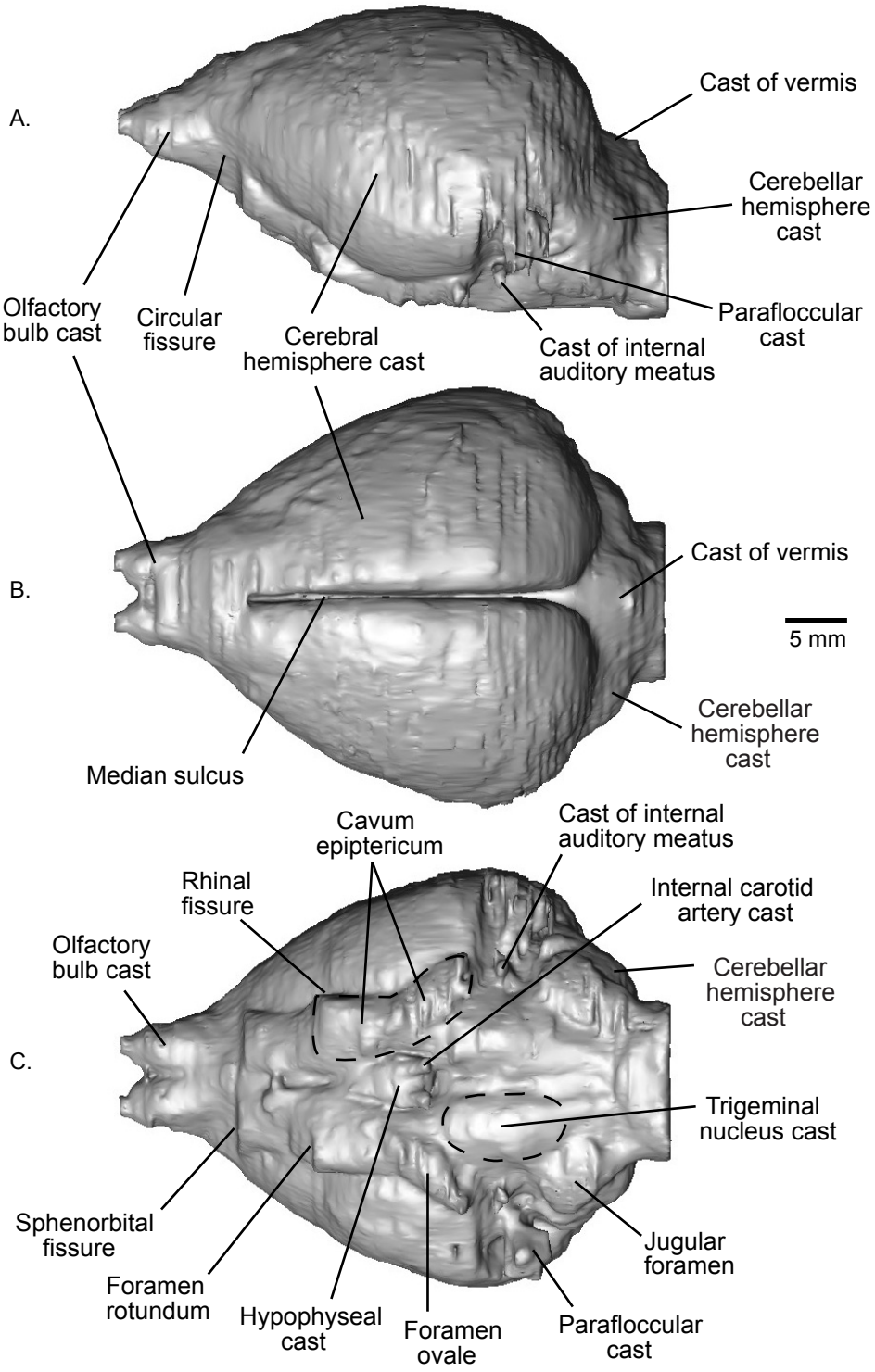


Figure 7. Digital rendering of the cranial endocast of *Obdurodon dicksoni* (QM F20568) shown in (A) left lateral, (B) dorsal, and (C) ventral views.

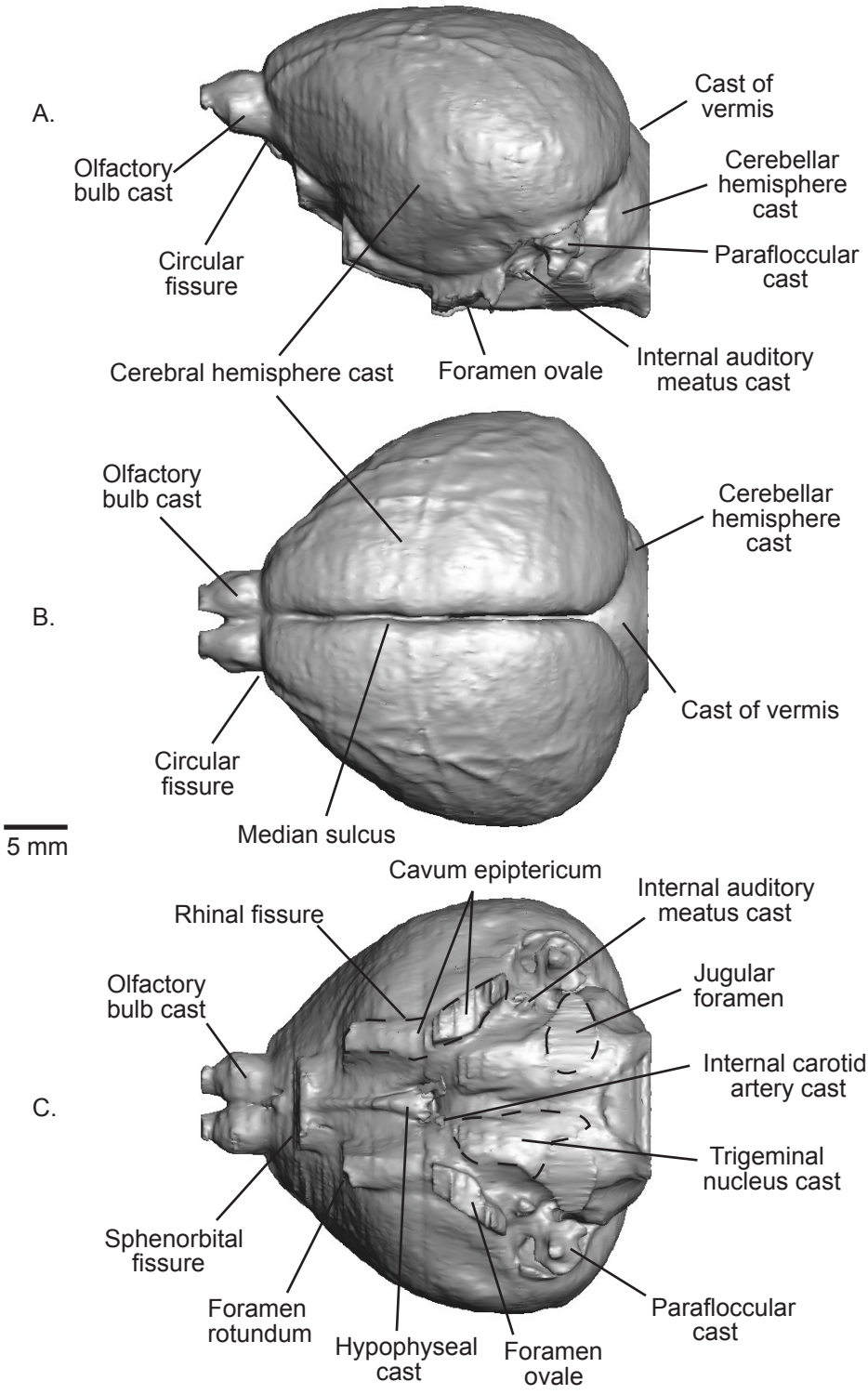


Figure 8. Digital rendering of the cranial endocast of an adult *Ornithorhynchus anatinus* (AMNH 200255) shown in (A) left lateral, (B) dorsal, and (C) ventral views.

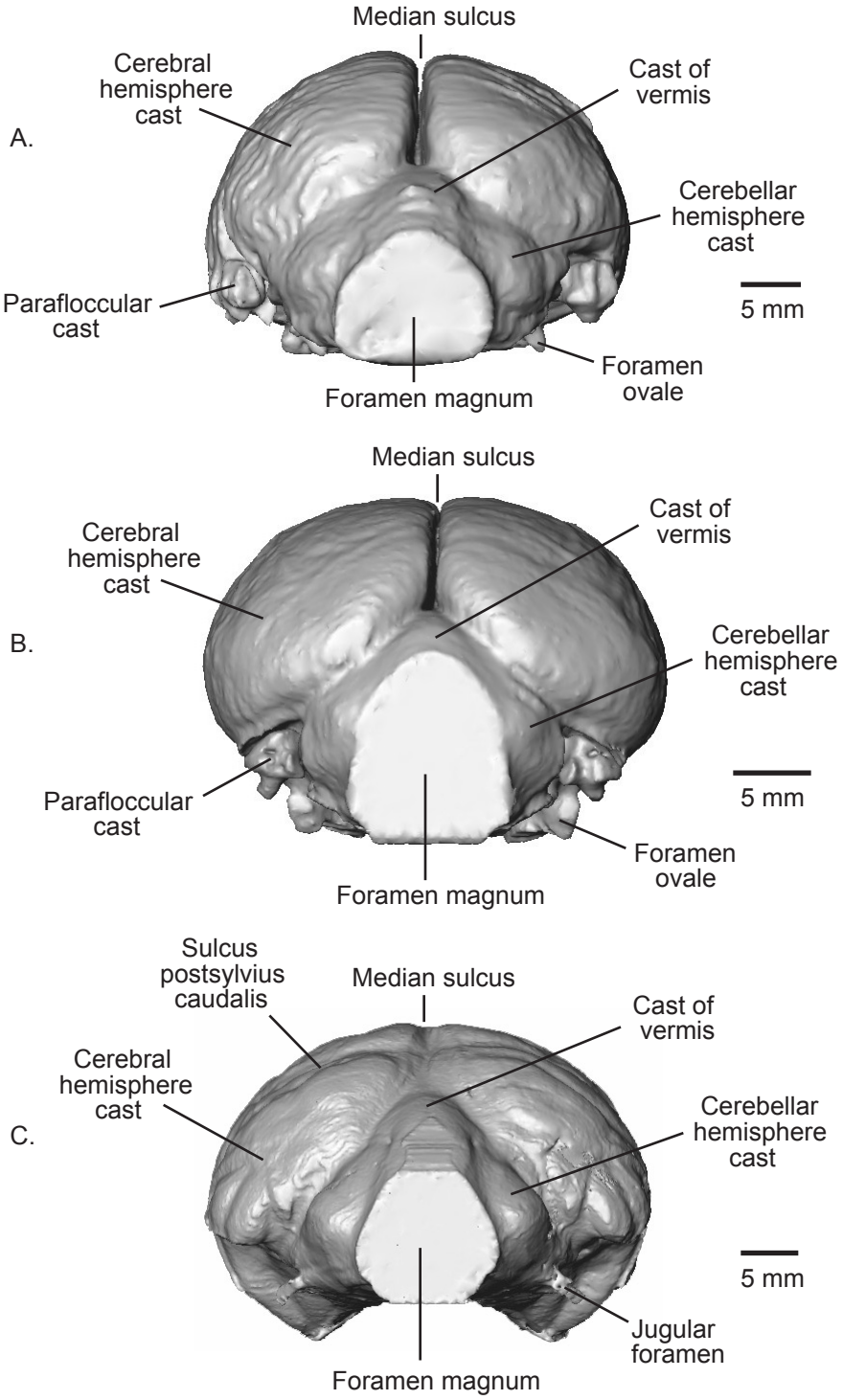


Figure 9. Digital renderings of posterior views of cranial endocasts: (A) *Obdurodon dicksoni* (QM F20568), (B) adult *Ornithorhynchus anatinus* (AMNH 200255), (C) *Tachyglossus aculeatus* (AMNH 154457). Note that scale is different for each image.

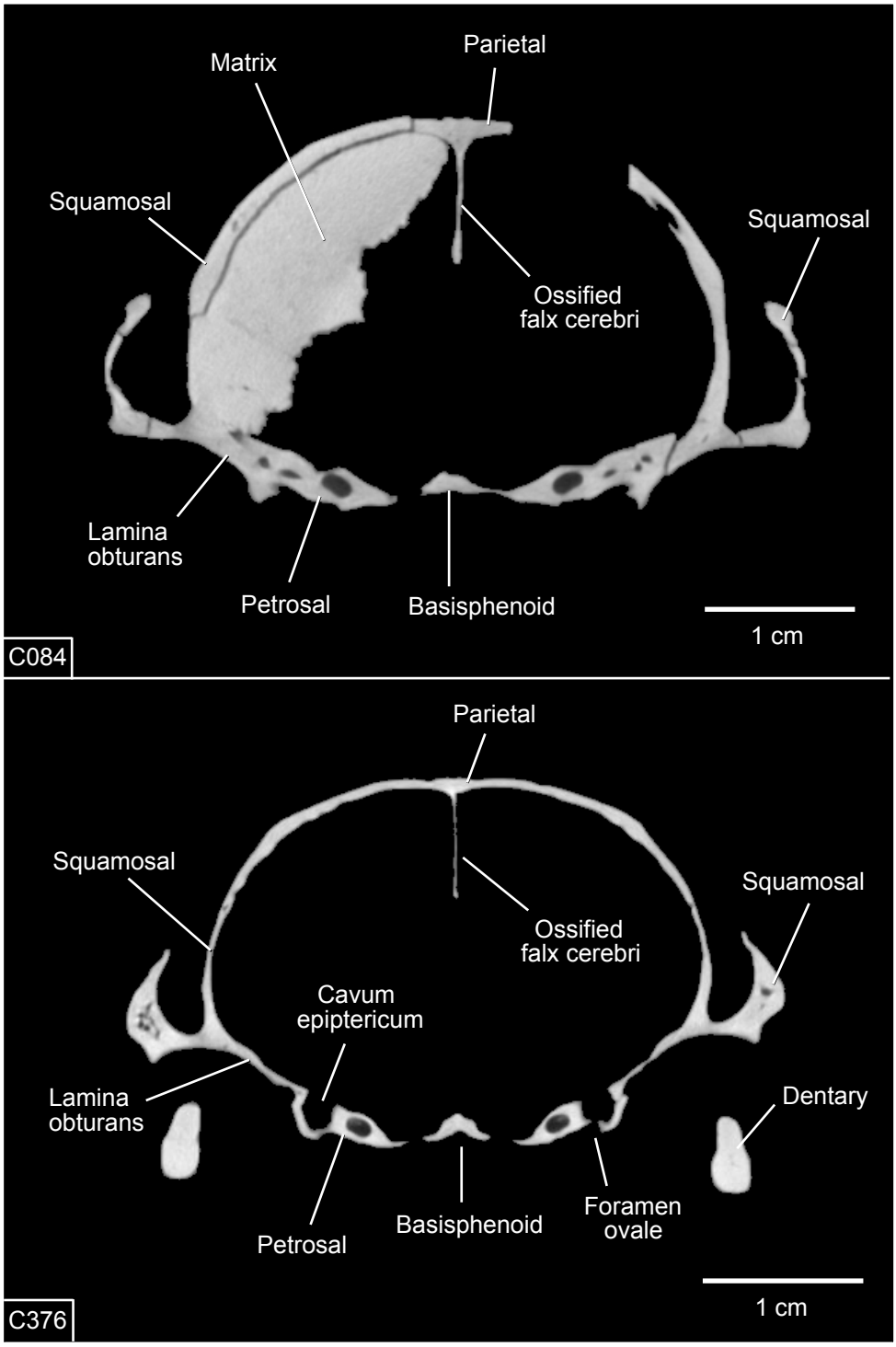


Figure 10. Coronal CT images through the skull of *Obdurodon dicksoni*, QM F20568 (top image) and an adult *Ornithorhynchus anatinus*, AMNH 200255 (bottom image) showing the ossified falx cerebri.

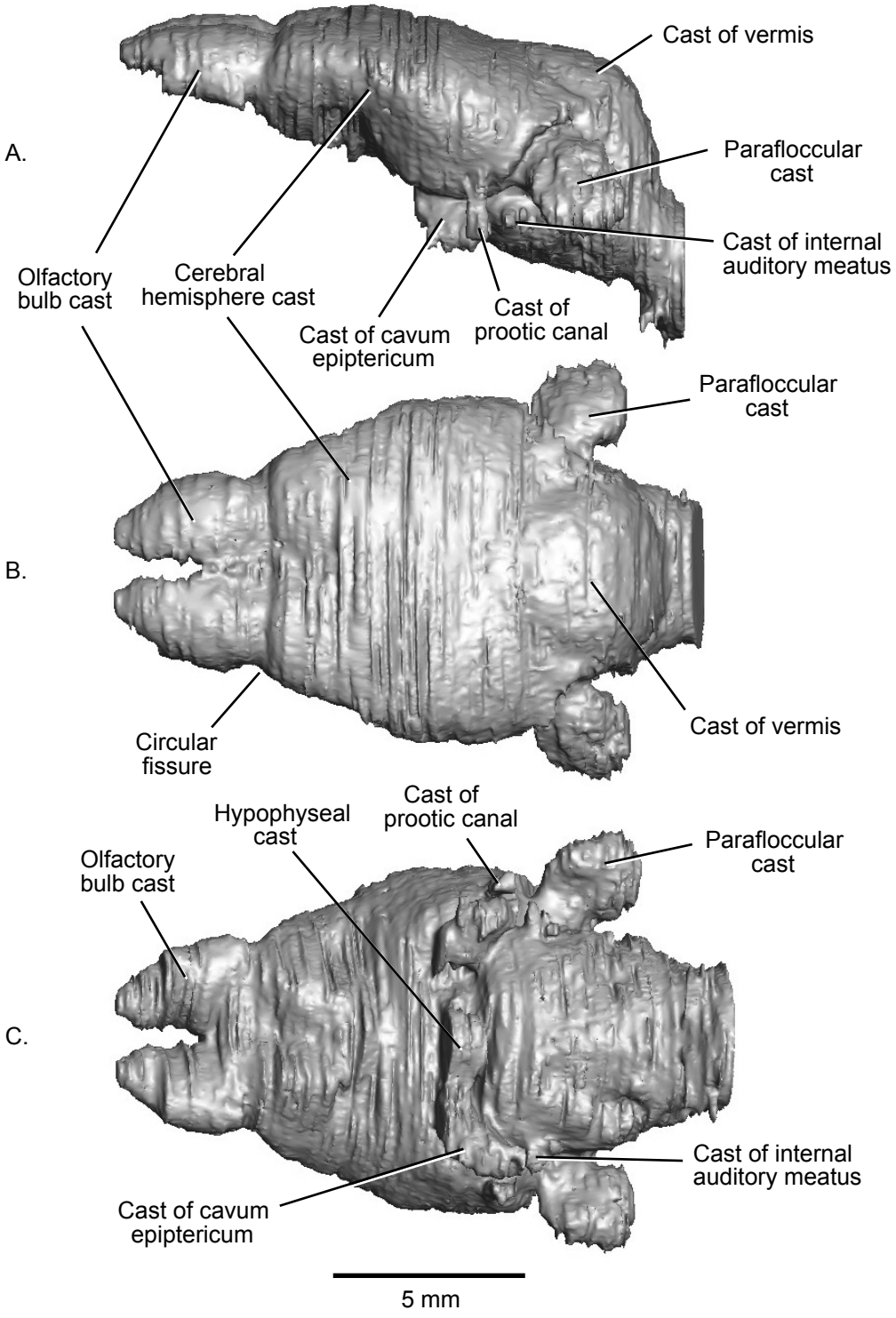


Figure 11. Digital rendering of the cranial endocast of *Kryptobaatar dashzevegi* (PSS-MAE 101) shown in (A) left lateral, (B) dorsal, and (C) ventral views.

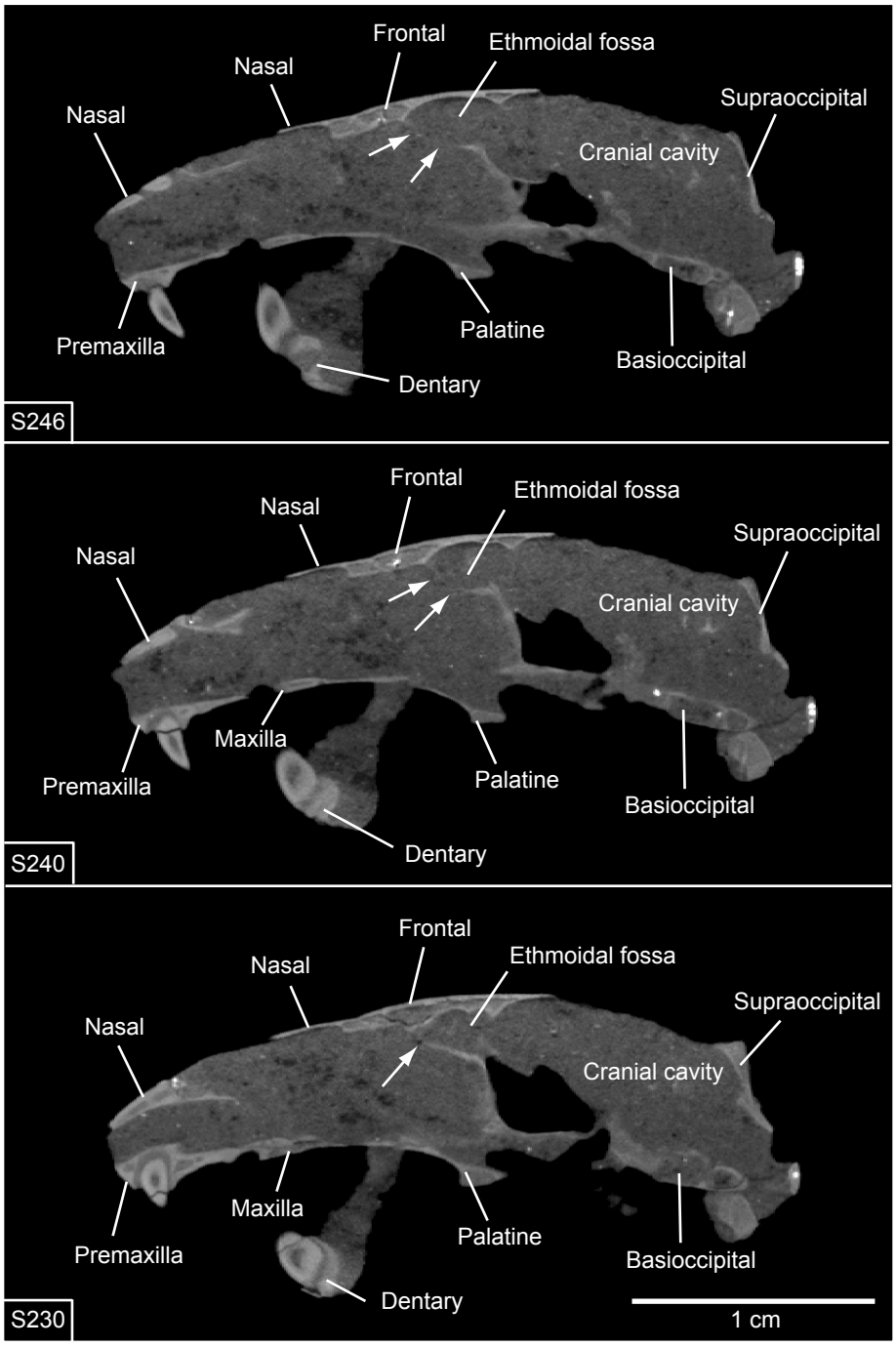


Figure 12. Three sagittal CT images of *Kryptobaatar dashzevegi* (PSS-MAE 101) taken through the right side of the skull and showing the cribriform plate (indicated by arrows). The top image is just to the right of the skull midline, the middle image is lateral to the first image, and the bottom image is lateralmost of the three.

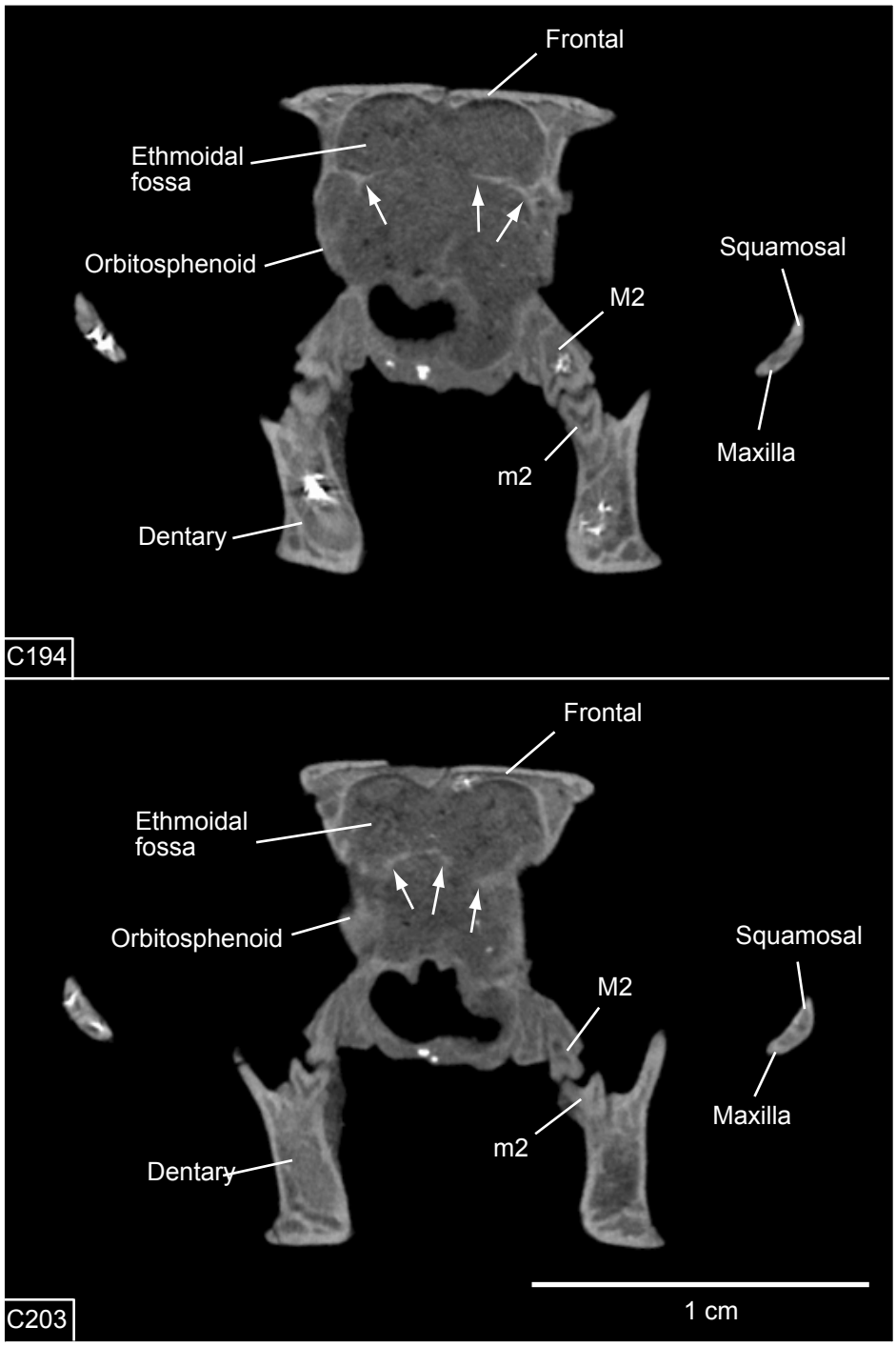


Figure 13. Two coronal CT images of *Kryptobaatar dashzevegi* (PSS-MAE 101) showing the cribriform plate (indicated by arrows). The top image is more anterior in the skull than the bottom one.

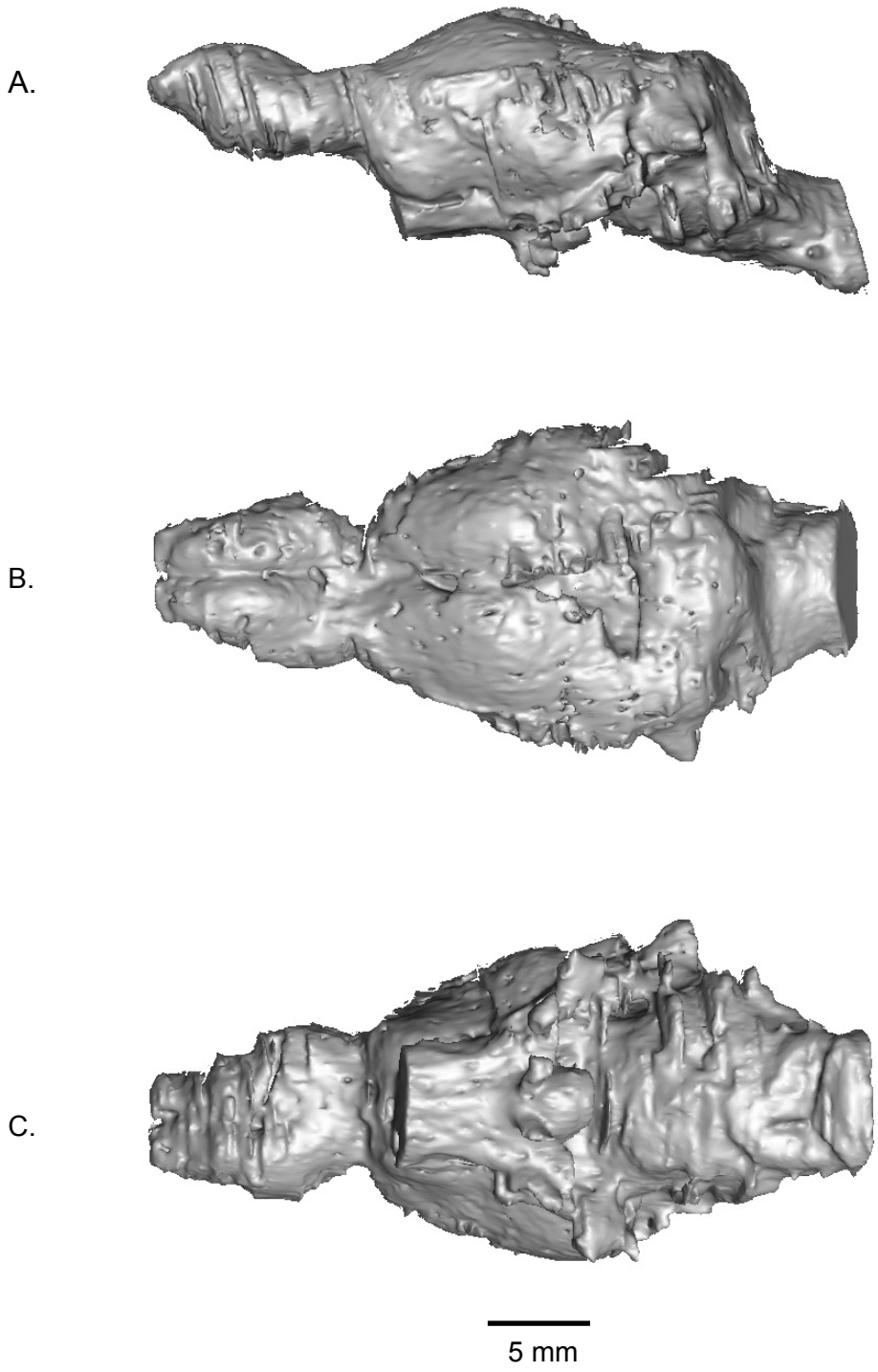


Figure 14. Digital rendering of the cranial endocast of *Vincelestes neuquenianus* (MACN-N 04) shown in (A) left lateral, (B) dorsal, and (C) ventral views. Anatomical structures are labeled on Figure 15.

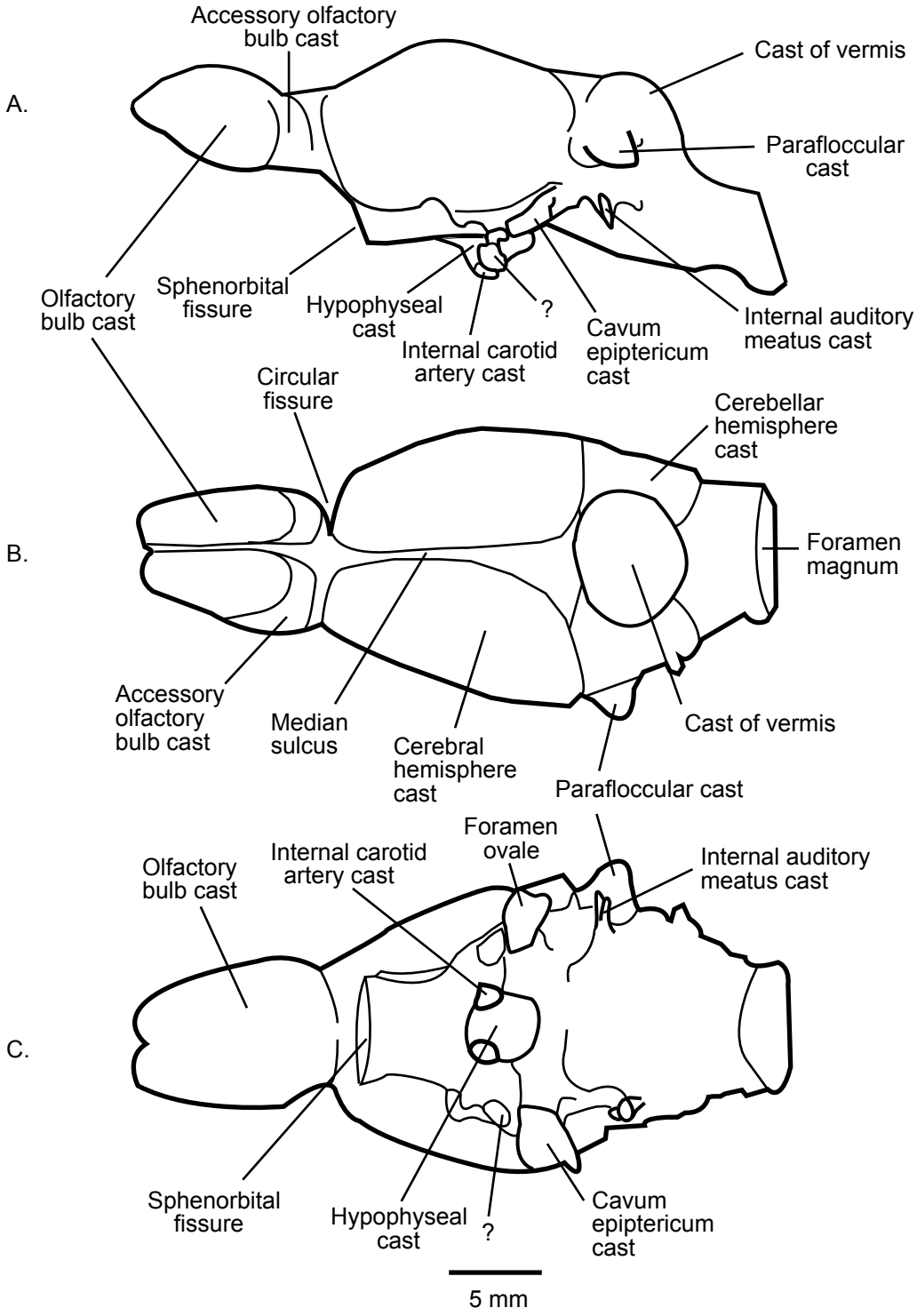


Figure 15. Line drawings of the cranial endocast of *Vincelestes neuquenianus* (MACN-N 04) shown in (A) left lateral, (B) dorsal, and (C) ventral views.

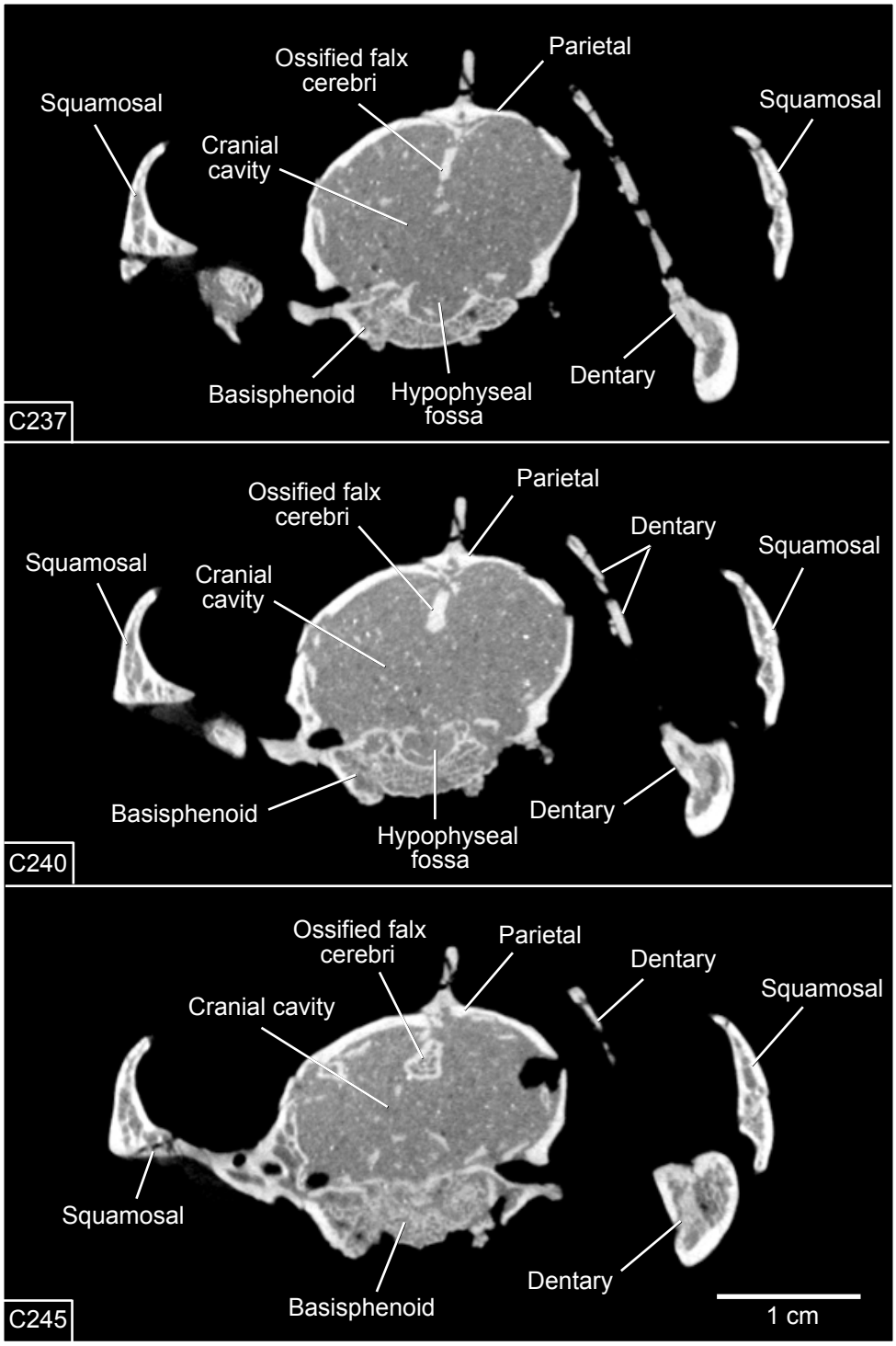


Figure 16. Coronal CT images through the braincase of *Vincelestes neuquenianus* (MACN-N 04) showing the ossified falx cerebri.

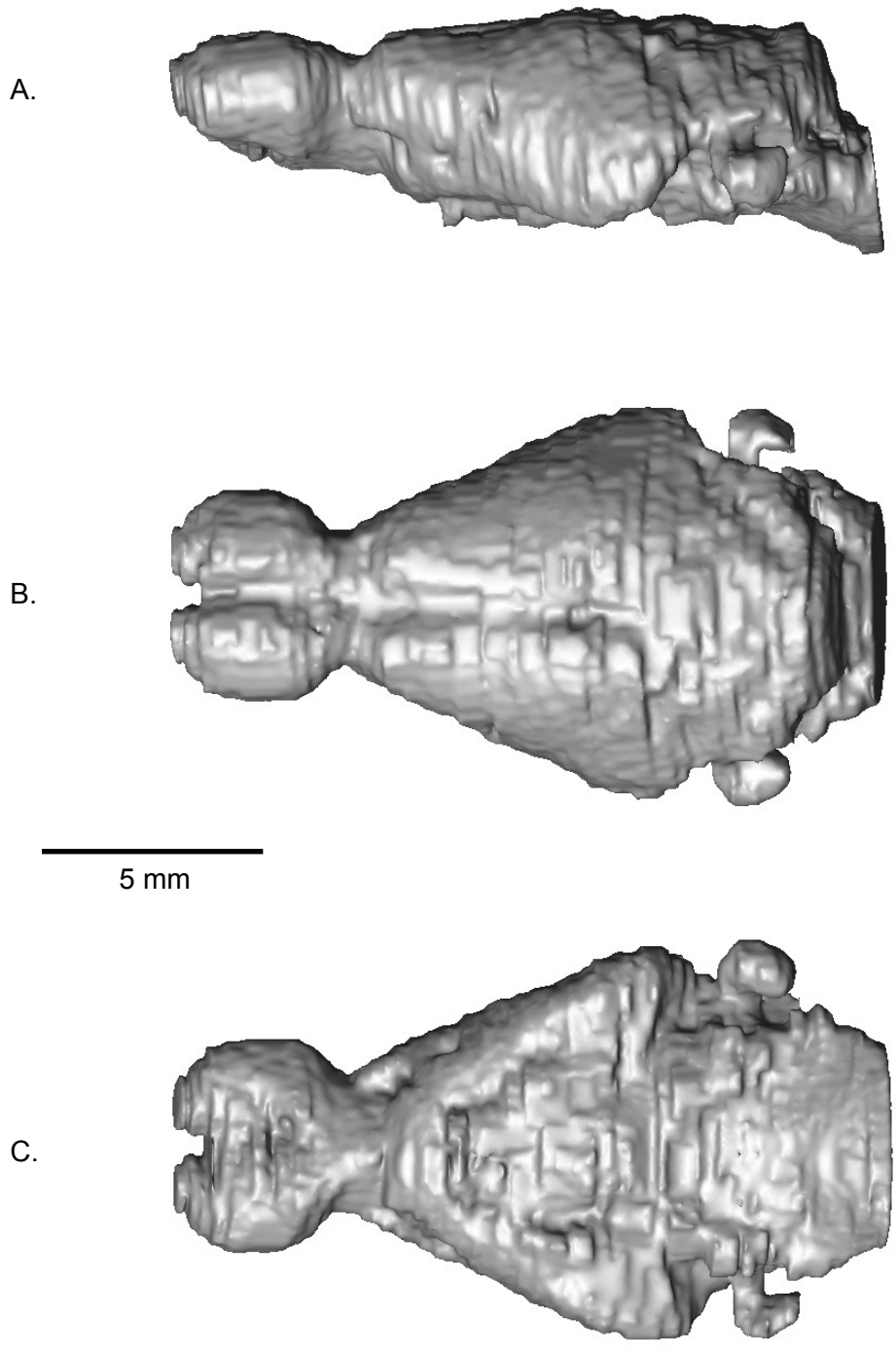


Figure 17. Digital rendering of the cranial endocast of *Pucadelphys andinus* (MHNC 8266) shown in (A) left lateral, (B) dorsal, and (C) ventral views. Anatomical structures are labeled on Figure 18.

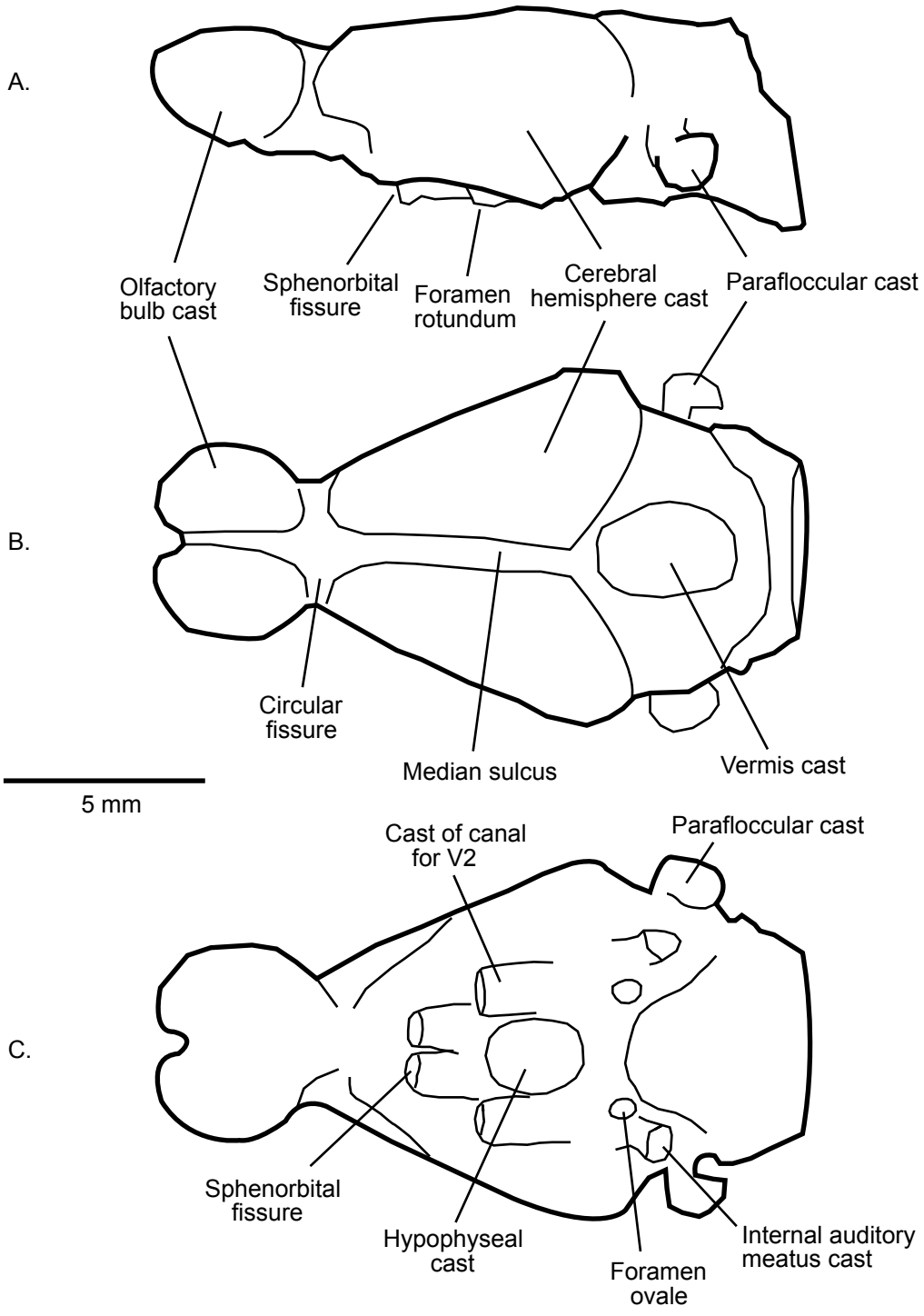


Figure 18. Line drawings of the cranial endocast of *Pucadelphys andinus* (MHNC 8266) with anatomical labels shown in (A) left lateral, (B) dorsal, and (C) ventral views.

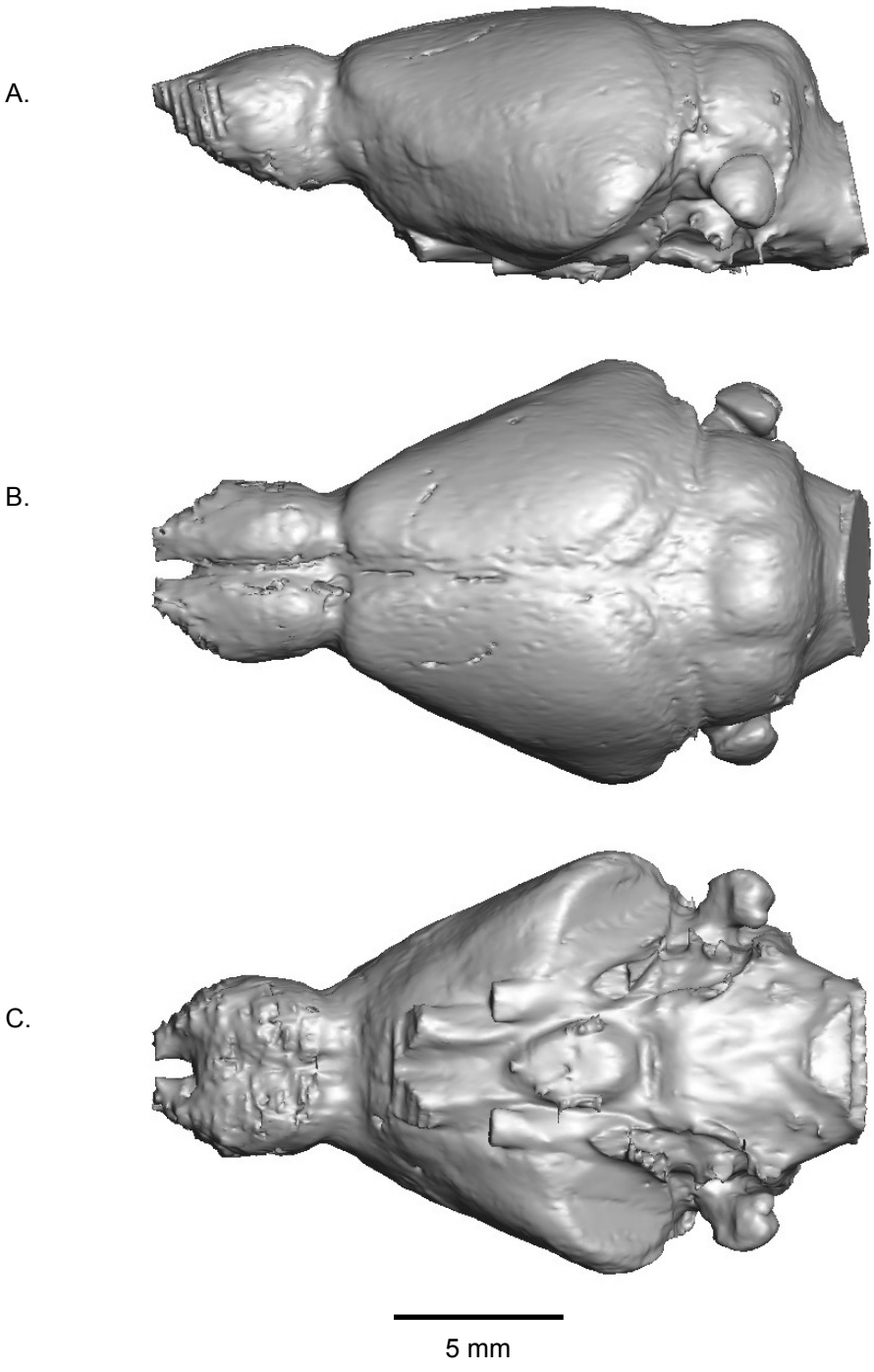


Figure 19. Digital rendering of a cranial endocast of *Monodelphis domestica* (TMM M-7599) shown for comparison in (A) left lateral, (B) dorsal, and (C) ventral views. Anatomical structures are labeled on Figure 20.

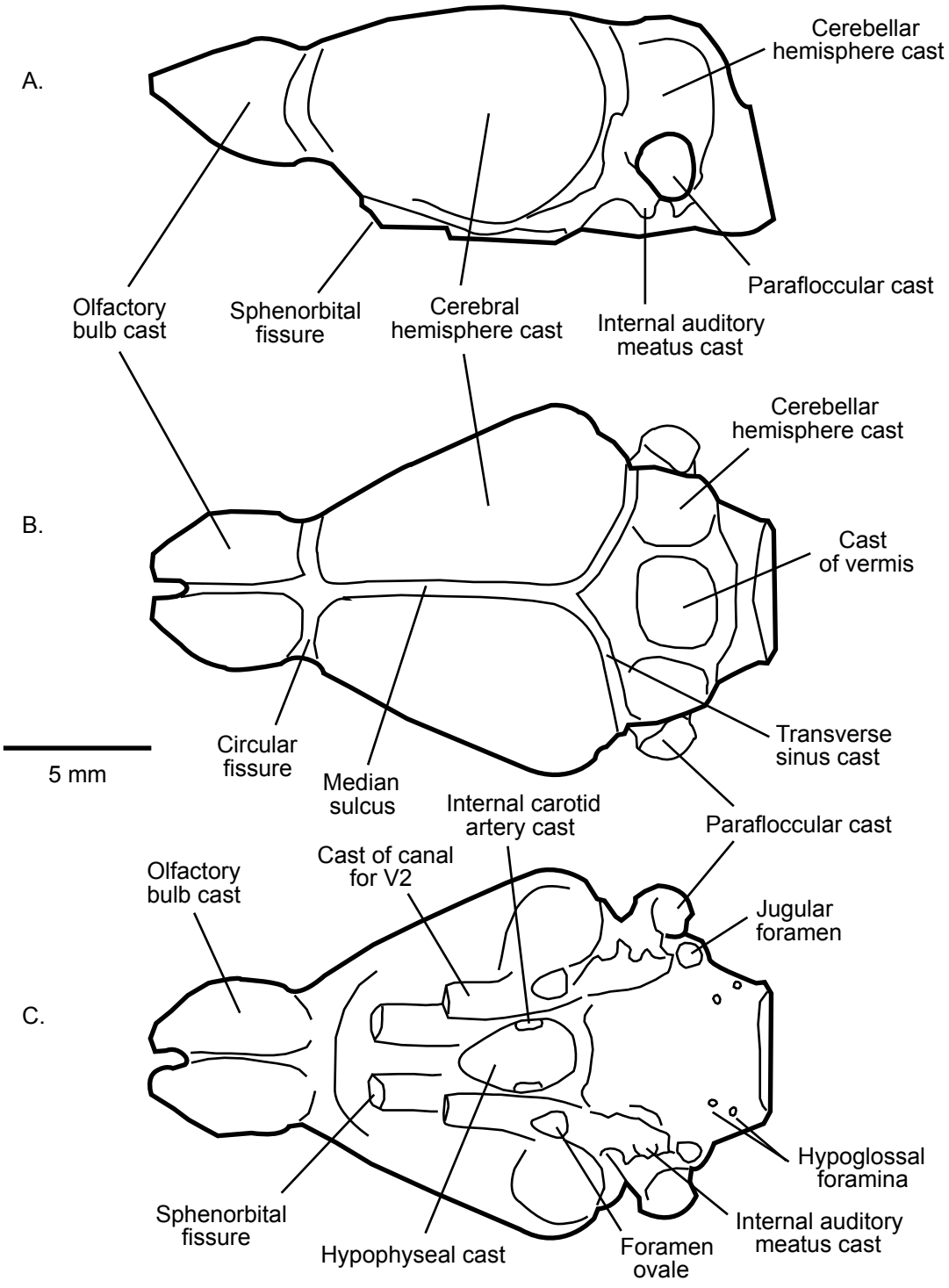


Figure 20. Line drawings of a cranial endocast of *Monodelphis domestica* (TMM M-7599) with anatomical labels in (A) left lateral, (B) dorsal, and (C) ventral views.

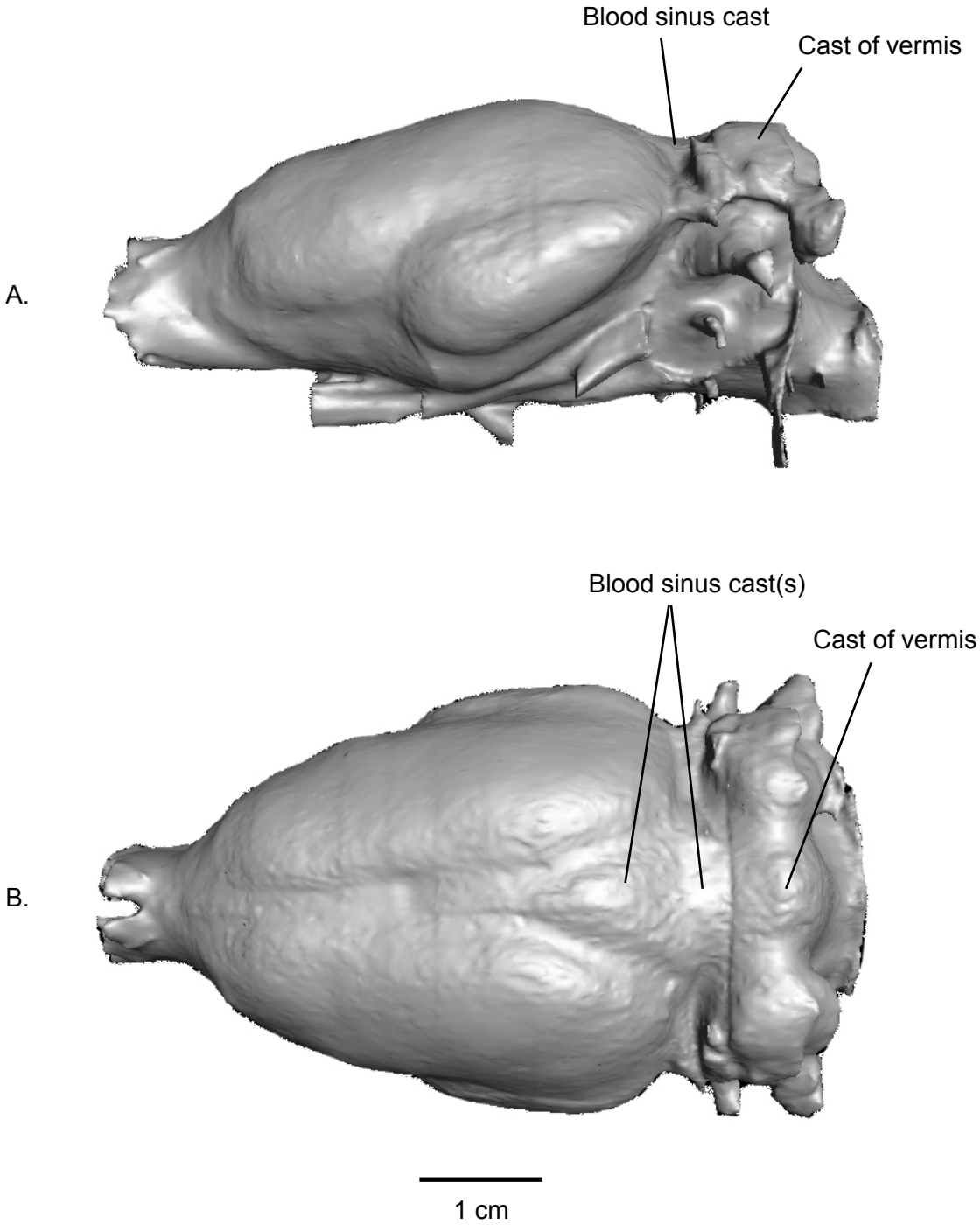


Figure 21. Digital rendering of the cranial endocast of *Phascolarctos cinereus* (TMM M-2946) shown in (A) left lateral, and (B) dorsal views.

# Chapter 3: Evolution of Cranial Endocast Characters

## INTRODUCTION

The cranial cavity houses many sensory structures including the brain, the organ in which sensory information and motor response are coordinated. Behavior is response to stimuli and thus cranial endocasts which serve as proxies of brains in fossil mammals can be used to interpret the evolution of some aspects of behavior in these animals. Relatively few studies have examined the evolution of the endocranial space in a phylogenetic context (e.g., Northcutt, 1984, 1985; Roth and Wullimann, 2001; Franzosa, 2004; Kielan-Jaworowska et al., 2004; Striedter, 2005). The primary goal of this chapter is to examine the evolution of endocast characters in the context of the evolutionary history of mammals and non-mammalian cynodonts.

A secondary goal of this study is to determine if inclusion of these characters into a sizeable, previously published phylogenetic matrix of skeletal and dental characters (Luo and Wible, 2005) has any bearing on the outcome on the phylogenetic analysis. The skull is the most important source of morphological data for diagnosing and determining relationships among different clades of mammals. However, most currently analyzed cranial characters come from external aspects of the skull, especially the dentition. For example, a recent analysis by Luo and Wible (2005) exploring the relationships of extinct and extant mammals and non-mammalian cynodonts included 422 morphological characters, of which 129 (31%) were dental characters, and 181 (43%)

characters dealt with the rest of the skull. Only 33 of the latter characters were based on internal features (24 from the petrosal, 7 from the endocranial cavity, and 2 from the nasal cavity).

The internal osteology and cavities of the skull serve to house and support many soft-tissue sensory structures (e.g., olfactory epithelium in the nasal cavity, and brain in the endocranial cavity) and are therefore morphologically complex. The anatomical complexity and taxonomic variation of the endocranial cavity has long been recognized as important for central nervous system comparisons among extinct and extant mammals (e.g., Edinger, 1948, 1975; Jerison, 1973; Radinsky, 1973b, 1977). Even so, morphological characters from the nervous system are rarely incorporated in phylogenetic analyses of mammals (but notable exceptions are: Johnson et al., 1982a, b, 1994; Kirsch, 1983; Kirsch and Johnson, 1983; Kirsch et al., 1983). Thus, the nervous system represents a large and virtually untapped potential source of new phylogenetic data.

## MATERIALS AND METHODS

### Distribution of endocast characters across phylogeny

This analysis incorporated 23 taxa including four non-mammalian cynodont species, nine extinct mammal species or clades, and 10 extant mammal species. These taxa were chosen to represent the major extant clades of Mammalia (Monotremata, Marsupialia, Placentalia) as well as some of the important fossil clades (e.g.,

Triconodontidae, Multituberculata). Based on previous phylogenetic analyses, I sampled basally-diverging taxa within these major mammalian clades. The addition of new fossil endocast material described in Chapter 2 provides data points along the branches connecting these major mammalian clades.

Digital cranial endocasts were extracted from 18 skulls representing 17 of these taxa. These skulls were scanned at UTCT and endocasts were extracted following the procedures outlined in Chapter 2. Cranial endocast data for the remaining six taxa were taken from the papers describing natural endocast material. These include *Probainognathus* sp. (Quiroga, 1980a, b; CT slices of PVSJ 410 [Museo de Ciencias Naturales, Universidad de San Juan, Argentina]), Triconodontidae (Simpson, 1927; Kermack, 1963), *Leptictis dakotensis* (Novacek, 1982, 1986), *Zalambdalestes lechei* (Kielan-Jaworowska, 1984, 1986), *Kennalestes gobiensis* (Kielan-Jaworowska, 1984, 1986), and *Asioryctes nemegetensis* (Kielan-Jaworowska, 1984). Digital cranial endocasts were also extracted from 19 other specimens representing six additional taxa (*Manis tricuspis*, *Monodelphis domestica*, *Orycteropus afer*, *Procavia capensis*, *Trichechus senegalensis*, *Zaglossus bruijni*) but these taxa were not included in this analysis for reasons explained below.

These endocast data were used to score a matrix of 39 morphological characters. These characters comprise both quantitative and qualitative data. Ratio data were converted into discrete characters. The remaining quantitative data were treated as both continuous and discrete characters (6.1, 6.2, 10.1, 10.2, 19.1, 19.2, 31.1, 31.2, 36.1, 36.2). For example, character 6 is the angle of cranial flexure. The continuous version of this character (6.1) places the angle data in bins of 5% and weights gaps between data points

(e.g., segment coding; Thiele, 1993). Letters (e.g., A, B, C, etc.) were used to designate character states when greater than 10 states were required to describe the range of variation (e.g., character 6.1). The discrete version of character 6 (6.2) has two character states: endocranial flexure greater than 38° (0), or 38° or less (1). Thirty-eight degrees is the mean value for endocranial flexure for the data examined here.

The distribution of the 39 endocast characters was examined on a pruned version of the strict consensus tree published by Luo and Wible (2005). The taxa in the Luo and Wible (2005) matrix for which endocast material is unavailable were pruned from the tree. *Thrinaxodon liorhinus* was designated as an outgroup and *Diademodon* sp., which is not in the Luo and Wible (2005) matrix, was added as a second outgroup for this analysis. Following the Luo and Wible (2005) analysis, *Kennalestes*, *Asioryctes*, *Zalambdalestes*, and *Leptictis* are non-placental eutherians but *Felis silvestris catus*, *Canis lupus*, and *Dasypus novemcinctus* are crown placentals. *Pucadelphys andinus* lies outside of crown Marsupialia but along its stem according to the Luo and Wible (2005) analysis. The distribution of the 39 characters was examined in the program MacClade using the DELTRAN optimization. For characters that were treated as both continuous and discrete (e.g., characters 6, 10, 19, 31, 36), both the discrete and continuous versions were optimized separately on the Luo and Wible tree.

I chose the Luo and Wible (2005) tree because it includes significant taxonomic sampling of both extinct and extant mammals and non-mammalian cynodonts. Several other independent phylogenetic analyses of non-mammalian cynodonts (Kemp, 1982, 1983, 1988; Hopson and Barghusen, 1986; Gauthier et al., 1988; Rowe, 1988, 1993; Hopson, 1991; Wible, 1991, Luo, 1994; Martinez et al., 1996; Sidor and Hopson, 1998;

Hopson and Kitching, 2001) and basal mammals were published over the past 19 years (Novacek et al., 1988; Novacek, 1992; Hopson and Rougier, 1993; Wible et al., 1995; Rougier et al., 1996a, b, 1998; Hu et al., 1997; Ji et al., 1999; Luo et al., 2001a, b; Wang et al., 2001; Luo et al., 2002). These studies examined overlapping but different segments of the cynodont lineage using a variety of data (e.g., dental, cranial osteology, and postcranial osteology), but none of these possess as large a sample of extinct and extant taxa as the Luo and Wible (2005) matrix. An even more complete matrix of extinct and extant mammals is warranted for future phylogenetic analyses. A preliminary attempt to address this problem revealed that such work is beyond the scope and goals of this dissertation. When more inclusive phylogenies are available, then endocast data from other taxa collected in this dissertation can be included.

**Phylogenetic analyses incorporating endocast characters**

Three sets of phylogenetic analyses incorporating the endocast character matrix were conducted in PAUP 4.0b (Swofford, 1998). The first set of analyses included the endocast character matrix only (Appendix 5). All of the taxa in the matrix were incorporated in the analysis, including *Manis*, *Monodelphis*, *Orycteropus*, *Procavia*, *Trichechus*, and *Zaglossus*. The quantitative characters were all treated as discrete (e.g., characters 6.2, 10.2, 19.2, 31.2, 36.2). All characters were initially analyzed as unordered; however, in a subsequent round of analyses, continuous characters were ordered (#2, 3, 4, 9, 32, 33). *Thrinaxodon* and *Diademodon* were designated as the outgroups. A heuristic parsimony search was conducted with 1000 addition sequence

replicates and using the tree-bisection-connection (TBR) branch-swapping algorithm. The starting tree was obtained via stepwise addition using a random addition sequence. The endocast matrix was also analyzed using the same parameters but with the monophyly of Mammalia, Eutheria, and Metatheria constrained. A second analysis of the endocast matrix excluded the taxa not present in the Luo and Wible (2005) matrix. This subset of the endocast matrix was analyzed using the same parameters described above.

The second set of phylogenetic analyses combined the Luo and Wible (2005) published character matrix with my endocast matrix. The endocast data for the *Diademodon*, Triconodontidae, *Manis*, *Monodelphis*, *Orycteropus*, *Procavia*, *Trichechus*, and *Zaglossus* were excluded from the analysis because these taxa were not included in the original Luo and Wible matrix. *Kryptobaatar dashzevegi* is a cimolodontan multituberculate, and therefore the *Kryptobaatar* endocast data were incorporated with the cimolodontan data of the Luo and Wible matrix. Character redundancies were removed such that the resulting combined matrix contained 96 taxa and 456 characters of which 448 are parsimony-informative. I used data from my matrix in cases of conflict between my matrix and the Luo and Wible (2005) matrix. The quantitative characters were all treated as discrete (e.g., characters 6.2, 10.2, 19.2, 31.2, 36.2). All characters were initially analyzed as unordered; however, in a subsequent round of analyses, continuous characters were ordered (#32, 76, 78, 79, 80, 91, 97, 99, 104, 135, 136, 145, 146, 147, 148, 149, 150, 184, 200, 212, 359, 381, 409 from the Luo and Wible [2005] matrix, and #2, 3, 4, 9, 32, 33 from my endocast matrix). *Thrinaxodon* was designated as the outgroup. A heuristic parsimony search was conducted with 100 addition sequence

replicates and using the TBR branch-swapping algorithm. The starting tree was obtained via stepwise addition using a random addition sequence.

The third set of phylogenetic analyses combined the Luo and Wible (2005) published character matrix with my endocast matrix, but the taxa not common to both matrices were cropped prior to the analysis. Similar to the previously discussed analyses, the *Kryptobaatar* endocast data were incorporated with the cimolodontan data of the Luo and Wible matrix. Character redundancies were removed such that the resulting combined matrix contained 21 taxa and 456 characters of which 448 are parsimony-informative. I used data from my matrix in cases of conflict between my matrix and the Luo and Wible (2005) matrix. The quantitative characters were all treated as discrete (e.g., characters 6.2, 10.2, 19.2, 31.2, 36.2). All characters were initially analyzed as unordered; however, in a subsequent round of analyses, continuous characters were ordered (#32, 76, 78, 79, 80, 91, 97, 99, 104, 135, 136, 145, 146, 147, 148, 149, 150, 184, 200, 212, 359, 381, 409 from the Luo and Wible [2005] matrix, and #2, 3, 4, 9, 32, 33 from my endocast matrix). *Thrinaxodon* was designated as the outgroup. A heuristic parsimony search was conducted with 1000 addition sequence replicates and using the TBR branch-swapping algorithm. The starting tree was obtained via stepwise addition using a random addition sequence. The pruned Luo and Wible (2005) matrix of 21 taxa was analyzed again using the same parameters but without the inclusion of my endocast matrix. This allows comparison of the effects of inclusion of the endocast characters with the pruned Luo and Wible (2005) matrix.

## CHARACTER LIST AND CHARACTER STATE DISTRIBUTIONS

Below is a description of the 39 endocast characters; distributions of the character states on the pruned version of the Luo and Wible (2005) consensus tree are discussed. The entire endocast character matrix is presented in Appendix 5. Some of these characters are uninformative for this particular sample of taxa when optimized on the Luo and Wible tree. Nonetheless, these characters are documented here because they might be informative for future analyses incorporating a more inclusive sample of taxa.

**Character 1**: Relative expansion of the braincase: braincase is narrow in the parietal region (0); cerebral cast expanded (the parietal part of the cranial vault is wider than the frontal part, but does not extend to lambdoidal region) (1); or greatly expanded (cerebellar cast is transversely expanded as much as cerebral cast) (2). This character is modified from Luo and Wible (2005, character 414). *Thrinaxodon* (Figure 22), *Diademodon* (Figure 23), and *Probainognathus* exhibit character state (0). Therefore presence of lateral expansion of the braincase in the parietal region (state 1) is a synapomorphy for the clade including *Hadrocodium* (Figure 6, Chapter 2) and Mammalia. Within some members of each of the major extant clades of crown Mammalia (Monotremata, Marsupialia, Placentalia), the braincase shows lateral expansion back to the lambdoidal crest (state 2) (e.g., *Ornithorhynchus*, Figures 8, 9, Chapter 2). The optimization of character 1 on the pruned version of the strict consensus tree of Luo and Wible (2005) is illustrated in Figure 24. Expansion of the braincase in Mammalia results from expansion of the cerebral hemispheres and, in particular, the isocortex.

**Character 2**: Maximum width vs. anteroposterior length aspect ratio of entire endocast: endocast longer than wide (aspect ratio < 0.9) (0); endocast length and width about equal (aspect ratio = 0.9-1.1) (1); or endocast wider than long (aspect ratio > 1.1) (2). The character is uninformative for the taxa examined here; only *Ornithorhynchus* and *Zaglossus* exhibit character state (1) but all of the other taxa show character state (0).

**Character 3**: Maximum height vs. anteroposterior length aspect ratio of entire endocast: endocast longer than tall (aspect ratio < 0.9) (0); endocast length and height about equal (aspect ratio = 0.9-1.1) (1); or endocast taller than long (aspect ratio > 1.1) (2). This character is uninformative for the taxa examined on the Luo and Wible (2005) tree; all exhibit character state (0).

**Character 4**: Maximum height vs. maximum width aspect ratio of entire endocast: endocast width and height about equal (aspect ratio = 0.9-1.1) (0); endocast taller than wide (aspect ratio > 1.1) (1); or endocast wider than tall (aspect ratio < 0.9) (2). *Thrinaxodon* exhibits state (0) and *Diademodon* exhibits character state (1) while presence of an endocast that is wider than tall is a synapomorphy for the clade that includes *Probainognathus*, *Hadrocodium*, and Mammalia. The large height/width aspect ratio in *Thrinaxodon* and *Diademodon* is explained by the presence of a prominent parietal tube associated with the parietal foramen on the endocast. Loss of a parietal foramen and the associated tall parietal tube is a synapomorphy for the clade including *Probainognathus*, *Hadrocodium*, and Mammalia. This explains why many of the taxa in this clade have a relatively short endocast, compared to maximum width (state 2). In this regard, character 4 shows some correlation with character 30 (presence or absence of parietal tube and foramen on the endocast). However, the distribution of taxa without a

parietal tube and foramen (character 30, state 1) is not identical to the distribution of taxa with state 2 for character 4. *Dasypus* and *Didelphis* show character state (1) indicating a reversal from state (2). *Vombatus*, *Canis*, and *Felis* show character state (0), also a reversal. These reversals from state 2 cannot be easily explained. The optimization of character 4 is illustrated in Figure 25.

**Character 5**: Cranial sutures: not visible on endocast of adult (0); or visible on endocast of adult (1). This character is uninformative for the taxa examined on the Luo and Wible (2005) tree; only *Felis*, *Dasypus*, *Dasyurus*, and *Didelphis* (Figure 26) show cranial sutures on the adult endocast. However, *Orycteropus* and *Trichechus* also have sutures on the adult endocast. Perhaps the distribution of this character is a reflection of ossification or calcification of the outer portion of the dura mater of the meninges. Cranial sutures would not be visible on endocasts if the outer layer of the meninges is ossified or calcified. Ossification or calcification of portions of the meninges occurs in some cetaceans (e.g., *Tursiops truncatus*, the bottlenose dolphin, Colbert et al., 2005) and occasionally in humans, most commonly among the elderly (Cheon et al., 2002). Alternatively, presence or absence of cranial sutures on an endocast may simply be a reflection of the degree of fusion of the braincase bones during the ontogeny of the individual (see Chapter 4).

**Character 6.1**: Endocast flexure: 1-5º (0); 6-10º (1); 11-15º (2); 16-20º (3); 21-25º (4); 26-30º (5); 31-35º (6); 36-40º (7); 41-45º (8); 46-50º (9); 51-55º (A); or 56-60º (B). Endocast flexure measures were rounded to the closest integer. Endocast flexure was measured in lateral view by taking the acute angle between two lines, both of which pass through the hypophyseal cast (Figure 5, Chapter 2). The first line passes through the

middle of the olfactory bulb casts to the middle of the hypophyseal cast. The second line passes from the middle of the hypophyseal cast to the middle of the foramen magnum. The angle between these two lines captures the amount of basicranial flexion of the skull as reflected on an endocast. Basicranial flexion is typically measured using landmarks on skulls and recorded as an obtuse angle (e.g., Ross et al., 2004). The angle measured here utilizes landmarks on endocasts rather than landmarks on skulls and is measured as an acute angle. Variation in basicranial flexion among taxa is largely a consequence of increase in overall brain size relative to basicranial length (Ross et al., 2004). Functional advantages or constraints of basicranial flexion are debated in the literature (Ross et al., 2004).

Other measures of endocast flexure discussed in the literature include cephalic and pontine flexures. Cephalic flexure is determined as the angle of flexure between the forebrain and midbrain (Hopson, 1979). This corresponds to embryonic 'cranial flexure' (Senn, 1979). Pontine flexure is measured as the angle of flexure between the metencephalon and myelencephalon of the hindbrain (Hopson, 1979). Pontine flexure is also commonly measured in embryonic brains (Senn, 1979). Cephalic and pontine flexures were not measured here because the forebrain, midbrain, and different portions of the hindbrain are often not clearly divisible on endocasts.

The distribution of the character states for character 6.1 are discussed below. *Hadrocodium* has an endocranial flexure of 41-45º as does *Tachyglossus* suggesting that this state might be ancestral for Mammalia. Endocranial flexure of 26-30º appears to be a synapomorphy for Theria, although taxa within the crown show both significantly higher and lower flexure angles. The optimization of character 6.1 is illustrated in Figure 27.

**Character 6.2**: Endocast flexure: greater than 38º (0); or 38º or less (1). This is the discrete version of 6.1. As stated above, 38º is the mean for the values measured for taxa examined on the Luo and Wible (2005) tree. Presence of an endocast flexure of 38º or less is a synapomorphy for the clade including *Kryptobaatar*, *Vincelestes*, and Theria. A reversal to state (0) is seen in *Didelphis*. The optimization of character 6.2 is illustrated in Figure 28.

**Character 7**: Well-developed olfactory bulb casts: present on endocast (0); or absent from endocast (1). This character is uninformative for the taxa examined on the Luo and Wible (2005) tree, all exhibit state 0. However, *Trichechus* and other aquatic mammals such as cetaceans lack well-developed olfactory bulbs (state 1; Meisami and Bhatnagar, 1998; Colbert et al., 2005).

**Character 8**: Well-defined bony anterior terminus of the olfactory bulb casts (i.e., well-developed cribriform plate): absent (0); or present (1). The cribriform plate is formed by the coalescence of the turbinal elements of the ethmoid bone (summarized by Rowe et al., 2005). Presence of an ossified cribriform plate indicates that the turbinals are also ossified and this is an adaptation for increased structural support for olfactory and respiratory epithelia in mammals (summarized by Rowe et al., 2005). Turbinals increase the surface area of respiratory epithelium by 50% and olfactory epithelium by 600% over the surface area of the enclosing walls of the nasal cavity of *Monodelphis domestica*, the gray short-tailed opossum (Rowe et al., 2005).

Presence of a well-developed cribriform plate is a synapomorphy of Mammalia (Rowe, 1988, 1993). *Ornithorhynchus* (Zeller, 1988) and *Obdurodon* (Chapter 2) possess a partially ossified cribriform plate, but *Tachyglossus* and *Zaglossus* have a

completely ossified cribriform plate. The optimization of character 8 is illustrated in Figure 29.

**Character 9**: Olfactory bulb cast width vs. length aspect ratio: longer than wide (aspect ratio < 0.9) (0); wider than long (aspect ratio > 1.1) (1); or length and width are about equivalent (aspect ratio = 0.9-1.1) (2). Presence of olfactory bulb casts that are longer than wide is a plesiomorphy for Mammalia, Theria, Monotremata, and Marsupialia. This is also the condition for Placentalia, but it represents a reversal for this clade. The optimization of character 9 is illustrated in Figure 30.

**Character 10.1**: Percent of endocast composed by olfactory bulb casts: 0.0-0.9% (0); 1.0-1.9% (1); 2.0-2.9% (2); 3.0-3.9% (3); 4.0-4.9% (4); 5.0-5.9% (5); 6.0-6.9% (6); 7.0-7.9% (7); 8.0-8.9% (8); 9.0-9.9% (9); 10.0-10.9% (A); 11.0-11.9% (B); 12.0-12.9% (C); 13.0-13.9% (D); 14.0-14.9% (E); 15.0-15.9% (F); or 16.0-16.9% (G). Percent data were rounded to the nearest 0.1%. It is clear that *Ornithorhynchus* and *Obdurodon* have relatively small olfactory bulbs. The ancestral condition for Theria, however, is unclear based on these character states and this taxon sampling. *Vincelestes* and *Kryptobaatar* have relatively large olfactory bulb casts, but within Theria, metatherians have relatively larger olfactory bulb casts compared to eutherians ancestrally.

**Character 10.2**: Percent of endocast composed by olfactory bulb casts: greater than 6% (0); or less than 6% (1). This is the discrete version of character 10.1 and helps clear up some ambiguity about the ancestral condition for Theria. The olfactory bulb casts comprise about 6% of the total endocranial space on average for the taxa examined on the Luo and Wible (2005) tree. Presence of relatively large olfactory bulb casts occur in *Probainognathus*, *Hadrocodium*, Triconodontidae, *Vincelestes*, and ancestrally in

Theria. Reduction of relative olfactory bulb size has occurred in multiple lineages including *Ornithorhynchus*, *Obdurodon*, and Marsupialia as well as in aquatic placental mammals (e.g., sirenians and cetaceans; Meisami and Bhatnagar, 1998; Colbert et al., 2005). The cribriform plate extends posterior to the circular fissure in *Tachyglossus* (Figure 4, Chapter 2) and *Zaglossus* as do the corresponding olfactory nerve fibers and the olfactory bulb because the olfactory bulb surface area and volume are correlated to the surface area of the cribriform plate (Rowe et al., 2005). There are no distinctive bony markers to segregate the posterior portion of the olfactory bulb space from the rest of the endocranial cavity and, therefore, the volume of the olfactory bulb casts in the two species of echidnas are underestimated. The optimization of character 10.2 is illustrated in Figure 31.

**Character 11**: Circular fissure (separating olfactory bulbs from cerebral hemisphere) on endocast: poorly defined or absent (0); or well-defined (1). This character was modified from Luo and Wible (2005, character 418). The annular ridge of the frontal is the bony element that sits in the circular fissure of the brain (and corresponding endocast) and separates the olfactory bulbs from the rest of the brain. Thus, the circular fissure marks the posterior extent of the olfactory bulbs. Presence of a well-defined circular fissure is certainly ancestral for Theria based on its occurrence in Triconodontidae, *Kryptobaatar* (Figure 11, Chapter 2), and *Vincelestes* (Figures 14, 15, Chapter 2). This character state might be a synapomorphy for Mammalia based on its occurrence in *Ornithorhynchus* but absence in *Hadrocodium* (Figure 6, Chapter 2) and other non-mammalian cynodonts. The optimization of character 11 is illustrated in Figure 32.

**Character 12**: Casts of olfactory tracts: absent from endocast (0); or visible on endocast (1). The olfactory tracts are the projections of the olfactory bulbs to the cortex. In many mammals, the underlying meninges obscure the view of the olfactory bulb tracts from view in the corresponding endocasts. This character is basically uninformative for the taxa examined on the Luo and Wible (2005) tree because only the *Didelphis* endocast shows distinguishable olfactory tracts (Figure 26). However, *Orycteropus* also has distinctive olfactory tracts on its endocast.

**Character 13**: Surface of cerebral hemisphere casts: lissencephalic (= smooth) (0); or gyrencephalic (= convoluted) (1). An example of a lissencephalic endocast is that of *Ornithorhynchus* (Figure 8, Chapter 2); *Tachyglossus* has a gyrencephalic endocast (Figure 4, Chapter 2). Presumably, fossil mammals with lissencephalic cerebral hemisphere casts such as *Vincelestes* actually possessed lissencephalic cerebral hemispheres. However, this is not always the case in extant mammals. For example, the brain of *Tursiops truncatus*, the bottlenose dolphin, is very convoluted, but its cranial endocast is smooth, a condition that might be explained by ossification or calcification of some meninges surrounding the brain (Colbert et al., 2005). This character is also affected by the overall volume of the brain, because larger brains are more likely to be convoluted than smaller-sized brains. Volume increases as the cube of a linear unit but surface area only increases by the square of the linear unit. Assuming that a brain is roughly spherical in shape, convolutions increase the amount of cortical surface area relative to volume as the brain size or number of cells increases.

Even so, the ancestral conditions for Mammalia and Theria are for presence of lissencephalic cerebral hemisphere surfaces on endocasts. Gyrencephaly has evolved

independently in Monotremata, Marsupialia, and Placentalia. The optimization of character 13 is illustrated in Figure 33.

**Character 14**: Well-developed rhinal fissure on endocast: absent (0); or present (1). As stated previously, the rhinal fissure is typically used as an indication of the ventral boundary of isocortex in mammals and thus can be used to record the expansion of the isocortex in extinct taxa (Jerison, 1991). Absence of a rhinal fissure on endocasts is the ancestral condition for Mammalia and Theria. All the monotremes (Figures 4, 7, 8, Chapter 2) examined in this study and some members of Placentalia and Marsupialia have distinctive rhinal fissures on their endocasts. Lack of a rhinal fissure on a cranial endocast is not necessarily an indication of absence of isocortex as the rhinal fissure is absent on the endocasts of extant taxa that clearly possess the fissure on the exteriors of their brains (Jerison, 1991; e.g., *Monodelphis domestica*, Figures 19, 20, Chapter 2). In addition, lack of a rhinal fissure on endocasts may be an artifact of small brain size or isocortex size of some mammals (Rowe, 1996a, b). The optimization of character 14 is illustrated in Figure 34. Because of its variable appearance on endocasts, the rhinal fissure is not a reliable indicator of relative isocortex expansion. The relative width of the cranial endocast in the posterior portion of the cerebral hemisphere casts is perhaps a better indicator of isocortex expansion.

**Character 15**: Position of rhinal fissure on endocast: on lateral wall (0); or on ventral surface (1). This character is equivocal for Mammalia. The condition for Monotremata is to have the rhinal fissure located on the ventral surface of the brain and corresponding cranial endocast (Figures 4, 7, 8, Chapter 2). In contrast, the condition for Theria is to have the rhinal fissure on the lateral surface of the endocast (e.g., *Didelphis*,

Figure 26). Within Theria, the rhinal fissure is located on the ventral surface of endocasts of some taxa. The position of the rhinal fissure is likely correlated with the overall size of the brain or isocortex and this is reflected on the corresponding cranial endocast. The polarization of this character is unclear based on the taxa sampled here. The optimization of character 15 is illustrated in Figure 35.

**Character 16**: Well-developed median sulcus (i.e., division of the cortex into separate hemispheres) on endocast: absent (0); or present (1). *Thrinaxodon* (Figure 22) and *Diademodon* (Figure 23) lack a median sulcus whereas *Probainognathus*, *Hadrocodium*, and most crown mammals possess a well-developed median sulcus. Some therians such as *Didelphis* have a poorly developed median sulcus on their endocast because the superior sagittal sinus mostly fills the space and also possibly because of a reduced amount of ossification or calcification of the falx cerebri. The optimization of character 16 is illustrated in Figure 36.

**Character 17**: Exposure of midbrain (mainly superior and inferior colliculi) on dorsal surface of endocast: absent (0); or present (1). The ancestral condition for Theria and Mammalia is for the midbrain to not be exposed on the dorsal surface of cranial endocasts (e.g., *Didelphis*, Figure 26). The midbrain is either covered by blood sinuses and associated meninges, a posteriorly expanded cerebrum, an anteriorly expanded cerebellum, or some combination of these structures (Edinger, 1964). The midbrain is reportedly exposed on endocasts of *Probainognathus* (Quiroga, 1980a, b), *Zalambdalestes* (Kielan-Jaworowska, 1984, 1986), *Kennalestes* (Kielan-Jaworowska, 1984, 1986), and *Asioryctes* (Kielan-Jaworowska, 1984).

**Character 18**: Well-developed paraflocculus of the cerebellum cast: present (0); or absent (1). The paraflocculus occupies the space within the subarcuate fossa of the petrosal bone. Previous studies of extant marsupials suggest that the parafloccular lobes completely fill the subarcuate fossa early in postnatal ontogeny but only fill about half the space in adults (Sánchez-Villagra, 2002). However, the effects of desiccation of dead specimens on brain shape remain unexplored and, therefore, I assume that the space within the subarcuate fossa is an accurate representation of the size of the paraflocculus. The ancestral condition for Theria and Mammalia is for presence of a well-developed paraflocculus on the endocast (e.g., *Kryptobaatar*, Figure 11, Chapter 2). Complete lack of a parafloccular cast is observed in *Diademodon* (Figure 23) and some members of each of the three major clades of extant mammals (e.g., *Tachyglossus*, Figure 4, Chapter 2). The paraflocculus of the cerebellum is associated with coordination, balance, and vestibular sensory acquisition. The optimization of character 18 is illustrated in Figure 37.

**Character 19.1**: Percent of endocast composed by parafloccular casts: 0.0-0.5% (0); 0.6-1.0% (1); 1.1-1.5% (2); 1.6-2.0% (3); 2.1-2.5% (4); 2.6-3.0% (5); 3.1-3.5% (6); 3.6-4.0% (7); or 4.1-4.5% (8). Percent data were rounded to the nearest 0.1%. The ancestral condition for Mammalia is state (0) based on the taxa examined on the Luo and Wible (2005) tree. The optimization of character 19.1 is illustrated in Figure 38.

**Character 19.2**: Percent of endocast composed by parafloccular casts: greater than 1% (0); or less than 1% (1). This is the discrete version of character 19.1. The parafloccular casts constitute about 1% of the total endocranial space on average for the taxa examined on the Luo and Wible (2005) tree. Character state (1) is possibly a

synapomorphy for the clade including Mammalia and *Hadrocodium*; the condition in *Diademodon* and *Probainognathus* are unknown. *Thrinaxodon*, *Kryptobaatar*, *Dasyurus*, and *Dromiciops* exhibit character state (0) while all the others show state (1).

**Character 20**: Vermis of cerebellum: not visible on endocast (0); or clearly visible on endocast (1). The vermis is not a separate organ of the cerebellum with a specific identifiable function but rather is a topological feature signifying expansion of the cerebellum in the dorsoventral direction. The presence of a well-developed vermis on the endocast is a possible synapomorphy for Mammalia (e.g., *Didelphis*, Figure 26). The condition for *Hadrocodium* for this character is unknown because the back roof of the braincase is damaged. *Thrinaxodon* (Figure 22), *Diademodon* (Figure 23), and *Probainognathus* (Quiroga, 1980a, b) show no evidence of a vermis on their endocasts. The optimization of character 20 is illustrated in Figure 39.

**Character 21**: Cast of vermis of cerebellum: extends anterior to the paraflocculars casts (0); or vermis remains behind paraflocculars casts (1). This character is modified from Luo and Wible (2005, character 415). Character state (1) occurs in each of the three major extant clades of Mammalia (e.g., *Didelphis*, Figure 26). Character state (0) is exhibited in Triconodontidae, *Kryptobaatar* (Figure 11, Chapter 2), *Vincelestes* (Figures 14, 15, Chapter 2), and *Pucadelphys* (Figures 17, 18, Chapter 2). Character state (1) is the derived state for Marsupialia. The optimization of character 21 is illustrated in Figure 40.

**Character 22**: Cerebellar hemisphere casts on endocast: not visible on endocast (0); or well-developed on endocast (1). This character is modified from Luo and Wible (2005, character 417). Similar to the vermis, the hemispheres do not perform different

functions from the rest of the cerebellum, but rather indicate lateral expansion of the cerebellum. Presence of well-developed cerebellar hemispheres on the endocast (e.g., *Didelphis*, Figure 26) is the ancestral condition for Mammalia based on their presence in the non-mammalian cynodont *Probainognathus*. The optimization of character 22 is illustrated in Figure 41.

**Character 23**: Cast of pons on endocast: not well demarked on endocast (0); or clearly exposed on endocast (1). This character is uninformative for the taxa examined on the Luo and Wible (2005) tree. However, the pons is visible on the endocast of *Manis tricuspis*. In most mammals, the pons is obscured from view on the corresponding endocast by meninges and associated cistern sinuses.

**Character 24**: Cast of medulla oblongata on endocast: not well-demarked on endocast (0); or clearly exposed on endocast (1). This character is uninformative for the taxa examined in this analysis; none of the taxa have a well-demarked medulla oblongata on their endocast. To my knowledge, a medulla oblongata cast is not visible on any mammalian endocast. The pontine cistern and surrounding meninges fills in the space around the medulla oblongata and thus smooths this portion of the corresponding endocast.

**Character 25**: Transverse sinus cast: absent (0); or visible on endocast (1). Presence of the transverse sinus cast on the endocast is a synapomorphy for the clade that includes Triconodontidae, *Kryptobaatar* (Kielan-Jaworowska and Lancaster, 2004), *Vincelestes* (Rougier et al., 1992), and Theria (e.g., *Didelphis*, Figure 26). Reversals are seen in *Vincelestes* and *Pucadelphys* within this clade. The optimization of character 25 is illustrated in Figure 42.

**Character 26**: Sigmoid sinus cast: absent (0); or visible on endocast (1). This character is uninformative for the taxa examined on the Luo and Wible (2005) tree. Most taxa exhibit state (0) but *Didelphis*, *Dromiciops*, *Felis silvestris catus*, *Leptictis*, *Manis*, and *Zalambdalestes* show state (1) (e.g., *Didelphis*, Figure 26). The ancestral condition for Theria is state (0).

**Character 27**: Prootic vein cast: absent (0); or visible on endocast (1). This character is uninformative for the taxa examined on the Luo and Wible (2005) tree. Most taxa exhibit state (0) but *Didelphis*, *Monodelphis*, *Dromiciops*, *Vombatus*, *Canis lupus*, *Felis silvestris catus*, *Leptictis*, and *Manis* show state (1) (e.g., *Didelphis*, Figure 26). The ancestral condition for Theria is equivocal.

**Character 28**: Position of pons relative to insertion of cranial nerve V: pons lies anterior to insertion of cranial nerve V (0); or pons lies wholly posterior to the insertion of cranial nerve V (1). This character usually cannot be evaluated on fossil taxa because the pons does not usually leave an impression on endocasts. Consequently, this character was only scored from published data on actual brains of extant mammals. Based on extant phylogenetic bracketing, I infer that *Leptictis*, *Zalambdalestes*, *Kennalestes*, *Asioryctes*, and *Pucadelphys* exhibited state (0). Monotremes exhibit state (1) but all the extant therians show state (0). The ancestral condition for Mammalia is likely state (0) because this is the ancestral condition in Vertebrata. The optimization of character 28 is illustrated in Figure 43.

**Character 29**: Superior sagittal sinus: located in a space within the supraoccipital (0); or located within meninges of the brain (1). This character is uninformative for the

taxa examined on the Luo and Wible (2005) tree. *Thrinaxodon* exhibits state (0) (Figure 44), the condition in *Diademodon* is unknown, and the remaining taxa show state (1).

**Character 30**: Prominent parietal tube and foramen: present (0); or absent on endocast (1). The parietal foramen is associated with the parietal eye and pineal body, both of which comprise the epiphysis portion of the epithalamus (Butler and Hodos, 1996). Extinct taxa lacking a parietal foramen are assumed to have lacked a parietal eye, but the pineal body leaves little if any bony signature and therefore the organ's presence or absence cannot be easily inferred from fossils (Roth et al., 1986). The parietal eye has thermoreceptive and photoreceptive functions that regulate circadian rhythm and reproductive cycles (Roth et al., 1986; Butler and Hodos, 1996). In non-mammalian synapsids, the parietal eye likely aided in the detection of seasonality for reproductive purposes and survival tactics (Roth et al., 1986). The optimization of character 30 on the pruned version of the strict consensus tree of Luo and Wible (2005) is illustrated in Figure 45. *Thrinaxodon* (Figure 22), and *Diademodon* (Figure 23) show a prominent parietal tube and foramen on their endocasts. Character state (1) is a synapomorphy for the clade that includes *Probainognathus* (Quiroga, 1980a, b), *Hadrocodium*, and Mammalia. It was previously suggested that during the Permian and early Triassic, there was a strong selective pressure for presence of a parietal eye in non-mammalian synapsids that inhabited high latitudes with harsh and seasonal climates (Roth et al., 1986). In the Middle Triassic, worldwide reduction in seasonality associated with the Pangaea supercontinent possibly eased selection pressures for maintenance of a parietal eye, resulting in the closure of the parietal foramen in cynodonts (Roth et al., 1986).

**Character 31.1**: Percent endocast composed by hypophyseal fossa: 0.00-0.09% (0); 0.10-0.19% (1); 0.20-0.29% (2); 0.30-0.39% (3); 0.40-0.49% (4); 0.50-0.59% (5); 0.60-0.69% (6); 0.70-0.79% (7); 0.80-0.89% (8); 0.90-0.99% (9); 1.00-1.09% (A); 1.10-1.19% (B); 1.20-1.29% (C); or 1.30-1.39% (D). Percent data were rounded to the nearest 0.01%. The development of the hypophyseal fossa is variable in different mammals, and may not be an accurate measure of the size of the pituitary gland in some mammalian taxa (Edinger, 1942). However, the hypophyseal fossa is the only available bony proxy for the pituitary gland in extinct taxa (Edinger, 1942). The pituitary gland regulates growth and effectively overall body size through the release of hormones. Larger glands are expected to release more hormones resulting in larger body size (Edinger, 1942). Among the taxa examined here, hypophyseal volume shows positive correlations with endocranial volume and body mass; however, these data were not examined using independent contrasts. Relative hypophyseal fossa size; that is, hypophyseal volume expressed as a percentage of endocranial volume, does not show a correlation with body mass. The optimization of relative hypophyseal fossa size (character 31.1) on the pruned version of the strict consensus tree of Luo and Wible (2005) is complex (Figure 46). Character state (0) is a synapomorphy for Theria, but the ancestral condition for Mammalia is state (1). This suggests that the hypophyseal fossa occupies a smaller percentage of the endocranial volume in therian mammals compared to more basally diverging mammals such as monotremes. The biological significance of this character distribution is not immediately obvious because, as stated above, body mass does not scale with relative hypophyseal fossa size. Perhaps the pituitary gland is significantly larger than the hypophyseal fossa in therian mammals such that the gland extends above

the fossa. Alternatively, maybe there really is a relationship between relative hypophyseal fossa size and body size, but the taxonomic sampling here is too small.

**Character 31.2**: Percent endocast composed by hypophyseal fossa: less than 0.2% (0); or greater than 0.2% (1). This is the discrete version of character 31.1. The hypophyseal fossa accounts for about 0.2% of the total endocranial space on average for the taxa examined on the Luo and Wible (2005) tree. Character state (1) is ancestral for Mammalia but state (0) is seen in all monotremes examined here as well as the placentals and some marsupials. The optimization of character 31.2 is illustrated in Figure 47.

**Character 32**: Width vs. length aspect ratio for hypophyseal fossa: wider than long (aspect ratio > 1.1) (0); longer than wide (aspect ratio < 0.9) (1); or hypophyseal length and width are about equal (aspect ratio = 0.9-1.1) (2). Character state (0) is the ancestral condition for Mammalia and Theria. Character state (1) is a synapomorphy for both Monotremata and Marsupialia. The optimization of character 32 is illustrated in Figure 48.

**Character 33**: Depth of hypophyseal fossa with respect to its length: fossa deeper than long (aspect ratio > 1.1) (0); fossa longer than deep (aspect ratio < 0.9) (1); or hypophyseal fossa depth and length about equal (aspect ratio = 0.9-1.1) (2). Character state (0) is the ancestral condition for Mammalia and the ancestral condition for Theria is equivocal. Character state (1) is a synapomorphy for both Monotremata and Marsupialia. The optimization of character 33 is illustrated in Figure 49.

**Character 34**: Trigeminal nucleus casts: absent from endocast (0); or visible on hindbrain portion of endocast (1). *Obdurodon* and *Ornithorhynchus* exhibit state (1)

(Figures 7, 8, Chapter 2) but all other taxa examined on the Luo and Wible (2005) tree show state (0).

**Character 35**: Cavum epiptericum: visible on ventral surface of endocast (0); not distinguishable on endocast (1); or visible when endocast is viewed from above (2). The cavum supracochleare for the geniculate ganglion was considered for this character only if the cavum epiptericum and cavum supracochleare are confluent in a particular taxon. This character is uninformative for the taxa examined on the Luo and Wible (2005) tree. Character state (0) is the ancestral condition for Mammalia (e.g., *Vincelestes*, Figures 14, 15, Chapter 2) and Theria. *Diademodon* (Figure 23) exhibits state (1) and *Hadrocodium* shows state (2) (Figure 6, Chapter 2).

**Character 36.1**: Percent of endocast composed by cava epipterica: 0.10-0.19% (0), 0.20-0.29% (1), 0.30-0.39% (2), 0.40-0.49% (3), 0.50-0.59% (4), 0.60-0.69% (5), 0.70-0.79% (6), 0.80-0.89% (7), 0.90-0.99% (8), 1.00-1.09% (9), 1.10-1.19% (A), 1.20-1.29% (B), or 1.30-1.39% (C). Percent data were rounded to the nearest 0.01%. Character state (C) is reconstructed at the node for Mammalia. The ancestral condition for Theria is equivocal. The optimization of character 36.1 is illustrated in Figure 50.

**Character 36.2**: Percent of endocast composed by cava epipterica: greater than 0.5% (0); or less than 0.5% (1). This is the discrete version of character 36.1. The cava epipterica comprise about 0.5% of the total endocranial space on average for the taxa examined on the Luo and Wible (2005) tree. Character state (1) is a synapomorphy for Theria but reversals are present within this clade. The optimization of character 36.2 is illustrated in Figure 51.

**Character 37**: Cavum epiptericum: confluent with cavum supracochleare (0); or separate from cavum supracochleare which houses the geniculate ganglion (1). This character was modified from Luo and Wible (2005, character 313). There is at least a partial separation of the two cavities in *Tachyglossus*, triconodonts, *Vincelestes*, and therians (Rougier et al., 1996a; Luo and Wible, 2005). Optimization on the Luo and Wible (2005) tree suggests that separation of the cavum epiptericum and cavum supracochleare is a synapomorphy comprising *Vincelestes* and Theria. If this is true, this condition also evolved independently in *Tachyglossus* and Triconodontidae. The ancestral character state is visible in the CT slices of the adult *Ornithorhynchus anatinus* skull (e.g., coronal slice #348-380, visible on the Digimorph website; Appendix 3). The derived character state is visible in the CT slices of the *Didelphis virginiana* skull (e.g., coronal slice #700-747, visible on the Digimorph website; Appendix 3). The optimization of character 37 is illustrated in Figure 52.

**Character 38**: Cast of orbital fissure canal: right and left canals are separate at exit of skull (0); or canals are confluent at exit (1). This character is uninformative for the taxa examined on the Luo and Wible (2005) tree. *Ornithorhynchus* (Figure 8, Chapter 2) and *Vincelestes* (Figures 14, 15, Chapter 2) exhibit state (1) but the other taxa all show state (0) (e.g., *Didelphis*, Figure 26). Therefore, the ancestral condition for Mammalia and Theria is for the right and left orbital fissure canals to remain separate at their exit of the skull.

**Character 39**: Optic chiasm: absent from endocast (0); or visible on endocast (1). This character is uninformative for the taxa examined on the Luo and Wible (2005) tree. The ancestral state for Mammalia and Theria is for the optic chiasm to not be visible on

the endocast. The optic chiasm is typically surrounded by meninges and therefore this structure is not visible on many cranial endocasts. However, the optic chiasm is visible on the endocast of *Tachyglossus* (Figure 4, Chapter 2) and on a few placental endocasts (*Canis lupus*, *Leptictis*, *Zalambdalestes*).

## ANCESTRAL CHARACTER STATE RECONSTRUCTIONS

Based on the distribution of the characters discussed above, the ancestral endocast character states are reconstructed for the following clades: Mammalia, Monotremata, Theria, Marsupialia, and Placentalia. Character states for each of these clades are presented in Appendix 6. Synapomorphies for each of these clades are discussed below.

**Mammalia**. There are three probable synapomorphies for Mammalia among the endocast characters examined in this analysis. Presence of at least a partial ossified cribriform plate (8[+1]) is a synapomorphy for Mammalia (Rowe, 1988, 1993). A second possible synapomorphy for Mammalia is the presence of a clearly visible vermis of the cerebellum on endocasts (20[+1]). The condition for *Hadrocodium* for this character is unknown because the back roof of the braincase is damaged. The third synapomorphy is that the cava epipterica together compose 1.3-1.4% of the total endocranial space (36.1[+C]).

**Monotremata**. There are six probable synapomorphies for Monotremata among the endocast characters examined in this analysis. One possible synapomorphy for Monotremata is the presence of a well-developed rhinal fissure on the endocast (14[+1]).

However, as discussed above, lack of a rhinal fissure on some endocasts may be an artifact of small brain size of some mammals. A second possible monotreme synapomorphy is the position of the rhinal fissure on the ventral surface of the endocast. However, again this character is possibly correlated with overall size of the brain, and particularly of the isocortex. A third possible synapomorphy is the position of the pons completely posterior to the insertion of cranial nerve V (28[+1]). This character is based on the study of actual brain material and therefore cannot be evaluated on fossil taxa. The fourth possible synapomorphy for Monotremata relates to the percent of the total endocranial space that is composed by the hypophyseal fossa. For the discrete version of this character, Monotremata exhibits state (0), the hypophyseal fossa comprises less than 0.2% of the total endocranial space (31.2[+0]). This represents a reversal because the ancestral condition for Mammalia is for the hypophyseal fossa to comprise greater than 0.2% of the total endocranial space (state 1). The fifth synapomorphy for Monotremata is that the hypophyseal fossa is longer than wide (32[+1]). The sixth synapomorphy also concerns the hypophyseal fossa dimensions. In monotremes, the fossa is longer than it is deep (33[+1]).

The olfactory bulb casts together constitute 6% of the total endocranial space (10.2[+1]) in monotremes. However, as mentioned above in the description of character 10.2, the volumes of the olfactory bulb casts of *Tachyglossus* and *Zaglossus* are underestimated and, therefore, I do not consider this character to be a synapomorphy for Monotremata.

**Theria**. There are four probable synapomorphies for Theria among the endocast characters examined in this analysis. The first synapomorphy for Theria is that the range

of endocast flexure around the hypophysis is 26-30º (6.1[+5]). The second possible synapomorphy is that the rhinal fissure is visible on the lateral wall of the endocast (15[+0]). As stated above, the polarity of this character is uncertain at this time. The third endocast synapomorphy for Theria is that the hypophyseal fossa composes 0-0.1% of the total endocranial space (31.1[+0]). The fourth synapomorphy for Theria is that the cava epipterica together constitute less than 0.5% of endocranial space (36.2[+1]).

**Marsupialia**. There are five probable synapomorphies for Marsupialia among the endocast characters examined in this analysis. The first synapomorphy for Marsupialia is that the range of endocast flexure around the hypophysis is 36-40º (6.1[+7]). The second synapomorphy is that a well-developed rhinal fissure is visible on the endocast (14[+1]). However, as discussed above lack of a rhinal fissure on some endocasts may be an artifact of small brain size of some mammals because all mammalian brains observed directly have the fissure. A third possible synapomorphy is that the cast of the vermis of cerebellum is located completely posterior to the parafloccular casts (21[+1]). However, the ancestral condition for Theria is equivocal (0/1). A fourth synapomorphy is that the hypophyseal fossa is longer than wide (32[+1]). The fifth endocast synapomorphy for Marsupialia is that the hypophyseal fossa is longer than deep (33[+1]). Monotremata also possesses the same character states for characters 32 and 33. However, because extinct taxa on the branches separating monotremes and marsupials have different character states, the similarities in the hypophyses of Monotremata and Marsupialia described by these characters must have evolved independently, based on the Luo and Wible (2005) phylogenetic hypothesis.

**Placentalia**. There are four probable synapomorphies for Placentalia among the endocast characters examined in this analysis. The first synapomorphy is that the lateral expansion of braincase extends posteriorly to the lambdoidal region of the skull (1[+2]). The second synapomorphy is the presence of olfactory bulb casts that are longer than wide (9[+0]). This represents a reversal from character state (1). The third synapomorphy for Placentalia is that the hypophyseal fossa composes less than 0.2% of the total endocranial space (31.2[+0]). This represents a reversal because the ancestral condition for Theria for this character is for the hypophyseal fossa to constitute greater than 0.2% of endocranial space (state 1). The fourth synapomorphy for Placentalia is that the depth and length of the hypophyseal fossa are essentially equivalent (33[+2]).

## RESULTS FROM PHYLOGENETIC ANALYSES

When the complete endocast character matrix was analyzed by itself with all character unordered, I obtained 19,263 most parsimonious trees (MPTs) with a tree length (TL) = 125, consistency index (CI) = 0.3680, and retention index (RI) = 0.5842. Strict consensus (Figure 53) and Adams consensus (Figure 54) trees summarize these results. When the same matrix was analyzed with the continuous characters ordered, I obtained 16,312 MPTs with a TL = 120, CI = 0.3667, and RI = 0.5870. For the most part, the endocast characters alone provide little resolution for this set of taxa. However, Monotremata is fully resolved as a monophyletic group that is diagnosed by a single unambiguous synapomorphy (character 28), when all the characters are unordered.

When the continuous characters are ordered and a strict consensus tree is calculated, the Monotremata clade breaks apart, but *Obdurodon* and *Ornithorhynchus* form a clade, and *Tachyglossus* and *Zaglossus* form a clade as well. The Adams consensus tree for the ordered analysis places *Procavia* as the sister taxon to the echidna clade (*Tachyglossus* + *Zaglossus*), and finds the *Procavia* +echidna clade as sister taxon to the platyus clade (*Obdurodon* + *Ornithorhynchus*).

It is interesting to note that *Kryptobaatar* is nested within non-mammalian cynodonts and *Pucadelphys* and *Vincelestes* fall outside of crown Mammalia for both the unordered (Figure 53) and ordered analyses. All three of these taxa are considered to be crown mammals based on several other phylogenetic analyses, including that of Luo and Wible (2005). I am not suggesting that these taxa are not crown mammals but rather that the endocast characters alone do not place them within the crown clade. Brain evolution did not follow the dominant systematic signal obtained from the rest of the mammalian anatomy.

The endocast matrix was pruned to exclude taxa not included in the Luo and Wible (2005) matrix. Analysis of the pruned matrix with all characters unordered resulted in 2,032 MPTs with TL = 96, CI = 0.4479, and RI = 0.6015. When continuous characters were ordered, the analysis resulted in 264 MPTs with TL = 94, CI = 0.4362, and RI = 0.6074. Strict consensus (Figure 55) and Adams consensus (Figure 56) trees from the unordered analysis summarize these results. A monophyletic Mammalia and a monophyletic Monotremata was obtained in all of the MPTs. However, the clades Theria, Marsupialia, and Placentalia were not obtained in any of the MPTs. When the

continuous characters were ordered, *Kryptobaatar* nested outside crown Mammalia; otherwise, the results were nearly identical to those of the unordered analysis.

The phylogenetic analysis including the combined matrix of Luo and Wible (2005) and my endocast character data, and treating all characters as unordered, resulted in 3,772 MPTs of TL = 2122, CI = 0.3577, and RI = 0.7832. The ordered and unordered analyses resulted in strict consensus trees with minimal differences; from hereon, the results from the unordered analysis are described. The strict consensus tree from this analysis does not differ greatly from the strict consensus tree obtained by Luo and Wible (2005) (Figure 57). Within Eutriconodontidae (sensu Kielan-Jaworowska et al., 2004), *Amphilestes* is the sister taxon to the clade containing *Jeholodens*, *Priacodon*, and *Trioracodon* in the combined matrix analysis. This result contrasts with the Luo and Wible analysis in which *Amphilestes* and *Gobiconodon* form a polytomy with the clade containing *Jeholodens*, *Priacodon*, and *Trioracodon*. In my analysis, *Bradypus* and *Tamandua* form a clade that is the sister taxon to the other xenarthrans. In contrast in the Luo and Wible analysis, *Bradypus* and *Tamandua* form a polytomy with a clade containing the remaining xenarthrans.

The most significant differences between results from my combined matrix analysis and the Luo and Wible (2005) study occur in the metatherian portion of the tree. In the combined matrix analysis, *Kokopellia* is the sister taxon to a clade including *Asiatherium*, *Anchistodelphys*, *Albertatherium*, *Didelphodon*, *Pediomys*, *Turgidodon*, *Mayulestes*, *Pucadelphys*, *Andinodelphys*, and crown Marsupialia. Nested within this larger clade, *Pucadelphys* and *Andinodelphys* form a clade with crown marsupials. These

results contrast with the strict consensus tree of Luo and Wible (2005) in which all of the above mentioned non-marsupial metatherians form a polytomy with crown Marsupialia.

Despite these differences, there is little net effect from inclusion of my endocast characters with the Luo and Wible matrix. The large amount of missing data from the additional endocast characters likely mitigates the phylogenetic significance of these characters. The missing data results from lack of cranial material for many of these taxa, or at least lack of cranial material that is suitable for study of endocranial space.

The phylogenetic analysis of the Luo and Wible (2005) matrix with my endocast character matrix, but with taxa not common to both matrices pruned prior to the analysis, and all characters unordered resulted in 1 MPT with a TL = 1070, CI = 0.6318, and RI = 0.7437. When the continuous characters were ordered, I obtained 2 MPTs of TL = 1097, CI = 0.6171, and RI = 0.7407. The unordered analysis placed *Hadrocodium* within crown Mammalia in a polytomy with cimolodontans and the clade including *Vincelestes* + Theria (Figure 58). Monotremata and Marsupialia are recovered as monophyletic, but the relationships within Marsupialia are unusual. Marsupialia is nested within a paraphyletic Placentalia. A bootstrap analysis of 1000 replicates was subsequently performed; the results are presented in Figure 58. The clade containing *Hadrocodium*, cimolodontans, *Vincelestes*, and Theria is poorly sorted (bootstrap value = 56), but the clade of Marsupialia and three placentals (*Canis lupus*, *Felis silvestris catus*, and *Dasypus novemcinctus*) is supported by a bootstrap value of 83. The results from the ordered analysis differed from the unordered results by placing *Hadrocodium* as the sister taxon to Mammalia, and by placing *Dasyurus*, *Dromiciops*, and the *Pucadelphys-Didelphis* clade in a polytomy.

The analysis of the cropped Luo and Wible (2005) matrix of 21 taxa, but without my endocast matrix resulted in a 2 MPTs of TL = 969, CI = 0.6605, and RI = 0.7709. The strict consensus tree of the 2 MPTs (Figure 59) is nearly identical to the MPT of the analysis of the same taxa but including the endocast characters in the matrix. The only difference is that in the analysis without the endocast characters, *Hadrocodium* forms a polytomy with Monotremata, cimolodontans, and the clade containing *Vincelestes* + Theria (Figure 59).

The comparison between the analyses of the Luo and Wible (2005) matrix with and without my endocast characters again reveals that my endocast characters do not greatly alter the topology of the tree. The skeletal and dental characters in the Luo and Wible matrix outnumber my endocast characters by an order of magnitude. Because of this discrepancy, my endocast characters have little apparent effect on the tree topology.

## DISCUSSION

**Mammalia**. The ancestral mammal brain morphotype is characterized by the retention of a number of characters from its non-mammalian cynodont ancestors. These characters include presence of relatively large olfactory bulbs, a smooth cerebrum, and well-developed parafloccular lobes of the cerebellum. As noted by some authors (Kielan-Jaworowska, 1986, 1997; Kielan-Jaworowska et al., 2004), the cerebellum is laterally expanded in basal mammals relative to some non-mammalian cynodonts. This is supported by the expansion of the braincase in the parietal region and presence of well-

developed parafloccular casts. However, both of these characters are plesiomorphic for Mammalia because they are also present in *Hadrocodium*.

Even so, the transition from non-mammalian cynodonts to mammals likely involved a number of neurological changes. Among these was an increase in overall brain size, a result of increase in size of the isocortex and expansion of the striatum (Jerison, 1973; Kielan-Jaworowska et al., 2004). In addition, a vermis is clearly visible for the first time on the endocasts of basal mammals, suggesting that the cerebellum had expanded vertically. Basal mammals show an increase in the relative size of the cavum epiptericum which houses the trigeminal ganglion, suggesting that the trigeminal nerve is relatively large in these taxa.

These neurological changes are correlated with increased perception and increased neural control of the skeletomuscular system for mastication and locomotion (Kielan-Jaworowska et al., 2004). Expansion of the cerebral hemisphere region of endocasts suggests expansion of the isocortex to provide increased surface area for projection of sensory information. This expansion of the cortical sensory areas is possibly related to modification in the inner ear associated with higher frequency hearing and the acquisition of hair as a peripheral sense organ (Ulinski, 1986). Curvature of the cochlea and incorporation of three miniaturized ear ossicles in the adult mammalian middle ear also enhanced auditory capabilities in early mammals (Rowe, 1996a, b). Presence of relatively large olfactory bulb casts associated with extensive, ossified turbinals in the snout suggests that basal mammals had increased olfactory capabilities compared with their non-mammalian cynodont ancestors. Increased size of the trigeminal nerve possibly provided increased sensitivity to the snout and vibrissae for

greater detection of tactile information. In addition, in extant mammals pathways from the cerebellum and basal ganglia to specific motor nuclei of the thalamus allow for smooth functional control of the skeleton and associated muscles (Ulinski, 1986). It seems likely that these neurological pathways evolved in association with postcranial skeletal and muscular modifications in mammals as adaptations for improved locomotion (Ulinski, 1986). All of these neural modifications for increased sensory perception (auditory, olfactory, tactile information) and associated motor response were interpreted (Jerison, 1973) as adaptations for early mammals to be successful in nocturnal niches.

Increase in brain size in early mammals is associated with a number of modifications to the skull (Kielan-Jaworowska et al., 2004). These include posterior displacement of the braincase relative to the craniomandibular joint (Rowe, 1996a, b; Kielan-Jaworowska et al., 2004), increase in depth of the frontal region of the braincase in relation to enlargement of the olfactory bulbs, widening of the parietal region of the skull in association with expansion of the isocortex, and widening of the occipital region of the skull related to differentiation of the cerebellum. Expansion of the isocortex is associated with separation of the postdentary elements from the mandible and incorporation of these bones into the middle ear and other changes (Rowe, 1993, 1996a, b).

**Monotremata**. Monotreme brains are characterized by the presence of a clearly visible rhinal fissure on the ventral surface of the cranial endocast, a pons that lies completely posterior to the insertion of the trigeminal nerve, and a relatively small hypophyseal fossa. Based on a study of extant mammalian brains, bifurcation of the termination of the optic tract in the thalamus is a synapomorphy for Monotremata

(Johnson et al., 1982a, b). In addition, extant monotremes are also the only mammals known to have electroreceptive capabilities (Scheich et al., 1986; Augee and Gooden, 1992; Bohringer, 1992; Manger et al., 1997; Proske et al., 1998). Electroreceptors located in the snouts of the platypus and both species of echidnas are innervated by the trigeminal nerve, which is very large in all of these taxa and passes through 14 foramina in the skull and mandible en route to innervating the upper and lower jaws or bills (Huber, 1930; Abbie, 1934; Griffiths, 1968; 1978; Musser and Archer, 1998). The extant platypus, *Ornithorhynchus anatinus*, relies on electroreception as well as tactile receptors in its bill for underwater navigation, because the eyes, ears, and olfactory organs are covered while the animal is submerged (Griffiths, 1978; Scheich et al., 1986; Bohringer, 1992). The electroreceptors are also used for tracking prey by both the platypus and the echidnas (Bohringer, 1992; Augee and Gooden, 1992). Electroreception is a synapomorphy for Vertebrata but has been lost and re-acquired multiple times within the lineage and innervation in other aquatic vertebrates differs from monotremes (Bullock et al., 1983; Fritzsch and Münz, 1986; Feng, 1991; Butler and Hodos, 1996; Schlosser, 2002). Electroreceptors are innervated by the trigeminal nerve only in monotremes, a probable synapomorphy for the group (Andres and von Düring, 1988).

The location of the pons behind the insertion of the trigeminal nerve is another potential synapomorphy for Monotremata (Griffiths, 1968, 1978). In all placental and marsupial taxa studied so far, the pons lies in front of the trigeminal nerve insertion. Cranial endocasts from two multituberculate mammals (*Chulsanbaatar* and *Nemegtbaatar*) were reported to also show the pons lying completely behind the insertion of the trigeminal nerve (Kielan-Jaworowska, 1986). However, the casts of the pons are

not conspicuous on these specimens (based on the description and illustrations presented by Kielan-Jaworowska [1986] and the digital endocast of *Kryptobaatar*), and their exact positions are open to interpretation. The pons also does not leave an obvious signature on monotreme endocasts, and therefore this character cannot be assessed for *Obdurodon*.

Finally, the monotreme brain is fairly large for its body size with an EQ value that is just below the average for mammals but significantly larger compared to extinct taxa just outside Mammalia such as *Hadrocodium* (Chapter 2). As in many other mammals, much of the monotreme brain comprises the isocortex of the cerebral hemispheres. Much of the sensory information projected to the isocortex in monotremes is derived from the snout, undoubtedly resulting from the mechano- and electroreceptive capabilities located in the rostrum. So it is possible that increased brain size in monotremes is correlated in some degree with increased isocortex surface area and increased sensory information derived from the snout.

**Theria**. Therian cranial endocasts are characterized by a number of synapomorphies. The flexure of therian endocasts is 26-30º ancestrally compared with ancestral flexure for Mammalia of 36-40º. Other characters include the location of the rhinal fissure on the lateral surface of the endocast, the hypophyseal fossa composes a relatively small percentage of the total endocranial volume, and the cava epipterica are relatively small.

Comparative study of brain morphology reveals additional synapomorphies for Theria (Johnson et al., 1982a, b, 1994). For example, therian mammals have a complete secondary (SII) somatic sensory projection region of the cerebral cortex, but monotremes have only a primary (SI) somatic sensory projection region (Johnson et al., 1994). The

fibers of the optic tract run under a superficial gray layer in most therian mammals as opposed to the plesiomorphic condition in which the optic tract fibers run superficially over the anterior tectum (Johnson et al., 1982a, b). The external cuneate nucleus is clearly separated from the cuneate-gracile complex of the medulla oblongata (Johnson et al., 1994).

**Marsupialia**. Marsupial cranial endocasts are characterized by a number of features; these include an endocast flexure of 36-40º, the vermis of the cerebellum is located completely posterior to the parafloccular casts, and the hypophyseal fossa is longer than it is deep or wide. In addition, based on comparative study of brains, another synapomorphy of marsupials is that the arteries of the CNS terminate in individual non-anastomotic capillary loops (Wislocki and Campbell, 1937; Sunderland, 1941; Johnson et al., 1982a, b). This condition was observed in *Didelphis virginiana*, *Dasyurus viverrinus*, *Macropus giganteus*, *Pseudochirus* sp., *Trichosurus vulpecula*, and *Phascolarctos cinereus* (Wislocki and Campbell, 1937; Sunderland, 1941). This is in contrast to the ancestral condition found in other mammals in which the arterioles form free capillary anastomoses with a number of different venules (Johnson et al., 1982a, b).

**Placentalia**. Placental cranial endocasts are characterized by the lateral expansion of the braincase extending posterior to the lambdoidal region of the skull, presence of olfactory bulbs that are longer than wide, and presence of a relatively small hypophyseal fossa. In addition, based on comparative study of brains, there are some additional synapomorphies for Placentalia. Unlike other mammals, the cerebral hemispheres of placentals are connected by a corpus callosum (Johnson et al., 1982a, b). In addition, either some or all of the facial nerve fibers pass ventral to the trigeminal

column (Johnson et al., 1982a, b). This contrasts with other mammals in which all of the facial nerve fibers emerge dorsal to the trigeminal column (Johnson et al., 1982a, b). Finally, the ventral 'accessory' nucleus of the inferior olive has a medial position in placentals (Johnson et al., 1982a, b). This is in contrast to the lateral position of the ventral 'accessory' nucleus of the inferior olive that is seen in other mammals.

**Multituberculates and Triconodonts**. Multituberculates and triconodonts do not form a monophyletic group by themselves, but the similarity of cranial endocasts from the two groups was noted previously in the literature (Kielan-Jaworowska, 1983, 1986, 1997). Previously, multituberculate and tricondont endocasts were designated as 'cryptomesencephalic', a condition characterized by a large vermis, no cerebellar hemispheres, and lack of midbrain exposure on the endocast (Kielan-Jaworowska, 1986, 1997). The cryptomesencephalic type contrasts to the 'eumesencephalic' type seen in basal therians (Kielan-Jaworowska, 1986, 1997). The eumesencephalic condition is characterized by a wide cerebellum, presence of cerebellar hemispheres, and broad dorsal midbrain exposure on endocasts (Kielan-Jaworowska, 1986, 1997).

The terms 'cryptomesencephalic' and 'eumesencephalic' were later abandoned (Kielan-Jaworowska and Lancaster, 2004; Kielan-Jaworowska et al., 2004). Even so, the bearing of my work presented in this chapter is worth mentioning with respect to these terms. Based on my work in this chapter, the cryptomesencephalic endocast characters uniting multituberculates and tricondonts are all plesiomorphic for these two taxa. Evaluation of the eumesencephalic condition is more complicated. The first two eumesencephalic characters (presence of a wide cerebellum, and presence of cerebellar hemispheres) are correlated and should be represented by a single character.

Nonetheless, presence of well-developed cerebellar hemispheres correctly diagnoses Theria. Presence of broad dorsal midbrain exposure on the endocasts occurs independently in several lineages, including some non-mammalian cynodonts (character 17, this chapter; Edinger, 1964; Quiroga, 1980a, b; Kielan- Jaworowska, 1997).

## CONCLUSIONS

Thirty-nine endocast characters were examined in 23 mammalian and non-mammalian cynodont taxa on a pruned consensus tree from the Luo and Wible (2005) phylogenetic analysis. Some of the endocast characters I examine were previously used in other phylogenetic studies; however, a rigorous examination of many endocranial characters in a phylogenetic context including several taxa has yet to be published. The purpose of this chapter was to identify where major changes in the endocranial space occurred along the evolutionary lineages of Mammalia. I document which major changes in the evolution of endocranial space are diagnostic for major clades of Mammalia. In Chapter 4, I began to explore individual and ontogenetic variation by examining these 39 characters using a single taxon, *Monodelphis domestica*.

Approximately one-third of the characters examined here are uninformative for the sample of taxa I examined. Nonetheless, it is important to document these uninformative characters, because some may actually be informative if the taxonomic sampling is denser. Based on my taxonomic sampling (Appendix 5), I determined endocranial synapomorphies for the clades Mammalia, Monotremata, Theria, Placentalia,

and Marsupialia (Appendix 6). Most notably among these synapomorphies, Mammalia is diagnosed by the presence of a clearly visible vermis cast of the cerebellum and the presence of a relatively large cavum epiptericum for the trigeminal ganglion. Monotremata is most notably diagnosed by the pons being completely posterior to the insertion of the trigeminal nerve. Another important neural synapomorphy for Monotremata that cannot be accessed on endocasts is the presence of electroreceptors that are innervated by the trigeminal nerve. Marsupial endocasts are most notably diagnosed by a vermis of the cerebellum that is located completely posterior to the parafloccular casts. Placentalia is notably diagnosed by lateral expansion of endocranial space that extends posterior to the lambdoidal region of the skull.

Presence or absence of the rhinal fissure on cranial endocasts is a character that was historically considered greatly significant for the study of mammalian brain evolution (Jerison, 1973). The rhinal fissure marks the ventral border of the isocortex and therefore presumably the rhinal fissure can be used to track the expansion of the isocortex in mammals (Jerison, 1991). However, my survy finds that the rhinal fissure is a structure that is not always visible on cranial endocasts of extant mammals, corroborating the findings of others (e.g., Jerison, 1991). For example, there is no mark of the rhinal fissure on endocasts of adult *Monodelphis domestica* even though the fissure is clearly visible on the corresponding brains (Chapter 4). This taxonomic variability suggests that presence or absence of a rhinal fissure has little biological significance. Perhaps another character, such as the relative width of the endocast is a better proxy for measuring expansion of the isocortex in mammals.

Phylogenetic analysis of the matrix of the 39 endocast characters scored for 23 taxa shows little resolution. However, Monotremata was fully resolved based on this analysis, being diagnosed by a single character (the pons being completely posterior to the insertion of the trigeminal nerve). Analysis of the endocast matrix included with the original Luo and Wible (2005) matrix does not significantly alter the topology of the Luo and Wible (2005) strict consensus tree. Likewise, analysis of the Luo and Wible (2005) matrix combined with my endocast matrix, but to the exclusion of taxa not present in both, did not greatly alter the tree topology obtained from analysis of the taxon-pruned version of the Luo and Wible original matrix.

My endocast character had little effect on tree topology because of the overwhelming number of characters from other portions of the skull, denition, and postcranial skeleton. This problem is not unique to the study of endocranial characters. A similar situation exists when large amounts of molecular data are combined with a matrix of relatively few morphological characters. Differential character weighting is sometimes employed to downweight one group of characters relative to another (Felsenstein, 2004). For example, transitions and transversions are often weighted differently in analyses of DNA data (Felsenstein, 2004). Perhaps experimentation with differential weighting of distinctive anatomical character complexes in the Luo and Wible (2005) matrix will suggest that the endocranial characters are more informative for tree topology.

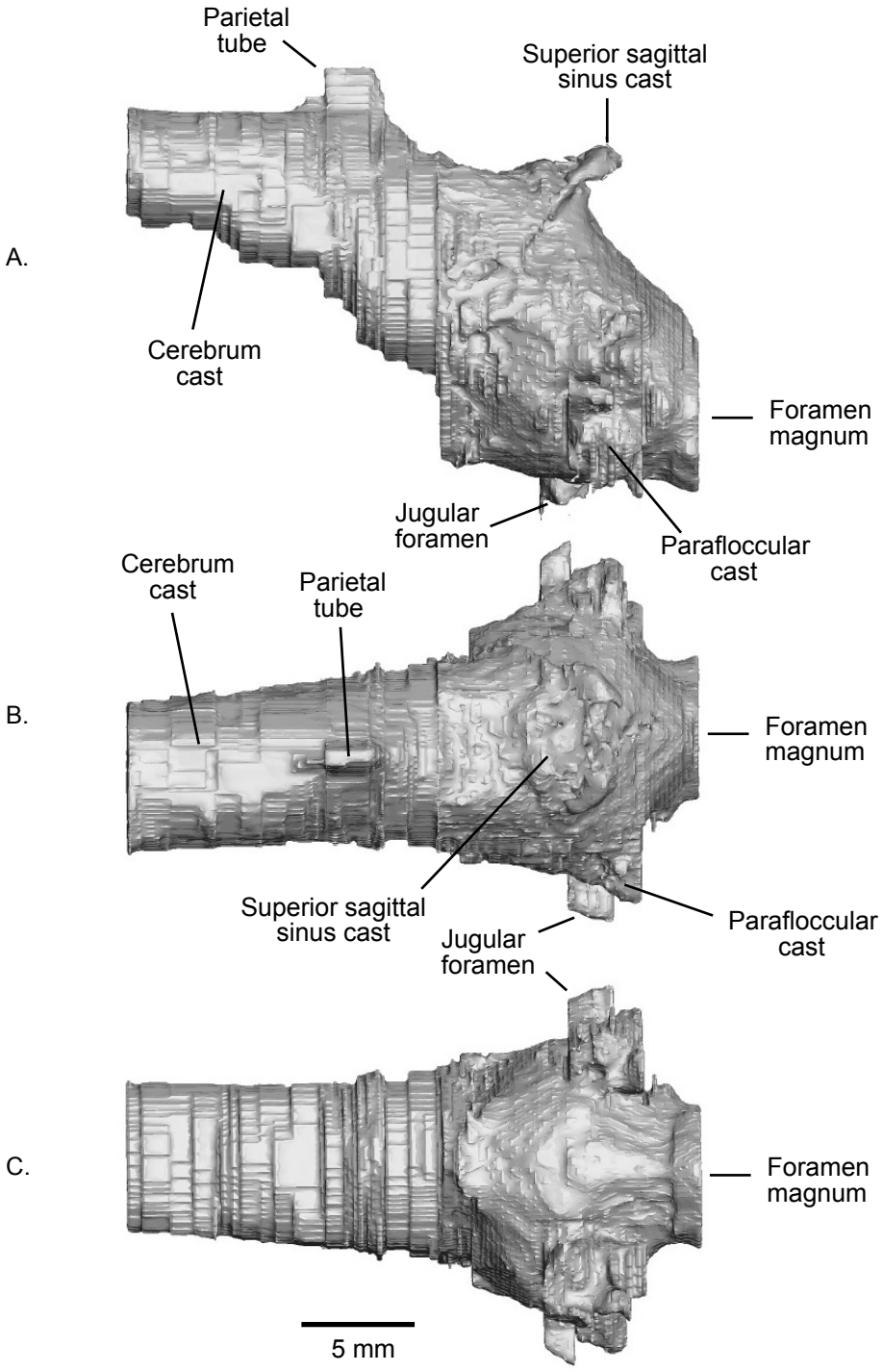


Figure 22. Digital rendering of the cranial endocast of a skull of *Thrinaxodon liorhinus* (UCMP 40466) shown in (A) left lateral, (B) dorsal, and (C) ventral views. The digital endocast was modified from data published in Rowe et al. (1995).

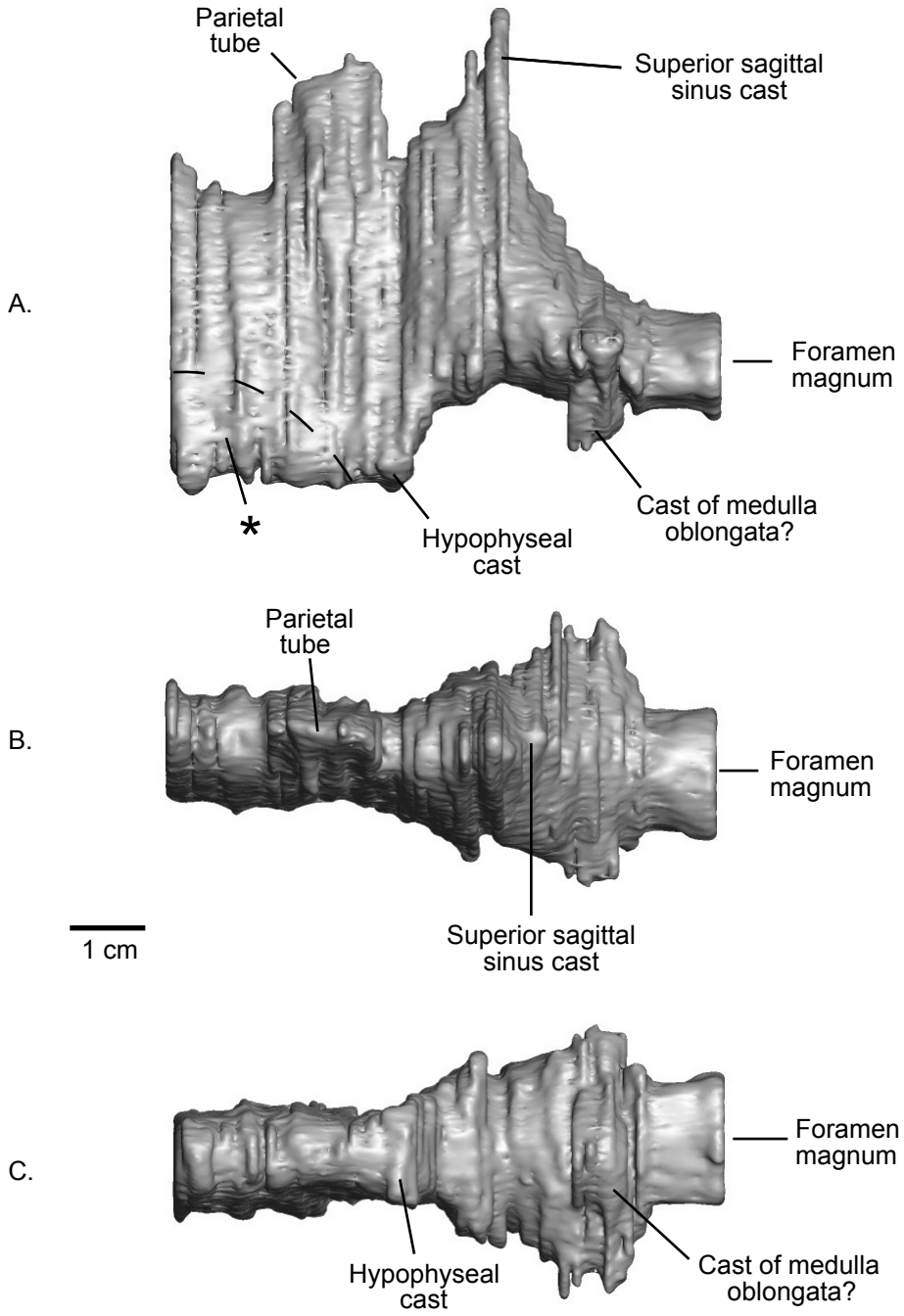


Figure 23. Digital rendering of the cranial endocast of a skull of *Diademodon* sp. (UCMP 42446) shown in (A) left lateral, (B) dorsal, and (C) ventral views. Abbreviation: "*" Represents unossified portion of skull anterior to the epipterygoid (Watson, 1911). This portion of the endocast was not filled by the brain (Watson, 1913), but the corresponding lateral opening in the skull probably transmitted cranial nerves II, III, IV, V-1, and VI (Watson, 1911).

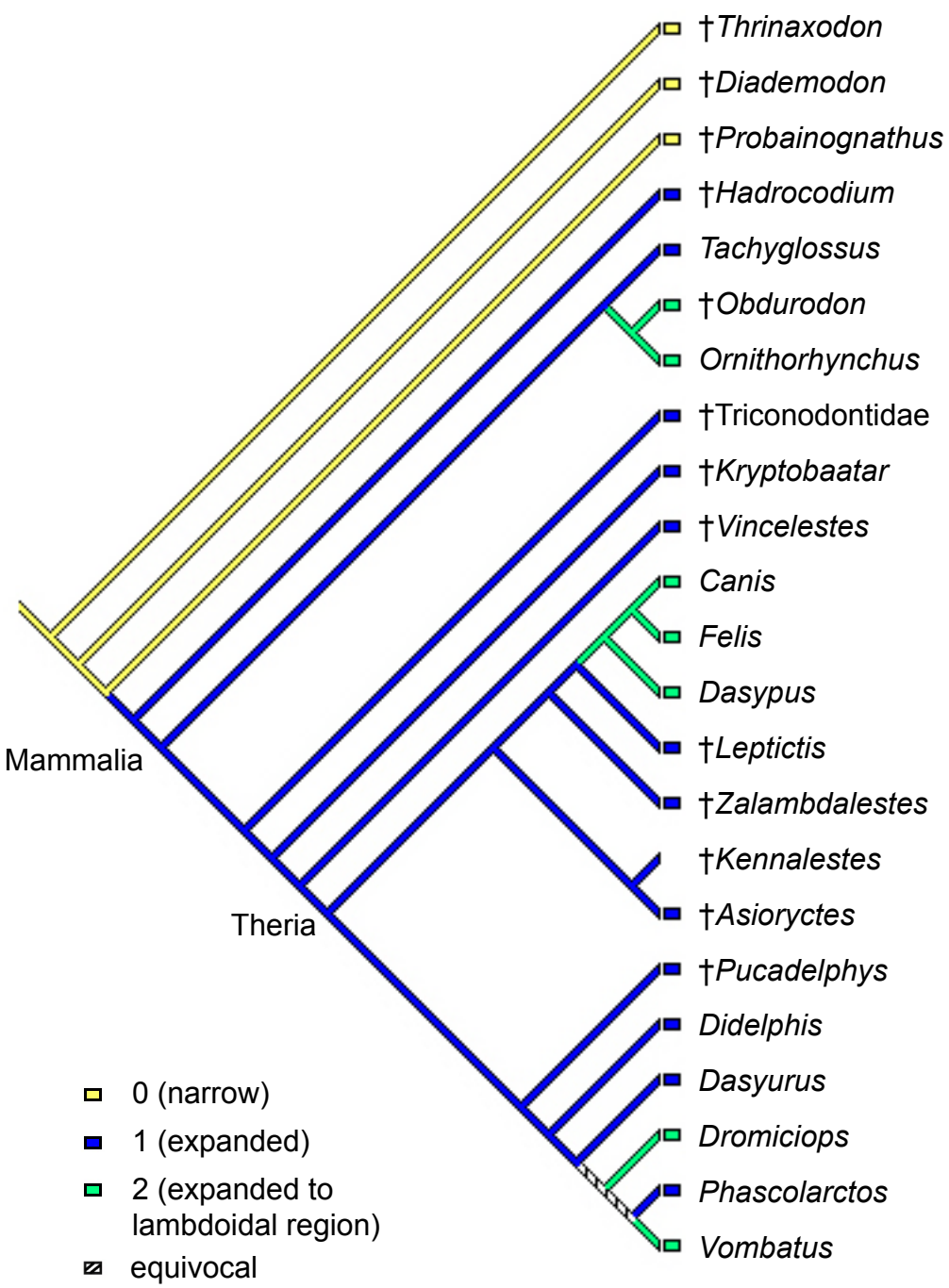


Figure 24. Character 1 (relative expansion of braincase in parietal region) optimized on a pruned version of the strict consensus tree of Luo and Wible (2005).

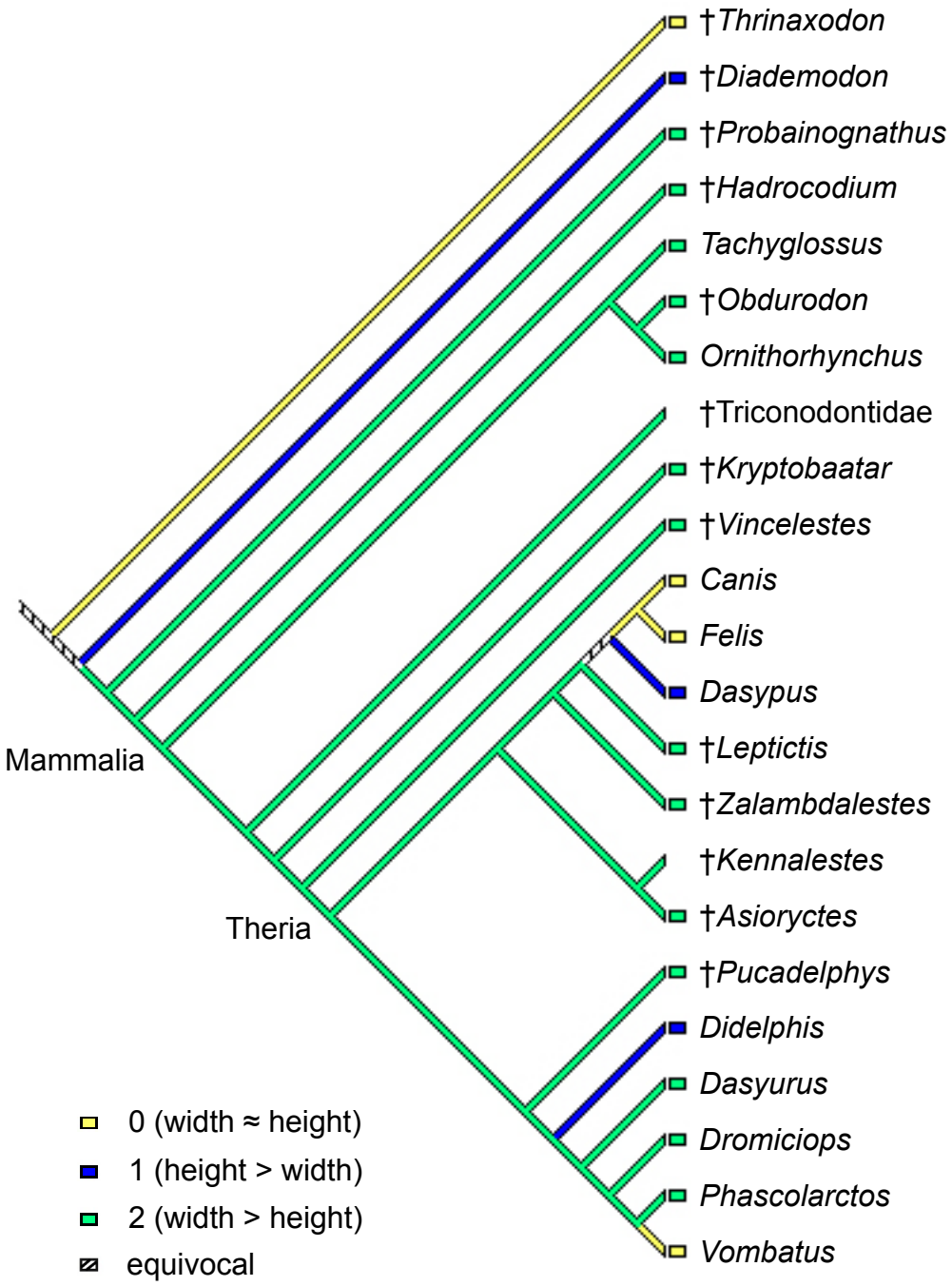


Figure 25. Character 4 (height/width aspect ratio of endocast) optimized on a pruned version of the strict consensus tree of Luo and Wible (2005).

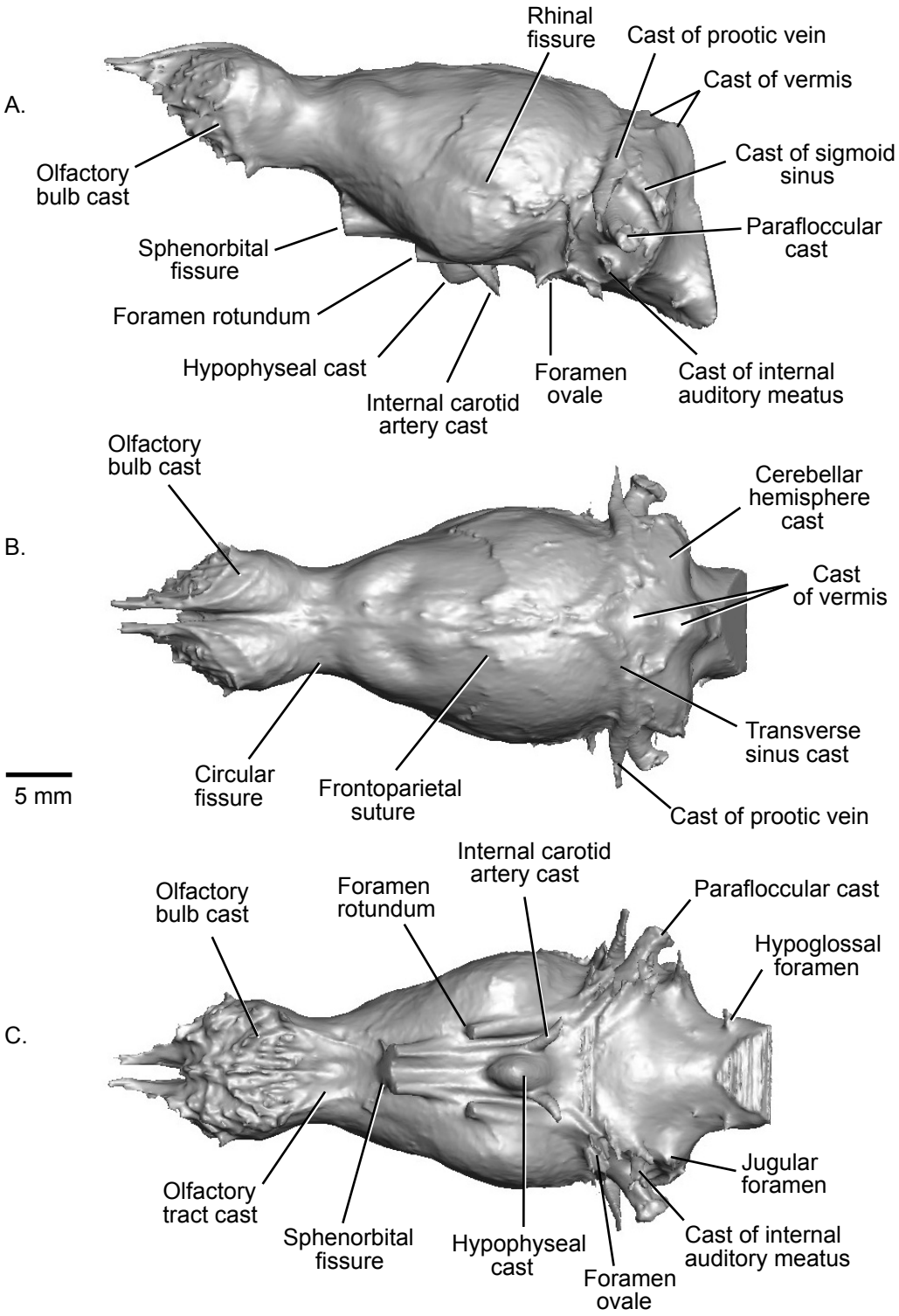


Figure 26. Digital rendering of the cranial endocast of *Didelphis virginiana* (TMM M-2517) shown in (A) left lateral, (B) dorsal, and (C) ventral views.

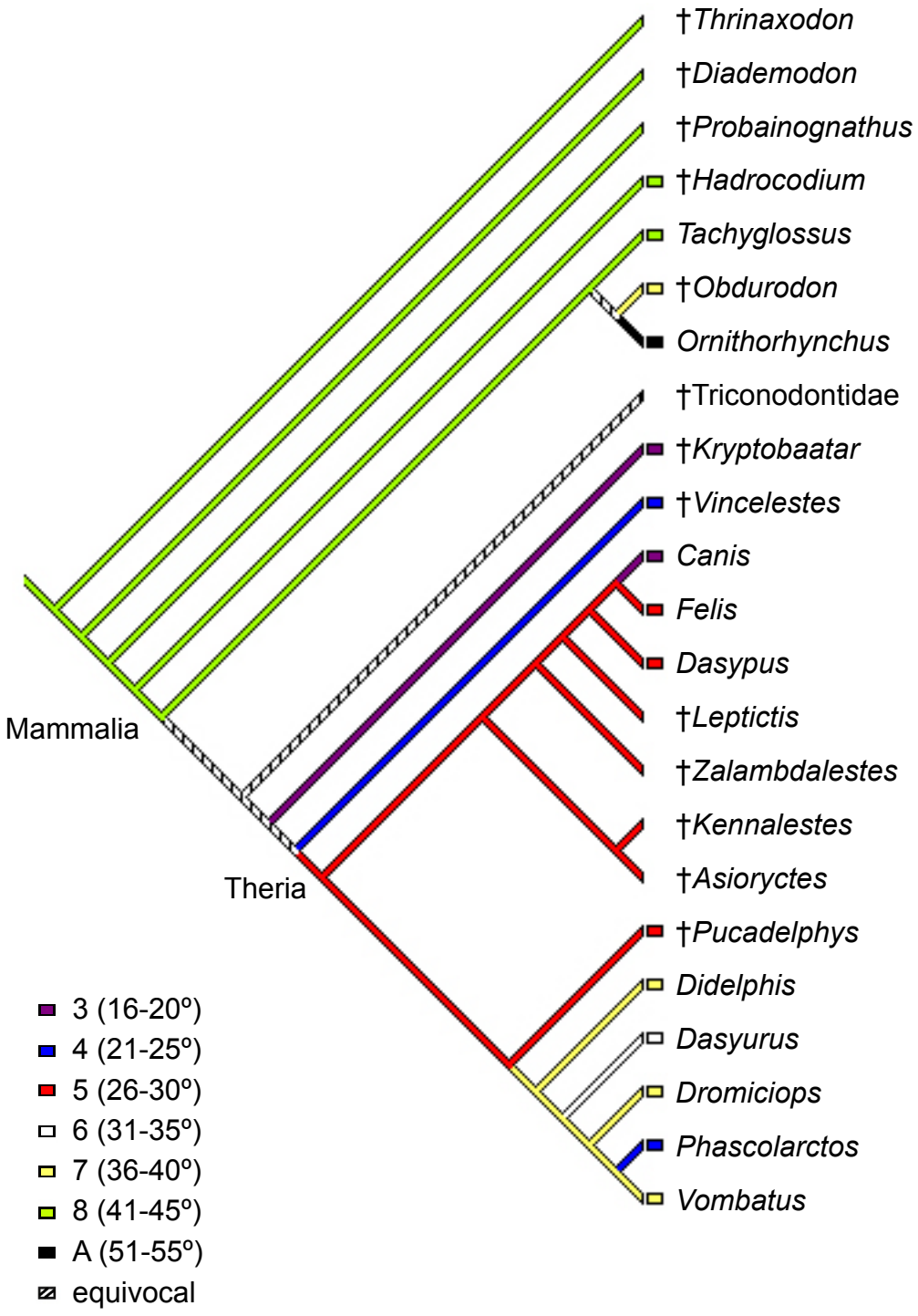


Figure 27. Character 6.1 (endocast flexure) optimized on a pruned version of the strict consensus tree of Luo and Wible (2005).

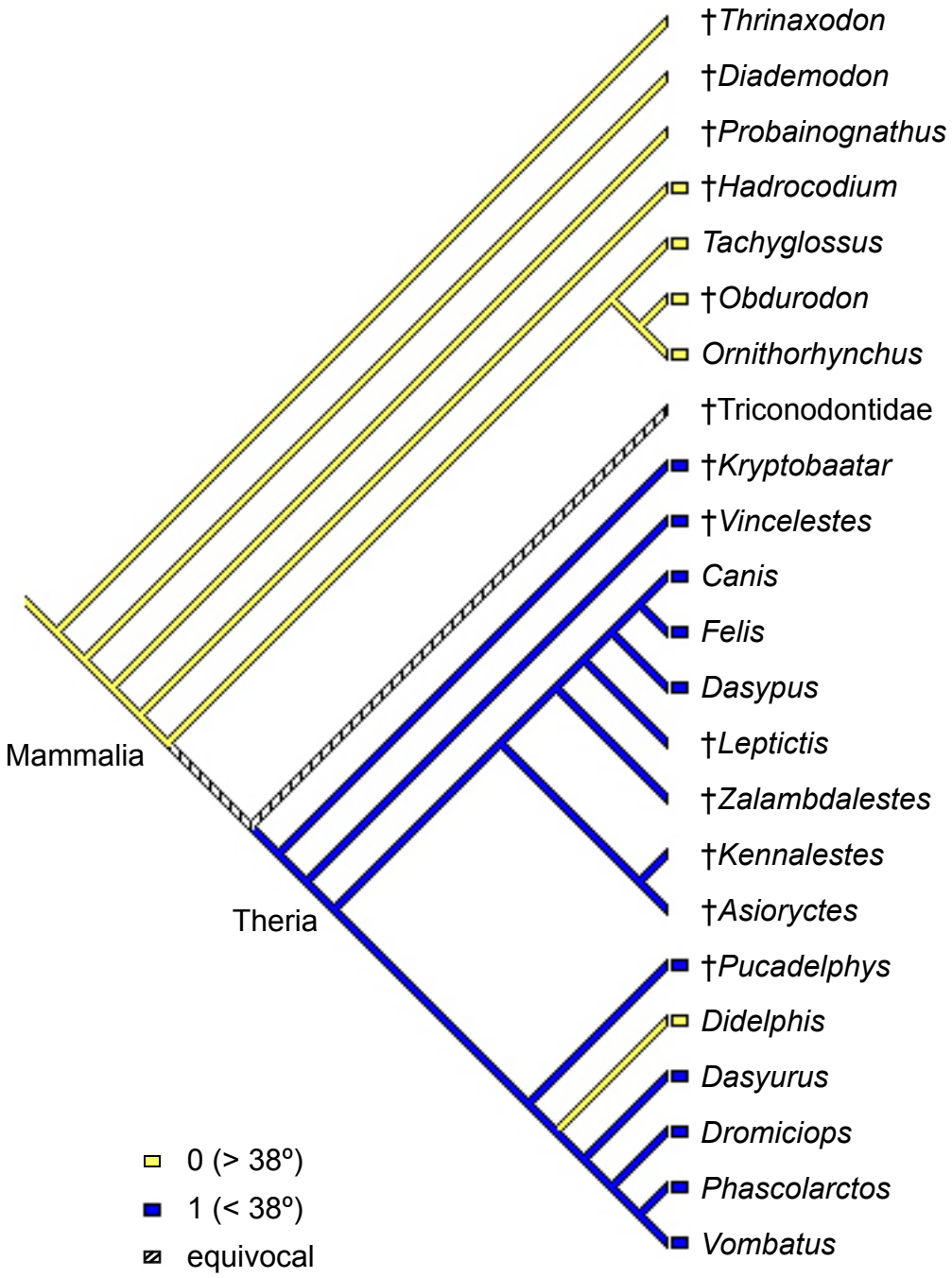


Figure 28. Character 6.2 (endocast flexure) optimized on a pruned version of the strict consensus tree of Luo and Wible (2005).

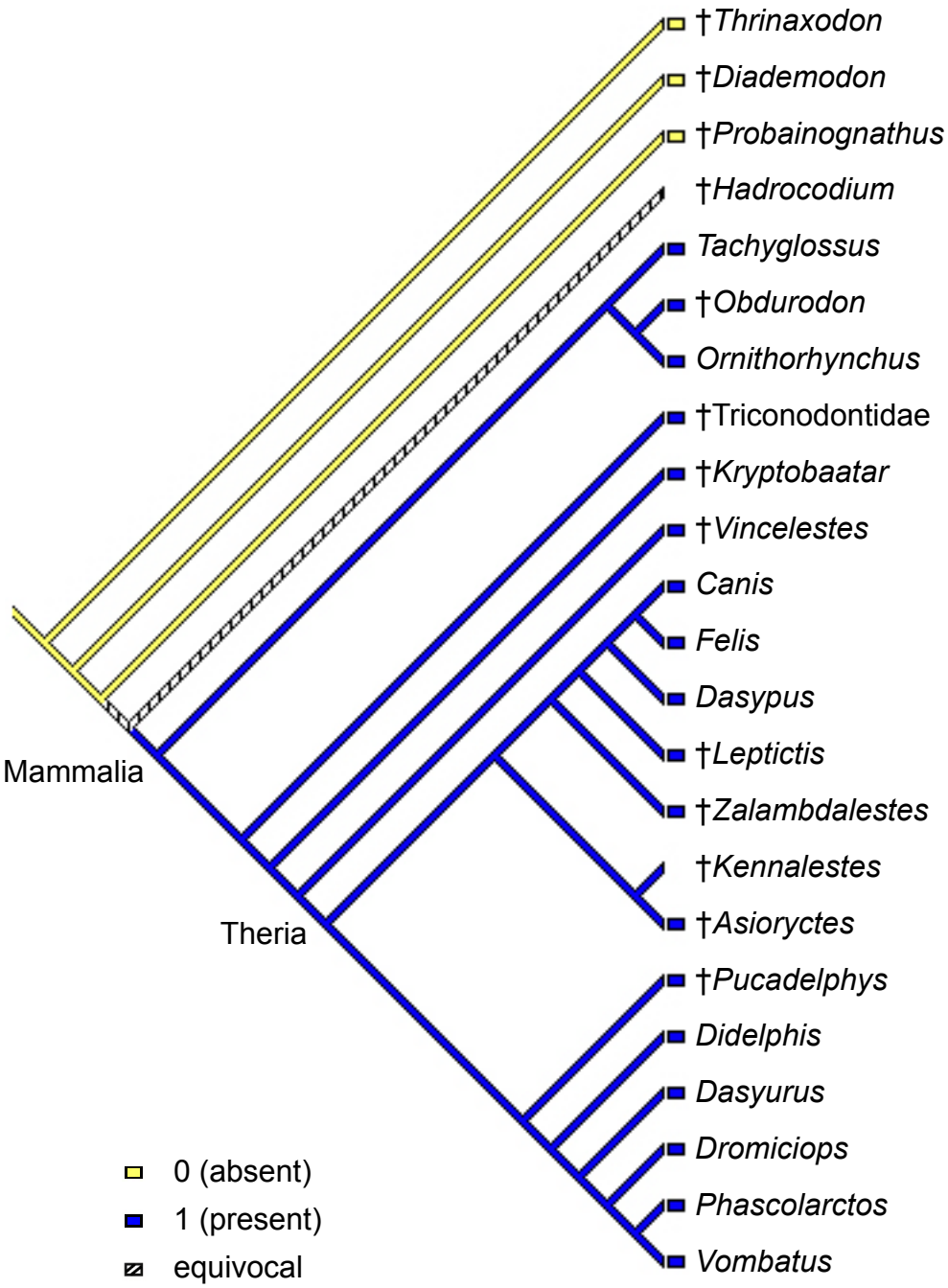


Figure 29. Character 8 (presence or absence of ossified cribriform plate) optimized on a pruned version of the strict consensus tree of Luo and Wible (2005).

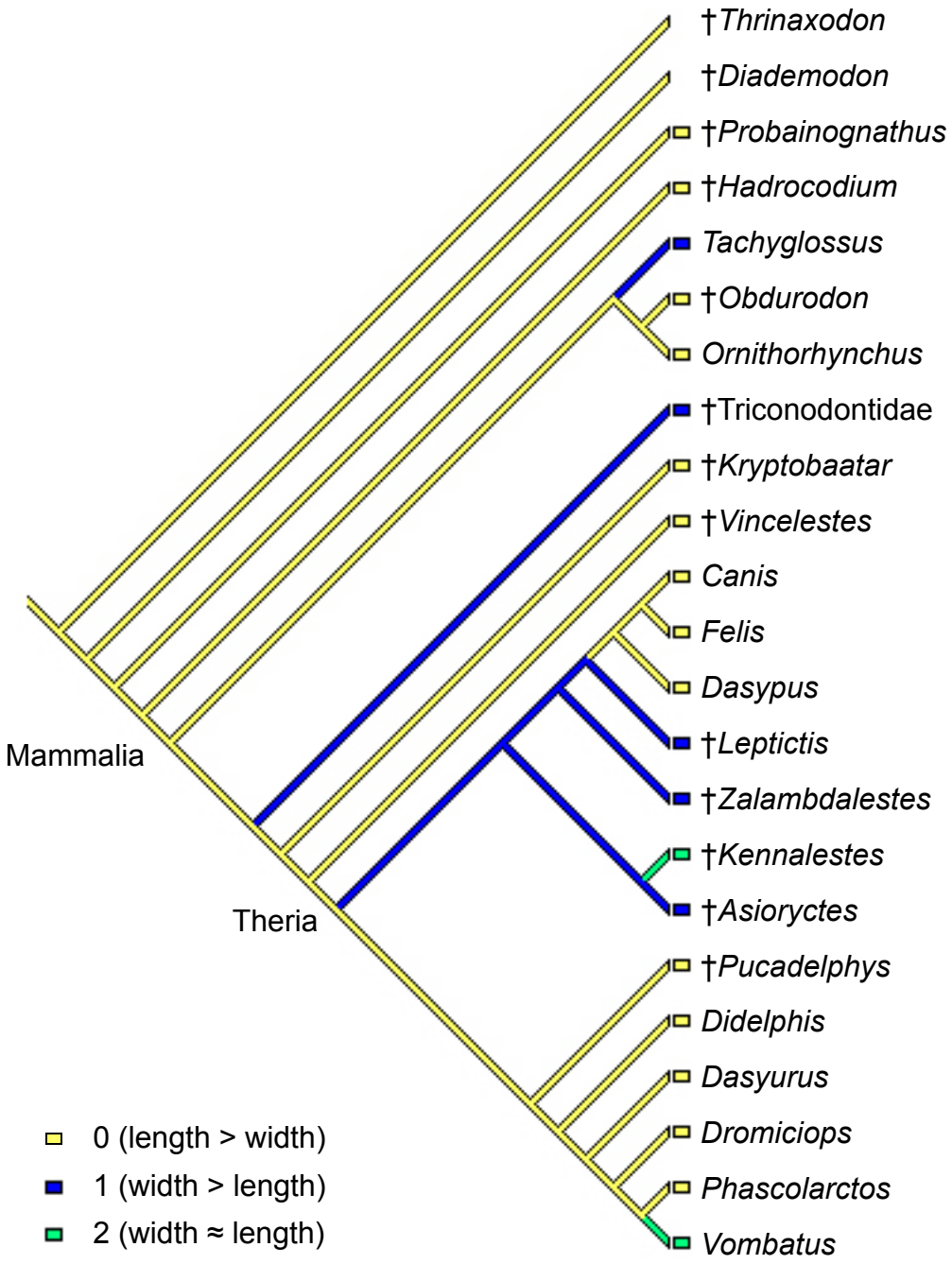


Figure 30. Character 9 (olfactory bulb cast width/length aspect ratio) optimized on a pruned version of the strict consensus tree of Luo and Wible (2005).

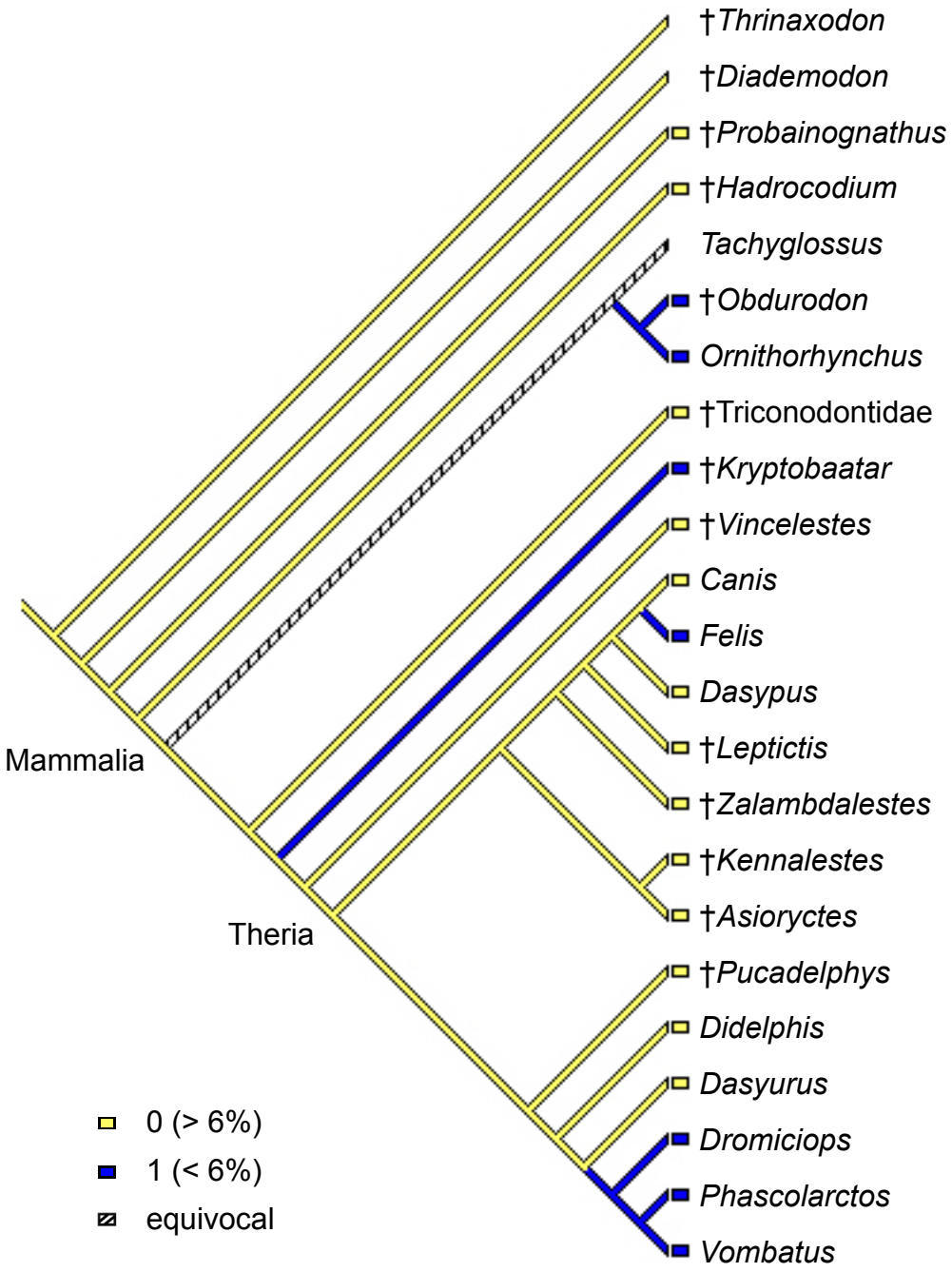


Figure 31. Character 10.2 (% endocast composed by olfactory bulb casts) optimized on a pruned version of the strict consensus tree of Luo and Wible (2005).

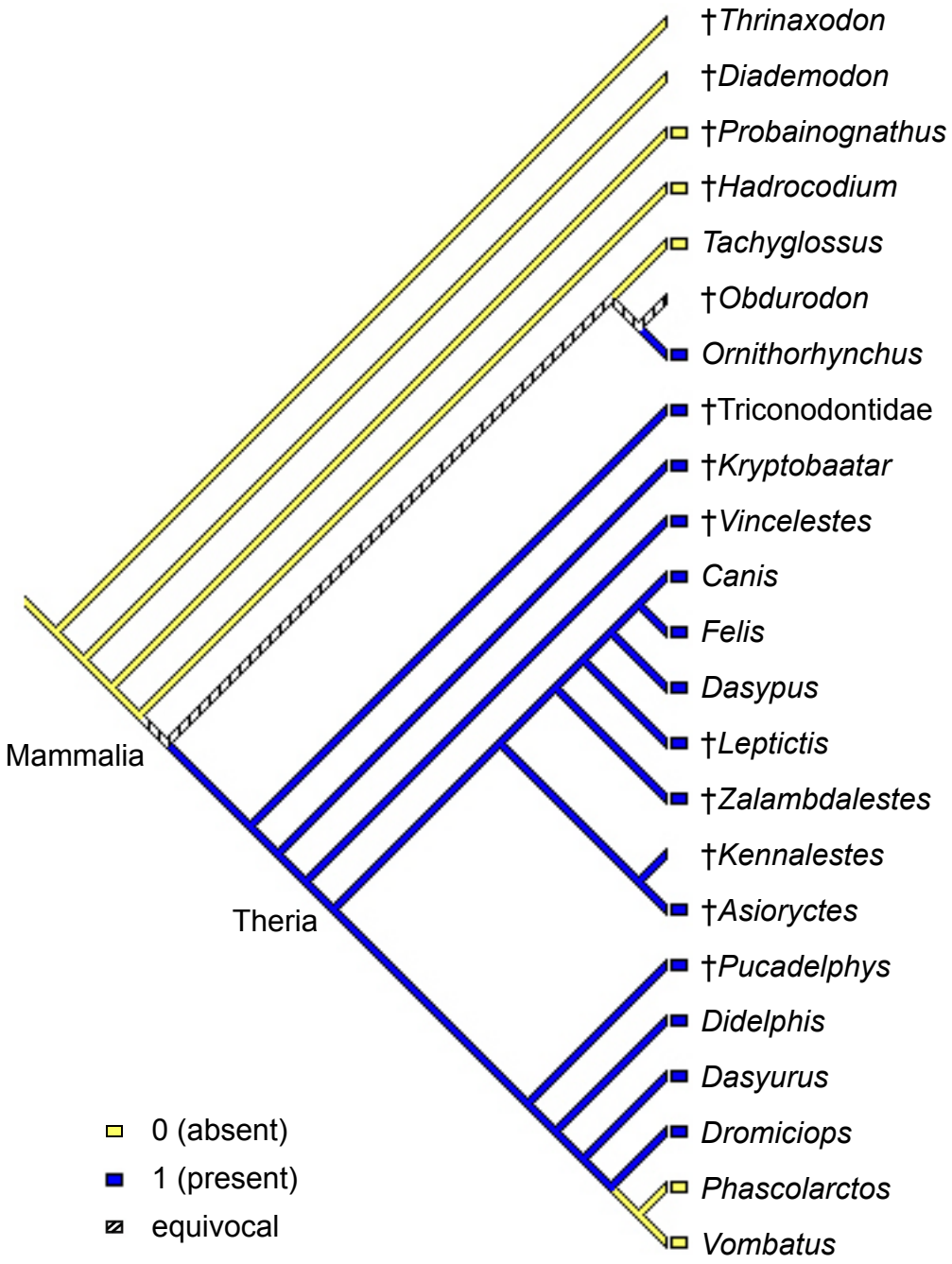


Figure 32. Character 11 (circular fissure: present or absent on endocast) optimized on a pruned version of the strict consensus tree of Luo and Wible (2005).

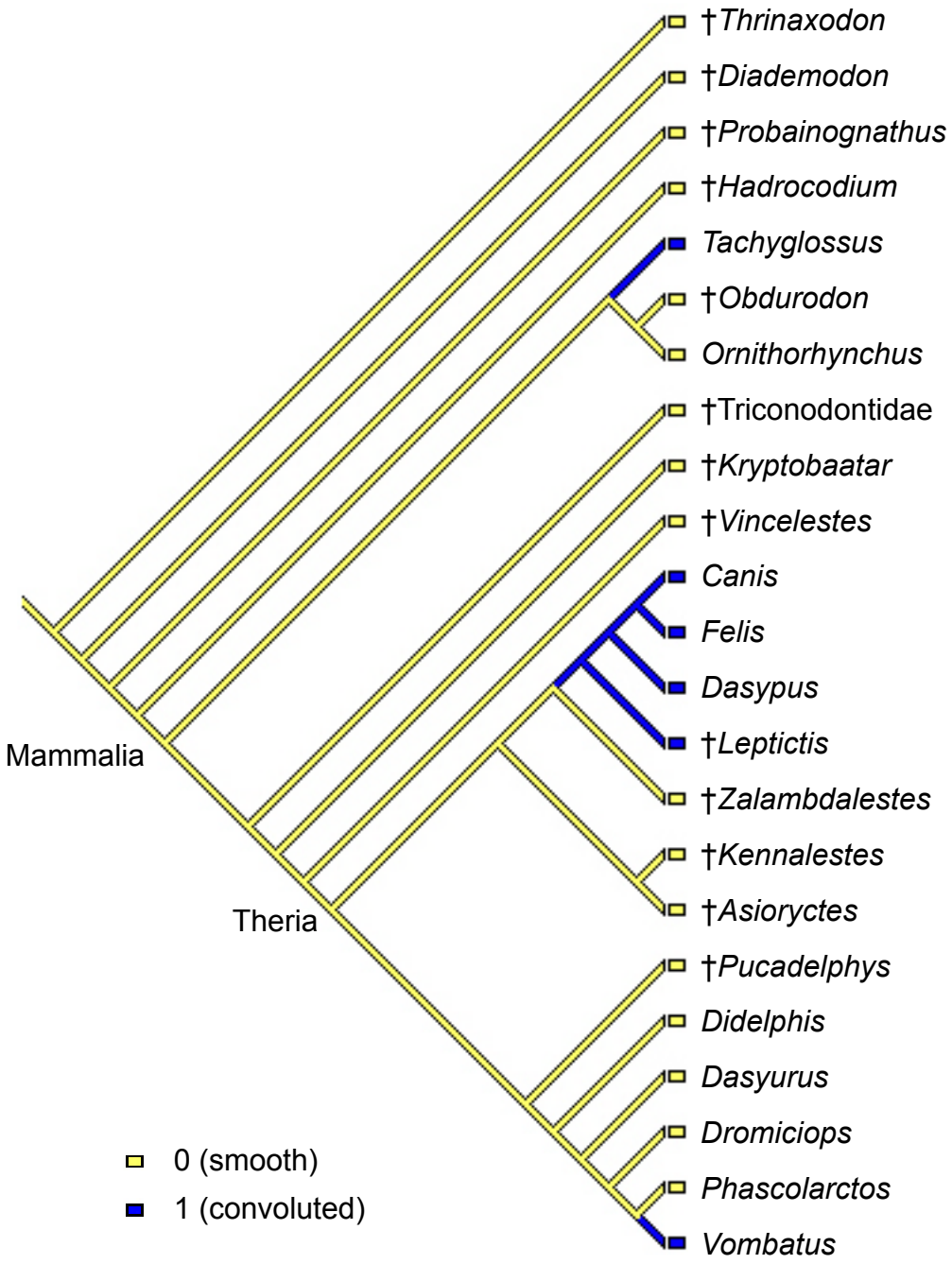


Figure 33. Character 13 (cerebral hemisphere casts: smooth or convoluted) optimized on a pruned version of the strict consensus tree of Luo and Wible (2005).

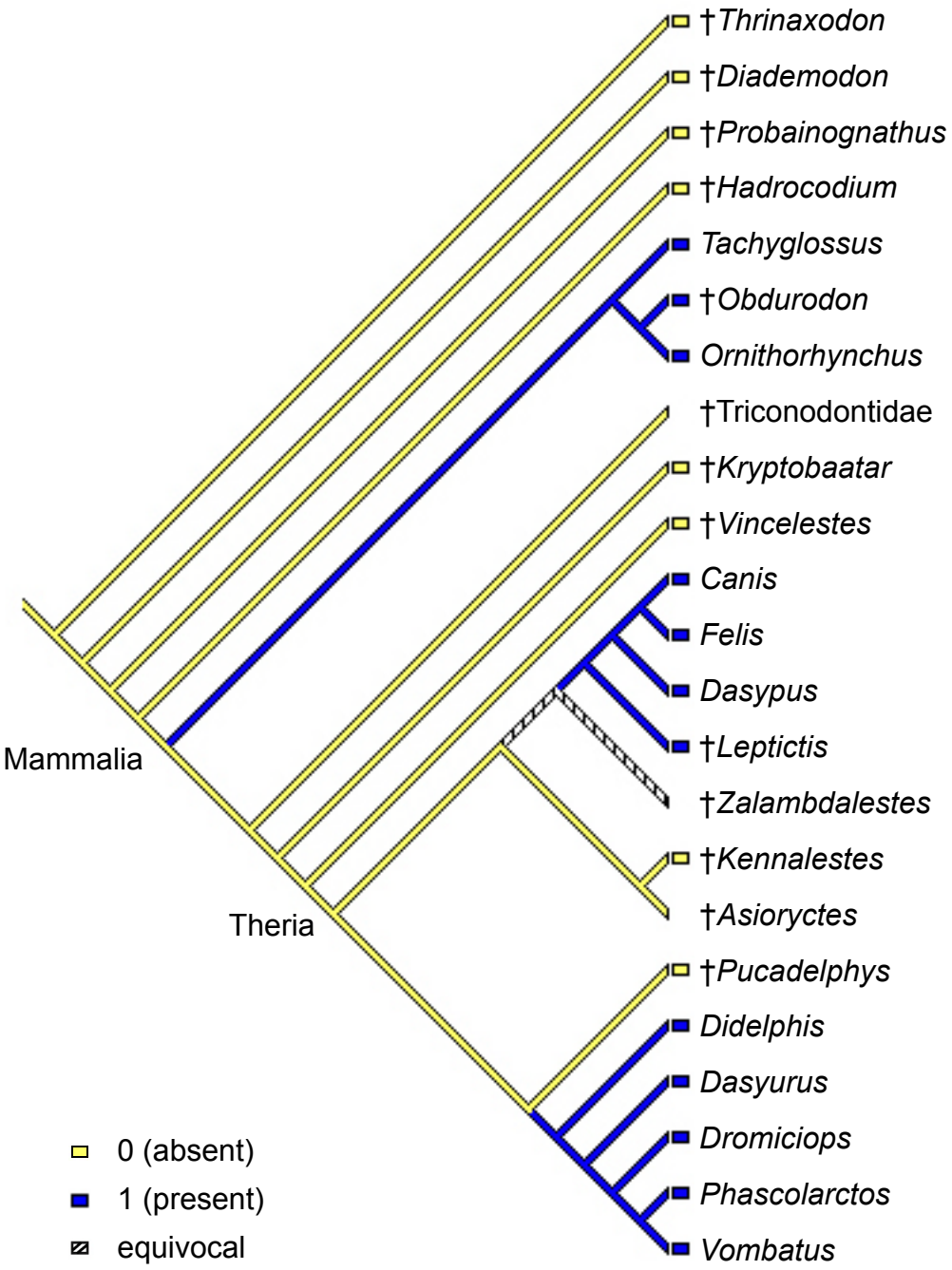


Figure 34. Character 14 (rhinal fissure on endocast: present or absent) optimized on a pruned version of the strict consensus tree of Luo and Wible (2005).

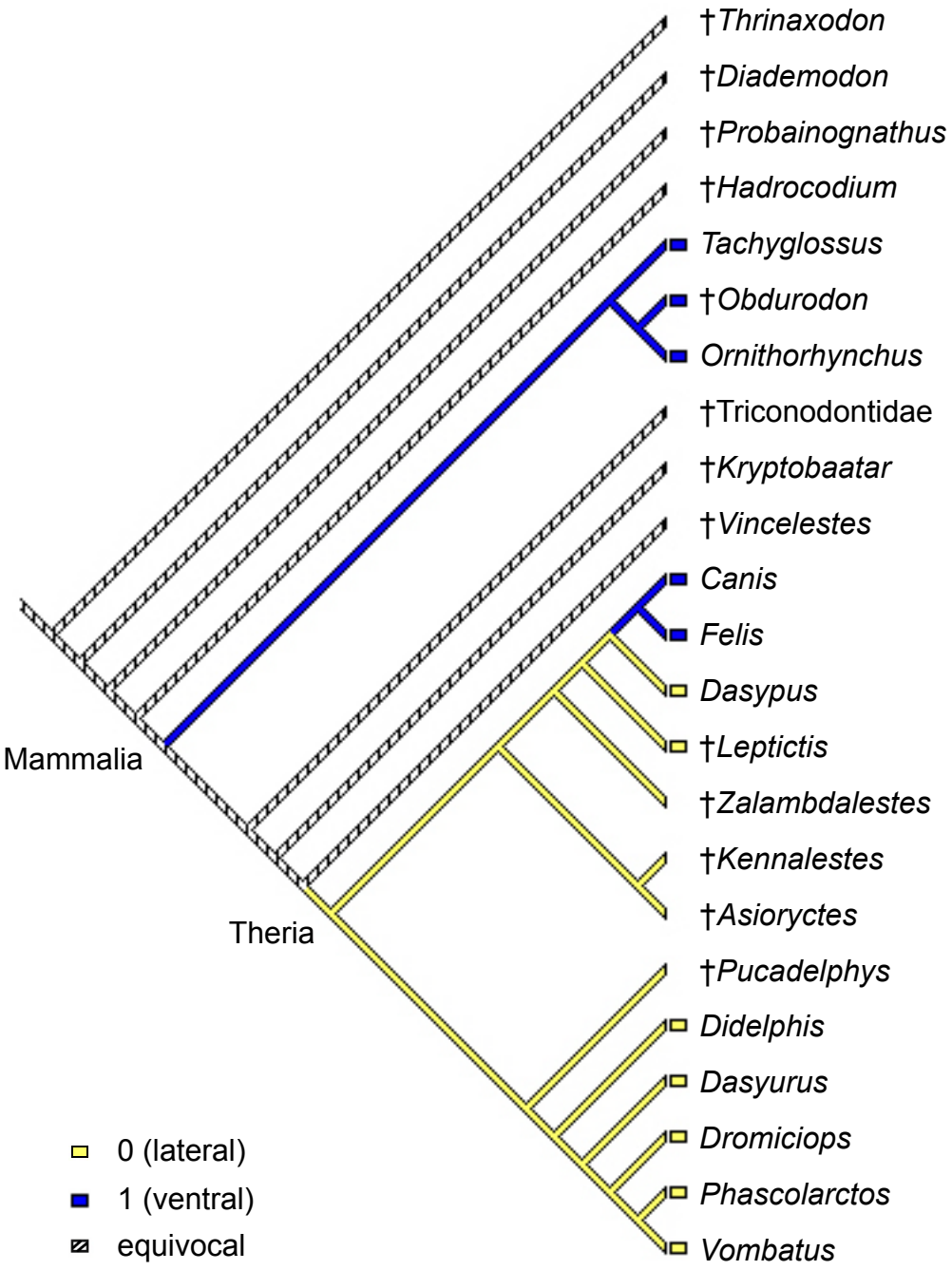


Figure 35. Character 15 (rhinal fissure on lateral wall or ventrum of endocast) optimized on a pruned version of the strict consensus tree of Luo and Wible (2005).

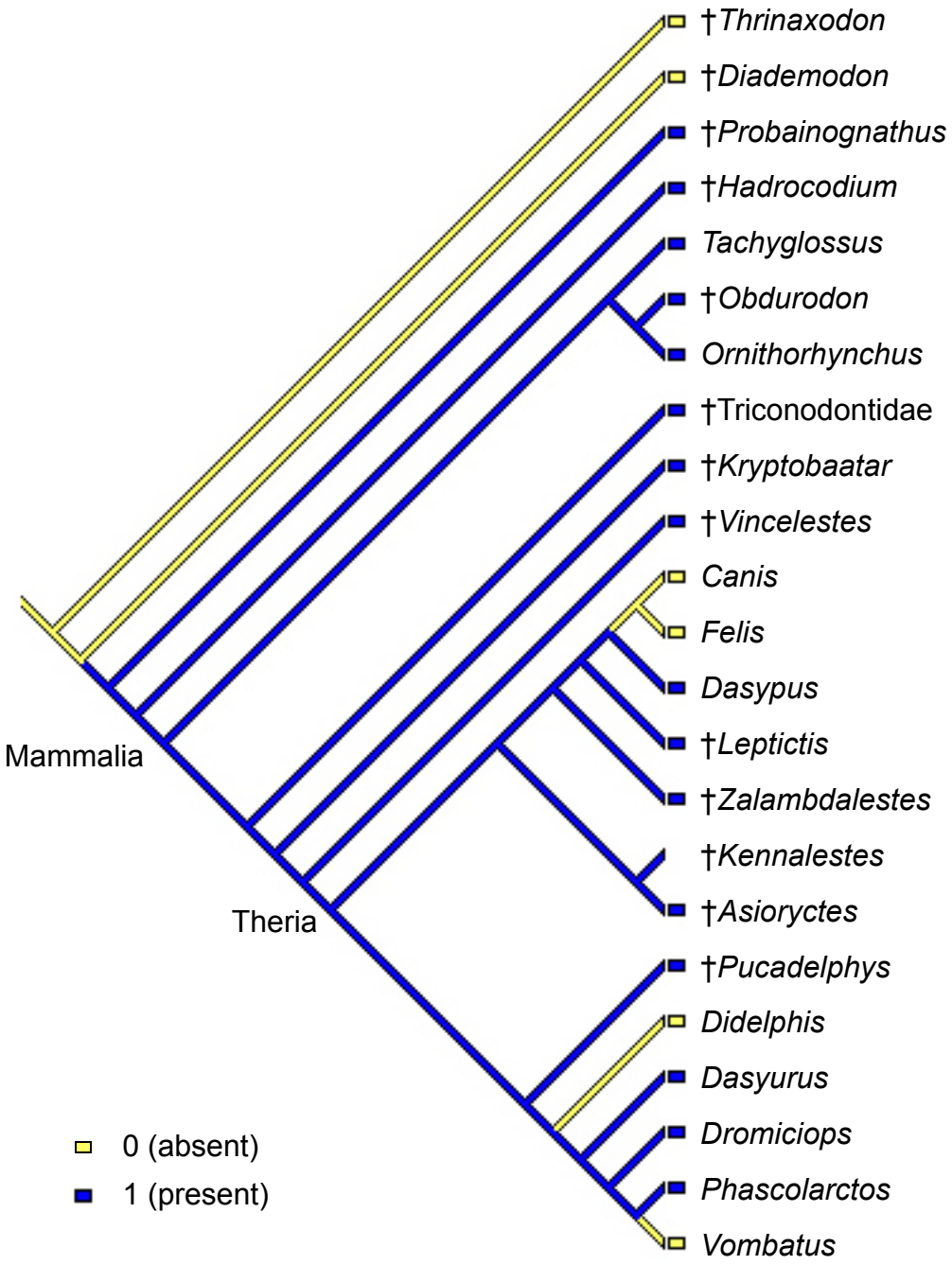


Figure 36. Character 16 (median sulcus present or absent on endocast) optimized on a pruned version of the strict consensus tree of Luo and Wible (2005).

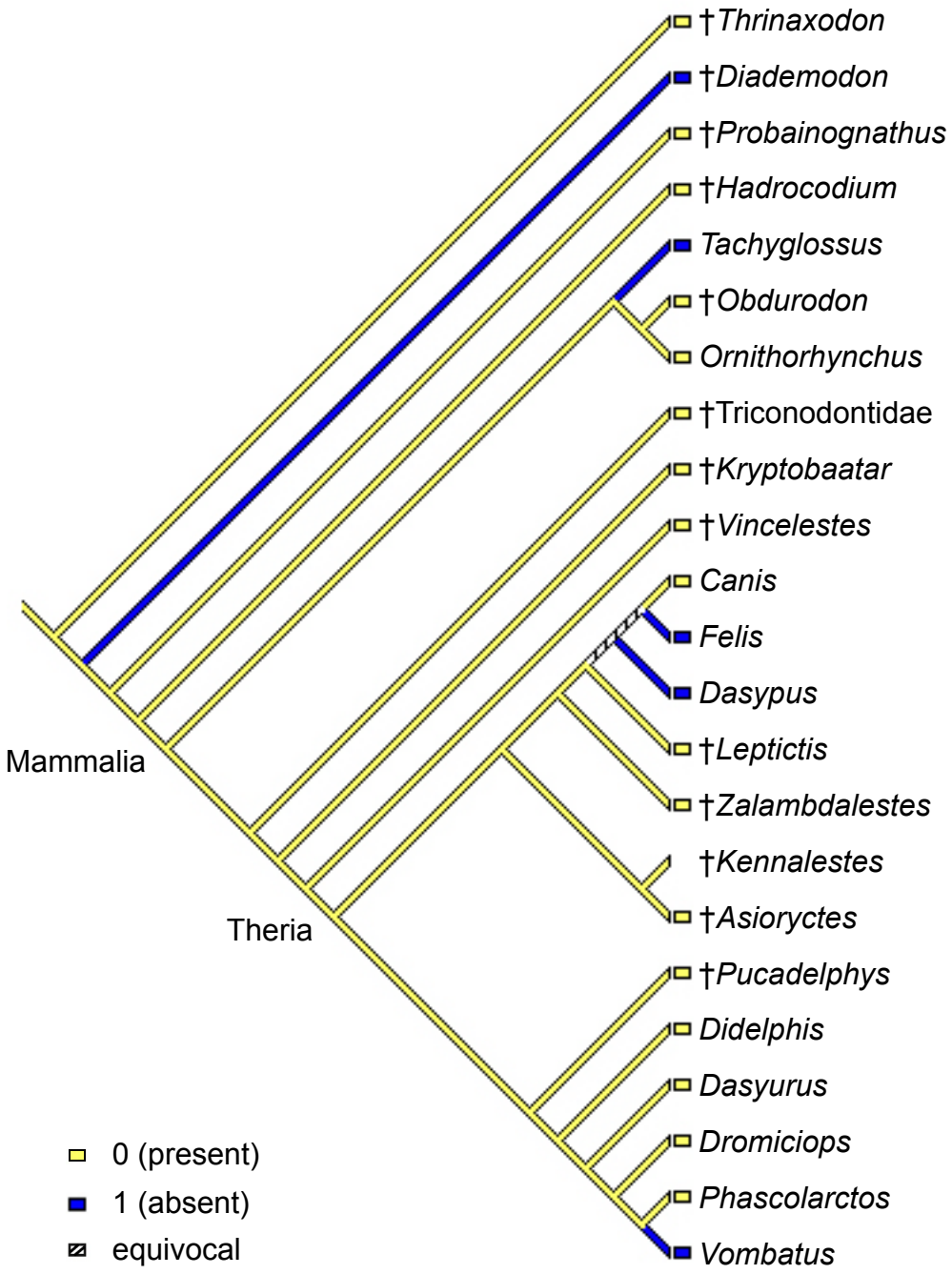


Figure 37. Character 18 (paraflocculi present or absent on endocast) optimized on a pruned version of the strict consensus tree of Luo and Wible (2005).

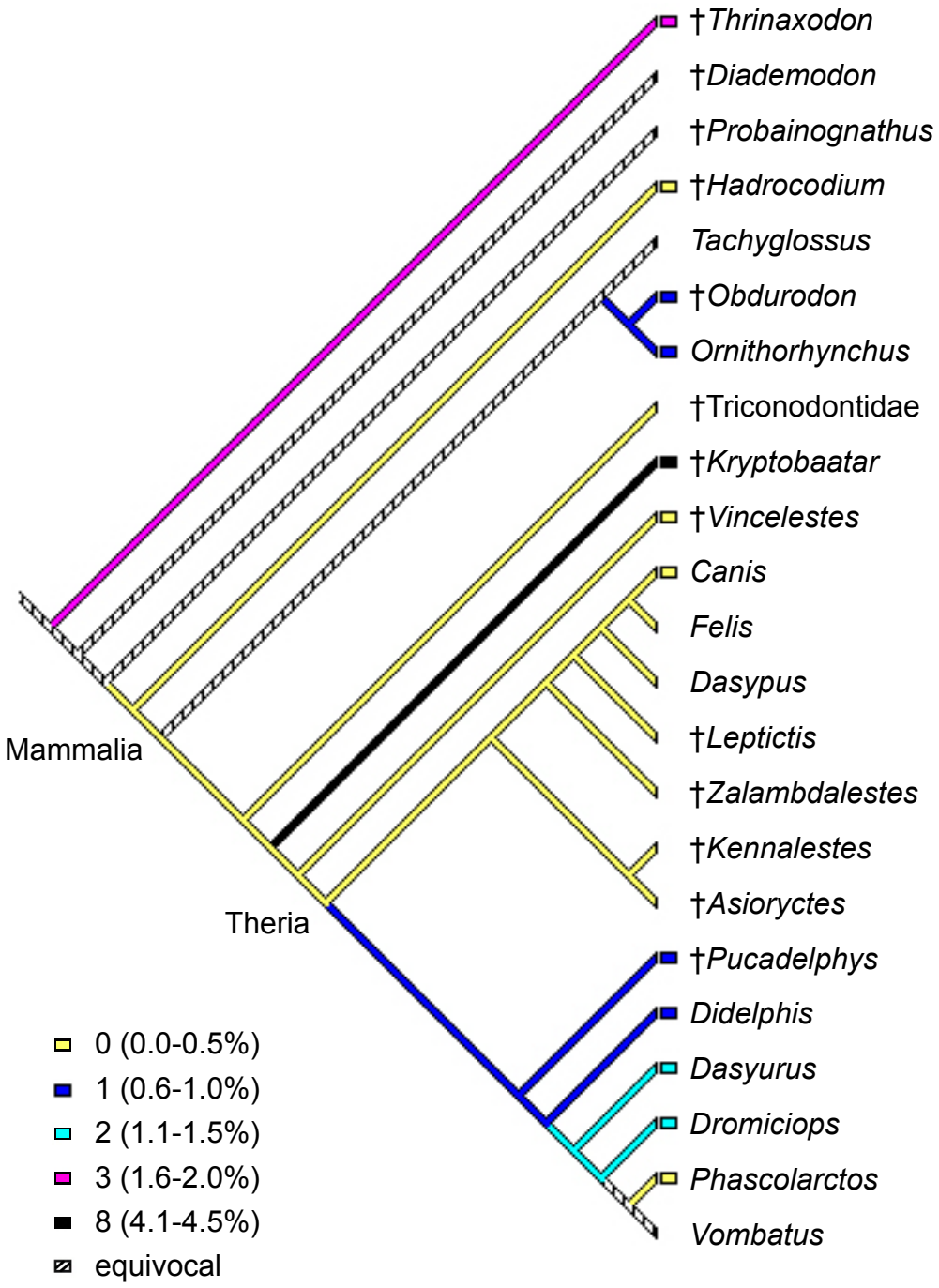


Figure 38. Character 19.1 (% endocast composed by parafloccular casts) optimized on a pruned version of the strict consensus tree of Luo and Wible (2005).

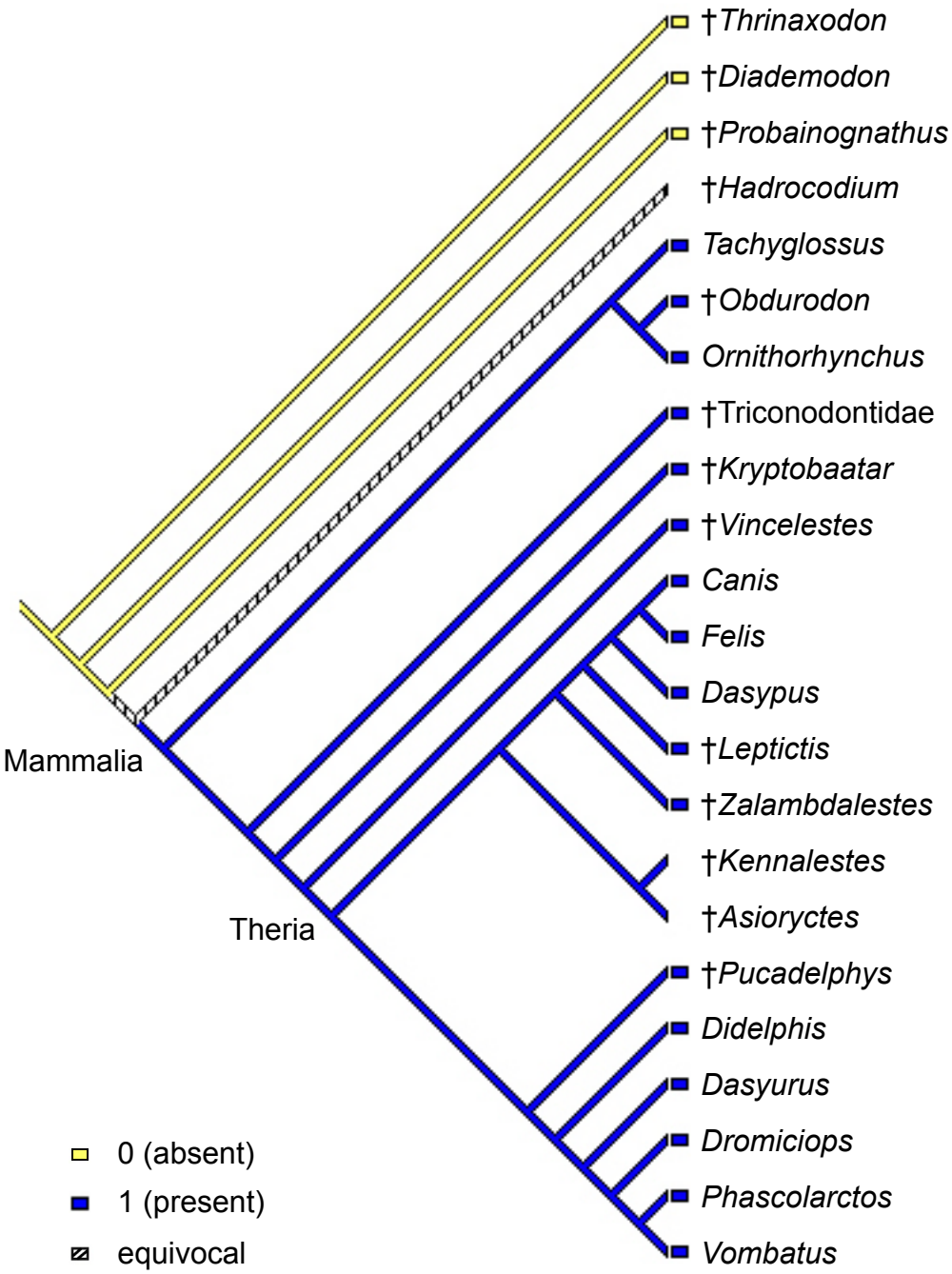


Figure 39. Character 20 (vermis present or absent on endocast) optimized on a pruned version of the strict consensus tree of Luo and Wible (2005).

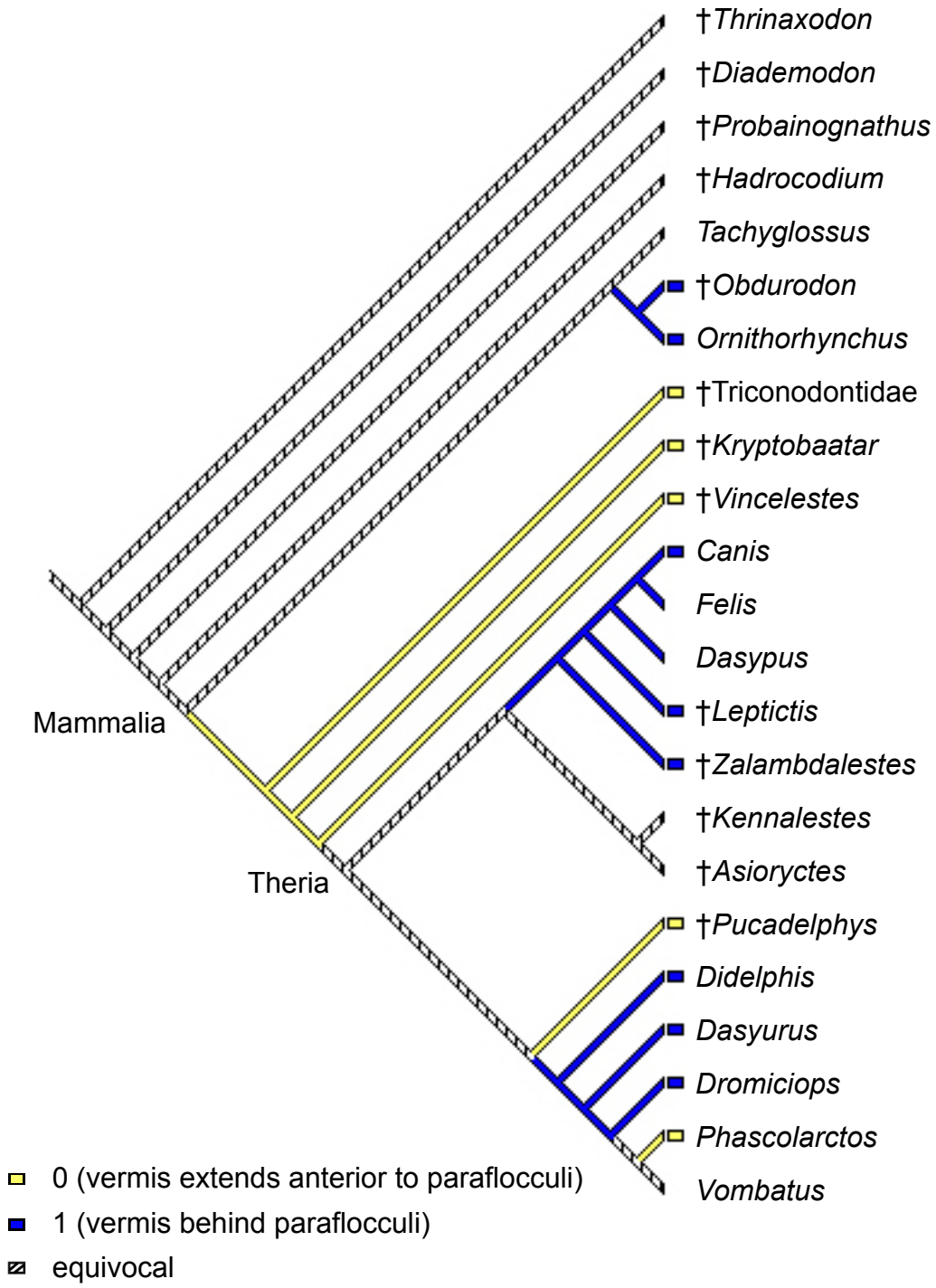


Figure 40. Character 21 (cast of vermis anterior extent) optimized on a pruned version of the strict consensus tree of Luo and Wible (2005).

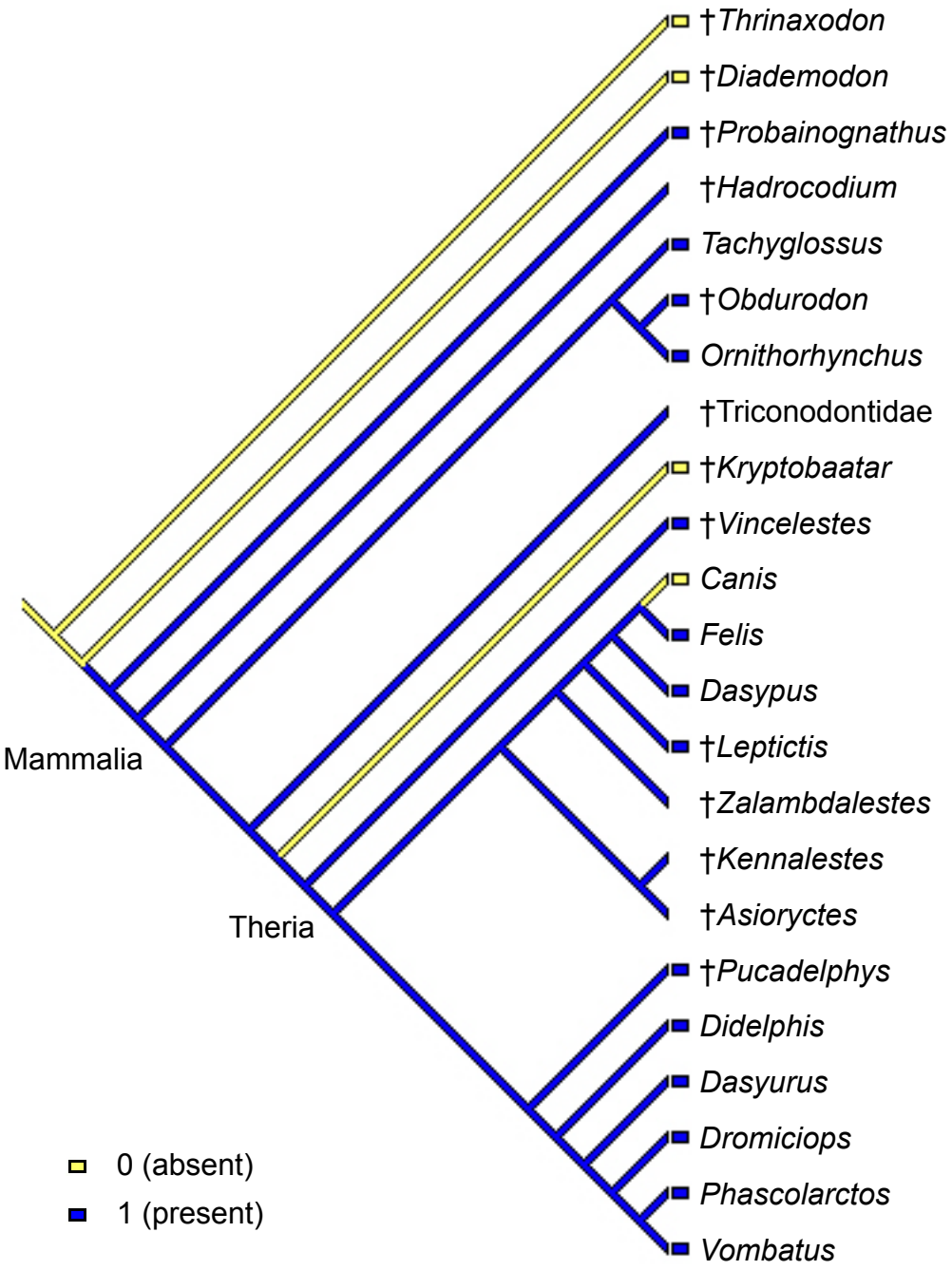


Figure 41. Character 22 (cerebellar hemispheres on endocast) optimized on a pruned version of the strict consensus tree of Luo and Wible (2005).

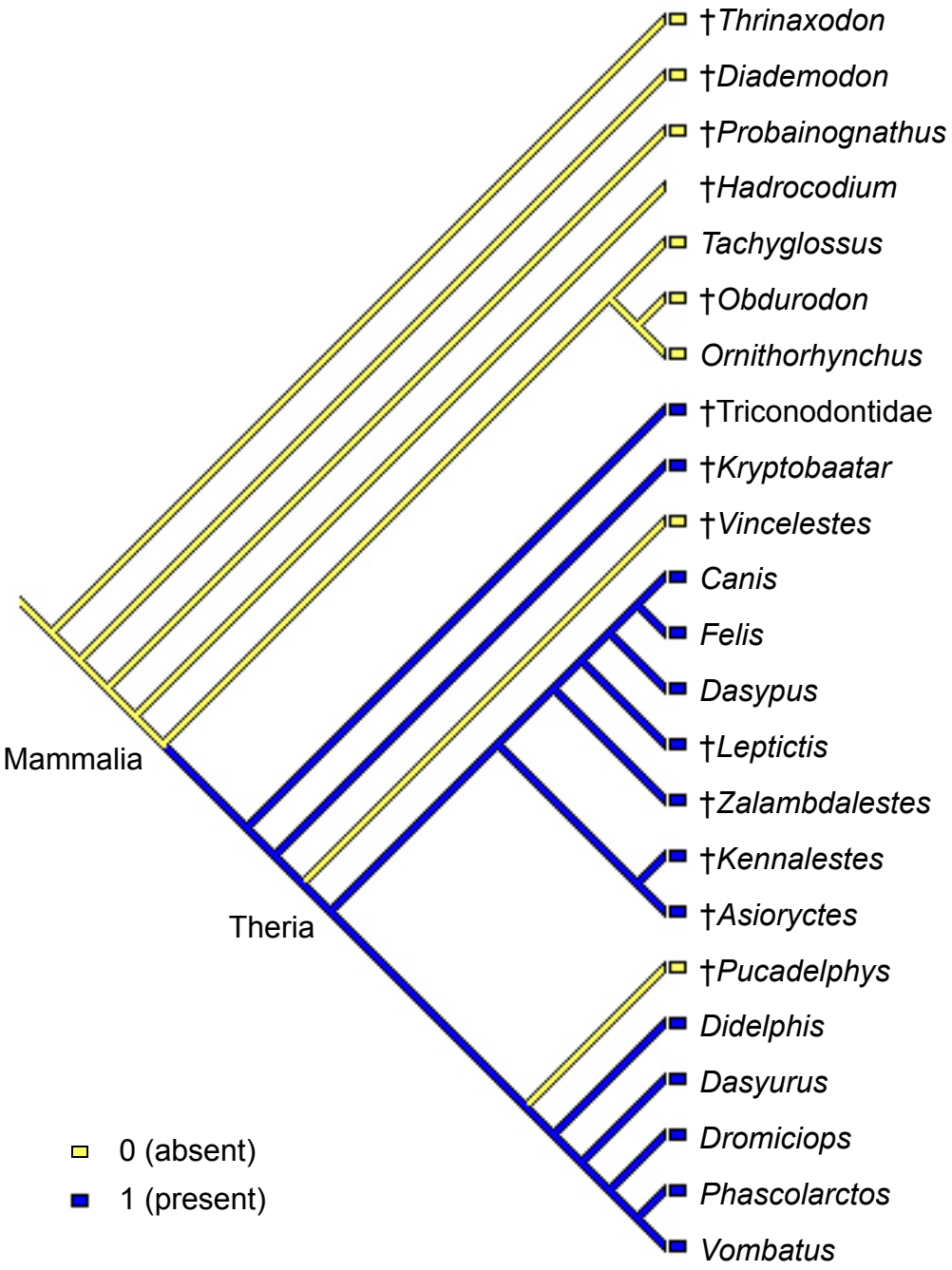


Figure 42. Character 25 (transverse sinus canal presence or absence on endocast) optimized on a pruned version of the strict consensus tree of Luo and Wible (2005).

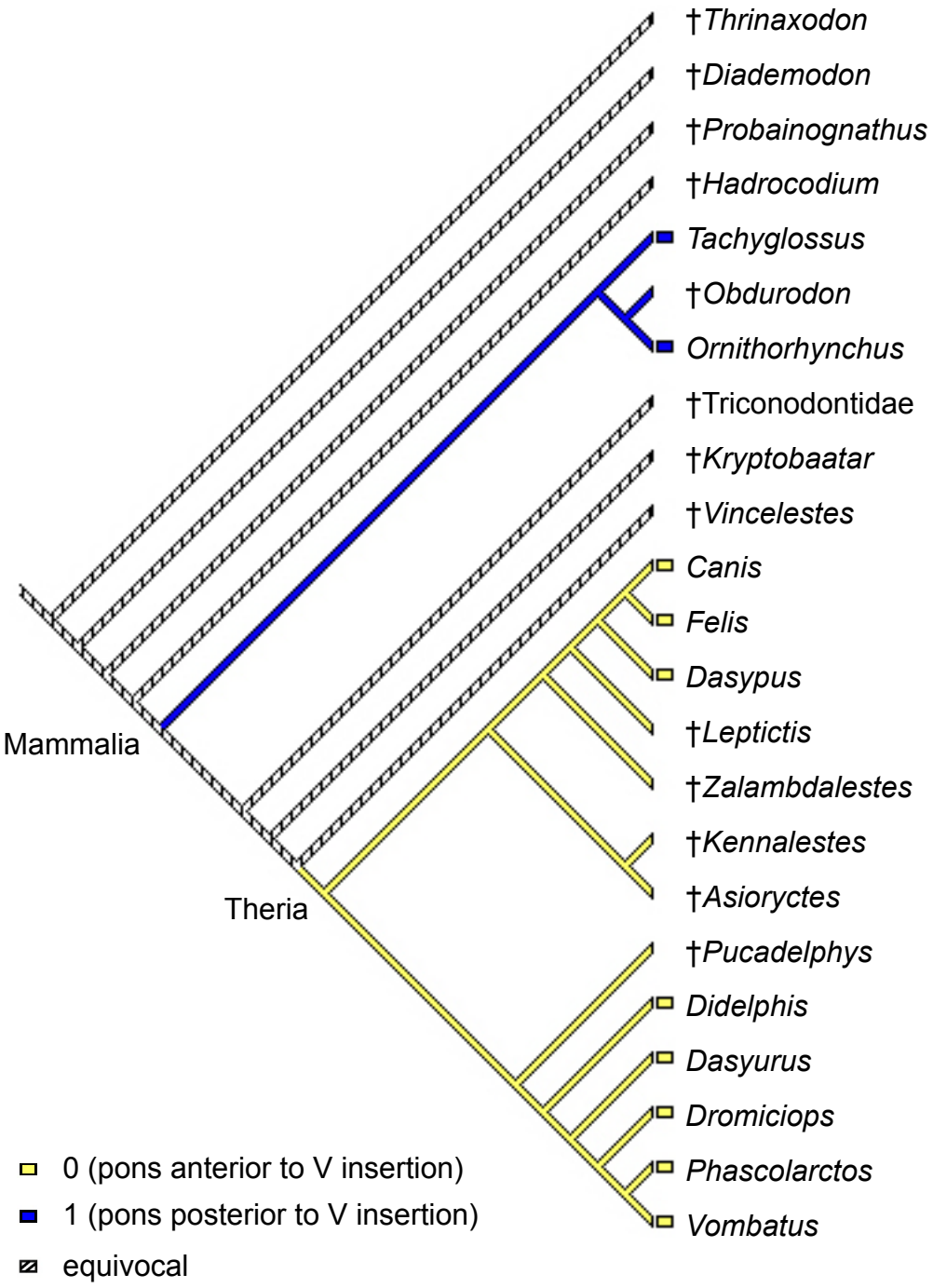


Figure 43. Character 28 (position of pons relative to insertion of nerve V) optimized on a pruned version of the strict consensus tree of Luo and Wible (2005).

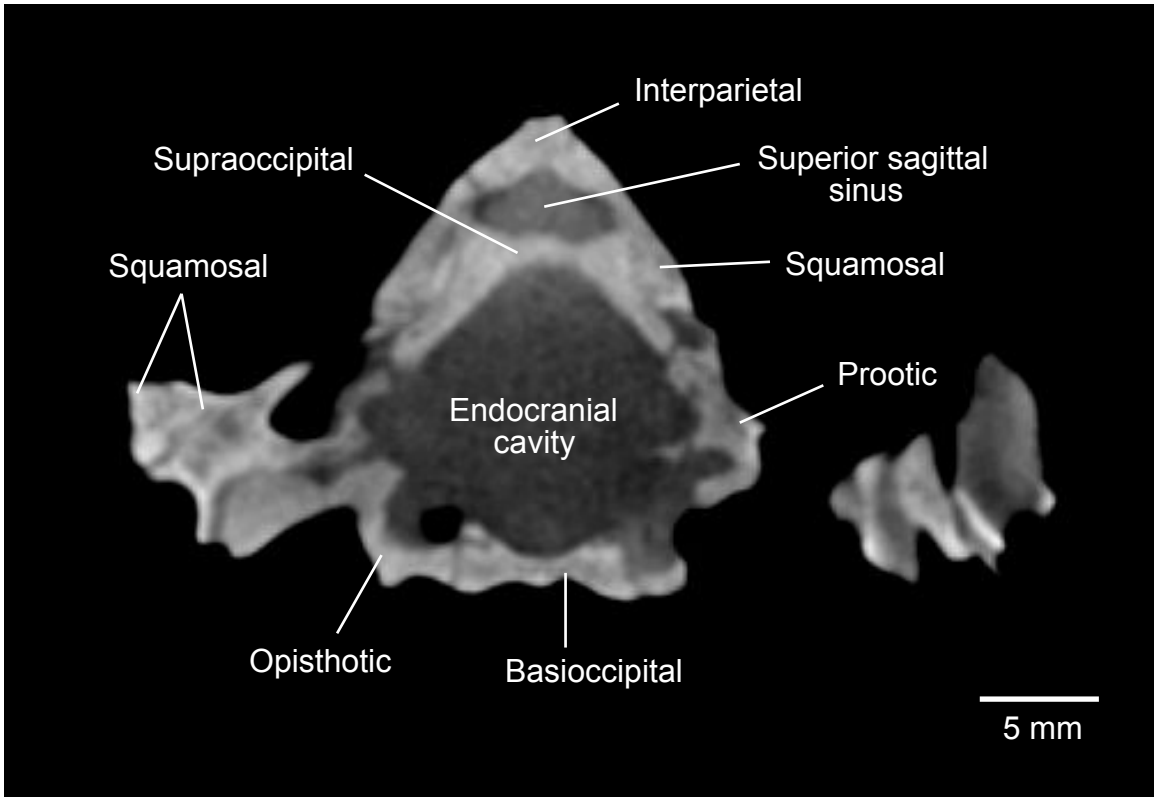


Figure 44. Coronal CT slice #035 through skull of *Thrinaxodon liorhinus* (UCMP 40466) showing the bony boundary between the superior sagittal sinus and endocranial cavity. Image modified from Rowe et al. (1995).

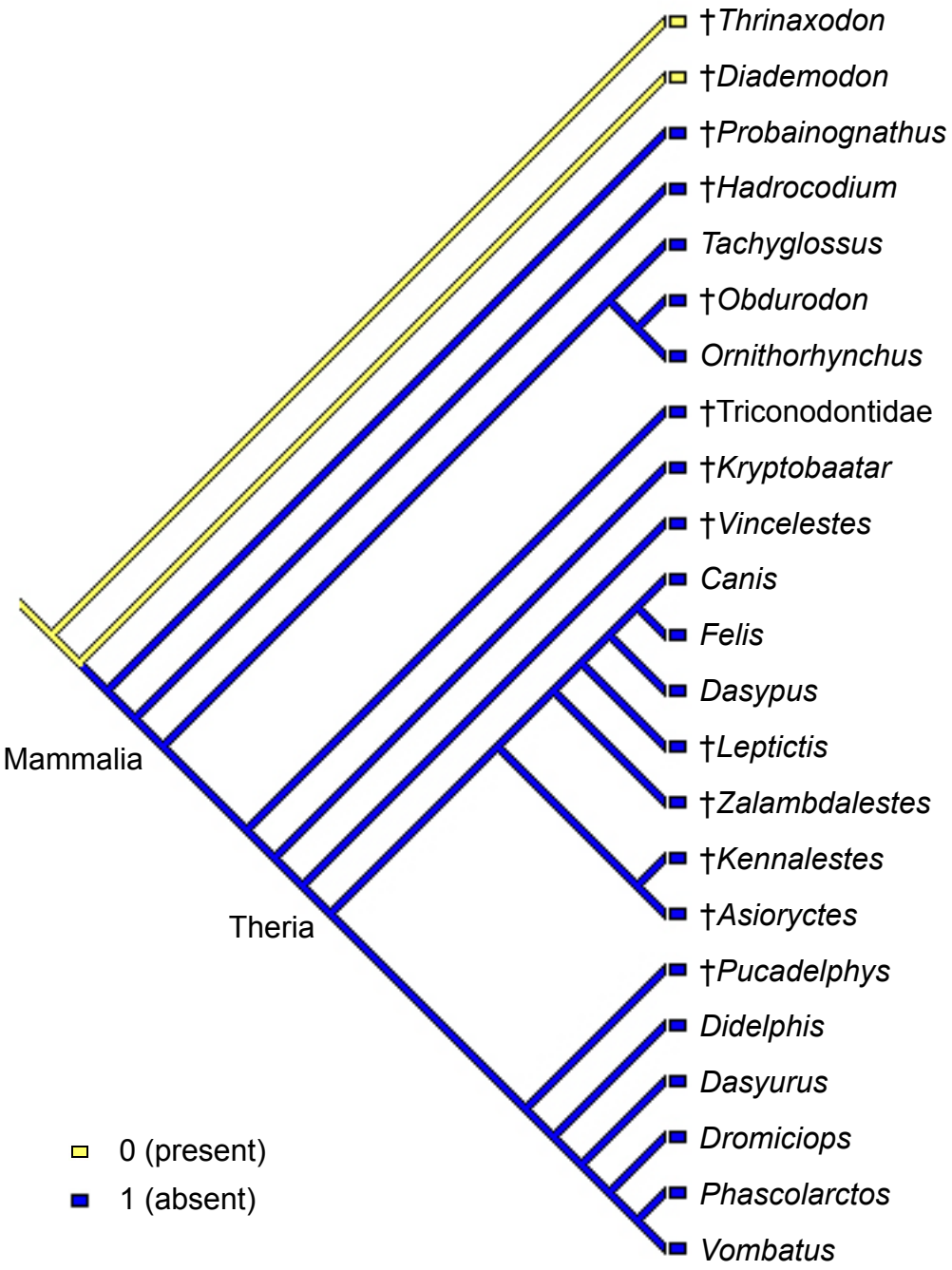


Figure 45. Character 30 (presence of parietal tube and foramen) optimized on a pruned version of the strict consensus tree of Luo and Wible (2005).

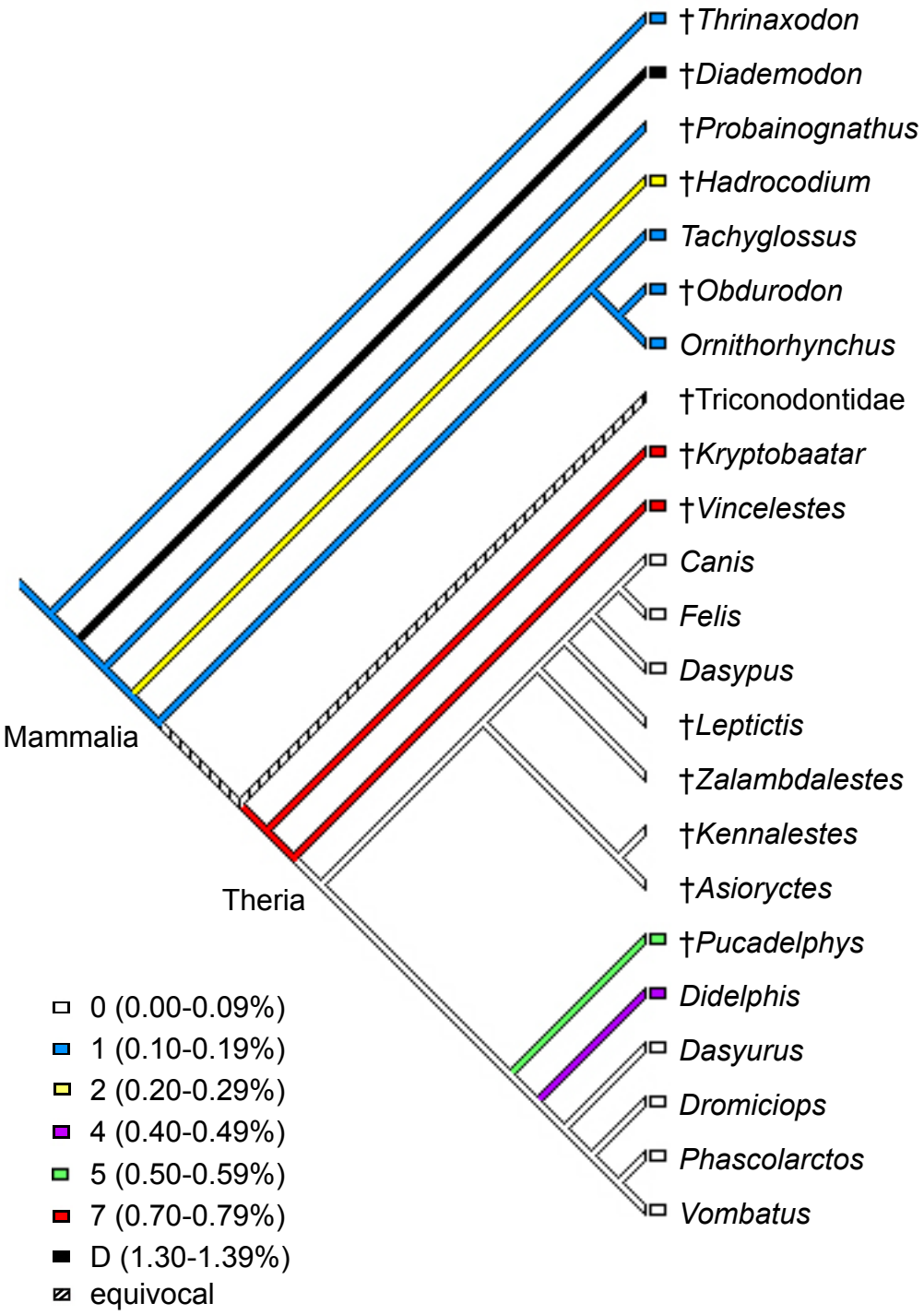


Figure 46. Character 31.1 (% endocast composed by hypophyseal fossa) optimized on a pruned version of the strict consensus tree of Luo and Wible (2005).

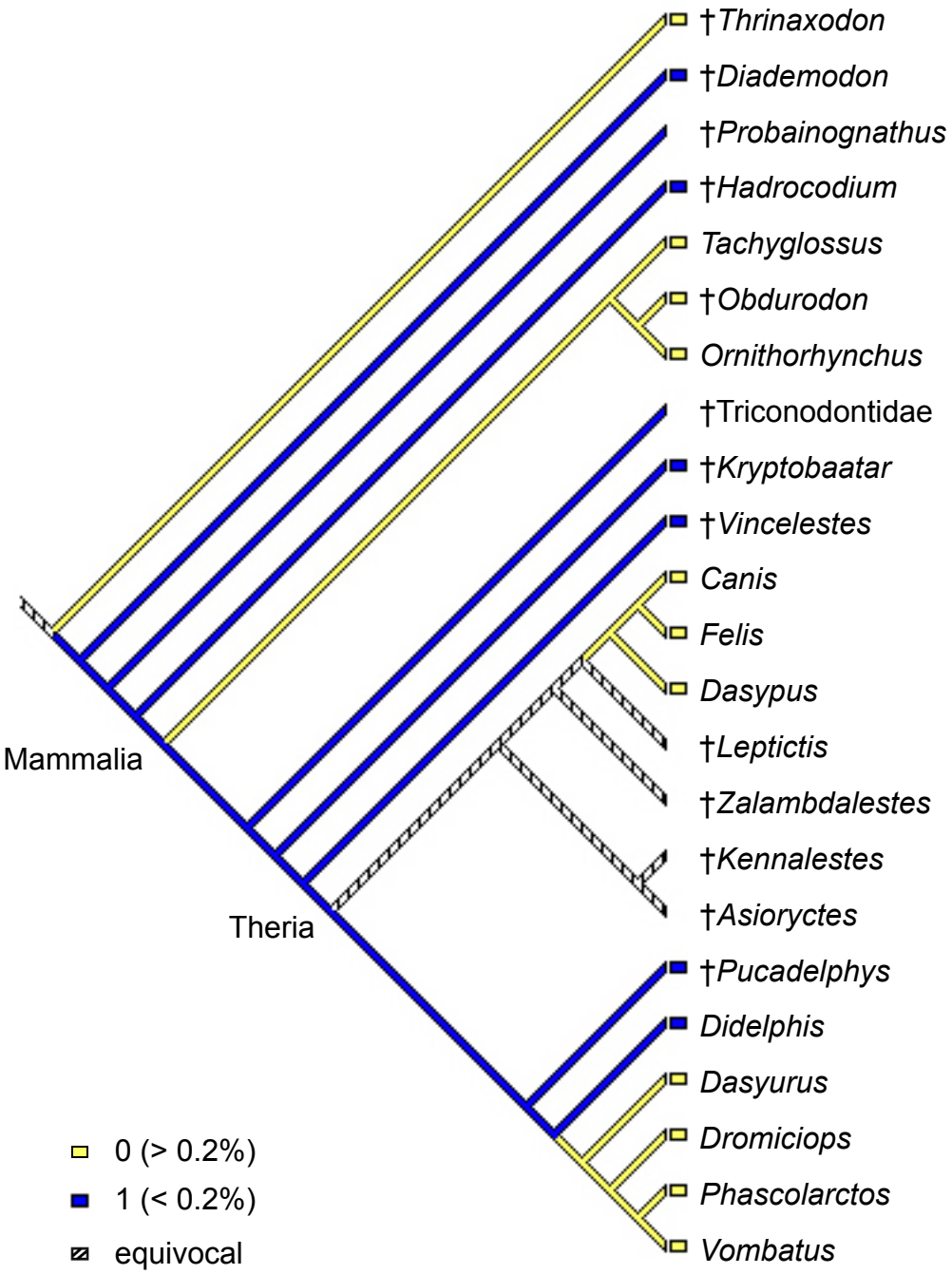


Figure 47. Character 31.2 (% endocast composed by hypophyseal fossa) optimized on a pruned version of the strict consensus tree of Luo and Wible (2005).

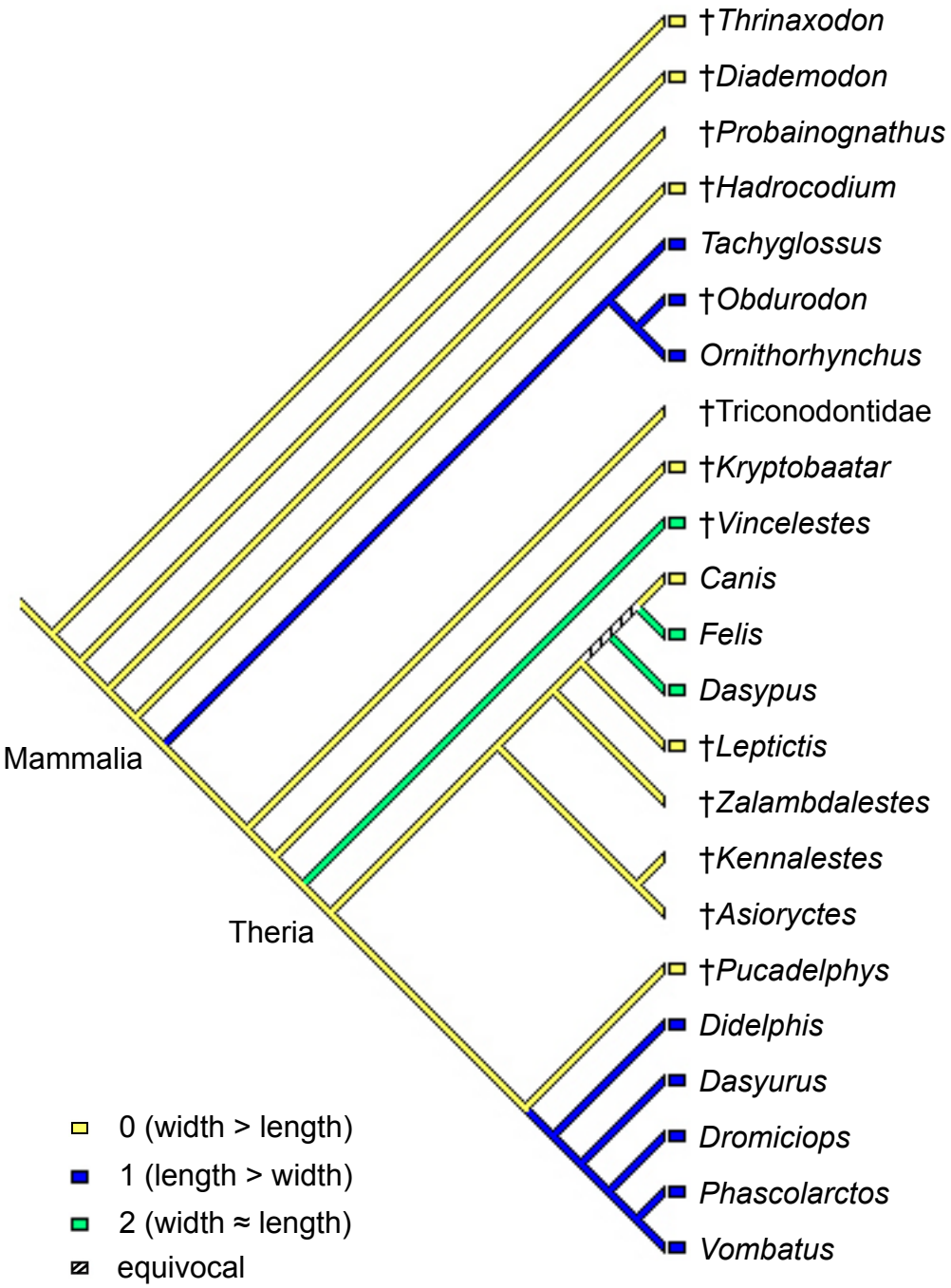


Figure 48. Character 32 (width/length aspect ratio of hypophyseal fossa) optimized on a pruned version of the strict consensus tree of Luo and Wible (2005).

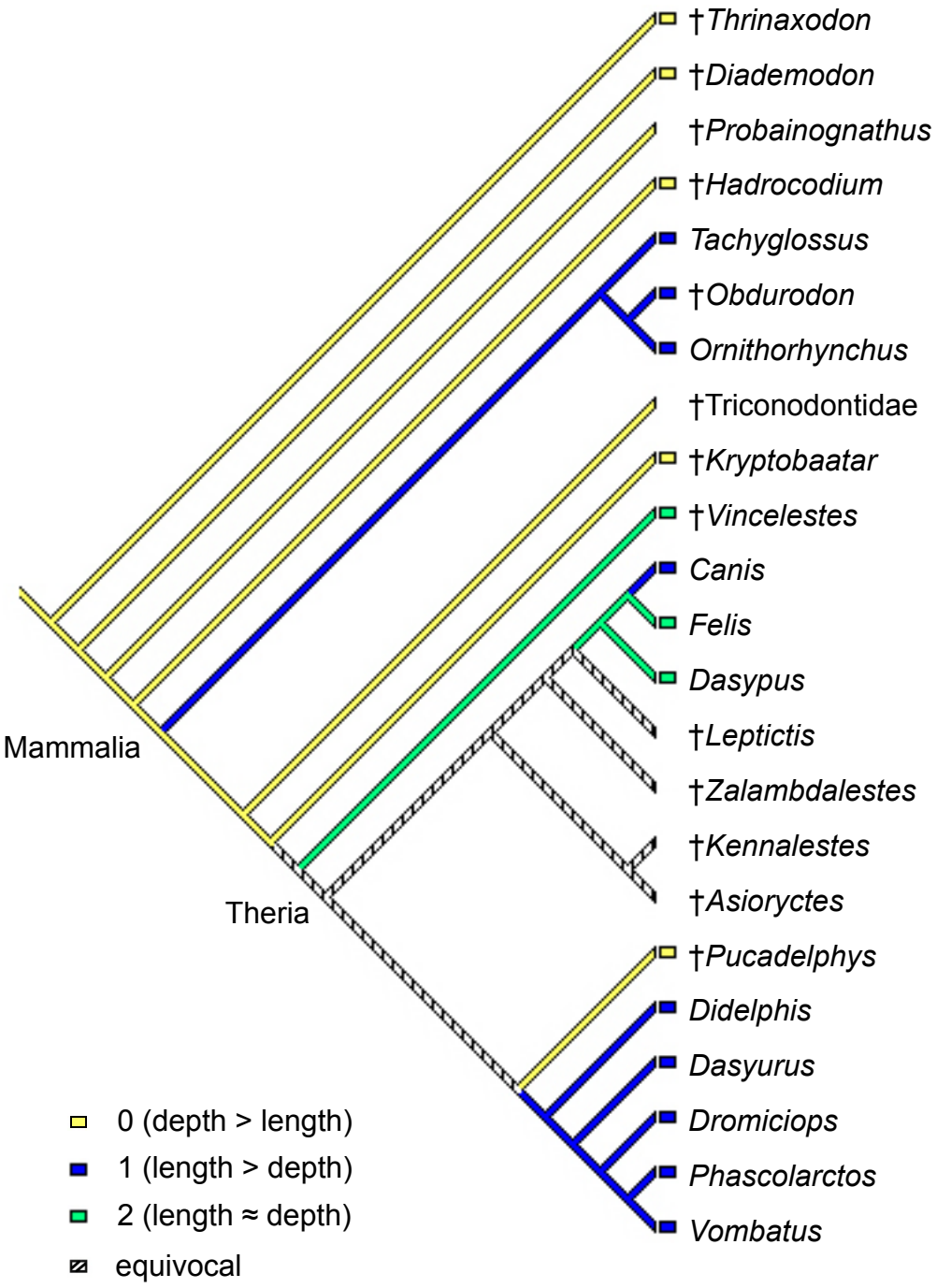


Figure 49. Character 33 (depth/length aspect ratio for hypophyseal fossa) optimized on a pruned version of the strict consensus tree of Luo and Wible (2005).

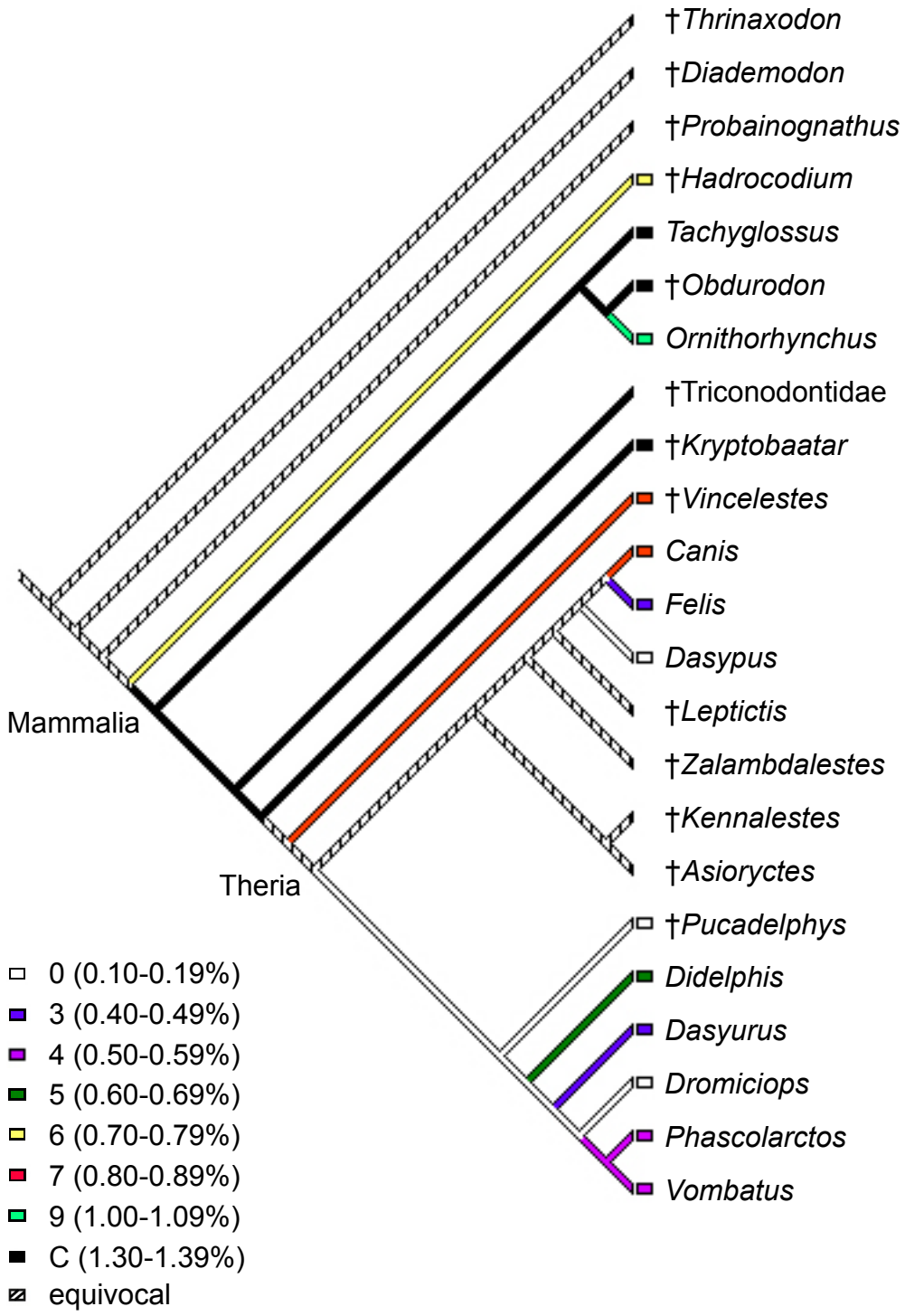


Figure 50. Character 36.1 (% endocast composed by cava epipterica) optimized on a pruned version of the strict consensus tree of Luo and Wible (2005).

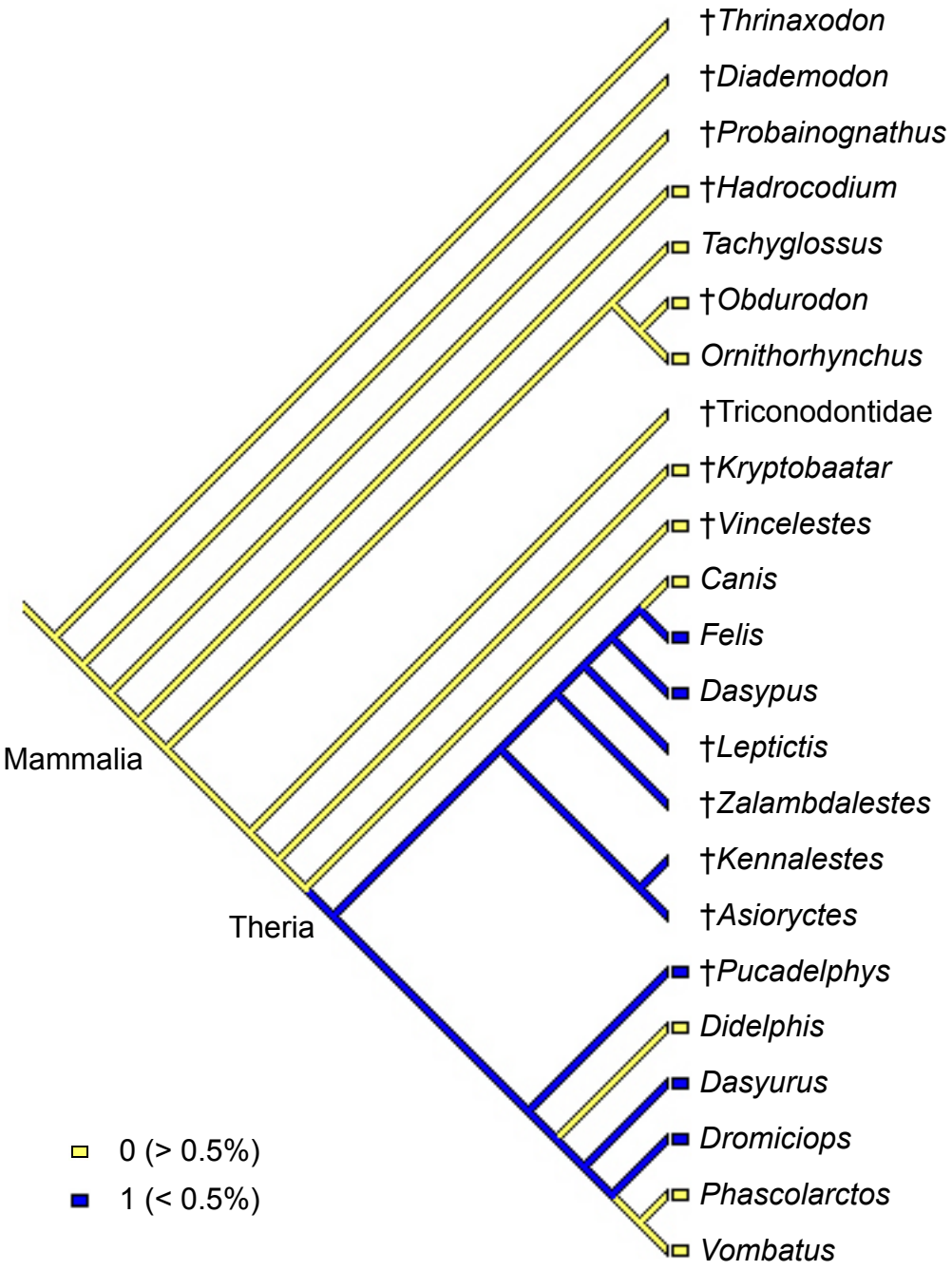


Figure 51. Character 36.2 (% endocast composed by cava epipterica) optimized on a pruned version of the strict consensus tree of Luo and Wible (2005).

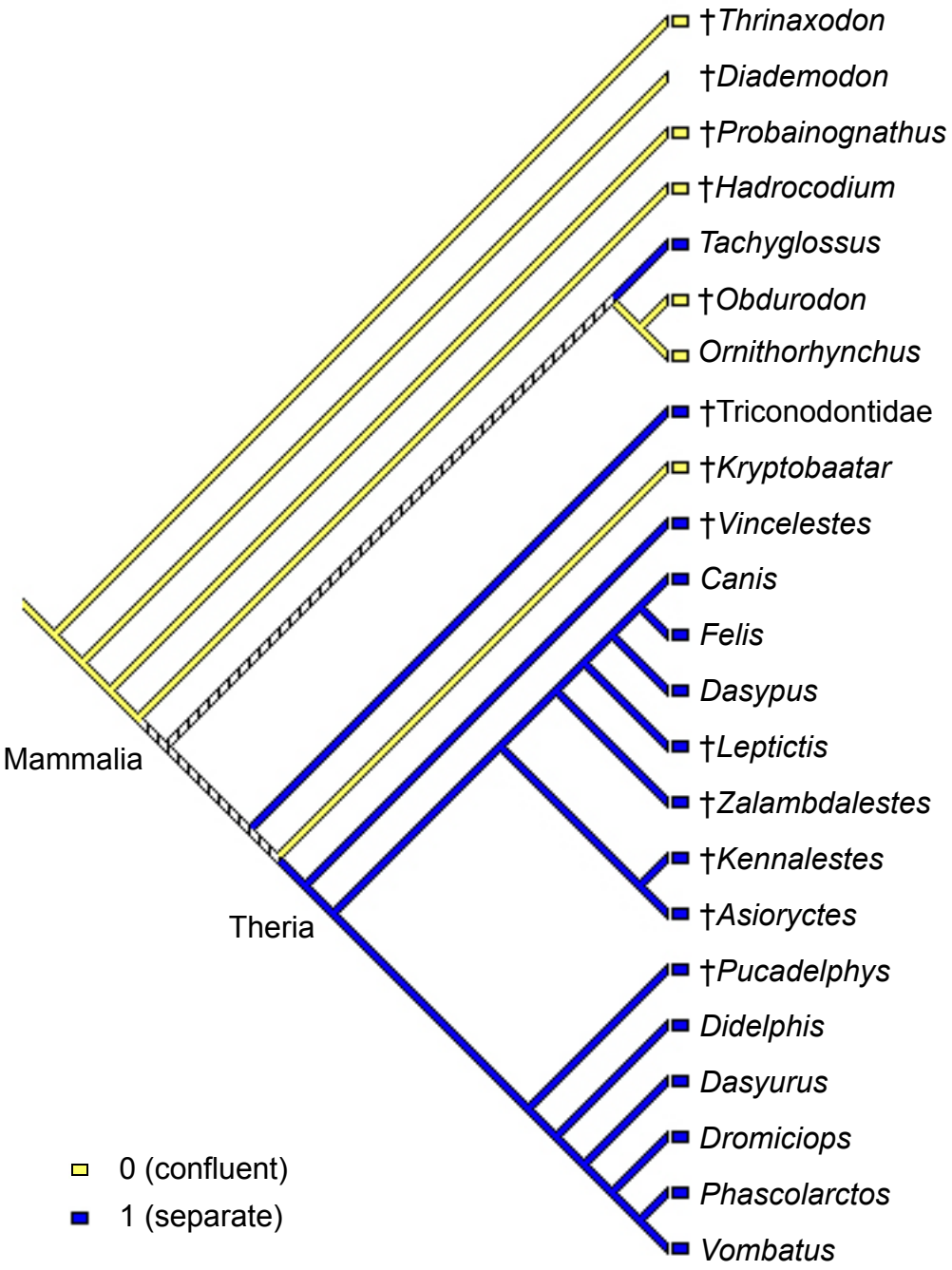


Figure 52. Character 37 (cavum epiptericum and cavum supracochleare confluence) optimized on a pruned version of the strict consensus tree of Luo and Wible (2005).


Figure 53. Strict consensus tree obtained from unordered character analysis of endocast character matrix alone (Appendix 5).


Figure 54. Adams consensus tree obtained from unordered character analysis of endocast character matrix alone (Appendix 5).

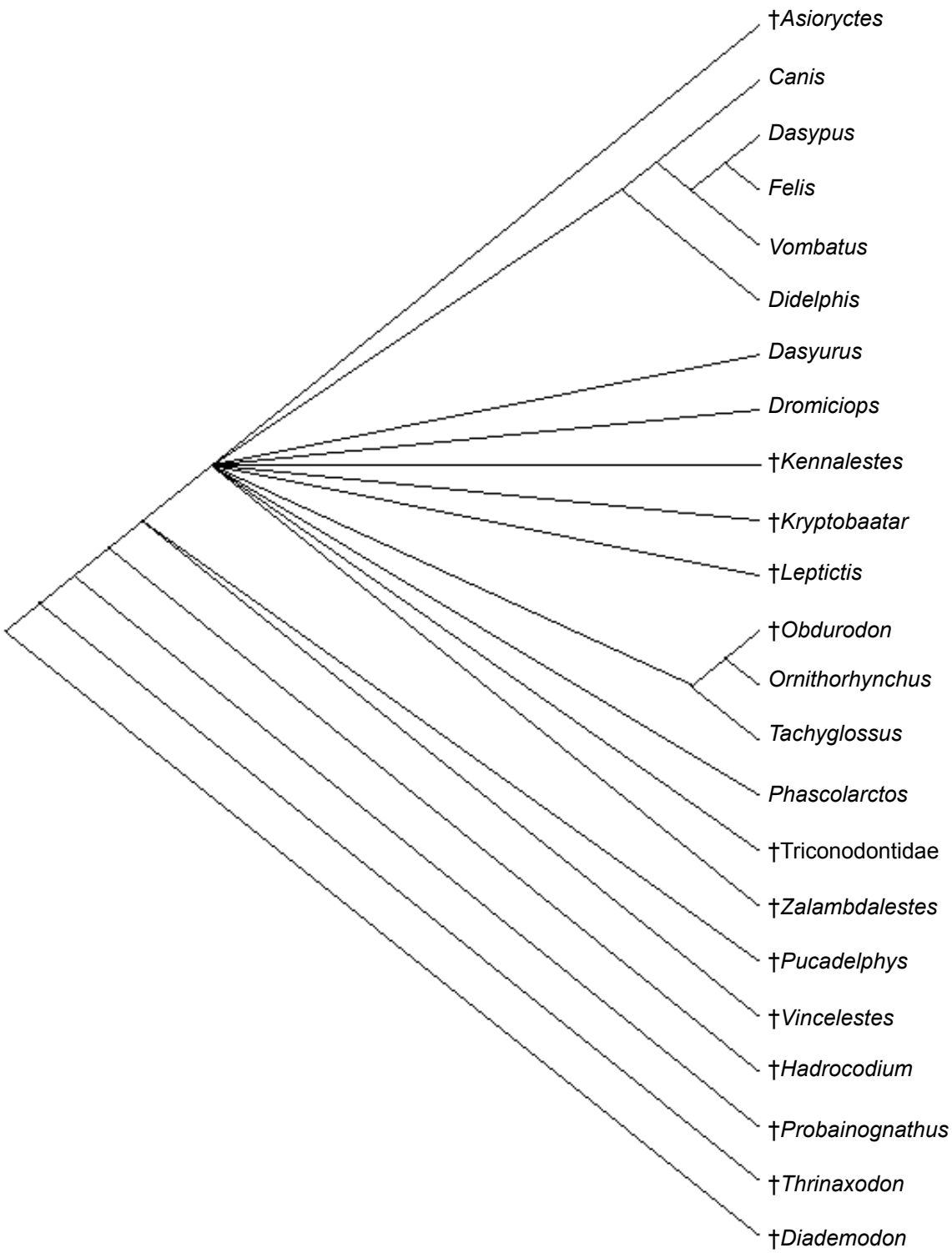


Figure 55. Strict consensus tree obtained from unordered character analysis of cropped endocast matrix. Taxa not included in the Luo and Wible (2005) matrix were pruned prior to the analysis.

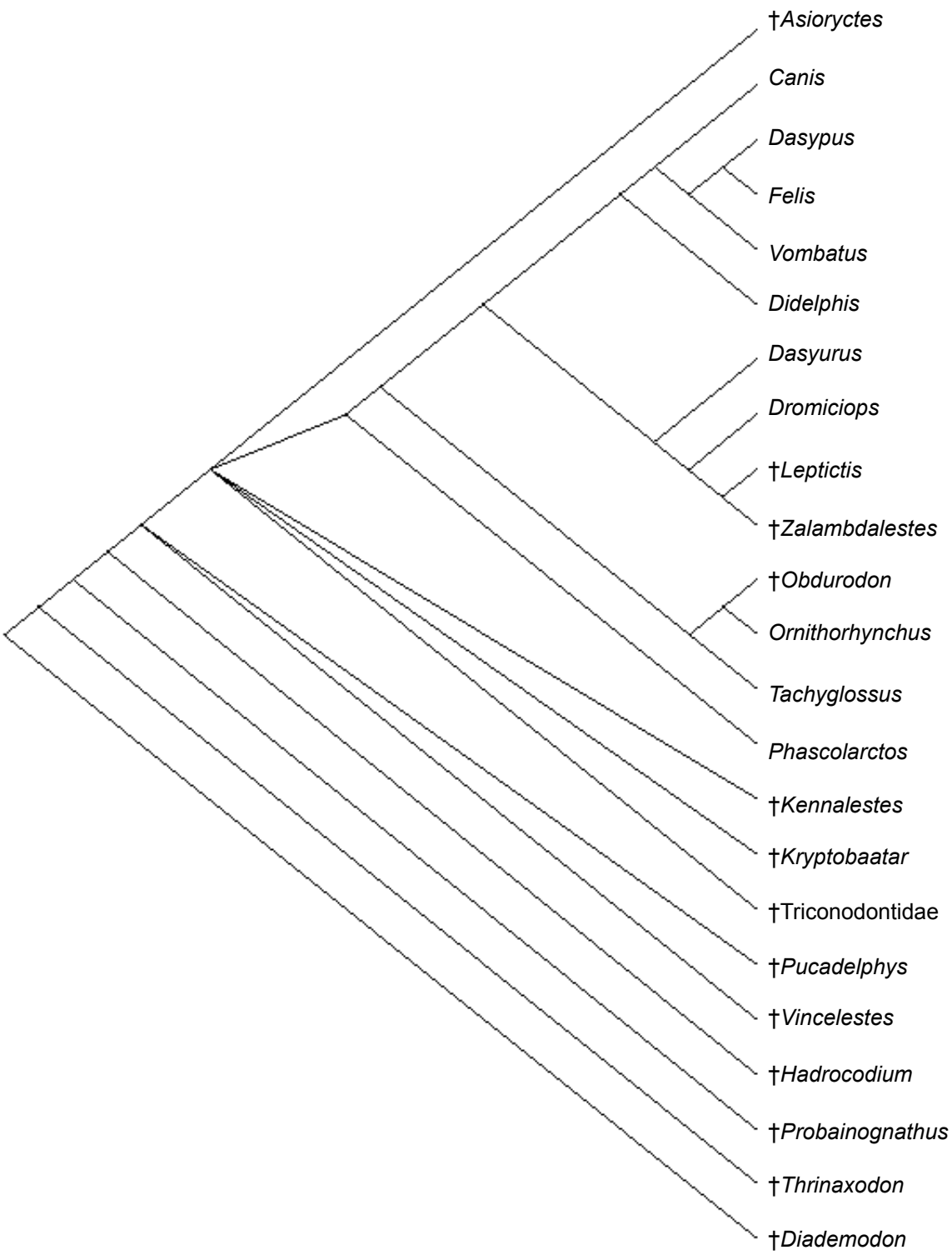


Figure 56. Adams consensus tree obtained from unordered character analysis of cropped endocast matrix. Taxa not included in the Luo and Wible (2005) matrix were pruned prior to the analysis.

Figure 57. Strict consensus tree obtained from unordered character analysis of combined Luo and Wible (2005) matrix and my endocast matrix.

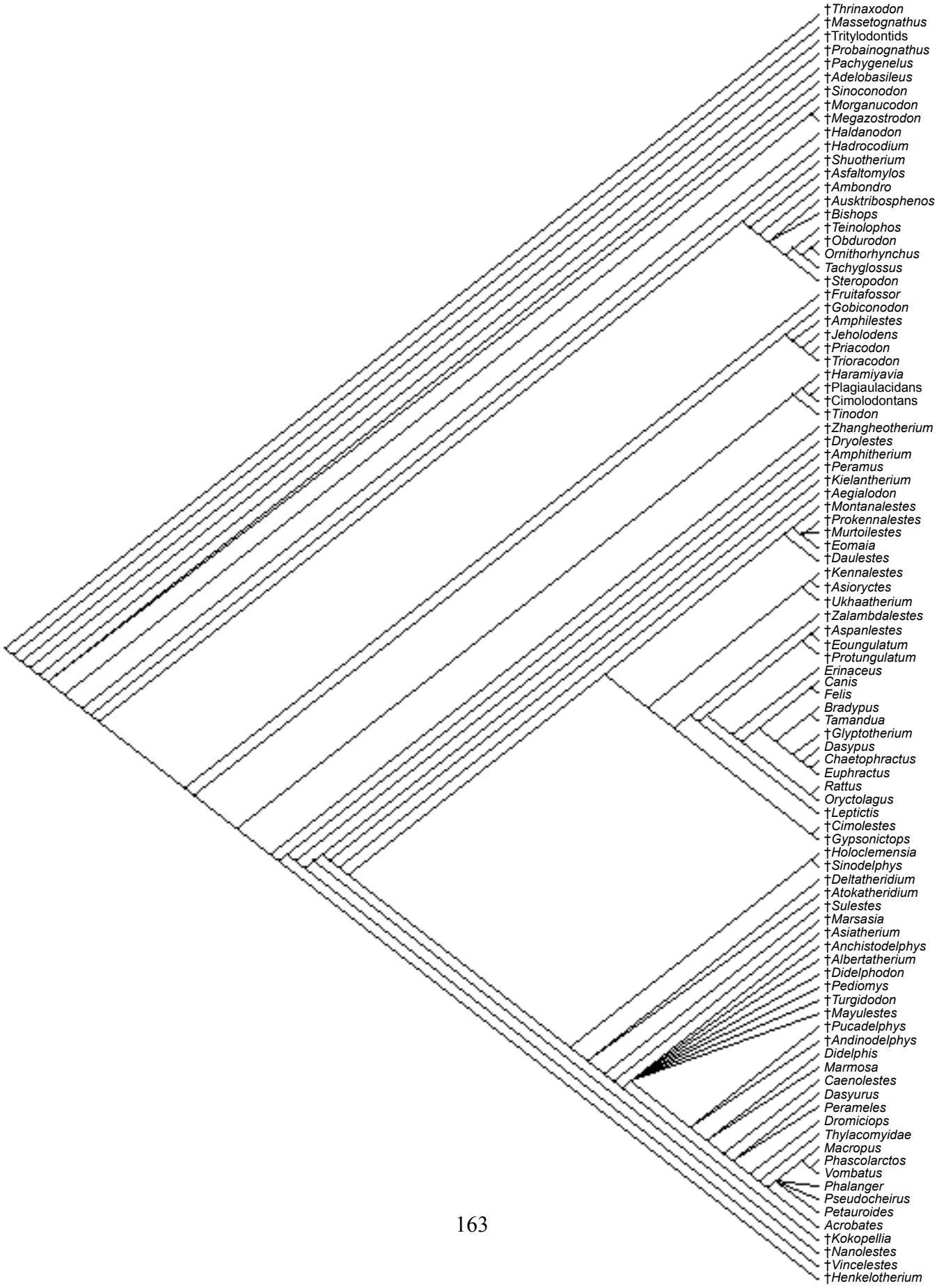
†Thrinaxodon
†Massetognathus
†Tritylodontids
†Probainognathus
†Pachygenelus
†Adelobasileus
†Sinoconodon
†Morganucodon
†Megazostrodon
†Haldanodon
†Hadrocodium
†Shuotherium
†Asfaltomylos
†Ambondro
†Ausktribosphenos
†Bishops
†Teinolophos
†Obdurodon
Ornithorhynchus
Tachyglossus
†Steropodon
†Fruitafossor
†Gobiconodon
†Amphilestes
†Jeholodens
†Priacodon
†Trioracodon
†Haramiyavia
†Plagiaulacidans
†Cimolodontans
†Tinodon
†Zhangheotherium
†Dryolestes
†Amphitherium
†Peramus
†Kielantherium
†Aegialodon
†Montanalestes
†Prokennalestes
†Murtoilestes
†Eomaia
†Daulestes
†Kennalestes
†Asioryctes
†Ukhaatherium
†Zalambdalestes
†Aspanlestes
†Eoungulatum
†Protungulatum
Erinaceus
Canis
Felis
Bradypus
Tamandua
†Glyptotherium
Dasypus
Chaetophractus
Euphractus
Rattus
Oryctolagus
†Leptictis
†Cimolestes
†Gypsonictops
†Holoclemensia
†Sinodelphys
†Deltatheridium
†Atokatheridium
†Sulestes
†Marsasia
†Asiatherium
†Anchistodelphys
†Albertatherium
†Didelphodon
†Pediomys
†Turgidodon
†Mayulestes
†Pucadelphys
†Andinodelphys
Didelphis
Marmosa
Caenolestes
Dasyurus
Perameles
Dromiciops
Thylacomyidae
Macropus
Phascolarctos
Vombatus
Phalanger
Pseudocheirus
Petauroides
Acrobates
†Kokopellia
†Nanolestes
†Vincelestes
†Henkelotherium

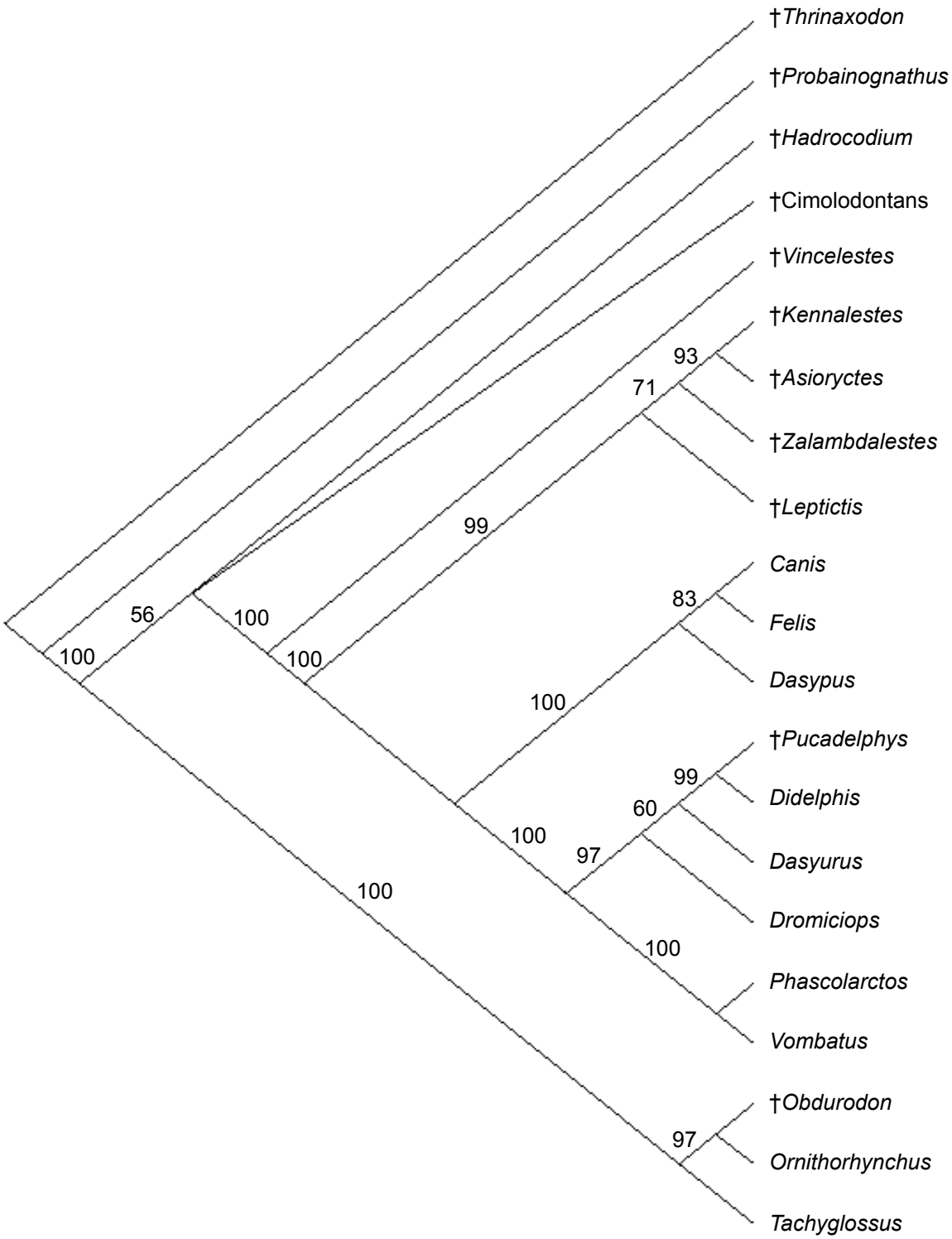


Figure 58. Single most parsimonious tree obtained from unordered character analysis of combined Luo and Wible (2005) matrix and my endocast matrix; taxa not common to both matrices were pruned. Bootstrap values shown above branches.

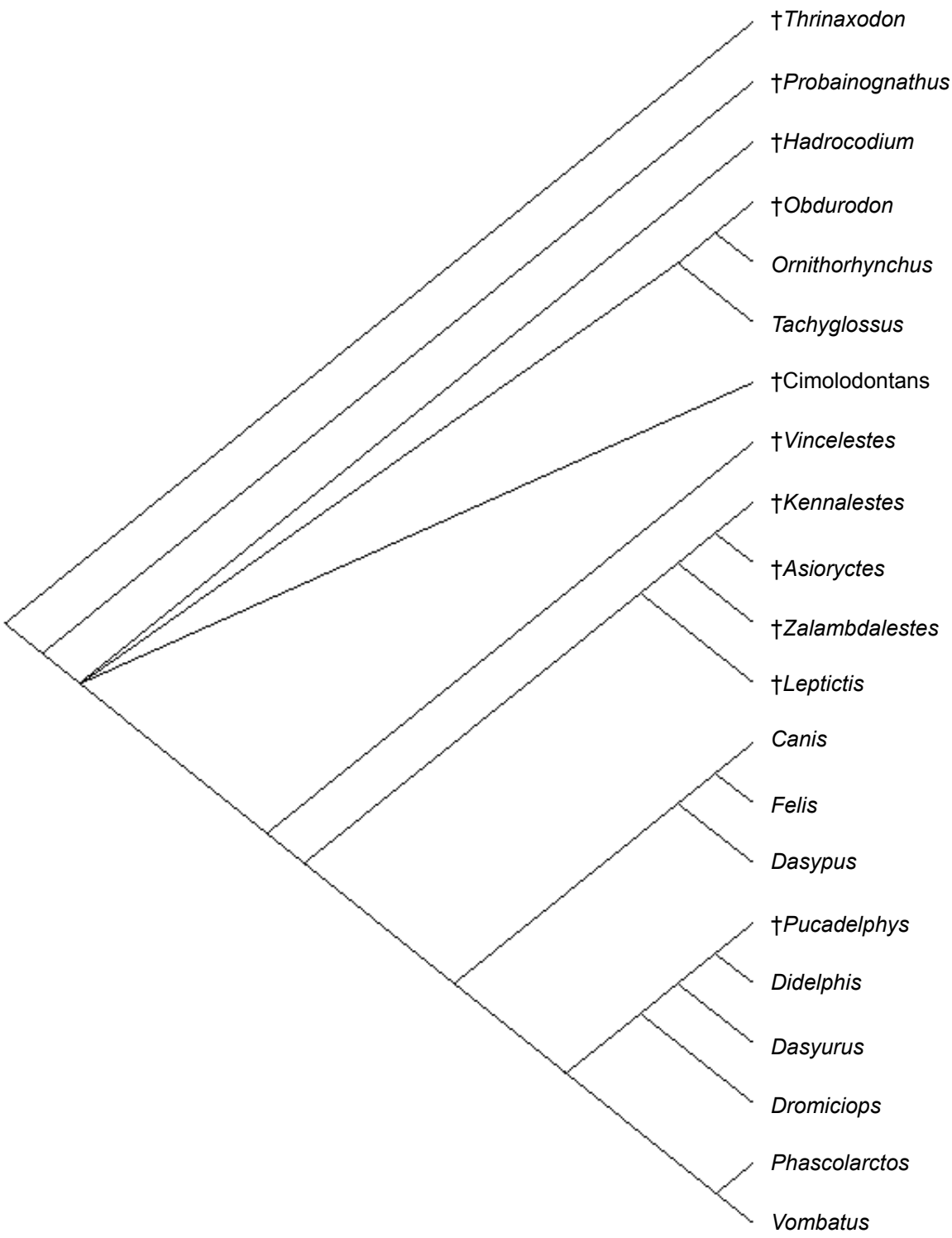


Figure 59. Strict consensus tree obtained from unordered character analysis of cropped Luo and Wible (2005) matrix; taxa not present in my endocast matrix were pruned prior to analysis. My endocast matrix was not added to the Luo and Wible matrix in this analysis.

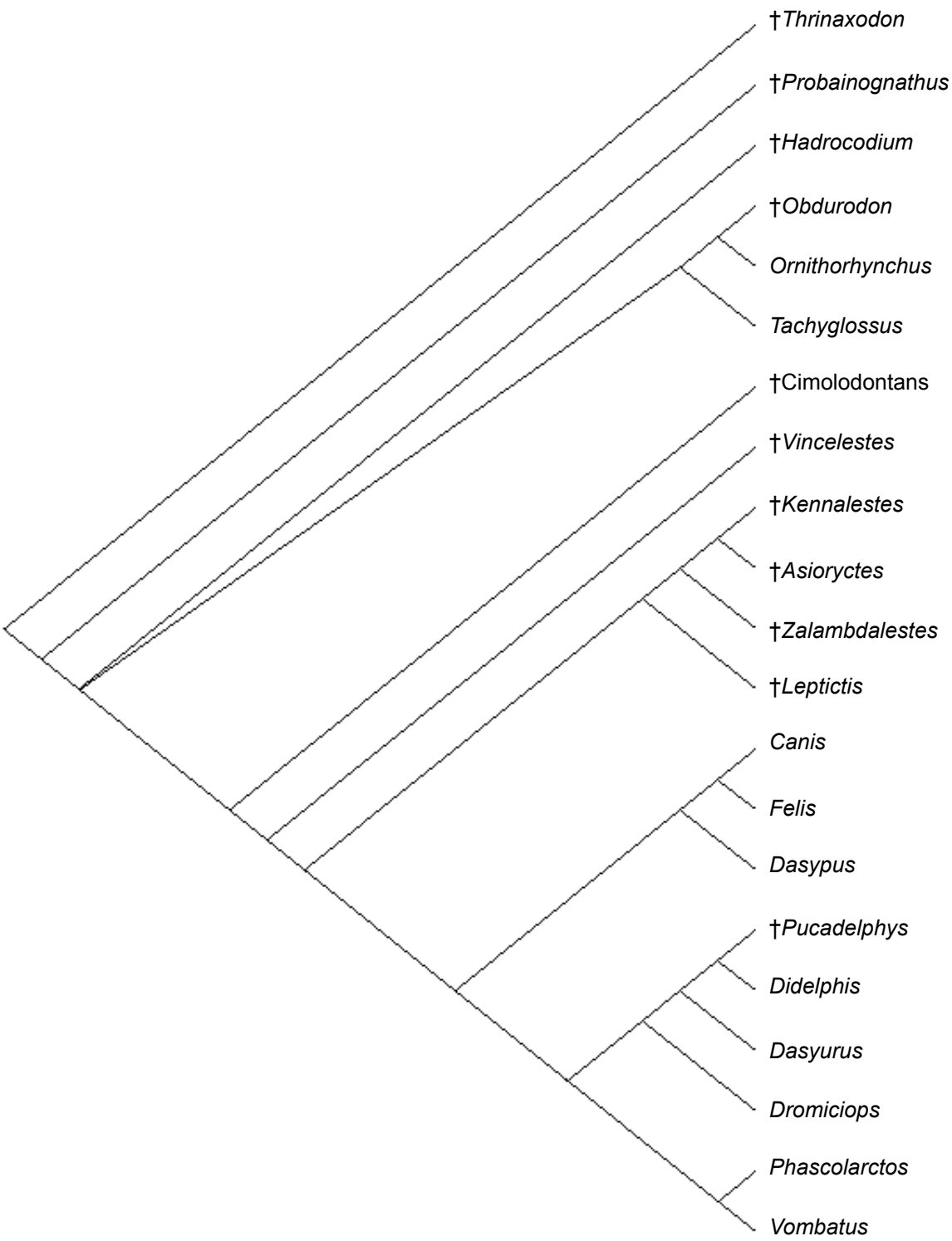


Figure 60. Adams consensus tree obtained from unordered character analysis of cropped Luo and Wible (2005) matrix; taxa not present in my endocast matrix were pruned prior to analysis. My endocast matrix was not added to the Luo and Wible matrix in this analysis.

# Chapter 4: Cranial Endocasts from an Ontogenetic Series of *Monodelphis domestica* (Didelphidae, Marsupialia)

## INTRODUCTION

Historically, studies of the brains of fossils were restricted to those with natural endocast material or specimens from which artificial endocasts could be easily extracted using conventional methods. However, the cranial cavities of many fossil specimens are filled with matrix and their endocranial space could only be studied through destructive serial sectioning. In recent years, high-resolution X-ray computed tomography was established as a proven technology for extracting endocasts from virtually any skull in a non-destructive fashion (e.g., Rowe et al., 1995; Brochu, 2000; Larsson et al., 2000; Witmer et al., 2003; Franzosa and Rowe, 2005). Consequently, our knowledge of the evolution of endocranial space in mammals has expanded with the study of additional taxa. Even so, some basic questions about the study of endocasts remain unanswered, such as the range of ontogenetic and individual variation for a particular species. Relatively few studies of cranial endocasts have examined multiple individuals of a particular taxon to understand individual variation (notable exceptions are Edinger, 1948; Radinsky, 1968b, 1973a; Novacek, 1982, 1986), and virtually no studies have examined ontogenetic variation of endocasts for a particular taxon. Morphological characters that show intraspecific variation are known to contain phylogenetic signal, and different treatments of these characters can greatly affect the results of phylogenetic analyses

(Wiens, 1995, 1998, 1999). Therefore, it is important to get an idea of the degree of intraspecific variation among endocasts so that characters related to this system can be properly treated in phylogenetic analyses.

To address these and other issues, I present a description of cranial endocasts of *Monodelphis domestica*, the gray short-tailed opossum, based on multiple individuals from different ages of postnatal ontogeny. I also compared these endocasts with the gross anatomy of brains of *M. domestica* that were extracted by dissection from individuals of comparable age. I investigate three questions in this chapter. 1) Should ontogenetic (post-organogenesis) variation be taken into consideration when studying endocasts? That is, apart from size alone is there significant ontogenetic variation such that it would affect scoring phylogenetic characters? 2) Should individual variation be taken into consideration when studying endocasts? 3) Is the brain growth trajectory for a single species of mammal (*M. domestica*) different from a brain allometry trajectory based on adults from a higher taxonomic group of mammals?

*Monodelphis domestica* is a good choice for this type of study for a number of reasons. First, *M. domestica* is a laboratory animal and therefore a growth series of specimens of known absolute ages is easily obtainable. Second, the skull and the biology, in general, of *Monodelphis* are well studied (Macrini, 2000, 2004; Wible, 2003; Macrini and Rowe, in preparation). Third, the gross anatomy of the brain of *Didelphis virginiana*, a didelphid marsupial, is well described (Voris, 1928; Loo, 1930; Voris and Hoerr, 1932; Larsell, 1936; Krabbe, 1942), but endocasts of opossums are not. Comparisons are made here between endocasts of *D. virginiana* and *M. domestica*. Finally, *M. domestica* is a member of Didelphidae, the basal-most diverging clade of

marsupials (Jansa and Voss, 2000; Horowitz and Sánchez-Villagra, 2003; Voss and Jansa, 2003) and, therefore, results from this study might be used as a standard for other marsupial (and even therian) endocast variation studies, at least until further work is conducted.

**Institution Abbreviations—AMNH**, American Museum of Natural History, New York, New York, U.S.A.; **SFBR**, Southwest Foundation for Biomedical Research, San Antonio, Texas, U.S.A.; **TMM M**, extant mammal collections of the Texas Memorial Museum/ Texas Natural Science Center housed at the Vertebrate Paleontology Laboratory, Austin, Texas, U.S.A.; **UTCT**, University of Texas High-Resolution X-ray CT Facility in Austin, Texas, U.S.A.

## MATERIALS AND METHODS

### Specimens examined

All specimens of *Monodelphis domestica* used in this study (Table 4.1) were obtained from the laboratory colonies of the SFBR. Because these were laboratory animals, I have precise absolute age data on the individuals. These specimens were accessioned into the Texas Natural History Center and are housed at the Vertebrate Paleontology Laboratory as part of the extant mammal collection.

Heads or skulls of 14 individuals were CT scanned including two adult 'retired breeder' females, one adult 'retired breeder' male, one day 90 postnatal male, one day 90 female, one day 76 male, one day 75 male, one day 57 female, one day 56 female, two

day 48 females, and three day 27 individuals (Table 4.1). The day 56 and 57 individuals are considered to be a single age group, and similarly the day 75 and 76 individuals are treated as comparable in age. The material examined includes frozen, alcohol preserved, and skeletonized specimens. Frozen and preserved specimens were dissected to extract their brains. When possible, brains were extracted from individuals that were also CT scanned. In all, 10 specimens were dissected: two adult females, one adult male, one day 90, one day 76, one day 56, one day 48, and three day 27. The brain masses of these individuals are presented in Table 4.1.

The skull of a day 27 individual (TMM M-7595) is distorted, probably a result of desiccation during skeletal preparation. Portions of the braincase roof, lateral walls, and the basicranium are caved in. The hypophyseal fossa is damaged on this specimen and consequently a volume cannot be accurately determined for this structure.

At day 27, the deciduous upper and lower third premolars are in place, as are the first upper and lower molars. The upper and lower second molars are in the process of eruption. At day 48, the second lower molar is present and the second upper and third lower molars are erupting. The day 27 and day 48 individuals belong to the first dental age class for didelphids (Gardner, 1973). At day 57, the second upper and lower molars are in place and the third lower molar is erupting. At day 75, the third lower molar is in place and the third upper and fourth lower molars are erupting. The day 57 and day 75 individuals belong to the second dental age class for didelphids (Gardner, 1973). At age 90, the third upper molar is in place and the fourth lower molar is present but not functional. This corresponds to the third dental age class for didelphids (Gardner, 1973). The three 'retired breeder' *Monodelphis* specimens used in this study correspond to the

seventh dental age class (Gardner, 1973) because all adult dentition is present and cusp wear is present. A single skull of *Didelphis virginiana*, the Virginia opossum, (TMM M-2517; adult male collected in Travis County, Texas) was also CT scanned and its digital cranial endocast was extracted for comparison with those of *M. domestica*.

A description of CT scanning was provided in Chapter 2. Extraction of the endocasts and acquisition of endocast measurements follows the techniques described in Chapter 2.

**Examination of endocast characters**

Thirty-nine endocast characters were examined on individuals of the *Monodelphis* growth series. Some of these characters are uninformative for the sample of *Monodelphis* examined here, but these characters do vary across a broader sample of Theria or Mammalia (Chapter 3, Appendices 1, 4). For this reason and for the sake of completeness, I report the variability of all of the 39 endocast characters.

**Extraction of brains**

I dissected specimens of *Monodelphis* to isolate the brain in order to confirm identification of features on endocasts. Two of the individuals were alcohol-preserved specimens. I used forcepts to remove pieces of the skull roofs of two frozen individuals (TMM M-8272, an adult female; TMM M-8270, an adult male). The neural tissue lost rigidity as the specimens thawed, making it impossible to remove an intact brain from the

skull. However, brain volume was recorded from a thawed brain extracted from one of the frozen specimens. The remaining six frozen specimens were fixed in formalin prior to dissection. These specimens were soaked in 10% formalin for 10 to 12.5 days, rinsed in 95% ethanol, and then stored in 70% ethanol (Williams et al., 1977).

Extracted brains were weighed using a Mettler AE 50 scale (accurate to the nearest 0.0001 g) at the UTCT. Skull length was measured using calipers accurate to the nearest 0.01 mm for dry skulls or by using VGStudioMax© for skulls that could not be extracted intact.

**Determination of body mass**

Frozen and whole preserved specimens were weighed using 5, 10, 30, 100, and 1000 g Pesola spring scales with increments of 0.05, 01, 0.25, 1.0, and 10.0 g, respectively. Body masses were estimated for skeletonized specimens using two different techniques. The first technique was to take an average mass of different individuals of the same age. These mass data were taken from the LL2 stock of the laboratory colony of the SFBR; these data are provided in Table 4.2. The LL2 stock was selected for the robustness of its individuals and its large litter sizes (n=10-12). This technique was applied to the non-adult skeletonized specimens. For skeletonized individuals of known sex, only masses from individuals of that sex were used to determine an average mass. In the instance when the sex is unknown for the skeletonized individual (e.g., day 27, TMM M-7595), masses from both males and females of that age

were used for determining the average mass. These *Monodelphis* were weighed using a Mettler PE 2000 scale (accurate to the nearest 0.1 g) at the SFBR.

A different mass estimate technique was applied to a single adult opossum skeleton (TMM M-7599) because the exact age of this individual is unknown and because *Monodelphis domestica* exhibits continual growth (Cothran et al., 1985). The second technique estimates body mass from total skull length measured from the anterior tip of the premaxillae to the back of the occiput. Skull length was measured from adult wild-caught and laboratory-raised individuals housed at the AMNH for which body mass is known (Table 4.3). Skull length was measured using calipers accurate to 0.01 mm and body mass was taken from specimen tags. The skull length and body mass data were plotted and an equation for estimation of body mass was determined (Figure 61).

**Encephalization quotients**

To determine encephalization quotients, $\log_{10}$ (body mass) was plotted versus $\log_{10}$ (endocranial volume) for a sample of adult didelphids (Eisenberg and Wilson, 1981). Similarly, $\log_{10}$ (body mass) was plotted versus $\log_{10}$ (endocranial volume) for the *Monodelphis* growth series. *Monodelphis* endocranial volume data were converted to cubic cm to facilitate comparison with the adult didelphid data.

To determine EQ equations, three types of regression analyses were performed: least-squares (model 1 regression), major-axis (model 2 regression), and reduced-major axis. Least-squares regression assumes that the Y variable contains error but the X variable does not (Sokal and Rohlf, 1998). This is an unrealistic assumption for most

allometric analyses. Major-axis regression assumes that both variables have error and the variances of the two variables are equal (Sokal and Rohlf, 1998). Reduced-major axis assumes that the ratio of the two error variances equals the ratio of the actual variances of the raw data (i.e., the ratio of the standard deviation of variable Y divided by the standard deviation of variable X; Sokal and Rohlf, 1998).

Some have advocated use of reduced-major axis for EQ analyses (e.g., Hurlburt, 1996). However, major-axis and reduced-major axis analyses can over- or underestimate the true slope if their respective assumptions are a significant departure from reality (Pagel and Harvey, 1988; Harvey and Krebs, 1990). If there is a high correlation between the X and Y variables, then all three regression methods perform well (Pagel and Harvey, 1988; Harvey and Krebs, 1990).

Quantitative data sampled from closely related taxa are non-independent; therefore, the phylogenetic relationships of the sampled taxa need to be taken into account (Felsenstein, 1985). However, to facilitate comparison between the EQ lines determined from multiple adult species of didelphids and a growth series of a single species (*Monodelphis domestica*), independent contrasts were not calculated. Otherwise, regression lines from an independent contrast versus independent contrast plot would be compared with regression lines from a log(body mass) versus log(endocranial volume) plot.

# RESULTS

## Description of endocasts

Changes in shape account for the greatest amount of morphological variation between the endocasts of the growth series of *Monodelphis domestica* (Figures 19, 20, 62, 63, 64). The endocasts of the adult *M. domestica* are wedge-shaped in dorsal view, whereas endocasts of younger individuals of the growth series are more rounded in overall shape (Figures 19, 20, 62). In lateral view, the olfactory bulb casts of the *Monodelphis* are tear drop shaped with the wider end pressed against the cast of the egg-shaped cerebral hemispheres (Figures 19, 20, 63). Endocast flexures around the hypophyseal cast are presented in Appendix 1.

Anteroposterior maximum length, maximum width, maximum height, and endocast flexure measurements for all 14 *Monodelphis* endocasts are presented in Appendix 1. Endocast length and width both increase with age for the growth series (Figure 65). The endocast width/length aspect ratio decreases through ontogeny from 0.68-0.80 (n=3) in day 27 individuals to 0.58-0.63 (n=3) in adults. Similarly, the height/length aspect ratio decreases from 0.48-0.60 (n=3) in day 27 individuals to 0.39-0.49 (n=3) in adults. The endocast height/width ratio remains fairly constant throughout ontogeny (range 0.67-0.79, mean=0.73, n=14).

Endocranial volumes and brain masses of the *Monodelphis* specimens are presented in Table 4.1. Endocranial volume increases with absolute age in the growth series (Figure 66). Based on the assumption that brain tissue has a specific gravity of one, the brain of a single day 56 individual (TMM M-8266) of *Monodelphis* fills 72.9%

of the endocranial volume. The brain fills 67.8% of the endocranial volume of a day 76 individual (TMM M-8267), and 86.6% of the endocranial volume of a day 90 individual (TMM M-8268).

The endocast from a single adult male *Didelphis virginiana* (Figure 67) appears more laterally constricted than those of the adult *M. domestica*. The width/length aspect ratio from the *D. virginiana* endocast is 0.57, which is near the lower range for the three adult *M. domestica* endocasts examined here. *Didelphis* lacks the large epitympanic recess present in *Monodelphis* and this is possibly correlated with the relatively narrow endocast of *Didelphis*. The height/length ratio of the *D. virginiana* endocast (ratio=0.65) is similar to those of the adult *M. domestica* endocasts, but the height/width endocast aspect ratio is considerable larger in *Didelphis* (ratio=1.14) than in *Monodelphis*. The *Didelphis* endocast shows flexure of 40º around the hypophyseal cast.

The olfactory bulb casts compose 3.55-7.77% (n=3) of endocranial space in the day 27 endocasts; this increases to 8.00-8.43% (n=3) in adult *Monodelphis* (Figure 68). Younger individuals of the growth series have more circular olfactory bulb casts (day 27 width/length aspect ratios: 0.82-1.28; n=3) than those of adult specimens (width/length aspect ratios: 0.55-0.60; n=3). The circular fissure (sensu Loo, 1930; Rowe 1996a, b; = transverse fissure of Krause and Kielan-Jaworowska, 1993) is well developed in all 14 *Monodelphis* endocasts as well as the *Didelphis* endocast examined here (Figure 67). The olfactory bulb casts constitute 11.04% of endocranial space in the single *Didelphis* specimen examined. The *Didelphis* olfactory bulb casts width/length aspect ratio (=0.52) is similar to those from the adult *Monodelphis* endocasts.

All specimens of *Monodelphis* examined have enlarged cerebral hemisphere casts that are lissencephalic (Figure 69). The median sulcus is poorly developed on two of three day 27 endocasts (TMM M-8261 and TMM M-8265) but is clearly visible on the remaining twelve endocasts examined in this study. The rhinal fissure is not visible on any of the *Monodelphis* endocasts, but it is clearly visible on dissected brains. However, several cranial sutures are visible on endocasts from the day 48, 56, 57, 75, 76, and 90 individuals. These include the frontal-parietal, alisphenoid-frontal, alisphenoid-parietal, alisphenoid-squamosal, and squamosal-parietal sutures.

The *Didelphis* endocast also has enlarged lissencephalic cerebral hemisphere casts. The median sulcus of the *Didelphis* endocast is obscured by a median blood sinus cast; however, the posterior portion of the rhinal fissure is visible on the lateral surface of the endocast. The frontal-parietal, alisphenoid-frontal, alisphenoid-parietal, alisphenoid-squamosal, and squamosal-parietal sutures are all visible on the *Didelphis* endocast.

The midbrain is completely obscured from the dorsal surface of all of the *Monodelphis* endocasts examined in this study. A similar situation is seen in *Didelphis virginiana*, and a number of other mammals. Conversely, the inferior and superior colliculi of the midbrain are visible on the dorsal surfaces of corresponding brains of *Monodelphis* (Figure 69) and *Didelphis*. The large, paired transverse sinus cast on the dorsoventral surface of the endocasts is responsible for covering the midbrain. This is visible on all of the *Monodelphis* endocasts examined here except for two of the day 27 individuals (TMM M-8261 and TMM M-8265). A well-developed prootic vein cast and sigmoid sinus cast are also visible anterior and dorsal (respectively) to the parafloccular casts of the day 48, 56, 57, 75, 76, and 90 individuals (n=8). The prootic vein cast is

visible on the adult endocasts but the sigmoid sinus cast is not. The transverse sinus, prootic vein, and sigmoid sinus all have casts on the *Didelphis* endocast.

Casts of the vermis and cerebellar hemispheres are visible on endocasts of individuals of age day 48 through adult (n=11). The cerebellum of *Monodelphis* is very convoluted (= gyrencephalic) but its appearance on the endocasts is smooth. This indicates that the meninges and/or venous sinuses are covering up the convolutions. The paraflocculars casts are well developed in all individuals of the growth series examined here. The relative size of the paraflocculars casts shows a slight negative allometric trend through ontogeny (Figure 68), constituting 1.36-1.83% (n=3) of endocranial space in day 27 individuals and 1.10-1.19% (n=3) in adults.

The casts of the vermis and cerebellar hemispheres are also visible on the *Didelphis* endocast and, similar to *Monodelphis*, meninges and/or venous sinuses cover the convolutions of the cerebellum. The paraflocculars casts are small in *Didelphis* (composing 0.59% of endocranial space) relative to those of adult *Monodelphis*.

On the ventral surface of the endocasts, the hypophyseal cast is the most prominent feature (Figures 19, 20, 64). The relative size of the hypophyseal fossa increases in *Monodelphis* ontogeny from composing 0.09-0.10% (n=2) of endocranial space in day 27 individuals to 0.25-0.58% (n=3) of endocranial space in adults. The width/length aspect ratio of the hypophyseal fossa decreases from 1.10-1.11 (n=2) in day 27 individuals to 0.68-0.80 (n=3) in adults. The depth of the hypophyseal fossa grows at a rate that is slightly slower with respect to hypophyseal length than width (height/length aspect ratio range 0.13-0.32, mean=0.25, n=13; height/width aspect ratio range 0.23-0.40, mean=0.31, n=13).

The hypophyseal cast of *Didelphis* is oval in shape (when viewed ventrally) and very deep (length=5.544 mm; width=4.527 mm; height=3.336 mm), constituting 0.47% of endocranial space in *Didelphis*. Each internal carotid artery curves anteriorly and dorsomedially to enter the posterolateral portion of the hypophyseal fossa (Figure 67).

The foramen ovale for the exit of the mandibular branch of the trigeminal nerve ($V_3$) is located just posterolateral to the hypophyseal cast. The foramen opens directly ventrally. The cavum epiptericum sits in the depression above the foramen ovale and extends forward to the foramen rotundum; this space is occupied by the trigeminal ganglion. In *Monodelphis*, the volume of both cava epipterica together compose between 0.15% and 0.44% of endocranial space (mean=0.31%, N=14; Appendix 1). The cava epipterica constitute a significantly greater percentage of the total endocranial space in older individuals (e.g., adults and day 90) than in younger individuals (e.g., day 27). In *Didelphis*, the cava epipterica have a volume of 41.428 $mm^3$, which composes 0.63% of the total endocranial space.

Posteriorly, the cavum epiptericum is confluent with the cavum supracochleare which sits in the petrosal and houses the geniculate ganglion (Wible, 2003). The foramen rotundum for the exit of the maxillary branch of the trigeminal nerve ($V_2$) is located on a horizontally oriented tube that ends anterolateral to the hypophyseal cast. A cast of the canal leading to the sphenorbital fissure is located slightly anterior and medial to the casts of $V_2$. Several cranial nerves pass through this canal including the optic nerve (II), the oculomotor nerve (III), the trochlear nerve (IV), a branch of the ophthalmic branch of the trigeminal nerve ($V_1$), and the abducent nerve (VI). The paired orbital fissure canals are in close proximity to each other but are not confluent. The *Monodelphis* and *Didelphis*

endocasts are nearly identical in the placement of the foramen ovale, cavum epiptericum, foramen rotundum, orbital fissure, and associated canals. However, the orbital fissure is much more anterior to the rotundum in *Didelphis* than in *Monodelphis*. The large epiptympanic recess of *Monodelphis* possibly accounts for the anterior displacement of the foramen rotundum in *Monodelphis*. The cavum epiptericum is deeper and better developed in *Didelphis* than in *Monodelphis*.

Casts of olfactory tracts are not visible on any of the *Monodelphis* endocasts examined here, but they are quite conspicuous on the *Didelphis* endocast (Figure 67C). The medulla oblongata and pons of the hindbrain do not leave distinctive marks on the ventral surface of any of the *Monodelphis* or *Didelphis* endocasts.

**Encephalization quotients**

The three regression methods produced similar results for the *Monodelphis* growth series (Table 4.4). Endocranial volume is positively correlated with body mass for individuals of the *Monodelphis* growth series (Figure 70). The three regression methods also produced similar results when the adult didelphid data were analyzed (Table 4.4). The 95% confidence intervals of the slopes of the *Monodelphis* growth series and adult didelphid analyses did not come close to overlapping, suggesting that the slopes of the allometry lines of the two groups are truly different (Figure 71; Table 4.4). However, the datum point for the adult sample of *Monodelphis brevicaudata* from the Eisenberg and Wilson (1981) dataset lies on the regression line from the *M. domestica*

growth series data. The *M. brevicaudata* datum point clusters with the data points for the adult *M. domestica*.

## DISCUSSION

### Comparison of changes in endocasts with changes in biology during ontogeny

The 14 *Monodelphis* endocasts comprise four distinct morphological groups. The first group consists of two of the day 27 individuals (TMM M-8261 and TMM M-8265); the third day 27 individual is excluded from all of the groups because desiccation of the skull resulted in a misshapen endocast. The day 27 endocasts are characterized by relatively small, spherical olfactory bulb casts and a large circular 'main body' of the endocast (Figure 62). This age group corresponds with the onset of hearing and sight in *Monodelphis*; hearing onset occurs around days 28-30 (Aitkin et al., 1997; Reimer, 1996) and the eyes open around days 28-35 (Kraus and Fadem, 1987). A number of other neurological changes associated with sensory adaptations occur shortly after day 27. The olfactory bulbs assume the adult form at the cellular level by day 30 (Brunjes et al., 1992). The reported adult condition of the parafloccular lobe of the cerebellum only filling half of the subarcuate fossa is assumed by day 35 (Sánchez-Villagra, 2002). The vomeronasal organ first opens into the nasopalatine duct by day 40 and thus becomes functional for pheromone detection (Sánchez-Villagra, 2001).

The second morphological group of endocasts consists of day 48 individuals. The olfactory bulb casts are relatively larger and less spherical in overall shape relative to the day 27 endocasts (Figure 62).

The third morphological group is the largest and includes five individuals from day 56-90. The cerebral hemisphere casts extend laterally beyond the maximum transverse extent of the cerebellar cast (Figure 62). In this age class, the differentiation of the cerebellar cortical layers is complete by day 75 (Sánchez-Villagra and Sultan, 2002). In addition, weaning in *Monodelphis* occurs around day 56 (Kraus and Fadem, 1987; VandeBerg, 1990).

The fourth morphological group of endocasts includes one day 90 individual (TMM M-8268) and the three 'retired breeder' adult individuals. The 'main body' of the endocast, the portion posterior to the olfactory bulbs, is hexagonal in shape (Figure 62). The flexure points between sides of the hexagonal are more angular than those in endocasts of the other morphological groups.

**Discussion of variation in endocast phylogenetic characters**

In this study, ontogenetic variation refers to variation between individuals of different ages whereas individual variation (= polymorphism of Wiens [1995, 1998, 1999]) is restricted to variation between individuals of comparable age. The majority of the variation observed between the *Monodelphis* endocasts is characterized as ontogenetic, although individual variation is also present in the sample. A large amount of the variation observed in this study is quantitative; this includes shape change as indicated by differences in aspect ratios, volume changes, and relative volume changes as

ontogeny progresses. However, some of the variation observed here can also be characterized as qualitative. Below is a list of qualitative and quantitative phylogenetic characters dealing with cranial endocasts that are part of a more extensive taxonomic study (Chapter 3). A discussion is presented of types or lack of variation observed in this sample of 14 *Monodelphis* endocasts for these 39 characters. Reference is also made to the single *Didelphis* endocast incorporated in this study, but obviously variation was not addressed for this taxon.

**Character 1**: Relative expansion of the braincase: braincase is narrow in the parietal region (0); cerebral cast expanded (the parietal part of the cranial vault is wider than the frontal part, but does not extend to lambdoidal region) (1); or greatly expanded (cerebellar cast is transversely expanded as much as cerebral cast) (2). This character was modified from Luo and Wible (2005, character 414). Endocasts of all ages of *Monodelphis* and *Didelphis* examined have braincases that show lateral extension but only anterior to the lambdoidal region of the endocranial cavity.

**Character 2**: Maximum width vs. anteroposterior length aspect ratio of entire endocast: endocast longer than wide (aspect ratio < 0.9) (0); endocast length and width about equal (aspect ratio = 0.9-1.1) (1); or endocast wider than long (aspect ratio > 1.1) (2). The endocast width/length aspect ratio decreases through ontogeny, suggesting that the length of the endocranial cavity is growing at an overall faster rate than endocast width from day 27 to adult (following Rowe, 1996a). A fair amount of individual variation is also noticeable between day 27 opossums (n=3) for which the endocast width/ length aspect ratio has a range of 0.68-0.80. However, there is no variation in how

this character is scored for *Monodelphis*, because all of the specimens examined in this study have aspect ratios less than 0.9; that is, their endocasts are longer than wide.

**Character 3**: Maximum height vs. anteroposterior length aspect ratio of entire endocast: endocast longer than tall (aspect ratio < 0.9) (0); endocast length and height about equal (aspect ratio = 0.9-1.1) (1); or endocast taller than long (aspect ratio > 1.1) (2). The endocast height/length aspect ratio decreases through *Monodelphis* ontogeny, suggesting that the length of the endocranial cavity is growing at an overall faster rate than endocast height from day 27 to adult. Variation is noticeable between individuals of comparable age, particularly those of day 27 and adult opossums. However, there is no variation in how this character is scored for *Monodelphis*, because all of the specimens examined in this study have aspect ratios less than 0.9; that is, their endocasts are longer than tall.

**Character 4**: Maximum height vs. maximum width aspect ratio of entire endocast: endocast width and height about equal (aspect ratio = 0.9-1.1) (0); endocast taller than wide (aspect ratio > 1.1) (1); or endocast wider than tall (aspect ratio < 0.9) (2). The endocast height/width ratio remains fairly constant throughout ontogeny, indicating that the height and width of endocranial space increase at a similar rate from day 27 to adult. There is moderate variation between individuals of comparable age, particularly those of day 27 and adult opossums. However, there is no variation in how this character is scored for *Monodelphis*, because all of the specimens examined in this study have aspect ratios less than 0.9; that is, their endocasts are taller than wide. This character is therefore uninformative for variation studies using this sample of *Monodelphis*.

**Character 5**: Cranial sutures: not visible on endocast of adult (0); or visible on endocast of adult (1). Several cranial sutures are visible on *Monodelphis* endocasts of day 48, 56, 57, 75, 76, and 90 individuals but not on any of the day 27 or the adults. The same cranial sutures are also visible on the adult *Didelphis* endocast.

**Character 6.1**: Endocast flexure: 1-5º (0); 6-10º (1); 11-15º (2); 16-20º (3); 21-25º (4); 26-30º (5); 31-35º (6); 36-40º (7); 41-45º (8); 46-50º (9); 51-55º (A); or 56-60º (B). Endocast flexure measures were rounded to the closest integer. The continuous version of this character shows both individual and ontogenetic variation for the *Monodelphis* endocasts examined.

**Character 6.2**: Endocast flexure: greater than 38º (0); or 38º or less (1). This is the discrete version of 6.1. Similar to the continuous version of this character, the discrete version also shows both individual and ontogenetic variation for the *Monodelphis* endocasts examined.

**Character 7**: Well-developed olfactory bulb casts: present on endocast (0); or absent from endocast (1). All the *Monodelphis* and *Didelphis* endocasts have well-developed olfactory bulb casts.

**Character 8**: Well-defined bony anterior terminus of the olfactory bulb casts (i.e., well-developed cribriform plate): absent (0); or present (1). All 14 *Monodelphis* skulls examined have an ossified cribriform plate; however, the cribriform plate is better ossified in later stages of ontogeny. Nonetheless, the cribriform plate is ossified enough in all specimens to determine the anterior terminus of the olfactory bulb casts. Therefore this character is uninformative for variation studies of this sample of *Monodelphis*.

However, quantification of the degree of ossification of the cribriform plate would make this character informative.

**Character 9**: Olfactory bulb cast width vs. length aspect ratio: longer than wide (aspect ratio < 0.9) (0); wider than long (aspect ratio > 1.1) (1); or length and width are about equivalent (aspect ratio = 0.9-1.1) (2). This character shows ontogenetic variation; younger individuals of the growth series have more circular olfactory bulb casts than those of adult specimens. The width/ length aspect ratio also varies between individuals of comparable age and how this character is scored for non-adult *Monodelphis* (e.g., day 27 individuals). There is no variation in how this character is scored for *Monodelphis* when considering adults only.

**Character 10.1**: Percent of endocast composed by olfactory bulb casts: 0.0-0.9% (0); 1.0-1.9% (1); 2.0-2.9% (2); 3.0-3.9% (3); 4.0-4.9% (4); 5.0-5.9% (5); 6.0-6.9% (6); 7.0-7.9% (7); 8.0-8.9% (8); 9.0-9.9% (9); 10.0-10.9% (A); 11.0-11.9% (B); 12.0-12.9% (C); 13.0-13.9% (D); 14.0-14.9% (E); 15.0-15.9% (F); or 16.0-16.9% (G). Percent data were rounded to the nearest 0.1%. This character exhibits both ontogenetic and individual variation. Relative olfactory bulb cast size increases with age in *Monodelphis* as illustrated by Figure 68. Considerable variation is also noticeable between individuals of comparable age for non-adult individuals. For example, in day 27 individuals (n=3), the olfactory bulb casts constitute a range of 3.55-7.77% of endocranial space. However, there is no variation in how this character is scored for *Monodelphis* when considering adults only.

**Character 10.2**: Percent of endocast composed by olfactory bulb casts: greater than 6% (0); or less than 6% (1). This is the discrete version of character 10.1. This

character shows both ontogenetic and individual variation when considering non-adult *Monodelphis*. But again, there is no variation in how this character is scored for *Monodelphis* when considering adults only.

**Character 11**: Circular fissure (separating olfactory bulbs from cerebral hemisphere) on endocast: poorly defined or absent (0); or well-defined (1). This character is modified from Luo and Wible (2005, character 418). The circular fissure is well demarked on all 14 *Monodelphis* and the *Didelphis* endocasts. This fissure on the endocasts results from a bony annular ridge that protrudes from the internal surface of the frontal bone.

**Character 12**: Casts of olfactory tracts: absent from endocast (0); or visible on endocast (1). The casts of the olfactory tracts are not distinguishable on any of the *Monodelphis* endocasts examined here; however, the tracts are clearly visible on the *Didelphis* endocast.

**Character 13**: Surface of cerebral hemisphere casts: lissencephalic (= smooth) (0); or gyrencephalic (= convoluted) (1). The cerebral hemisphere casts of all 14 *Monodelphis* and the *Didelphis* endocasts are without distinctive convolutions and are therefore considered lissencephalic (=smooth). Dissections confirm that the surfaces of the cerebral hemispheres themselves are also lissencephalic.

**Character 14**: Well-developed rhinal fissure on endocast: absent (0); or present (1). None of the *Monodelphis* endocasts display any trace of the rhinal fissure; however, the posterior portion of the fissure is visible on the *Didelphis* endocast. The rhinal fissure marks the ventral edge of the isocortex. Absence of this structure on an endocast does

not necessarily indicate that the brain of that animal lacked isocortex (Jerison, 1991). Dissections confirm that adult *Monodelphis* brains have a fully formed rhinal fissure.

**Character 15**: Position of rhinal fissure on endocast: on lateral wall (0); or on ventral surface (1). This character is non-applicable for the *Monodelphis* endocasts because they do not show the rhinal fissure. In *Didelphis*, the rhinal fissure appears on the lateral surface of the endocast.

**Character 16**: Well-developed median sulcus (i.e., division of the cortex into separate hemispheres) on endocast: absent (0); or present (1). The median sulcus is well-developed in all of the *Monodelphis* endocasts except for two of the day 27 opossums. A bony anteroposteriorly-oriented midline ridge hangs down from the ventral surface of the parietal and the posterior portion of the frontal to sit inside the median sulcus. This bony ridge is likely an ossification of the meninges of the brain. The median sulcus is obscured by a median blood sinus cast on the *Didelphis* endocast.

**Character 17**: Exposure of midbrain (mainly superior and inferior colliculi) on dorsal surface of endocast: absent (0); or present (1). The midbrain is not exposed on the dorsal surface of any of the endocasts of *Monodelphis* or on the *Didelphis* endocast. Dissections indicate that large blood sinuses, particularly the paired transverse sinus, are responsible for obscuring the midbrain on endocasts.

**Character 18**: Well-developed paraflocculus of the cerebellum cast: present (0); or absent (1). All of the *Monodelphis* and the *Didelphis* endocasts have well-developed parafloccular casts which are representations of the space within the subarcuate fossa of the petrosal bone. It is unclear how much of this space is actually filled with the parafloccular lobe of the cerebellum. Previous studies of *Monodelphis domestica* suggest

that the parafloccular lobes completely fill the subarcuate fossa early in postnatal ontogeny but only fill about half the space in adults (Sánchez-Villagra, 2002). However, the effects of desiccation of dead specimens on brain shape remain unexplored.

**Character 19.1**: Percent of endocast composed by parafloccular casts: 0.0-0.5% (0); 0.6-1.0% (1); 1.1-1.5% (2); 1.6-2.0% (3); 2.1-2.5% (4); 2.6-3.0% (5); 3.1-3.5% (6); 3.6-4.0% (7); or 4.1-4.5% (8). Percent data were rounded to the nearest 0.1%. The parafloccular casts are relatively larger early in *Monodelphis* ontogeny (e.g., day 27) than in adults (Figure 68). There is also some individual variation for this character; the percent of endocranial space composed by the parafloccular casts ranges from 1.36-1.83% in day 27 individuals. However, there is no variation in how this character is scored when considering adult *Monodelphis* only.

**Character 19.2**: Percent of endocast composed by parafloccular casts: greater than 1% (0); or less than 1% (1). For the discrete version of character 19, all of the *Monodelphis* specimens examined are scored the same.

**Character 20**: Vermis of cerebellum: not visible on endocast (0); or clearly visible on endocast (1). The vermis of the cerebellum leaves an impression on the dorsal surface of most of the *Monodelphis* and the *Didelphis* endocasts. The vermis cast is not discernable on any of the day 27 endocasts. Studies of endocasts of the extinct multituberculate mammal *Kryptobaatar* suggest that the vermis is obscured by a large cistern sinus (Kielan-Jaworowska and Lancaster, 2004). Dissections confirm that this is certainly not the case in *Monodelphis*.

**Character 21**: Cast of vermis of cerebellum: extends anterior to the parafloccular casts (0); or vermis remains behind parafloccular casts (1) (modified from Luo and

Wible, 2005, character 415). For the specimens in which the vermis is discernable on their endocast, the vermis is located behind the paraflocculars casts.

**Character 22**: Cerebellar hemisphere casts on endocast: not visible on endocast (0); or well-developed on endocast (1). This character is modified from Luo and Wible (2005, character 417). Cerebellar hemisphere casts are visible on most *Monodelphis* and the *Didelphis* endocasts. The cerebellar hemisphere casts are not discernable on any of the day 27 endocasts.

**Character 23**: Cast of pons on endocast: not well demarked on endocast (0); or clearly exposed on endocast (1). None of the *Monodelphis* or *Didelphis* endocasts show a cast of the pons on their ventral surfaces. This character is uninformative for variation studies using this sample of *Monodelphis*.

**Character 24**: Cast of medulla oblongata on endocast: not well-demarked on endocast (0); or clearly exposed on endocast (1). None of the *Monodelphis* or *Didelphis* endocasts show a cast of the medulla oblongata on their ventral surfaces. This character is uninformative for variation studies using this sample of *Monodelphis*.

**Character 25**: Transverse sinus cast: absent (0); or visible on endocast (1). Transverse sinus casts are visible on all *Monodelphis* and the *Didelphis* endocasts except for two of the day 27 individuals.

**Character 26**: Sigmoid sinus cast: absent (0); or visible on endocast (1). The sigmoid sinus cast is only visible on the day 48, 56, 57, 75, 76, and 90 *Monodelphis* and the adult *Didelphis*.

**Character 27**: Prootic vein cast: absent (0); or visible on endocast (1). The prootic vein casts are visible on all of the *Monodelphis* endocasts except for the day 27 individuals. The *Didelphis* endocast also has a prootic vein cast.

**Character 28**: Position of pons relative to insertion of cranial nerve V: pons lies anterior to insertion of cranial nerve V (0); or pons lies wholly posterior to the insertion of cranial nerve V (1). This character cannot be evaluated on either the *Monodelphis* or *Didelphis* endocasts because the pons is not visible on any of these. However, dissections reveal that the pons lies anterior to the insertion of cranial nerve V into the hindbrain for all *Monodelphis* specimens examined.

**Character 29**: Superior sagittal sinus: located in a space within the supraoccipital (0); or located within meninges of the brain (1). The superior sagittal sinus is located within the meninges of the brain in *Monodelphis* and *Didelphis* and therefore does not appear on any of the endocasts.

**Character 30**: Prominent parietal tube and foramen: present (0); or absent on endocast (1). The pineal organ in some non-mammalian cynodonts extends to a foramen in the skull roof and therefore is visible on cranial endocasts. *Monodelphis*, *Didelphis*, and other members of Mammalia (sensu Rowe [1988]) do not have a parietal tube and foramen visible on their endocasts because the pineal organ is covered by the extensive isocortex.

**Character 31.1**: Percent endocast composed by hypophyseal fossa: 0.00-0.09% (0); 0.10-0.19% (1); 0.20-0.29% (2); 0.30-0.39% (3); 0.40-0.49% (4); 0.50-0.59% (5); 0.60-0.69% (6); 0.70-0.79% (7); 0.80-0.89% (8); 0.90-0.99% (9); 1.00-1.09% (A); 1.10-1.19% (B); 1.20-1.29% (C); or 1.30-1.39% (D). Percent data were rounded to the nearest

0.01%. The relative size of the hypophyseal fossa shows ontogenetic variation in *Monodelphis*; the relative size of the fossa increases with age. This agrees with the observation that pituitary gland shows positive allometry with increasing body size across vertebrates (Edinger, 1942). This character also shows some individual variation, especially in adults.

**Character 31.2**: Percent endocast composed by hypophyseal fossa: less than 0.2% (0); or greater than 0.2% (1). This is the discrete version of character 31.1. Similar to the quantitative version of this character, the discrete version shows ontogenetic variation for *Monodelphis*. The adult specimens exhibit state (1) but all of the other specimens show state (0).

**Character 32**: Width vs. length aspect ratio for hypophyseal fossa: wider than long (aspect ratio > 1.1) (0); longer than wide (aspect ratio < 0.9) (1); or hypophyseal length and width are about equal (aspect ratio = 0.9-1.1) (2). The hypophyseal fossa width/length aspect ratio in *Monodelphis* decreases with age indicating that as ontogeny progresses, hypophyseal length increases at a faster rate than hypophyseal width. This character also shows some individual variation for the day 57 and day 75 age groups.

**Character 33**: Depth of hypophyseal fossa with respect to its length: fossa deeper than long (aspect ratio > 1.1) (0); fossa longer than deep (aspect ratio < 0.9) (1); or hypophyseal fossa depth and length about equal (aspect ratio = 0.9-1.1) (2). One of the day 27 (TMM M-7595) exhibits state (0), but all of the other *Monodelphis* specimens show state (1).

**Character 34**: Trigeminal nucleus casts: absent from endocast (0); or visible on hindbrain portion of endocast (1). Trigeminal nucleus casts are not visible on any of the *Monodelphis* or the *Didelphis* endocasts.

**Character 35**: Cavum epiptericum: visible on ventral surface of endocast (0); not distinguishable on endocast (1); or visible when endocast is viewed from above (2). The cavum epiptericum is visible on all of the *Monodelphis* and the *Didelphis* endocasts, but only in ventral view. This cavity is much deeper in *Didelphis* than in *Monodelphis*.

**Character 36.1**: Percent of endocast composed by cava epipterica: 0.10-0.19% (0), 0.20-0.29% (1), 0.30-0.39% (2), 0.40-0.49% (3), 0.50-0.59% (4), 0.60-0.69% (5), 0.70-0.79% (6), 0.80-0.89% (7), 0.90-0.99% (8), 1.00-1.09% (9), 1.10-1.19% (A), 1.20-1.29% (B), or 1.30-1.39% (C). Percent data were rounded to the nearest 0.01%. The relative size of the cavum epiptericum increases with ontogeny. This character also shows some individual variation, including among the adults.

**Character 36.2**: Percent of endocast composed by cava epipterica: greater than 0.5% (0); or less than 0.5% (1). Unlike the continuous version of this character, the discrete version of character 36 shows no variation among the *Monodelphis* specimens examined here.

**Character 37**: Cavum epiptericum: confluent with cavum supracochleare (0); or separate from cavum supracochleare which houses the geniculate ganglion (1). This character was modified from Luo and Wible (2005, character 313). The *Didelphis* specimen and all of the *Monodelphis* specimens examined here exhibit character state (1).

**Character 38**: Cast of orbital fissure canal: right and left canals are separate at exit of skull (0), or canals are confluent at exit (1). The right and left orbital fissure

canals are in close proximity to each other but are never confluent in the *Monodelphis* and *Didelphis* endocasts.

**Character 39**: Optic chiasm: absent from endocast (0); or visible on endocast (1). The optic chiasm is not visible on any of the *Monodelphis* or the *Didelphis* endocasts. This structure is surrounded by meninges that obscure its view in the ventral view of endocasts.

**Summary of variation among endocast characters and implications for this study**

Character 15 was not applicable for the *Monodelphis* endocasts. Of the remaining 38 characters, 13 (34%) showed some sort of variation (ontogenetic, individual, or both) and 25 (66%) were not variable. Nine of 38 characters (24%) showed significant individual variation and 13 (34%) showed ontogenetic variation.

Broken down in a different way, 11 of the 39 characters are quantitative and the remaining 28 are qualitative. Of the 11 quantitative characters, one only shows variation between individuals of comparable age, seven show both ontogenetic and individual variation, and three show no variation. Unsurprisingly, 72% of the quantitative endocast characters show some sort of variation. The qualitative characters show some variation (21%), but significantly less than the quantitative characters. Of the 28 qualitative characters, five only show ontogenetic variation, one character shows both ontogenetic and individual variation, 21 show no variation at all, and one character is not applicable to the *Monodelphis* endocasts.

These results indicate that both ontogenetic and individual variation affect how endocast characters are scored for phylogenetic analysis, at least for the taxon

*Monodelphis domestica*. However, the taxonomic extent to which these results are applicable is unclear at this point (e.g., Are these characters variable for all marsupials, all therians, or all mammals?). Further study is required to address this question.

But assuming that the polymorphism of at least some endocast characters is more widespread than the single species *Monodelphis domestica*, individual variation should be addressed by examination of multiple specimens of each taxon. Ontogenetic variation can be dealt with either by only scoring characters from individuals of comparable age (e.g., only adults) or by examining growth series for each taxon. Either approach requires a careful assessment of the ontogeny of each specimen. It is important to point out that only three characters (6, 31.1, 36.1) show variation among adult individuals examined and that all of these are quantitative characters. Therefore, if only qualitative characters are examined on adult specimens of *M. domestica*, none of the characters is variable.

Individual and ontogenetic variation of endocast characters can and should certainly be examined in other extant mammals; in particular, placentals and monotremes. However, obtaining multiple individuals of fossil taxa is not always feasible. Several key Mesozoic mammals and non-mammalian cynodonts are represented by a sample size of one and therefore variation cannot be evaluated. Even when multiple individuals of a fossil taxon are available, preservation biases further limit sample sizes. Specimens with missing, damaged, or distorted braincases will have at least some missing data for endocast characters. This is illustrated by the distortion of the hypophyseal fossa in one of the day 27 *Monodelphis* specimens (TMM M-7595). This being said, there are opportunities to examine multiple individuals of a single taxon of fossil mammal. For example, several dozen natural endocasts of the Eocene oreodont

*Bathygenys reevesi* are known from a single locality in West Texas (Wilson, 1971; Macrini, in preparation). In addition, *Kryptobaatar* (Wible and Rougier, 2000; Kielan-Jaworowska and Lancaster, 2004), *Pucadelphys* (Marshall and Muizon, 1995), and *Vincelestes* (Rougier et al., 1992) are represented by multiple complete skulls.

In closing, further studies such as this should be conducted to determine the taxonomic extent to which significant ontogenetic and individual variation of these endocast characters are present. Multiple individuals of a taxon should be examined, if possible, when scoring endocast characters for phylogenetic analysis. I chose to concentrate on examining phylogenetic variation of endocranial characters in my dissertation before beginning to rigorously examine other types of variation (e.g., individual, ontogenetic, sexual dimorphism). This chapter is only a preliminary study of polymorphism in mammalian endocasts; future studies are planned to examine variation in extant therians and monotremes as well as among taxa of fossil mammals.

TABLE 4.1. *Monodelphis domestica* specimens examined in this study. Abbreviations: [A] = body mass average for day 27 determined using data from male and female individuals of laboratory colony (Table 4.2); [B] = body mass from measurement; [C] = body mass average for a particular age determined using data from female individuals of laboratory colony (Table 4.2); [D] = body mass average for day 75 determined using data from male individuals of laboratory colony (Table 4.2); [E] = body mass estimated using skull length vs. body mass plot (Figure 61, Table 4.3); [F] = cerebellum was damaged during dissection resulting in a lower brain mass; [G] = 'retired breeder'; **BdM** = body mass; **BrM** = brain mass; **EV** = endocranial volume; **SL** = skull length.

| Specimen number | Preservation | Age | Sex | BdM (g) | SL (mm) | EV ($mm^3$) | BrM (g) |
|---|---|---|---|---|---|---|---|
| TMM M-7595 | dry skeleton | 27 | ? | 3.53[A] | 18.50 | 248.523 | ? |
| TMM M-8265 | Frozen | 27 | ? | 2.85[B] | 14.09 | 224.899 | ? |
| TMM M-8263 | Alcohol | 27 | ? | 3.15[B] | ? | ? | 0.3847 |
| TMM M-8261 | Alcohol | 27 | ? | 3.10[B] | 14.04 | 222.982 | 0.0834 |
| TMM M-7536 | dry skeleton | 48 | ♀ | 12.66[C] | 23.25 | 437.380 | ? |
| TMM M-8269 | Frozen | 48 | ♀ | 9.70[B] | 24.09 | 482.658 | ? |
| TMM M-8266 | Frozen | 56 | ♀ | 15.25[B] | 25.65 | 560.441 | 0.4085 |
| TMM M-7539 | dry skeleton | 57 | ♀ | 22.34[C] | 25.80 | 486.902 | ? |
| TMM M-7542 | dry skeleton | 75 | ♂ | 47.01[D] | 29.20 | 612.469 | ? |
| TMM M-8267 | Frozen | 76 | ♂ | 36.5[B] | 30.84 | 689.663 | 0.4677 |
| TMM M-7545 | dry skeleton | 90 | ♀ | 49.36[C] | 30.65 | 644.829 | ? |
| TMM M-8268 | Frozen | 90 | ♂ | 54.5[B] | 35.65 | 804.633 | 0.6972 |
| TMM M-8273 | Frozen | 456 | ♂ | 110.0[B] | 41.60 | 956.059 | ? |
| TMM M-8271 | Frozen | 837 | ♀ | 89.5[B] | 39.92 | 987.894 | 0.5977[F] |
| TMM M-7599 | dry skeleton | adult[G] | ♀ | 80.4[E] | 40.00 | 954.777 | ? |
| TMM M-8272 | Frozen | 467 | ♀ | 78.0[B] | 40.55 | ? | 0.7094 |
| TMM M-8270 | Frozen | 459 | ♂ | 149.0[B] | 42.35 | ? | ? |

TABLE 4.2. Weights (grams) of *M. domestica* collected from individuals of the LL2 stock from the SFBR. Data collected by John VandeBerg of SFBR. Abbreviations: **DAM** = ID number of mother, **DOB** = date of birth, **SIRE** = ID number of father.

| Parents | | | | | LL2 Litter Weights (g) | | | | |
|---|---|---|---|---|---|---|---|---|---|
| | | | | | Day 27 | Day 48 | Day 57 | Day 75 | Day 90 |
| DAM | SIRE | Litter Size | DOB | Sex | (04/10/05) | (05/01/05) | (05/10/05) | (05/28/05) | (06/12/05) |
| J2501♀ | J1159♂ | 10 | 03/14/05 | ♀ | 4.5 | 13.9 | 25.1 | 38.4 | 46.3 |
| | | | | ♀ | 4.4 | 13.7 | 24.2 | 39.9 | 52.8 |
| | | | | ♂ | 4.6 | 13.2 | 22.2 | 40.1 | 57.6 |
| | | | | ♂ | 4.5 | 14.0 | 25.7 | 33.8 | 54.2 |
| I7247♀ | J1091♂ | 11 | 03/15/05 | | (04/11/05) | (05/02/05) | (05/11/05) | (05/29/05) | (06/13/05) |
| Died | | | | ♀ | 3.5 | MATERNAL | | | |
| 04/30/05 | | | | ♀ | 3.1 | DEATH | | | |
| | | | | ♂ | 2.9 | | | | |
| | | | | ♂ | 3.3 | | | | |
| J0642♀ | J1346♂ | 11 | 03/16/05 | | (04/12/05) | (05/03/05) | (05/12/05) | (05/30/05) | (06/14/05) |
| | | | | ♀ | 3.4 | 13.4 | 21.6 | 39.0 | 53.6 |
| | | | | ♀ | 3.7 | 11.2 | 22.2 | 39.3 | 48.5 |
| | | | | ♂ | 3.2 | 13.4 | 23.9 | 53.6 | 57.0 |
| | | | | ♂ | 4.0 | 13.5 | 24.6 | 53.2 | 69.6 |
| J0403♀ | J0405♂ | 11 | 03/16/05 | | (04/12/05) | (05/03/05) | (05/12/05) | (05/30/05) | (06/14/05) |
| | | | | ♀ | 3.1 | 10.6 | LITTER | | |
| | | | | ♀ | 3.0 | 10.4 | DEATH | | |
| | | | | ♂ | 3.3 | 10.8 | | | |
| | | | | ♂ | 2.9 | 10.6 | | | |
| J1345♀ | J8871♂ | 10 | 03/17/05 | | (04/13/05) | (05/04/05) | (05/13/05) | (05/31/05) | (06/15/05) |
| | | | | ♀ | 3.7 | 13.0 | 21.5 | 39.9 | 45.2 |
| | | | | ♀ | 3.5 | 15.1 | 22.6 | 43.9 | 48.6 |
| | | | | ♂ | 3.8 | 13.3 | 26.1 | 46.2 | 48.8 |
| | | | | ♂ | 4.3 | 15.9 | 23.3 | 51.8 | 62.7 |
| J1200♀ | J3654♂ | 12 | 03/18/05 | | (04/14/05) | (05/05/05) | (05/14/05) | (06/01/05) | (06/16/05) |
| | | | | ♀ | 3.8 | WEIGHTS | 20.2 | 36.2 | 52.0 |
| | | | | ♀ | 3.1 | NOT | 21.3 | 40.2 | 47.9 |
| | | | | ♂ | 2.4 | RECORDED | 24.7 | 50.6 | 61.4 |
| | | | | ♂ | 2.8 | | 23.5 | 46.8 | 56.9 |

TABLE 4.3. Mass and total skull length data from wild and laboratory *M. domestica* specimens housed at AMNH.

| Specimen number | Sex | Mass (g) | Skull length (mm) | Specimen origin |
|---|---|---|---|---|
| AMNH 248302 | ♀ | 69 | 39.15 | wild |
| AMNH 133244 | ♂ | 90 | 39.20 | wild |
| AMNH 133247 | ♀ | 60 | 37.15 | wild |
| AMNH 133245 | ♀ | 50 | 35.25 | wild |
| AMNH 260024 | ♂ | 100 | 42.65 | wild |
| AMNH 261243 | ♀ | 42 | 34.65 | wild |
| AMNH 261242 | ♀ | 34 | 33.65 | wild |
| AMNH 261241 | ♂ | 53 | 36.20 | wild |
| AMNH 261240 | ♀ | 61 | 37.85 | wild |
| AMNH 261236 | ♂ | 49 | 37.05 | wild |
| AMNH 261235 | ♀ | 43 | 35.30 | wild |
| AMNH 261234 | ♀ | 33 | 33.95 | wild |
| AMNH 261233 | ♂ | 65 | 38.95 | wild |
| AMNH 261232 | ♀ | 47 | 34.75 | wild |
| AMNH 261231 | ♂ | 71 | 39.25 | wild |
| AMNH 263547 | ♀ | 70 | 40.30 | wild |
| AMNH 264481 | ♂ | 125 | 45.35 | laboratory |
| AMNH 264482 | ♀ | 92 | 40.20 | laboratory |

TABLE 4.4. Results from regression analyses of the adult didelphid EQ plot and the *Monodelphis* growth series EQ plot. Abbreviations: **lower CL** = lower bound of 95% confidence interval for the slope; **upper CL** = upper bound of 95% confidence interval for the slope.

| **Analysis** | y-**intercept** | **slope** | **lower CL** | **upper CL** |
|---|---|---|---|---|
| Adult didelphids | | | | |
| Least-squares | -1.0488 | 0.6099 | 0.5330 | 0.6870 |
| Major-axis | -1.0689 | 0.6187 | 0.5430 | 0.7000 |
| Reduced-major axis | -1.0763 | 0.6220 | 0.5467 | 0.7048 |
| *Monodelphis* growth series | | | | |
| Least-squares | -0.8057 | 0.3979 | 0.3410 | 0.4550 |
| Major-axis | -0.8095 | 0.4007 | 0.3443 | 0.4593 |
| Reduced-major axis | -0.8134 | 0.4037 | 0.3479 | 0.4641 |

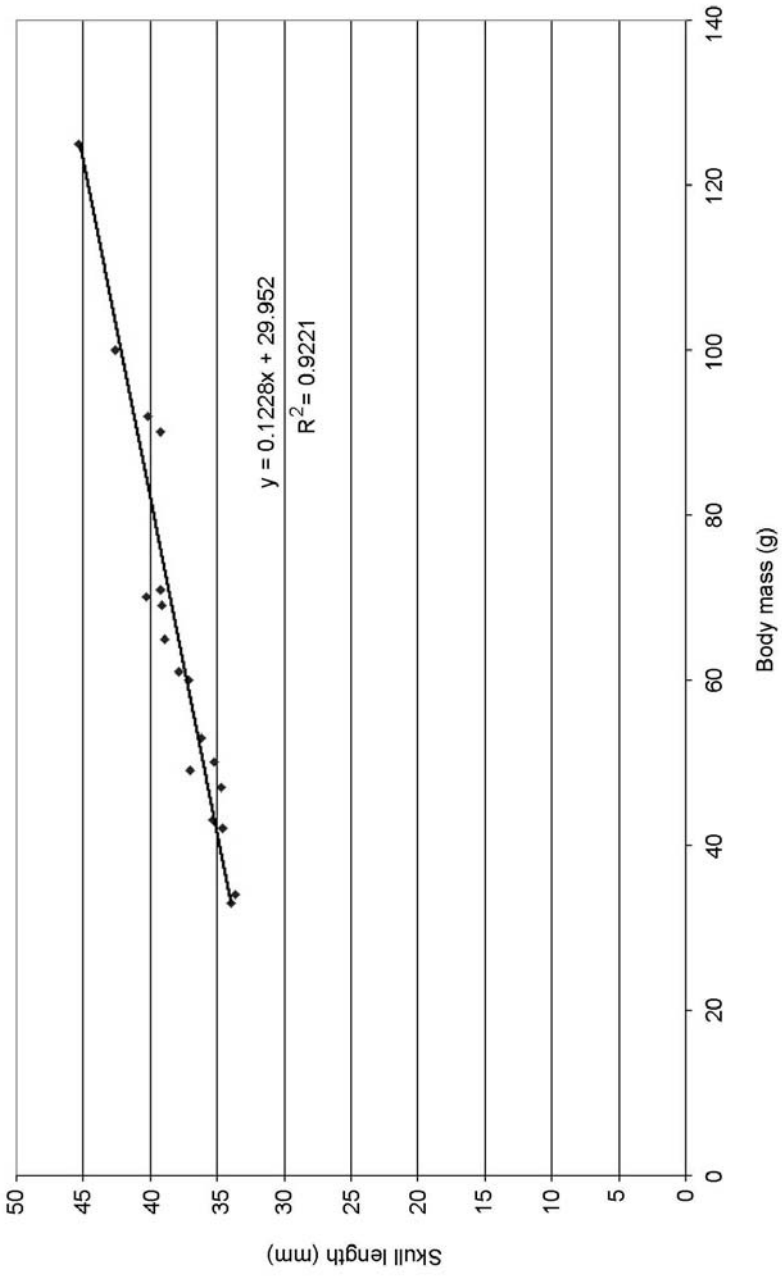


Figure 61. Bivariate plot of total skull length (mm) vs. body mass (g) for *Monodelphis domestica*. Data for plot reported in Table 4.3.

Figure 62. Dorsal views of all *Monodelphis* endocasts used in this study. Scale bars are below each corresponding endocast image. Each scale bar = 5 mm. (A) day 27 (TMM M-7595); (B) day 27 (TMM M-8261); (C) day 27 (TMM M-8265); (D) day 48 (TMM M-7536); (E) day 48 (TMM M-8269); (F) day 56 (TMM M-8266); (G) day 57 (TMM M-7539); (H) day 75 (TMM M-7542); (I) day 76 (TMM M-8267); (J) day 90 (TMM M-7545); (K) day 90 (TMM M-8268); (L) adult female (TMM M-7599); (M) adult female (TMM M-8271); (N) adult male (TMM M-8273).

A.
B.
C.
D.
E.
F.
G.
H.
I.
J.
K.
L.
M.
N.

Figure 63. Left lateral views of all *Monodelphis* endocasts used in this study. Scale bars are below each corresponding endocast image. Each scale bar = 5 mm. (A) day 27 (TMM M-7595); (B) day 27 (TMM M-8261); (C) day 27 (TMM M-8265); (D) day 48 (TMM M-7536); (E) day 48 (TMM M-8269); (F) day 56 (TMM M-8266); (G) day 57 (TMM M-7539); (H) day 75 (TMM M-7542); (I) day 76 (TMM M-8267); (J) day 90 (TMM M-7545); (K) day 90 (TMM M-8268); (L) adult female (TMM M-7599); (M) adult female (TMM M-8271); (N) adult male (TMM M-8273).

A.
B.
C.
D.
E.
F.
G.
H.
I.
J.
K.
L.
M.
N.

Figure 64. Ventral views of all *Monodelphis* endocasts used in this study. Scale bars are below each corresponding endocast image. Each scale bar = 5 mm. (A) day 27 (TMM M-7595); (B) day 27 (TMM M-8261); (C) day 27 (TMM M-8265); (D) day 48 (TMM M-7536); (E) day 48 (TMM M-8269); (F) day 56 (TMM M-8266); (G) day 57 (TMM M-7539); (H) day 75 (TMM M-7542); (I) day 76 (TMM M-8267); (J) day 90 (TMM M-7545); (K) day 90 (TMM M-8268); (L) adult female (TMM M-7599); (M) adult female (TMM M-8271); (N) adult male (TMM M-8273).

A.
B.
C.
D.
E.
F.
G.
H.
I.
J.
K.
L.
M.
N.

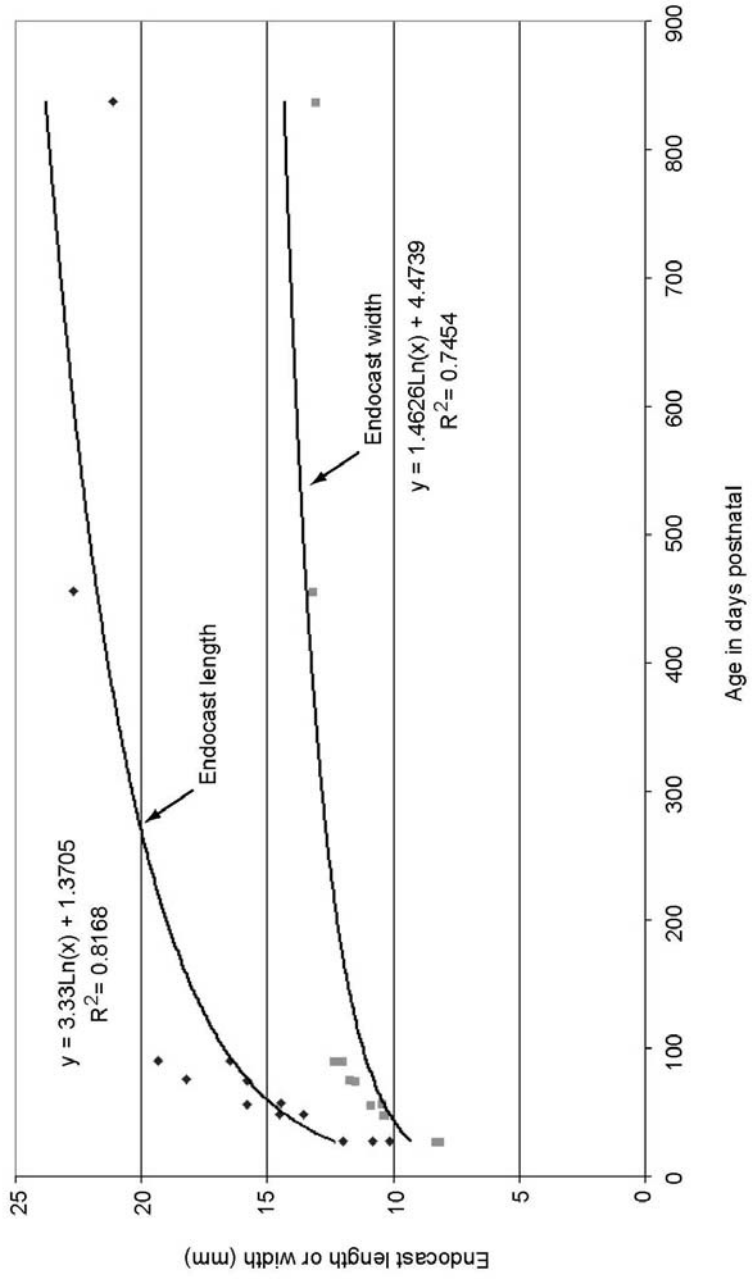


Figure 65. Bivariate plot of age vs. endocast length and age versus endocast width for *Monodelphis* growth series. Note: TMM M-7599, an adult female, was not included in plot because age in days postnatal is unknown.

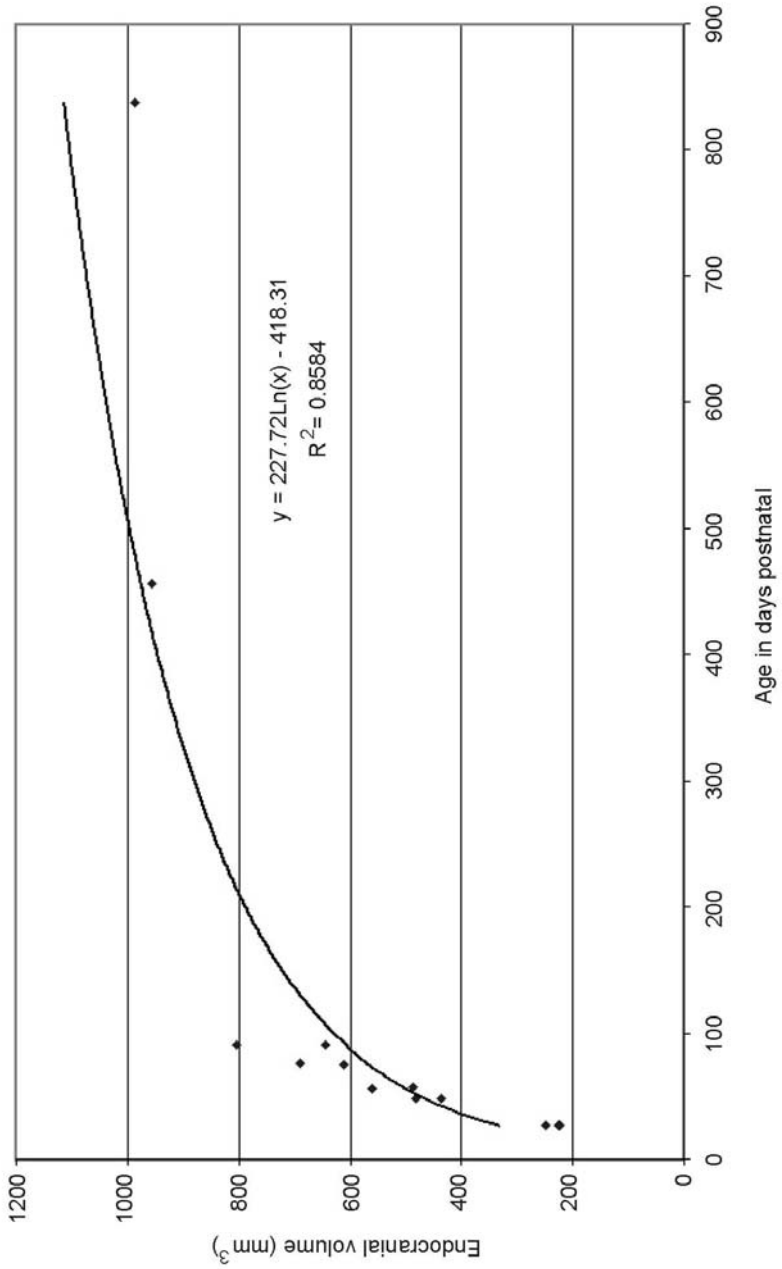


Figure 66. Bivariate plot of age vs. endocranial volume for *Monodelphis* growth series. Note: TMM M-7599, an adult female, was not included in plot because age in days postnatal is unknown.

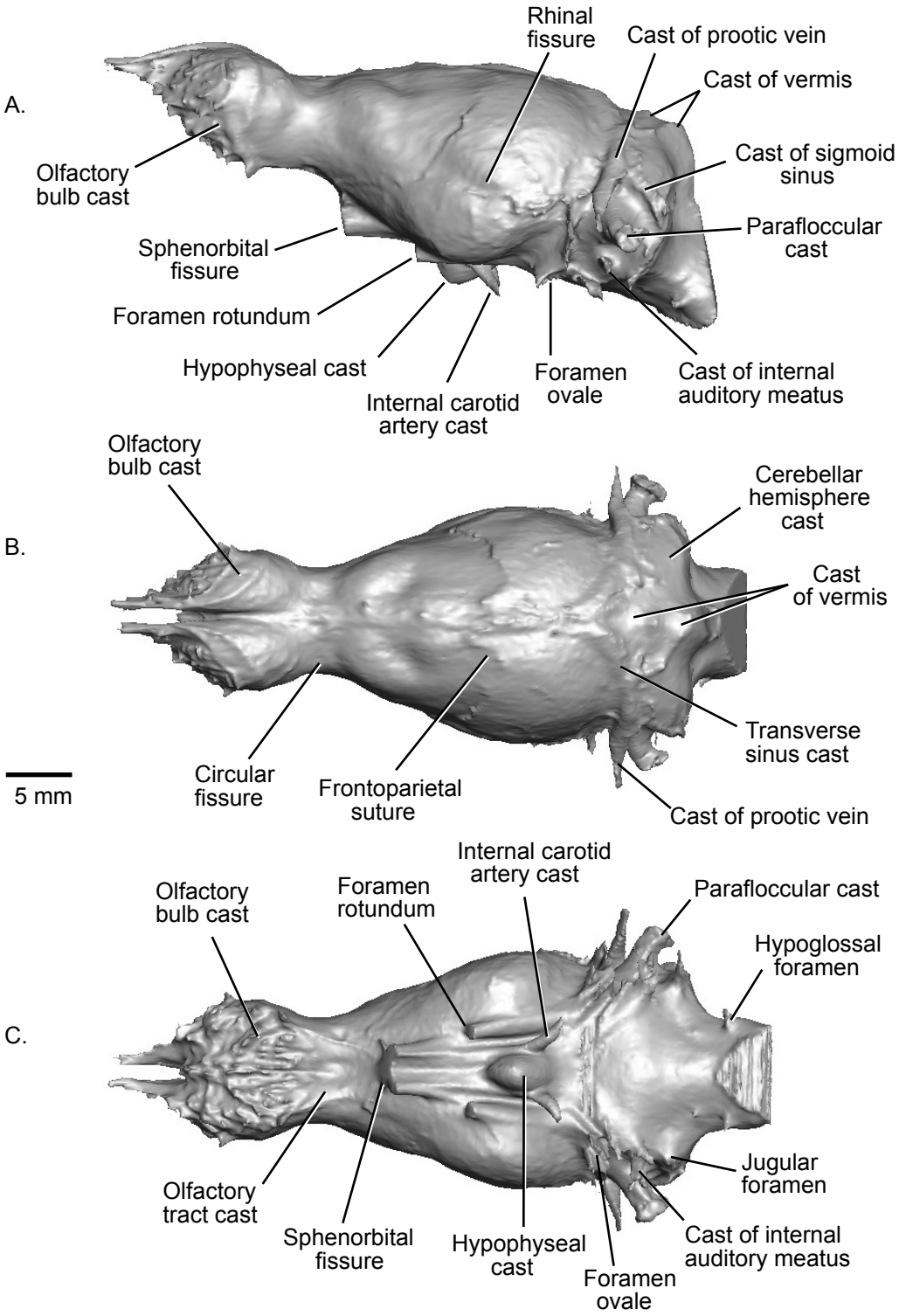


Figure 67. Digital rendering of the cranial endocast of *Didelphis virginiana* (TMM M-2517) shown in (A) left lateral, (B) dorsal, and (C) ventral views.

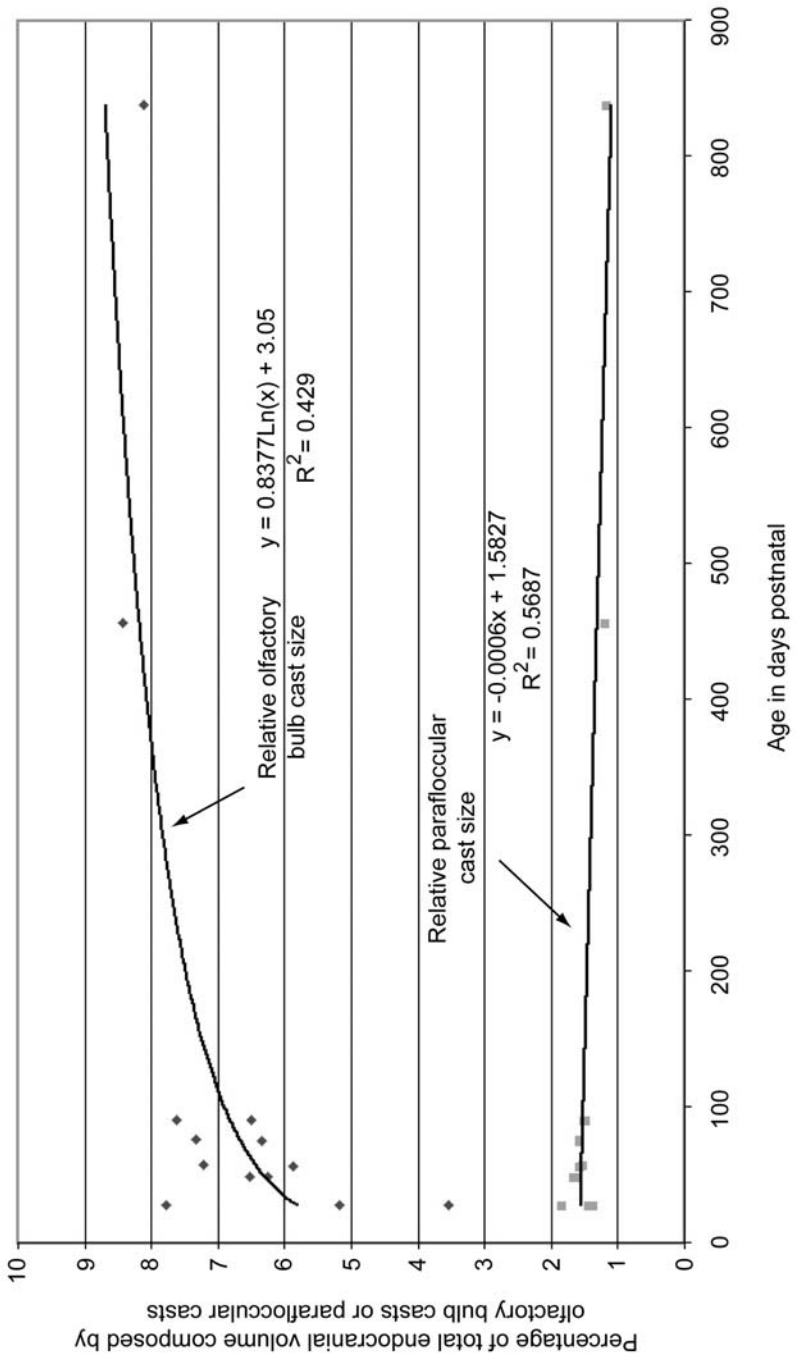


Figure 68. Bivariate plot of age vs. relative olfactory bulb cast and age vs. parafloccular cast size for *Monodelphis* growth series. Note: TMM M-7599, an adult female, was not included in plot because age in days postnatal is unknown.

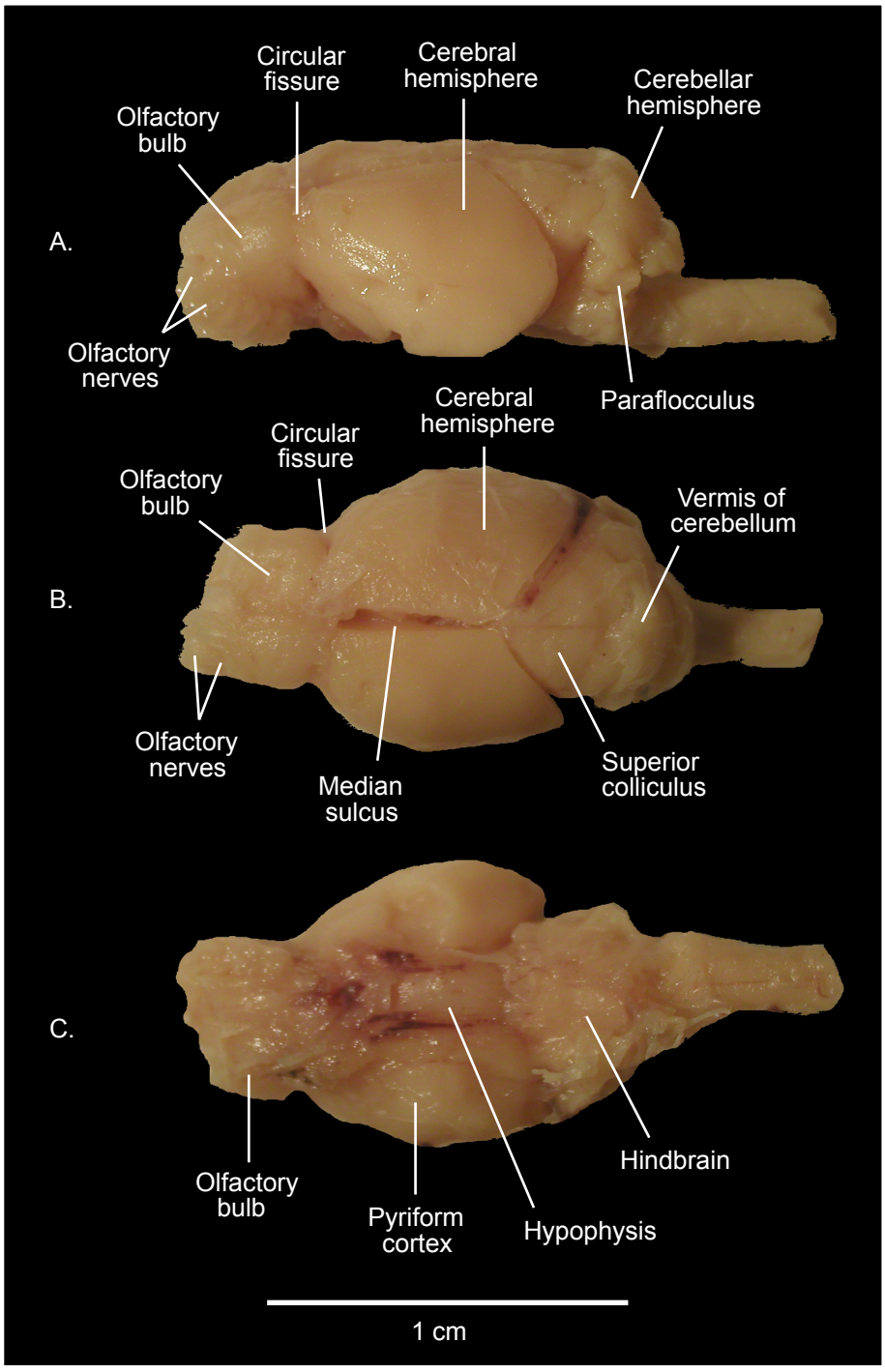


Figure 69. Photographs of the brain of a 27-day-old *Monodelphis domestica* (TMM M-8263) shown in (A) left lateral, (B) dorsal, and (C) ventral views.

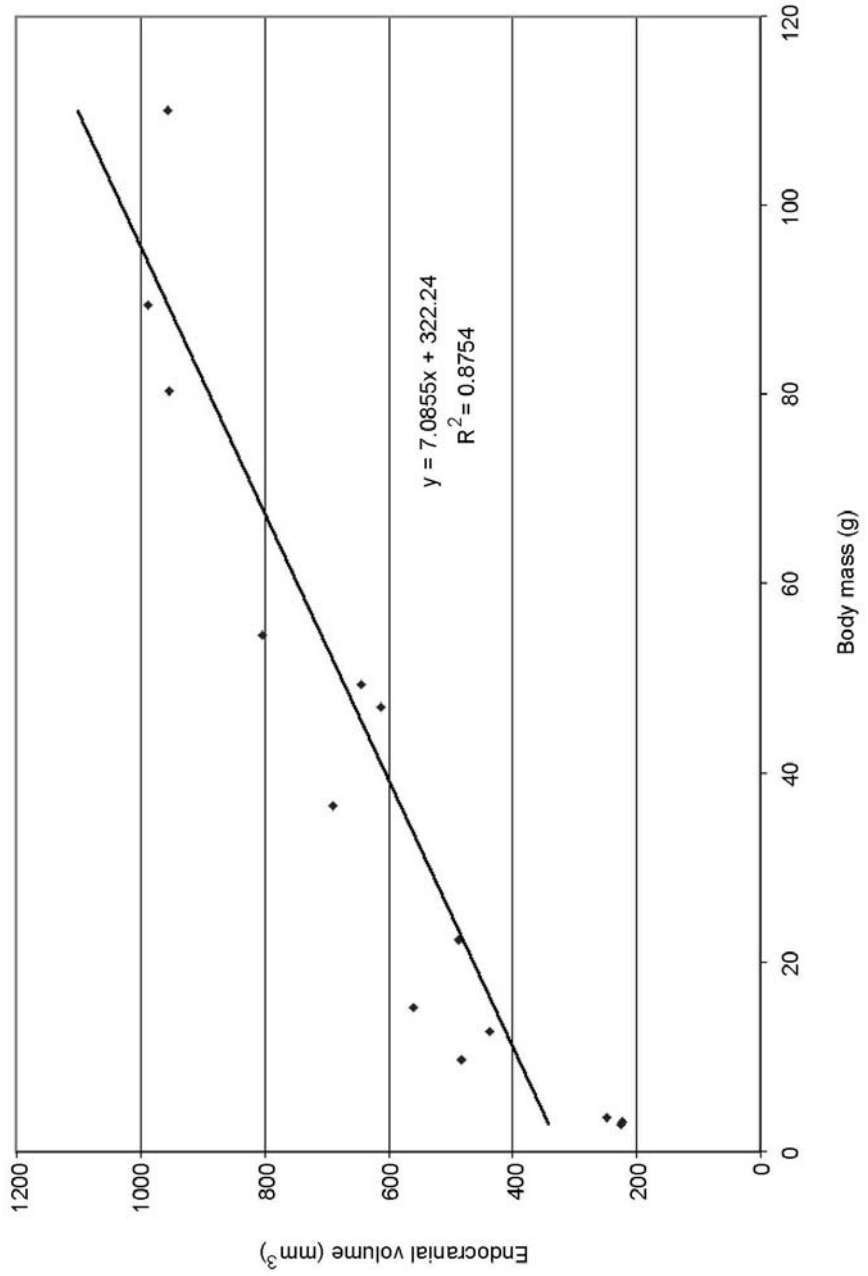


Figure 70. Bivariate plot of endocranial volume vs. body mass for *Monodelphis* growth series.

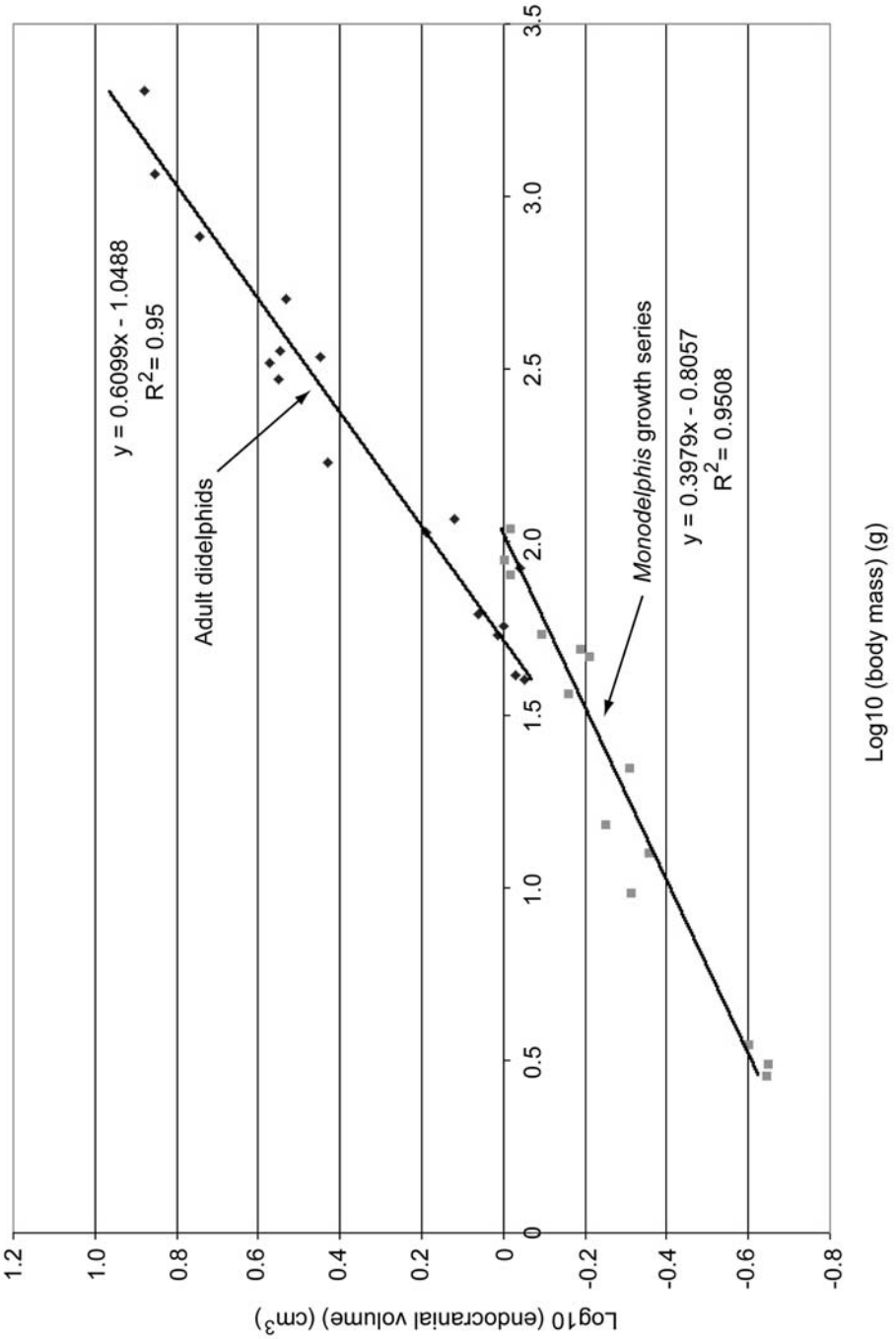


Figure 71. Bivariate plot of the endocranial volume vs. body mass for different didelphid species (data from Eisenberg and Wilson, 1981) with data from the *Monodelphis* growth series superimposed. *Monodelphis* growth series endocranial volume data were converted to $cm^3$. All data are $log_{10}$ transformed.

# Chapter 5: Summary and Discussion of Encephalization Quotients of Mammals

## SUMMARY

Historically, the evolution of endocranial space in mammals has been studied either through examination of changes in discrete characters on cranial endocasts (e.g., Edinger, 1948; Radinsky, 1977, 1981; Kielan-Jaworowska, 1986), or through quantitative comparisons of relative brain size (e.g., encephalization quotients; Jerison, 1973). The major goal of my dissertation was to cast new light on the study of endocranial space of mammals and non-mammalian cynodonts by contributing to the knowledge in terms of both discrete anatomical characters and quantitative data. The majority of my dissertation, up to this point, dealt with the first part of this goal, the examination of the evolution of discrete endocast characters.

In Chapter 2, I provided new anatomical descriptions of digital endocasts (four extinct mammals and one non-mammalian mammaliaform), and I presented endocranial volume measurements from these specimens (Appendix 1). Use of computed tomography (CT) allowed me to non-invasively isolate cranial endocasts of these rare and unique fossils in order to provide the first anatomical descriptions of the endocranial space of those taxa. Computed tomography also provides a means to accurately measure endocranial volumes (EVs) from intact skulls. I demonstrated this accuracy by comparing the EVs measured from CT data, and brain volumes of extant echidnas

(*Tachyglossus* and *Zaglossus*). Endocranial volumes measured from digital endocasts differ dramatically from endocranial volume estimates obtained by a commonly used technique that divides the endocranial space into cylinders. Differences in EV values affect calculations of EQs, particularly for extinct taxa (e.g., *Kryptobaatar*). Use of CT provides a means to standardize EV measures for fossils and, thus provides a way to aid in standardizing the methods for determining EQs. This is significant because relative brain size, as compared by EQs, is known to correlate with a number of biological and ecologically important variables (Jerison, 1973; Striedter, 2005).

In Chapter 3, I combined these new discrete anatomical data with comparative data from other fossil and extant digital endocasts, and previously published endocast data from other fossil taxa. I scored 39 anatomical characters from these endocast data, and then examined the phylogenetic distribution of these characters using a hypothesis of mammal and non-mammalian cynodont evolutionary relationships (a pruned strict consensus tree from Luo and Wible [2005]). The purpose of my analysis was to identify where major changes in the endocranial space occurred along the evolutionary lineages of Mammalia. Based on this analysis, I noted synapomorphies for the clades Mammalia, Monotremata, Theria, Placentalia, and Marsupialia (Appendix 6). I also documented the characters that were uninformative for my taxonomic sampling and based on the phylogenetic relationships depicted by Luo and Wible (2005). Some of these characters might be informative in subsequent analyses that use a denser taxonomic sampling or a different phylogenetic hypothesis.

One character I found to be uninformative (presence or absence of the rhinal fissure on cranial endocasts) was historically considered to have great significance for the

study of mammalian brain evolution (Jerison, 1973). The rhinal fissure marks the ventral border of the isocortex and therefore presumably the rhinal fissure can be used to track the expansion of the isocortex in mammals (Jerison, 1991). However, my survy finds that the rhinal fissure is a structure that is not always visible on cranial endocasts of extant mammals, corroborating the findings of others (e.g., Jerison, 1991). For example, there is no mark of the rhinal fissure on endocasts of adult *Monodelphis domestica* even though the fissure is clearly visible on the corresponding brains (Chapter 4). This taxonomic variability suggests that presence or absence of a rhinal fissure has little biological significance. Perhaps another character, such as the relative width of the endocast is a better proxy for measuring expansion of the isocortex in mammals.

In addition to examining the evolutionary history of the endocast characters, I also examined their phylogenetic utility by analyzing the endocast matrix both by itself and combined with the osteological and dental character matrix published by Luo and Wible (2005). Phylogenetic analysis of the matrix of the 39 endocast characters scored for 23 taxa shows little resolution. However, Monotremata was fully resolved based on this analysis, and was diagnosed by a single character: the pons being completely posterior to the insertion of the trigeminal nerve. Analysis of the endocast matrix included with the original Luo and Wible (2005) matrix does not significantly alter the topology of the Luo and Wible (2005) strict consensus tree. Likewise, analysis of the Luo and Wible (2005) matrix combined with my endocast matrix, but to the exclusion of taxa not present in both, did not greatly alter the tree topology obtained from analysis of the taxon-pruned version of the Luo and Wible original matrix. My endocast character had little effect on tree topology because of the overwhelming number of characters from other portions of

the skull, denition, and postcranial skeleton. Perhaps experimentation with differential weighting of distinctive anatomical character complexes in the Luo and Wible (2005) matrix will suggest that the endocranial characters are more informative for tree topology.

I chose to concentrate on examining phylogenetic variation of endocranial characters in my dissertation before beginning to rigorously examine other types of variation (e.g., individual, ontogenetic, sexual dimorphism). In Chapter 4, I presented a preliminary study of polymorphism in mammalian cranial endocasts using a single extant taxon, *Monodelphis domestica*. I examined the 39 endocast characters (from Chapter 3) for individual and ontogenetic variation among a postnatal growth series of *M. domestica*. The results indicate that to some degree both ontogenetic and individual variation affect how endocast characters are scored for phylogenetic analysis, at least for the taxon *M. domestica*. The taxonomic extent to which these results are applicable is unclear at this point and further study is required to address this question. But assuming that the variation is more widespread than the single species *M. domestica*, individual variation should be addressed by examination of multiple specimens of each taxon. Ontogenetic variation can be dealt with either by only scoring characters from individuals of comparable age (e.g., only adults) or by examining growth series for each taxon. Either approach requires a careful assessment of the ontogeny of each specimen.

Individual and ontogenetic variation of endocast characters can and should certainly be examined in other extant mammals; in particular, placentals and monotremes. Although obtaining multiple individuals of a fossil taxon is not always

feasible, there are some opportunities for variation studies of endocasts from a single taxon of fossil mammal (e.g., *Bathygenys* natural endocasts; Wilson, 1971).

## DISCUSSION OF ENCEPHALIZATION QUOTIENTS OF MAMMALS

Here I will discuss a preliminary examination of encephalization quotient data generated from endocasts I described in Chapter 2, among others. As stated in Chapter 1, an encephalization quotient (EQ) is the ratio of actual to expected brain size for a particular taxon (Jerison, 1973). These ratios are determined using plots of body size versus brain size among a number of closely related taxa. On these plots, EQs are equivalent to the residuals derived from the regression line of all the species examined in the study. These EQ plots show that brain size is allometrically related to body size among mammals and other groups of vertebrates (Jerison, 1973).

The exponent of 0.67 was originally fit for the plot of brain and body size data for mammals based on the idea that brain size scales to body surface by the same exponential factor (Jerison, 1973). Subsequent analyses were based on different statistical techniques applied to double log plots of brain size versus body size of a large sample of multiple extant mammal taxa. Most of these analyses converged on an exponent of 0.74 or 0.75 (e.g., Eisenberg and Wilson, 1978, 1981; Eisenberg, 1981; Hurlburt, 1996). In addition, a sample of brain and body mass data for 917 species of mammals was analyzed using independent contrasts, resulting in a line with a slope of 0.69 (Harvey and Krebs, 1990;

Harvey and Pagel, 1991). This suggests that brain size shows a strong allometric relationship across mammals, even when the phylogenetic effects are taken into account.

Encephalization quotients are widely utilized in the literature but also frequently criticized (e.g., Deacon, 1990; Striedter, 2005). Much of the criticism of EQ analyses revolves around their biological significance, but methodological issues associated with these analyses also raise concern. Despite all of the criticisms discussed in Chapter 1, EQs are useful for determining allometric relationships between endocranial volume and body mass for extinct animals. In addition, the degree of encephalization in mammals appears to correlate with a number of anatomical and functional correlates.

The purpose of the discussion presented here is not to determine a new encephalization quotient equation for Mammalia, but rather to examine the distribution of EQ values across mammal phylogeny for a sample of fossil and extant taxa. The first large-scale analysis of fossil and extant mammals EQs was presented by Jerison (1973). At that time, only a handful of cranial endocasts from Mesozoic/ early Tertiary mammals and non-mammalian cynodonts were available for study; these include *Thrinaxodon*, *Diademodon*, *Triconodon*, and *Ptilodus* (Jerison, 1973). Since the publication of Jerison's book in 1973, natural cranial endocasts from a number of additional taxa were described and their endocranial volumes were estimated (Quiroga, 1979, 1980a, 1980b, 1984; Kielan-Jaworowska, 1983, 1984, 1986; Kielan-Jaworowska et al., 1986; Krause and Kielan-Jaworowska, 1993; Kielan-Jaworowska and Lancaster, 2004; Zielan-Jaworowska et al., 2004). The EV data from these taxa have yet to be incorporated in a comprehensive study of EQs of fossil and extinct mammals. In addition, I provide new

data from fossil mammals and non-mammalian cynodonts that were obtained from digital endocasts described in this dissertation.

## Materials and Methods

Endocranial volumes were either obtained from the literature from natural endocast material or measured from new digital endocast material described in this dissertation. Ideally, endocranial volumes should only be measured using a standardized and accurate methodology, such as the methods presented in Chapter 2 for isolating digital endocasts from CT scans of skulls. Until more of the pertinent fossil taxa are CT scanned and digital endocasts are extracted, published volume estimates of natural endocasts have to be incorporated in EQ studies.

I measured body mass from extant specimens when possible and estimated body mass for the remanding specimens using a variety of different techniques. Endocranial volumes, body masses, and techniques for estimating body mass, when appropriate, are presented in Chapter 2 and Appendix 1. I calculated encephalization quotients for the taxa examined in this dissertation using the equations provided by three different studies (Jerison, 1973; Eisenberg, 1981; Hurlburt, 1996). These three studies provide different equations from analyses that employ different techniques and samples of mammals. For each taxon, EQs were calculated using two sets of endocranial volumes. One set of volumes includes the olfactory bulb casts, and the other set excludes the volume composed by the olfactory bulb casts. The three equations and the EQ values are provided in Appendix 4. For the purpose of the discussion in this chapter, I used

endocranial volumes that include the olfactory bulb casts to calculate EQ values from the Eisenberg (1981) equation. I chose the Eisenberg (1981) equation because the slope of the double log plot brain allometry line is 0.74, a value corroborated by several separate analyses.

**Observations**

Across vertebrate history, relative brain size has increased in a number of different lineages, with the most dramatic increases being in Chondrichthyes, Aves, and Mammalia (Striedter, 2005). The EQ data examined here, confirms that relative brain size increased initially in mammaliaforms (*Hadrocodium*, EQ = 0.49) compared to other non-mammalian cynodonts (EQs around 0.20; Jerison, 1973; Rowe, 1996a, b). Within Mammalia, relative brain size increased independently in monotremes, marsupials, and in multiple placental lineages (Figure 72). Monotremes have an average EQ (average = 0.87, range: 0.75-1.00) that is well above the EQ average for the stem mammals examined here (average = 0.25, range: 0.16-0.49). Increase in relative brain size in monotremes is possibly a result from increase in isocortex size to accommodate the additional sensory information gathered by mechano- and electroreceptors of the snout.

*Vincelestes*, a stem therian, has a relatively low EQ (0.28) compared to crown therians. This suggests that relative brain size increased in basal therians relative to their closest outgroups. Within Theria, relative brain size increases independently in marsupials and placentals. *Dromiciops australis*, el monito del monte, has a significantly larger EQ (1.54) compared to all of the other marsupials examined in this dissertation.

Didelphids, for example, have EQs that range from 0.34-1.09 (Eisenberg and Wilson, 1981; Appendix 4). The reason for this large relative brain size in *Dromiciops* is unclear. *Dromiciops* is a small (16.7-31.4 g body mass), scansorial marsupial found at high elevations in central Chile and western Argentina (Marshall, 1978). Arboreal and scansorial didelphids have relatively larger brains than terrestrial didelphid species (Eisenberg and Wilson, 1981). Arboreal and scansorial mammals might require a larger brain, and in particular a larger isocortex, to map additional sensory information to allow for navigation in a complex habitat (Eisenberg and Wilson, 1981). Perhaps the same holds true for *Dromiciops*. Within Placentalia, EQ increased independently in a number of lineages including odontocete cetaceans, primates, and elephants (summarized by Jerison, 1973; Striedter, 2005). EQ also appears to increase in sirenians (Figure 72).

**Anatomical Correlates of EQs**

In mammals, overall brain size as estimated from EQ is useful for estimating sizes of many constitute parts of the brain with the exception of the olfactory bulbs (Jerison, 1973). The parts that show positive correlation with brain size include the medulla, diencephalon, hippocampus, and cerebellum (Jerison, 1973).

In addition, overall brain size is correlated with cortical volume, neuron density, and neuronal connectivity (Jerison, 1973). Cortical volume is relatively larger in large brains than in small brains (Jerison, 1973). The relationships between brain size and the other two variables (neuron density and neuronal connectivity) require more explanation.

The number of neurons per unit volume decreases with increasing brain size, a result of a combination of causes. First, neurons increase in size with body size, but this increase is only slight and this relationship is far from isometric (Jerison, 1973; Deacon, 1990). Second, the ratio of the number of glial cells to neurons increases, therefore glia occupies more of the neuropil or inter-neural space within the brain (Jerison, 1973; Deacon, 1990). Third, axons and dendrites are larger in neurons of larger brains, thus occupying more of the neuropil than in smaller brains (Striedter, 2005).

The number of possible neuronal connections increases as the square of the number of neurons (Striedter, 2005). This makes it physically impossible for neurons to be completely connected with all other neurons in a large brain. Furthermore, large brains cannot possess a proportional amount of connectivity as present in smaller brains because of the increase in neuron number associated with increased brain size. Therefore, relative neuronal connectivity decreases with increasing brain size but absolute connectivity is maintained for the most part (Striedter, 2005). As a result of decreased neural connectivity, larger brains become more compartmentalized and functions are shared among different centers (Deacon, 1990; Striedter, 2005). It is important to point out that architectonic complexity does not necessarily increase with brain size; even if it does this does not translate into a 'measure of advancement' (Deacon, 1990). However, changes in modularity and integration of portions of the brain in response in brain size increase may not preserve the ancestral functions and inadvertently, useful modifications may occur that might be selected, leading to directional changes in evolution. Secondary modifications to size may indirectly lead to the evolution of new functionalities (Deacon, 1990).

An analogy is drawn between increasing brain size and expansion in a company. As a company becomes larger it must reorganize to remain efficient (Striedter, 2005). As the number of employees of a growing company increases they become distributed to different departments and are given more specialized tasks (Striedter, 2005). The trade-off in a larger company with more employees is the difficulty in maintaining communication among all of the employees (Striedter, 2005). This is analogous to a large brain with many neurons and a low relative neuronal connectivity.

**Other Correlates of EQs**

There have been several proposed functional correlates of high encephalization in mammals; some of these ideas are better supported than others. One general idea is that larger brains in mammals (as inferred from high EQs) serve to construct detailed maps based on sensory information obtained from the world around them (Jerison, 2001). This idea is consistent with the scaling of cortical size with overall brain size, the expansion of the isocortex in mammals, and the fact that sensory information is projected onto the surface of the cortex (Jerison, 1973, 2001).

Others have suggested that brain size and brain components have evolved to allow behavioral adaptations for changing environments (Butler and Hodos, 1996). Those animals with more complex neural networks have better opportunities for survival. This is because improved sensory capabilities allows for organisms to better detect changes in their environments (Butler and Hodos, 1996). Improved motor control allows improved locomotion behavior for escape and predation (Butler and Hodos, 1996). Expanded

neural integration provides better analysis, storage, and retrieval of information (Butler and Hodos, 1996). Therefore, larger and more complex brains allow for adaptive radiations (Butler and Hodos, 1996).

It was also proposed that overall brain size (as inferred from EQ) scales with body surface area (Jerison, 1973). If this were the case, then brain size would scale with body size by a factor of 0.67 as proposed by Jerison (1955, 1973). However, subsequent analyses have found little empirical data to support this idea and, in addition, this hypothesis does not explain why brain areas which are not associated with somatic information processing also scale with body surface area (Striedter, 2005).

The relationship between brain size and body size in mammals is similar to the relationship between basal metabolic rate and body size; with both power functions having an exponent of 0.75 (Armstrong, 1983; Striedter, 2005). An explanation for this relationship between basal metabolic rate and body size suggests that neonatal brain size is linked with maternal metabolic rate (Martin, 1981). This theory also suggests that gestation period relative to body size might account for variance in brain size for different mammalian taxa such that mammals with longer gestations produce neonates with larger brains (Martin, 1981). However, empirical evidence shows that mammals with high metabolic rates relative to their body size do not have young with large brains and, in addition, species with long gestations do not have high metabolic rates (Harvey and Krebs, 1990). Furthermore, it remains unclear why mammals would be selected to have brains as large as allowed by their metabolic rate (Harvey and Krebs, 1990). Relative brain size is poorly correlated with relative metabolic rate (as opposed to basal metabolic

rate), suggesting that if the two variables are correlated the relationship is complex (Striedter, 2005).

However, relative brain size appears to correlate with ecologically important variables, thus explaining deviations in some mammals from the brain allometry line (Harvey and Bennett, 1983; Elgar and Harvey, 1987; Harvey and Krebs, 1990; Striedter, 2005). For example, among chiropterans the frugivorous and nectivorous bats have the highest EQs and the insectivorous bats have the lowest EQs (Eisenberg and Wilson, 1978). It was suggested that foraging strategies based on locating relatively large amounts of energy-rich food sources that are temporally and spatially unpredictable require complicated information storage and retrieval capabilities and therefore larger brains (Eisenberg and Wilson, 1978). Among didelphid marsupials, relatively large brain size correlates with increased longevity, decreased litter size, and increased arboreal habitat use (Eisenberg and Wilson, 1981). A study comparing brain allometry at different taxonomic levels of mammals, suggested that at least in some cases, differences in brain size among distantly related species results from demands from different ecological niches (Pagel and Harvey, 1989).

The degree to which animals are social, that is interact and live together in groups of their own species, is possibly correlated with relative brain size (Striedter, 2005). This is referred to as 'social intelligence' or 'Machiavellian intelligence' (Dunbar, 1995; Striedter, 2005). Social intelligence is supported by the fact that highly encephalized mammals such as toothed whales, elephants, and primates are very social (Striedter, 2005). Social animals take part in a number of complex interactions with their peers which might require relatively larger brains (Striedter, 2005). An interesting idea is that

social intelligence and complex foraging behavior might both be correlated with increased brain size, especially isocortex size, in the ability of highly encephalized animals to manipulate other animals, both conspecifics and otherwise (Dunbar, 1995; Striedter, 2005).

It appears that relative brain size is also affected by sexual selection. For example, a study found that bats species with promiscuous females have relatively smaller brains than those species with females that are not promiscuous (Pitnick et al., 2006). Furthermore in species with promiscuous females, relative brain size shows negative correlation with testes size in males (Pitnick et al., 2006). This suggests that sexual selection favors a decrease in metabolically expensive brain tissue as a trade-off for increase in the amount of metabolically expensive testes (Pitnick et al., 2006).

**Causes of Increased Brain Size**

Relative brain size may increase as a result in size increase in absolute brain size or due to increase in overall body size. Selection for body size increase might cause brains to also increase in size, but not necessarily isometrically (Riska and Atchley, 1985). Experiments involving relative brain size and body size of different breeds of dogs confirm this explanation is plausible (Deacon, 1990). Furthermore, empirical evidence from rodents suggests that selection for body size during early ontogeny (prenatal or early postnatal) can explain differences in brain allometry between distantly related species (Riska and Atchley, 1985). Therefore, size increase in the brain is not necessarily caused by the increase of additional neural parts (Deacon, 1990).

However, there is some evidence that relative brain size has increased in some vertebrates independent of body size (Lande, 1979; Striedter, 2005). This can be accomplished by changes in the timing and rate of development of the brain. In many mammals, most of brain growth is completed prior to birth (exceptions are monotremes and marsupials), but body growth continues well after birth. This results in a decrease in relative brain size late in development (Striedter, 2005). Therefore, allometry plots are characterized by an initial steep phase of brain growth that scales with body growth, followed by a plateau in brain growth late in development during which time the body is continuing to grow at a steep rate (Striedter, 2005). In larger animals, the body grows for a longer period of time during the plateau stage of brain growth. The result is that, in general, larger animals have relatively smaller brains than smaller animals (Striedter, 2005).

Changes in brain growth can occur if the initial growth curve for the brain of a particular taxon is above that of its ancestors. This can occur if a larger portion of the embryo becomes neuronal precursor tissue during gastrulation (Striedter, 2005). This is the case in primates as the initial growth curve is higher and the initial steep brain growth period is prolonged in comparison to other groups of mammals (Striedter, 2005). In humans, the steep growth stage is prolonged and the plateau stage of brain growth is greatly abbreviated in comparison to other primates, resulting in a larger relative brain size (Striedter, 2005).

## Brain Size Constraints

Maximum brain size in mammals is ultimately constrained by the size of the skull and the amount of metabolic energy required by the brain to function (Aiello and Wheeler, 1995; Striedter, 2005). The brain requires a large amount of energy, 16% of the body's energy consumption in humans, which is second only to the digestive system (Striedter, 2005). In some mammals such as primates, larger brains are able to operate because the size of the gut is reduced making more metabolic energy available for the brain (Aiello and Wheeler, 1995; Striedter, 2005). The primates with smaller guts tend to eat less and consume more energy-rich foods than those taxa with larger guts (Aiello and Wheeler, 1995; Striedter, 2005).

Another idea is that brain size is constrained by the amount of metabolic resources contributed by the mother during gestation and lactation (Martin, 1996). This idea, dubbed the 'maternal energy hypothesis' is consistent with the fact that most brain growth in mammals occurs early in development (Martin, 1996); in placentals this is during an extended gestation period, and in marsupials and monotremes, the majority of brain growth occurs during an extended lactation period following birth. The maternal energy hypothesis proposes that gestation period and basal metabolic rate have a geater effect on brain size than body weight (Martin, 1996).

## Conclusions

It is apparent from the EQ data examined here, that brain size increased in a number of different lineages over the evolutionary history of Mammalia (middle Jurassic-

present). Many hypotheses were posited about the correlation of EQ with neuronal, behavioral, and physiological advantages. However, there is not one universal hypothesis that explains the EQ pattern across all of mammalian evolutionary history. The maternal energy hypothesis is particularly interesting but at this time there is not enough data to support this hypothesis for mammals outside Placentalia. It is more likely that increases of brain size in different lineages is attributed to a combinatorial effect of selective pressures from many different factors such as basal metabolic rate, length of gestation/ lactation period, behavior, and body weight. Regardless, EQ data will continue to be studied by paleoneurologists because of the availability of the pertenant data (e.g., endocranial volume) from cranial endocasts and because EQ is correlated with anatomical features of the brain (e.g., cortical volume, neuron density, neuronal connectivity) at some basic level. Cranial endocasts in general are significant because of the information they provide about gross anatomical regions of the brain in extinct animals, particularly mammals. The gross anatomy of the brain is correlated with sensory acquisition and behavior at some level.

Figure 72. Evolutionary relationships and encephalization quotient (EQ) values for a number of mammals and non-mammalian cynodonts. Cladogram is a composite from analyses by Rowe (1993), Martinez et al. (1996), Luo and Wible (2005). EQ was calculated using the Eisenberg (1981) equation; EQ values are presented in Appendix 4. Abbreviations for clades: 1 = Mammalia, 2 = Monotremata, 3 = Multituberculata, 4 = Theria, 5 = Eutheria, 6 = Placentalia, 7 = Metatheria, 8 = Marsupialia.

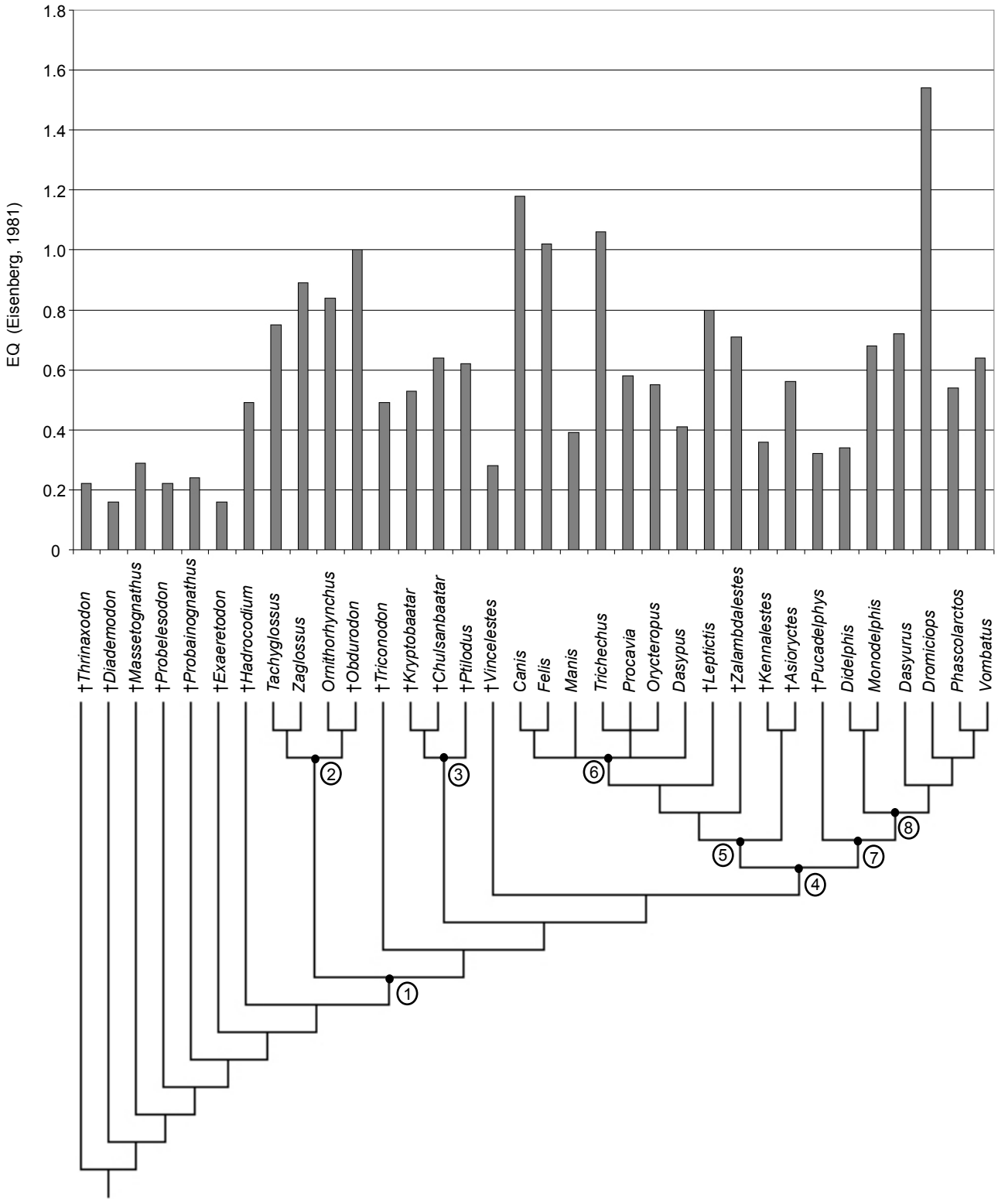
EQ (Eisenberg, 1981)
1.8
1.6
1.4
1.2
1.0
0.8
0.6
0.4
0.2
0
†Thrinaxodon
†Diademodon
†Massetognathus
†Probelesodon
†Probainognathus
†Exaeretodon
†Hadrocodium
Tachyglossus
Zaglossus
Ornithorhynchus
†Obdurodon
†Triconodon
†Kryptobaatar
†Chulsanbaatar
†Ptilodus
†Vincelestes
Canis
Felis
Manis
Trichechus
Procavia
Orycteropus
Dasypus
†Leptictis
†Zalambdalestes
†Kennalestes
†Asioryctes
†Pucadelphys
Didelphis
Monodelphis
Dasyurus
Dromiciops
Phascolarctos
Vombatus
1
2
3
4
5
6
7
8

# Appendix 1: Endocast Measurements

Abbreviations: **BM** = body mass; **CE** = cavum epiptericum; **EF** = endocast flexure; **EH** = maximum height of endocast; **E H/L ratio** = endocast height/ length aspect ratio; **E H/W ratio** = endocast height/ width aspect ratio; **EL** = anteroposterior endocast length; **EV** = endocranial volume; **EW** = maximum endocast width; **E W/L ratio** = endocast width/ length aspect ratio; **HF H** = hypophyseal fossa maximum height; **HF H/L ratio** = hypophyseal fossa height/ length aspect ratio; **HF L** = hypophyseal fossa anteroposterior length; **HF vol.** = hypophyseal fossa volume; **HF W** = hypophyseal fossa maximum width; **HF W/L ratio** = hypophyseal fossa width/ length aspect ratio; **OB H** = olfactory bulb cast height; **OB L** = olfactory bulb cast anteroposterior length; **OB vol.** = combined volume of olfactory bulb casts; **OB W** = olfactory bulb cast width; **OB W/L ratio** = olfactory bulb cast width/ length aspect ratio; **PF vol.** = combined volume of parafloccular casts; **% EV is CE** = percent of endocranial volume composed by cava epipterica; **% EV is HF** = percent of endocranial volume composed by hypophyseal fossa; **% EV is OB** = percent of endocranial volume composed by olfactory bulb casts; **% EV is PF** = percent of endocranial volume composed by parafloccular casts; **SL** = skull length; **[1]** = mass estimate from Mech (1974); **[2]** = mass estimate from McBee and Baker (1982); **[3]** = mass was measured; **[4]** = mass estimate based on lower bound of body mass range for adult *Sus scrofa*; **[5]** = mass estimate from McManus (1974); **[6]** = mass estimate from Menkhorst and Knight (2001); **[7]** = mass estimate from Luo et al. (2001b); **[8]** = mass estimate from Kielan-Jaworowska and Lancaster (2004); **[9]** = mass estimate from Nowak (1991); **[10]** = source of mass data described in Chapter 4; **[11]** = *Obdurodon* mass estimate scaled from adult *Ornithorhynchus* mass average; **[12]** = mass estimate from Pasitschniak-Arts and Marinelli (1998); **[13]** = mass estimate scaled from adult *Ornithorhynchus* mass average; **[14]** = mass estimate from Shoshani et al. (1988); **[15]** = mass estimate from Olds and Shoshani (1982); **[16]** = mass estimate scaled from *Monodelphis domestica* 90-day old individual averages; **[17]** = mass estimate from Hurlburt (1996); **[18]** = mass estimate from Rougier (1993).

| Taxon | Specimen # | Age | Sex | SL (mm) | BM (g) |
|---|---|---|---|---|---|
| *Canis lupus* | TMM M-1709 | adult | f | 224.9 | 36500[1] |
| *Dasypus novemcinctus* | TMM M-7417 | adult | ? | 86.8 | 4000[2] |
| *Dasyurus hallucatus* | TMM M-6921 | adult | f | 60.9 | 401[3] |
| *Diademodon* sp. | UCMP 42446 | adult | ? | 288 | 50000[4] |
| *Didelphis virginiana* | TMM M-2517 | adult | m | 109.6 | 2800[5] |
| *Dromiciops australis* | FMNH 127463 | adult | f | 27.7 | 21.5[3] |
| *Felis silvestris catus* | TMM M-628 | adult | ? | 90.6 | 4500[6] |
| *Hadrocodium wui* | IVPP 8275 | subadult | ? | 12 | 2.75[7] |
| *Kryptobaatar dashzevegi* | PSS-MAE 101 | adult | ? | 26.0 | 28.12[8] |
| *Manis tricuspis* | AMNH 53896 | adult | f | 73.2 | 4500[9] |
| *Monodelphis domestica* | TMM M-7595 | day 27 | ? | 18.5 | 3.53[10] |
| *Monodelphis domestica* | TMM M-8265 | day 27 | ? | 14.09 | 2.85[10] |
| *Monodelphis domestica* | TMM M-8261 | day 27 | ? | 14.04 | 3.1[10] |
| *Monodelphis domestica* | TMM M-7536 | day 48 | f | 23.25 | 12.66[10] |
| *Monodelphis domestica* | TMM M-8269 | day 48 | f | 24.09 | 9.7[10] |
| *Monodelphis domestica* | TMM M-8266 | day 56 | f | 25.65 | 15.25[10] |
| *Monodelphis domestica* | TMM M-7539 | day 57 | f | 25.8 | 22.34[10] |
| *Monodelphis domestica* | TMM M-7542 | day 75 | m | 29.2 | 47.01[10] |
| *Monodelphis domestica* | TMM M-8267 | day 76 | m | 30.84 | 36.5[10] |
| *Monodelphis domestica* | TMM M-7545 | day 90 | f | 30.65 | 49.36[10] |
| *Monodelphis domestica* | TMM M-8268 | day 90 | m | 35.65 | 54.5[10] |
| *Monodelphis domestica* | TMM M-8273 | adult | m | 41.6 | 110[10] |
| *Monodelphis domestica* | TMM M-8271 | adult | f | 39.92 | 89.5[10] |
| *Monodelphis domestica* | TMM M-7599 | adult | f | 40 | 80.4[10] |
| *Obdurodon dicksoni* | QM F20568 | adult | ? | 134.4 | 2038[11] |
| *Ornithorhynchus anatinus* | AMNH 200255 | adult | ? | 91.6 | 1389[12] |
| *Ornithorhynchus anatinus* | AMNH 252512 | juvenile | ? | 59.05 | 895[13] |
| *Orycteropus afer* | AMNH 51909 | adult | f | 250 | 60000[14] |
| *Phascolarctos cinereus* | TMM M-2946 | adult | ? | 142.9 | 9500[9] |
| *Procavia capensis* | TMM M-4351 | adult | ? | 78.7 | 3800[15] |
| *Pucadelphys andinus* | MHNC 8266 | adult | ? | 30.64 | 49[16] |
| *Tachyglossus aculeatus* | AMNH 154457 | adult | m | 99 | 4250[9] |
| *Thrinaxodon liorhinus* | UCMP 40466 | adult | ? | 68.64 | 700[17] |
| *Trichechus senegalensis* | AMNH 53939 | adult | f | 250.9 | 140000[9] |
| *Vincelestes neuquenianus* | MACN-N 04 | adult | f? | 63 | 900[18] |
| *Vombatus ursinus* | TMM M-2953 | adult | ? | 164.9 | 25000[9] |
| *Zaglossus bruijni* | AMNH 157072 | adult | m | 164 | 7500[9] |

**Appendix 1 continued.**

| Taxon | Specimen # | Log (BM) | EV (mm3) | EL (mm) |
|---|---|---|---|---|
| *Canis lupus* | TMM M-1709 | 4.562292864 | 153936.953 | 105.5 |
| *Dasypus novemcinctus* | TMM M-7417 | 3.602059991 | 10546.13 | 39.975 |
| *Dasyurus hallucatus* | TMM M-6921 | 2.603144373 | 3339.751 | 32.222 |
| *Diademodon* sp. | UCMP 42446 | 4.698970004 | 26971.117 | 68 |
| *Didelphis virginiana* | TMM M-2517 | 3.447158031 | 6608.008 | 45.672 |
| *Dromiciops australis* | FMNH 127463 | 1.33243846 | 820.999 | 16.748 |
| *Felis silvestris catus* | TMM M-628 | 3.653212514 | 28276.492 | 57.12 |
| *Hadrocodium wui* | IVPP 8275 | 0.439332694 | 45.122 | 7.201 |
| *Kryptobaatar dashzevegi* | PSS-MAE 101 | 1.449040027 | 342.87 | 15.04 |
| *Manis tricuspis* | AMNH 53896 | 3.653212514 | 10710.953 | 36.076 |
| *Monodelphis domestica* | TMM M-7595 | 0.547774705 | 248.523 | 12.02 |
| *Monodelphis domestica* | TMM M-8265 | 0.45484486 | 224.899 | 10.14 |
| *Monodelphis domestica* | TMM M-8261 | 0.491361694 | 222.982 | 10.803 |
| *Monodelphis domestica* | TMM M-7536 | 1.102433706 | 437.38 | 13.562 |
| *Monodelphis domestica* | TMM M-8269 | 0.986771734 | 482.658 | 14.515 |
| *Monodelphis domestica* | TMM M-8266 | 1.183269844 | 560.441 | 15.793 |
| *Monodelphis domestica* | TMM M-7539 | 1.349083169 | 486.902 | 14.466 |
| *Monodelphis domestica* | TMM M-7542 | 1.672190251 | 612.469 | 15.808 |
| *Monodelphis domestica* | TMM M-8267 | 1.562292864 | 689.663 | 18.2 |
| *Monodelphis domestica* | TMM M-7545 | 1.693375151 | 644.829 | 16.504 |
| *Monodelphis domestica* | TMM M-8268 | 1.736396502 | 804.633 | 19.352 |
| *Monodelphis domestica* | TMM M-8273 | 2.041392685 | 956.059 | 22.692 |
| *Monodelphis domestica* | TMM M-8271 | 1.951823035 | 987.894 | 21.105 |
| *Monodelphis domestica* | TMM M-7599 | 1.905256049 | 954.777 | 20.79 |
| *Obdurodon dicksoni* | QM F20568 | 3.30920418 | 15443.661 | 44.88 |
| *Ornithorhynchus anatinus* | AMNH 200255 | 3.142702246 | 9732.844 | 32.76 |
| *Ornithorhynchus anatinus* | AMNH 252512 | 2.951823035 | 4456.047 | 25.798 |
| *Orycteropus afer* | AMNH 51909 | 4.77815125 | 103943.078 | 112.11 |
| *Phascolarctos cinereus* | TMM M-2946 | 3.977723605 | 26275.291 | 64.26 |
| *Procavia capensis* | TMM M-4351 | 3.579783597 | 14337.555 | 50.392 |
| *Pucadelphys andinus* | MHNC 8266 | 1.69019608 | 311.506 | 16.042 |
| *Tachyglossus aculeatus* | AMNH 154457 | 3.62838893 | 20013.875 | 47.1 |
| *Thrinaxodon liorhinus* | UCMP 40466 | 2.84509804 | 1559.798 | 24.4 |
| *Trichechus senegalensis* | AMNH 53939 | 5.146128036 | 374556 | 113 |
| *Vincelestes neuquenianus* | MACN-N 04 | 2.954242509 | 2371.215 | 31.8 |
| *Vombatus ursinus* | TMM M-2953 | 4.397940009 | 63553.504 | 66.15 |
| *Zaglossus bruijni* | AMNH 157072 | 3.875061263 | 36049.008 | 53.55 |

**Appendix 1 continued.**

| Taxon | Specimen # | E W/ L ratio | EW (mm) | E H/ W ratio |
|---|---|---|---|---|
| *Canis lupus* | TMM M-1709 | 0.617412322 | 65.137 | 0.952162365 |
| *Dasypus novemcinctus* | TMM M-7417 | 0.665916198 | 26.62 | 1.141247183 |
| *Dasyurus hallucatus* | TMM M-6921 | 0.613990441 | 19.784 | 0.816467853 |
| *Diademodon* sp. | UCMP 42446 | 0.509338235 | 34.635 | 1.760011549 |
| *Didelphis virginiana* | TMM M-2517 | 0.573896479 | 26.211 | 1.136354965 |
| *Dromiciops australis* | FMNH 127463 | 0.754299021 | 12.633 | 0.855457928 |
| *Felis silvestris catus* | TMM M-628 | 0.701032913 | 40.043 | 1.016357416 |
| *Hadrocodium wui* | IVPP 8275 | 0.772948202 | 5.566 | 0.604204096 |
| *Kryptobaatar dashzevegi* | PSS-MAE 101 | 0.745478723 | 11.212 | 0.797716732 |
| *Manis tricuspis* | AMNH 53896 | 0.794406253 | 28.659 | 0.764506787 |
| *Monodelphis domestica* | TMM M-7595 | 0.680865225 | 8.184 | 0.698435973 |
| *Monodelphis domestica* | TMM M-8265 | 0.801282051 | 8.125 | 0.745846154 |
| *Monodelphis domestica* | TMM M-8261 | 0.766916597 | 8.285 | 0.786964393 |
| *Monodelphis domestica* | TMM M-7536 | 0.760138623 | 10.309 | 0.734697837 |
| *Monodelphis domestica* | TMM M-8269 | 0.713675508 | 10.359 | 0.709431412 |
| *Monodelphis domestica* | TMM M-8266 | 0.688152979 | 10.868 | 0.725064409 |
| *Monodelphis domestica* | TMM M-7539 | 0.722176137 | 10.447 | 0.757729492 |
| *Monodelphis domestica* | TMM M-7542 | 0.727606275 | 11.502 | 0.732568249 |
| *Monodelphis domestica* | TMM M-8267 | 0.642197802 | 11.688 | 0.742642026 |
| *Monodelphis domestica* | TMM M-7545 | 0.726248182 | 11.986 | 0.715167696 |
| *Monodelphis domestica* | TMM M-8268 | 0.637970236 | 12.346 | 0.70306172 |
| *Monodelphis domestica* | TMM M-8273 | 0.581173982 | 13.188 | 0.671064604 |
| *Monodelphis domestica* | TMM M-8271 | 0.619426676 | 13.073 | 0.693184426 |
| *Monodelphis domestica* | TMM M-7599 | 0.632804233 | 13.156 | 0.767862572 |
| *Obdurodon dicksoni* | QM F20568 | 0.772682709 | 34.678 | 0.740296442 |
| *Ornithorhynchus anatinus* | AMNH 200255 | 0.931043956 | 30.501 | 0.743746107 |
| *Ornithorhynchus anatinus* | AMNH 252512 | 0.969377471 | 25.008 | 0.75 |
| *Orycteropus afer* | AMNH 51909 | 0.56271519 | 63.086 | 0.891180294 |
| *Phascolarctos cinereus* | TMM M-2946 | 0.568518519 | 36.533 | 0.808447157 |
| *Procavia capensis* | TMM M-4351 | 0.567947293 | 28.62 | 0.863067785 |
| *Pucadelphys andinus* | MHNC 8266 | 0.58116195 | 9.323 | 0.750831277 |
| *Tachyglossus aculeatus* | AMNH 154457 | 0.835456476 | 39.35 | 0.716950445 |
| *Thrinaxodon liorhinus* | UCMP 40466 | 0.668278689 | 16.306 | 1.191831228 |
| *Trichechus senegalensis* | AMNH 53939 | 0.836486726 | 94.523 | 0.83483385 |
| *Vincelestes neuquenianus* | MACN-N 04 | 0.550754717 | 17.514 | 0.61213886 |
| *Vombatus ursinus* | TMM M-2953 | 0.787271353 | 52.078 | 1.079208111 |
| *Zaglossus bruijni* | AMNH 157072 | 0.944164332 | 50.56 | 0.703955696 |

**Appendix 1 continued.**

| Taxon | Specimen # | E H/ L ratio | EH (mm) | OB vol. (mm3) |
|---|---|---|---|---|
| *Canis lupus* | TMM M-1709 | 0.587876777 | 62.021 | 10385.096 |
| *Dasypus novemcinctus* | TMM M-7417 | 0.759974984 | 30.38 | 1291.994 |
| *Dasyurus hallucatus* | TMM M-6921 | 0.501303457 | 16.153 | 265.761 |
| *Diademodon* sp. | UCMP 42446 | 0.896441176 | 60.958 | ? |
| *Didelphis virginiana* | TMM M-2517 | 0.652150114 | 29.785 | 729.531 |
| *Dromiciops australis* | FMNH 127463 | 0.645271077 | 10.807 | 29.684 |
| *Felis silvestris catus* | TMM M-628 | 0.7125 | 40.698 | 691.65 |
| *Hadrocodium wui* | IVPP 8275 | 0.46701847 | 3.363 | 6.409 |
| *Kryptobaatar dashzevegi* | PSS-MAE 101 | 0.594680851 | 8.944 | 20.044 |
| *Manis tricuspis* | AMNH 53896 | 0.607328972 | 21.91 | 516.811 |
| *Monodelphis domestica* | TMM M-7595 | 0.475540765 | 5.716 | 19.318 |
| *Monodelphis domestica* | TMM M-8265 | 0.597633136 | 6.06 | 7.982 |
| *Monodelphis domestica* | TMM M-8261 | 0.603536055 | 6.52 | 11.532 |
| *Monodelphis domestica* | TMM M-7536 | 0.558472202 | 7.574 | 27.376 |
| *Monodelphis domestica* | TMM M-8269 | 0.506303824 | 7.349 | 31.491 |
| *Monodelphis domestica* | TMM M-8266 | 0.498955233 | 7.88 | 32.928 |
| *Monodelphis domestica* | TMM M-7539 | 0.547214157 | 7.916 | 35.134 |
| *Monodelphis domestica* | TMM M-7542 | 0.533021255 | 8.426 | 38.88 |
| *Monodelphis domestica* | TMM M-8267 | 0.476923077 | 8.68 | 50.655 |
| *Monodelphis domestica* | TMM M-7545 | 0.519389239 | 8.572 | 41.925 |
| *Monodelphis domestica* | TMM M-8268 | 0.448532451 | 8.68 | 61.277 |
| *Monodelphis domestica* | TMM M-8273 | 0.390005288 | 8.85 | 80.582 |
| *Monodelphis domestica* | TMM M-8271 | 0.429376925 | 9.062 | 80.249 |
| *Monodelphis domestica* | TMM M-7599 | 0.485906686 | 10.102 | 76.401 |
| *Obdurodon dicksoni* | QM F20568 | 0.57201426 | 25.672 | 293.077 |
| *Ornithorhynchus anatinus* | AMNH 200255 | 0.692460317 | 22.685 | 92.14 |
| *Ornithorhynchus anatinus* | AMNH 252512 | 0.727033103 | 18.756 | 80.359 |
| *Orycteropus afer* | AMNH 51909 | 0.501480689 | 56.221 | 10011.212 |
| *Phascolarctos cinereus* | TMM M-2946 | 0.45961718 | 29.535 | 671.817 |
| *Procavia capensis* | TMM M-4351 | 0.490177012 | 24.701 | 460.123 |
| *Pucadelphys andinus* | MHNC 8266 | 0.436354569 | 7 | 36.41 |
| *Tachyglossus aculeatus* | AMNH 154457 | 0.598980892 | 28.212 | 456.046 |
| *Thrinaxodon liorhinus* | UCMP 40466 | 0.79647541 | 19.434 | ? |
| *Trichechus senegalensis* | AMNH 53939 | 0.698327434 | 78.911 | n/a |
| *Vincelestes neuquenianus* | MACN-N 04 | 0.337138365 | 10.721 | 256.238 |
| *Vombatus ursinus* | TMM M-2953 | 0.84962963 | 56.203 | 1995.414 |
| *Zaglossus bruijni* | AMNH 157072 | 0.66464986 | 35.592 | 1108.623 |

**Appendix 1 continued.**

| Taxon | Specimen # | % EV is OB | OB L (mm) | OB W (mm) |
|---|---|---|---|---|
| *Canis lupus* | TMM M-1709 | 6.746330753 | 26 | 12.886 |
| *Dasypus novemcinctus* | TMM M-7417 | 12.25088255 | 11.562 | 10.02 |
| *Dasyurus hallucatus* | TMM M-6921 | 7.957509407 | 7.448 | 4.376 |
| *Diademodon* sp. | UCMP 42446 | n/a | ? | ? |
| *Didelphis virginiana* | TMM M-2517 | 11.04010467 | 14.916 | 6.354 |
| *Dromiciops australis* | FMNH 127463 | 3.615595147 | 3.397 | 2.578 |
| *Felis silvestris catus* | TMM M-628 | 2.446024776 | 11.662 | 5.365 |
| *Hadrocodium wui* | IVPP 8275 | 14.20371437 | 2.082 | 1.453 |
| *Kryptobaatar dashzevegi* | PSS-MAE 101 | 5.845947444 | 3.52 | 2.709 |
| *Manis tricuspis* | AMNH 53896 | 4.825070187 | 5.22 | 9.615 |
| *Monodelphis domestica* | TMM M-7595 | 7.773123614 | 2.857 | 2.331 |
| *Monodelphis domestica* | TMM M-8265 | 3.549148729 | 1.589 | 2.04 |
| *Monodelphis domestica* | TMM M-8261 | 5.171717897 | 2.097 | 1.974 |
| *Monodelphis domestica* | TMM M-7536 | 6.259088207 | 3.375 | 2.598 |
| *Monodelphis domestica* | TMM M-8269 | 6.524495606 | 3.478 | 2.457 |
| *Monodelphis domestica* | TMM M-8266 | 5.875373144 | 3.514 | 2.601 |
| *Monodelphis domestica* | TMM M-7539 | 7.215825772 | 3.853 | 2.678 |
| *Monodelphis domestica* | TMM M-7542 | 6.348076392 | 4.013 | 2.5 |
| *Monodelphis domestica* | TMM M-8267 | 7.344891635 | 5.042 | 2.679 |
| *Monodelphis domestica* | TMM M-7545 | 6.501723713 | 4.365 | 2.709 |
| *Monodelphis domestica* | TMM M-8268 | 7.61552161 | 4.85 | 2.765 |
| *Monodelphis domestica* | TMM M-8273 | 8.428559325 | 5 | 3.007 |
| *Monodelphis domestica* | TMM M-8271 | 8.123239943 | 5.04 | 2.813 |
| *Monodelphis domestica* | TMM M-7599 | 8.001973236 | 5.22 | 2.874 |
| *Obdurodon dicksoni* | QM F20568 | 1.897717128 | 7.48 | 5.745 |
| *Ornithorhynchus anatinus* | AMNH 200255 | 0.94669143 | 4.62 | 3.824 |
| *Ornithorhynchus anatinus* | AMNH 252512 | 1.803369668 | 4.241 | 3.481 |
| *Orycteropus afer* | AMNH 51909 | 9.631436929 | 23.836 | 18.277 |
| *Phascolarctos cinereus* | TMM M-2946 | 2.556839428 | 8.568 | 5.669 |
| *Procavia capensis* | TMM M-4351 | 3.209215239 | 9.184 | 8.841 |
| *Pucadelphys andinus* | MHNC 8266 | 11.68837839 | 3.976 | 2.468 |
| *Tachyglossus aculeatus* | AMNH 154457 | 2.278649187 | 8.4 | 10.71 |
| *Thrinaxodon liorhinus* | UCMP 40466 | n/a | ? | ? |
| *Trichechus senegalensis* | AMNH 53939 | n/a | n/a | n/a |
| *Vincelestes neuquenianus* | MACN-N 04 | 10.80619008 | 9.2 | 4.546 |
| *Vombatus ursinus* | TMM M-2953 | 3.139738762 | 10.35 | 11.086 |
| *Zaglossus bruijni* | AMNH 157072 | 3.075321795 | 12.425 | 14.108 |

**Appendix 1 continued.**

| Taxon | Specimen # | OB W/ L ratio | OB H (mm) | PF vol. (mm3) |
|---|---|---|---|---|
| *Canis lupus* | TMM M-1709 | 0.495615385 | 37.383 | 122.873 |
| *Dasypus novemcinctus* | TMM M-7417 | 0.866632071 | 15.982 | n/a |
| *Dasyurus hallucatus* | TMM M-6921 | 0.587540279 | 7.401 | 45.512 |
| *Diademodon* sp. | UCMP 42446 | n/a | ? | n/a |
| *Didelphis virginiana* | TMM M-2517 | 0.425985519 | 11.835 | 39.166 |
| *Dromiciops australis* | FMNH 127463 | 0.758904916 | 3.781 | 11.867 |
| *Felis silvestris catus* | TMM M-628 | 0.460041159 | 15.703 | n/a |
| *Hadrocodium wui* | IVPP 8275 | 0.697886647 | 2.355 | 0.127 |
| *Kryptobaatar dashzevegi* | PSS-MAE 101 | 0.769602273 | 2.646 | 13.844 |
| *Manis tricuspis* | AMNH 53896 | 1.841954023 | 12.157 | n/a |
| *Monodelphis domestica* | TMM M-7595 | 0.815890795 | 3.101 | 3.383 |
| *Monodelphis domestica* | TMM M-8265 | 1.283826306 | 2.454 | 3.211 |
| *Monodelphis domestica* | TMM M-8261 | 0.941344778 | 2.564 | 4.08 |
| *Monodelphis domestica* | TMM M-7536 | 0.769777778 | 3.363 | 7.276 |
| *Monodelphis domestica* | TMM M-8269 | 0.706440483 | 3.852 | 7.767 |
| *Monodelphis domestica* | TMM M-8266 | 0.740182129 | 4.095 | 8.752 |
| *Monodelphis domestica* | TMM M-7539 | 0.695042824 | 4.016 | 7.406 |
| *Monodelphis domestica* | TMM M-7542 | 0.62297533 | 4.23 | 9.68 |
| *Monodelphis domestica* | TMM M-8267 | 0.531336771 | 4.641 | 10.861 |
| *Monodelphis domestica* | TMM M-7545 | 0.620618557 | 3.934 | 9.549 |
| *Monodelphis domestica* | TMM M-8268 | 0.570103093 | 4.526 | 12.137 |
| *Monodelphis domestica* | TMM M-8273 | 0.6014 | 4.765 | 11.343 |
| *Monodelphis domestica* | TMM M-8271 | 0.558134921 | 4.792 | 11.491 |
| *Monodelphis domestica* | TMM M-7599 | 0.550574713 | 4.714 | 10.544 |
| *Obdurodon dicksoni* | QM F20568 | 0.768048128 | 9.213 | 88.484 |
| *Ornithorhynchus anatinus* | AMNH 200255 | 0.827705628 | 5.353 | 56.633 |
| *Ornithorhynchus anatinus* | AMNH 252512 | 0.820796982 | 6.188 | 31.608 |
| *Orycteropus afer* | AMNH 51909 | 0.766781339 | 26.162 | n/a |
| *Phascolarctos cinereus* | TMM M-2946 | 0.661647993 | 13.857 | 110.78 |
| *Procavia capensis* | TMM M-4351 | 0.962652439 | 13.034 | 12.589 |
| *Pucadelphys andinus* | MHNC 8266 | 0.620724346 | 3.7 | 2.971 |
| *Tachyglossus aculeatus* | AMNH 154457 | 1.275 | 7.711 | n/a |
| *Thrinaxodon liorhinus* | UCMP 40466 | n/a | ? | 29.37 |
| *Trichechus senegalensis* | AMNH 53939 | n/a | n/a | ? |
| *Vincelestes neuquenianus* | MACN-N 04 | 0.494130435 | 6.348 | 5.365 |
| *Vombatus ursinus* | TMM M-2953 | 1.071111111 | 19.25 | n/a |
| *Zaglossus bruijni* | AMNH 157072 | 1.135452716 | 12.174 | n/a |

**Appendix 1 continued.**

| Taxon | Specimen # | % EV is PF | HF vol. (mm3) | % EV is HF |
|---|---|---|---|---|
| *Canis lupus* | TMM M-1709 | 0.07982034 | 139.555 | 0.090657245 |
| *Dasypus novemcinctus* | TMM M-7417 | n/a | 2.102 | 0.019931482 |
| *Dasyurus hallucatus* | TMM M-6921 | 1.362736324 | 1.264 | 0.037847133 |
| *Diademodon* sp. | UCMP 42446 | n/a | 357.58 | 1.32578862 |
| *Didelphis virginiana* | TMM M-2517 | 0.592705094 | 31.375 | 0.474802694 |
| *Dromiciops australis* | FMNH 127463 | 1.44543416 | 0.277 | 0.033739383 |
| *Felis silvestris catus* | TMM M-628 | n/a | 23.928 | 0.084621529 |
| *Hadrocodium wui* | IVPP 8275 | 0.281459155 | 0.097 | 0.214972741 |
| *Kryptobaatar dashzevegi* | PSS-MAE 101 | 4.03768192 | 2.624 | 0.765304634 |
| *Manis tricuspis* | AMNH 53896 | n/a | 16.016 | 0.149529178 |
| *Monodelphis domestica* | TMM M-7595 | 1.361242219 | 0.118 | 0.047480515 |
| *Monodelphis domestica* | TMM M-8265 | 1.427752013 | 0.195 | 0.086705588 |
| *Monodelphis domestica* | TMM M-8261 | 1.829744105 | 0.229 | 0.102698873 |
| *Monodelphis domestica* | TMM M-7536 | 1.663542 | 0.29 | 0.0663039 |
| *Monodelphis domestica* | TMM M-8269 | 1.609213978 | 0.432 | 0.08950437 |
| *Monodelphis domestica* | TMM M-8266 | 1.561627361 | 0.407 | 0.072621382 |
| *Monodelphis domestica* | TMM M-7539 | 1.521045303 | 0.765 | 0.157115806 |
| *Monodelphis domestica* | TMM M-7542 | 1.580488155 | 0.492 | 0.080330596 |
| *Monodelphis domestica* | TMM M-8267 | 1.574827126 | 0.498 | 0.07220918 |
| *Monodelphis domestica* | TMM M-7545 | 1.480857716 | 0.541 | 0.083898212 |
| *Monodelphis domestica* | TMM M-8268 | 1.508389539 | 1.01 | 0.125523065 |
| *Monodelphis domestica* | TMM M-8273 | 1.186433055 | 2.358 | 0.246637498 |
| *Monodelphis domestica* | TMM M-8271 | 1.163181475 | 2.871 | 0.290618224 |
| *Monodelphis domestica* | TMM M-7599 | 1.104341642 | 5.558 | 0.58212546 |
| *Obdurodon dicksoni* | QM F20568 | 0.572947049 | 26.962 | 0.174582957 |
| *Ornithorhynchus anatinus* | AMNH 200255 | 0.581875144 | 9.53 | 0.097915882 |
| *Ornithorhynchus anatinus* | AMNH 252512 | 0.709328245 | 3.383 | 0.075919307 |
| *Orycteropus afer* | AMNH 51909 | n/a | 160.368 | 0.154284444 |
| *Phascolarctos cinereus* | TMM M-2946 | 0.421612838 | 18.228 | 0.069373161 |
| *Procavia capensis* | TMM M-4351 | 0.087804371 | 25.448 | 0.177491908 |
| *Pucadelphys andinus* | MHNC 8266 | 0.9537537 | 1.687 | 0.541562602 |
| *Tachyglossus aculeatus* | AMNH 154457 | n/a | 32.385 | 0.161812742 |
| *Thrinaxodon liorhinus* | UCMP 40466 | 1.882936124 | 2.448 | 0.156943399 |
| *Trichechus senegalensis* | AMNH 53939 | n/a | 317.297 | 0.084712833 |
| *Vincelestes neuquenianus* | MACN-N 04 | 0.226255316 | 16.935 | 0.714190826 |
| *Vombatus ursinus* | TMM M-2953 | n/a | 42.579 | 0.066997093 |
| *Zaglossus bruijni* | AMNH 157072 | n/a | 15.108 | 0.041909614 |

**Appendix 1 continued.**

| Taxon | Specimen # | HF L (mm) | HF W/ L ratio | HF W (mm) |
|---|---|---|---|---|
| *Canis lupus* | TMM M-1709 | 6.5 | 2.352769231 | 15.293 |
| *Dasypus novemcinctus* | TMM M-7417 | 2.952 | 0.938685637 | 2.771 |
| *Dasyurus hallucatus* | TMM M-6921 | 2.509 | 0.797927461 | 2.002 |
| *Diademodon* sp. | UCMP 42446 | 6.4 | 2.92234375 | 18.703 |
| *Didelphis virginiana* | TMM M-2517 | 5.544 | 0.816558442 | 4.527 |
| *Dromiciops australis* | FMNH 127463 | 1.501 | 0.586942039 | 0.881 |
| *Felis silvestris catus* | TMM M-628 | 5.474 | 1.099744246 | 6.02 |
| *Hadrocodium wui* | IVPP 8275 | 0.917 | 1.264994547 | 1.16 |
| *Kryptobaatar dashzevegi* | PSS-MAE 101 | 1.6 | 1.33875 | 2.142 |
| *Manis tricuspis* | AMNH 53896 | 5.452 | 0.915627293 | 4.992 |
| *Monodelphis domestica* | TMM M-7595 | 0.445 | 3.934831461 | 1.751 |
| *Monodelphis domestica* | TMM M-8265 | 1.318 | 1.104704097 | 1.456 |
| *Monodelphis domestica* | TMM M-8261 | 1.289 | 1.108611327 | 1.429 |
| *Monodelphis domestica* | TMM M-7536 | 1.812 | 0.799668874 | 1.449 |
| *Monodelphis domestica* | TMM M-8269 | 2.058 | 0.634596696 | 1.306 |
| *Monodelphis domestica* | TMM M-8266 | 2.52 | 0.518253968 | 1.306 |
| *Monodelphis domestica* | TMM M-7539 | 1.96 | 1.158163265 | 2.27 |
| *Monodelphis domestica* | TMM M-7542 | 1.824 | 1.264802632 | 2.307 |
| *Monodelphis domestica* | TMM M-8267 | 2.737 | 0.470953599 | 1.289 |
| *Monodelphis domestica* | TMM M-7545 | 2.182 | 0.850137489 | 1.855 |
| *Monodelphis domestica* | TMM M-8268 | 3.265 | 0.482695253 | 1.576 |
| *Monodelphis domestica* | TMM M-8273 | 3.188 | 0.795483061 | 2.536 |
| *Monodelphis domestica* | TMM M-8271 | 3.78 | 0.675132275 | 2.552 |
| *Monodelphis domestica* | TMM M-7599 | 3.96 | 0.793686869 | 3.143 |
| *Obdurodon dicksoni* | QM F20568 | 6.6 | 0.690151515 | 4.555 |
| *Ornithorhynchus anatinus* | AMNH 200255 | 4.41 | 0.597278912 | 2.634 |
| *Ornithorhynchus anatinus* | AMNH 252512 | 3.416 | 0.679156909 | 2.32 |
| *Orycteropus afer* | AMNH 51909 | 17.776 | 0.490605311 | 8.721 |
| *Phascolarctos cinereus* | TMM M-2946 | 4.522 | 0.773772667 | 3.499 |
| *Procavia capensis* | TMM M-4351 | 7.986 | 0.650513398 | 5.195 |
| *Pucadelphys andinus* | MHNC 8266 | 2.674 | 1.102468212 | 2.948 |
| *Tachyglossus aculeatus* | AMNH 154457 | 9.45 | 0.563386243 | 5.324 |
| *Thrinaxodon liorhinus* | UCMP 40466 | 2.6 | 1.130384615 | 2.939 |
| *Trichechus senegalensis* | AMNH 53939 | 11 | 1.703090909 | 18.734 |
| *Vincelestes neuquenianus* | MACN-N 04 | 4.211 | 0.997387794 | 4.2 |
| *Vombatus ursinus* | TMM M-2953 | 6.75 | 0.789333333 | 5.328 |
| *Zaglossus bruijni* | AMNH 157072 | 7 | 0.726428571 | 5.085 |

**Appendix 1 continued.**

| Taxon | Specimen # | HF H/ L ratio | HF H (mm) | EF (degrees) |
|---|---|---|---|---|
| *Canis lupus* | TMM M-1709 | 0.740615385 | 4.814 | 16 |
| *Dasypus novemcinctus* | TMM M-7417 | 0.201219512 | 0.594 | 27 |
| *Dasyurus hallucatus* | TMM M-6921 | 0.278198485 | 0.698 | 34 |
| *Diademodon* sp. | UCMP 42446 | 1.35296875 | 8.659 | ? |
| *Didelphis virginiana* | TMM M-2517 | 0.601731602 | 3.336 | 40 |
| *Dromiciops australis* | FMNH 127463 | 0.372418388 | 0.559 | 36 |
| *Felis silvestris catus* | TMM M-628 | 0.717208623 | 3.926 | 26 |
| *Hadrocodium wui* | IVPP 8275 | 0.625954198 | 0.574 | 45 |
| *Kryptobaatar dashzevegi* | PSS-MAE 101 | 0.97125 | 1.554 | 20 |
| *Manis tricuspis* | AMNH 53896 | 0.228906823 | 1.248 | ? |
| *Monodelphis domestica* | TMM M-7595 | 1.137078652 | 0.506 | 38 |
| *Monodelphis domestica* | TMM M-8265 | 0.269347496 | 0.355 | 52 |
| *Monodelphis domestica* | TMM M-8261 | 0.321955004 | 0.415 | 32 |
| *Monodelphis domestica* | TMM M-7536 | 0.316777042 | 0.574 | 42 |
| *Monodelphis domestica* | TMM M-8269 | 0.172011662 | 0.354 | 45 |
| *Monodelphis domestica* | TMM M-8266 | 0.167063492 | 0.421 | 48 |
| *Monodelphis domestica* | TMM M-7539 | 0.296938776 | 0.582 | 46 |
| *Monodelphis domestica* | TMM M-7542 | 0.287280702 | 0.524 | 37 |
| *Monodelphis domestica* | TMM M-8267 | 0.177932042 | 0.487 | 45 |
| *Monodelphis domestica* | TMM M-7545 | 0.323098075 | 0.705 | 38 |
| *Monodelphis domestica* | TMM M-8268 | 0.131699847 | 0.43 | 41 |
| *Monodelphis domestica* | TMM M-8273 | 0.257214555 | 0.82 | 38 |
| *Monodelphis domestica* | TMM M-8271 | 0.22037037 | 0.833 | 46 |
| *Monodelphis domestica* | TMM M-7599 | 0.317424242 | 1.257 | 46 |
| *Obdurodon dicksoni* | QM F20568 | 0.345 | 2.277 | 40 |
| *Ornithorhynchus anatinus* | AMNH 200255 | 0.500907029 | 2.209 | 52 |
| *Ornithorhynchus anatinus* | AMNH 252512 | 0.37734192 | 1.289 | 42 |
| *Orycteropus afer* | AMNH 51909 | 0.459270927 | 8.164 | ? |
| *Phascolarctos cinereus* | TMM M-2946 | 0.464396285 | 2.1 | 24 |
| *Procavia capensis* | TMM M-4351 | 0.22827448 | 1.823 | ? |
| *Pucadelphys andinus* | MHNC 8266 | 0.261780105 | 0.7 | 26 |
| *Tachyglossus aculeatus* | AMNH 154457 | 0.226666667 | 2.142 | 43 |
| *Thrinaxodon liorhinus* | UCMP 40466 | 0.546923077 | 1.422 | ? |
| *Trichechus senegalensis* | AMNH 53939 | 0.387090909 | 4.258 | n/a |
| *Vincelestes neuquenianus* | MACN-N 04 | 0.613630967 | 2.584 | 23 |
| *Vombatus ursinus* | TMM M-2953 | 0.763851852 | 5.156 | 36 |
| *Zaglossus bruijni* | AMNH 157072 | 0.204571429 | 1.432 | 49 |

**Appendix 1 continued.**

| Taxon | Specimen # | CE vol. | % EV is CE |
|---|---|---|---|
| *Canis lupus* | TMM M-1709 | 1345.863 | 0.874294946 |
| *Dasypus novemcinctus* | TMM M-7417 | 12.987 | 0.123144699 |
| *Dasyurus hallucatus* | TMM M-6921 | 15.978 | 0.4784189 |
| *Diademodon* sp. | UCMP 42446 | n/a | n/a |
| *Didelphis virginiana* | TMM M-2517 | 41.428 | 0.626936287 |
| *Dromiciops australis* | FMNH 127463 | 1.178 | 0.143483731 |
| *Felis silvestris catus* | TMM M-628 | 115.852 | 0.40971136 |
| *Hadrocodium wui* | IVPP 8275 | 0.325 | 0.720269492 |
| *Kryptobaatar dashzevegi* | PSS-MAE 101 | 4.666 | 1.360865634 |
| *Manis tricuspis* | AMNH 53896 | ? | ? |
| *Monodelphis domestica* | TMM M-7595 | 0.418 | 0.168193688 |
| *Monodelphis domestica* | TMM M-8265 | 0.345 | 0.153402194 |
| *Monodelphis domestica* | TMM M-8261 | 0.413 | 0.185216744 |
| *Monodelphis domestica* | TMM M-7536 | 1.267 | 0.289679455 |
| *Monodelphis domestica* | TMM M-8269 | 1.474 | 0.305392224 |
| *Monodelphis domestica* | TMM M-8266 | 1.44 | 0.256940516 |
| *Monodelphis domestica* | TMM M-7539 | 1.24 | 0.254671371 |
| *Monodelphis domestica* | TMM M-7542 | 2.097 | 0.342384676 |
| *Monodelphis domestica* | TMM M-8267 | 2.308 | 0.334656202 |
| *Monodelphis domestica* | TMM M-7545 | 2.724 | 0.422437576 |
| *Monodelphis domestica* | TMM M-8268 | 2.825 | 0.35109174 |
| *Monodelphis domestica* | TMM M-8273 | 4.212 | 0.440558585 |
| *Monodelphis domestica* | TMM M-8271 | 3.855 | 0.390224052 |
| *Monodelphis domestica* | TMM M-7599 | 4.032 | 0.422297563 |
| *Obdurodon dicksoni* | QM F20568 | 207.51 | 1.343658087 |
| *Ornithorhynchus anatinus* | AMNH 200255 | 106.201 | 1.091161021 |
| *Ornithorhynchus anatinus* | AMNH 252512 | 55.238 | 1.239618882 |
| *Orycteropus afer* | AMNH 51909 | ? | ? |
| *Phascolarctos cinereus* | TMM M-2946 | 151.722 | 0.577432235 |
| *Procavia capensis* | TMM M-4351 | ? | ? |
| *Pucadelphys andinus* | MHNC 8266 | 0.521 | 0.167251995 |
| *Tachyglossus aculeatus* | AMNH 154457 | 260.505 | 1.301622 |
| *Thrinaxodon liorhinus* | UCMP 40466 | n/a | n/a |
| *Trichechus senegalensis* | AMNH 53939 | ? | n/a |
| *Vincelestes neuquenianus* | MACN-N 04 | 19.335 | 0.815404761 |
| *Vombatus ursinus* | TMM M-2953 | 375.567 | 0.590946173 |
| *Zaglossus bruijni* | AMNH 157072 | 398.766 | 1.106177457 |

# Appendix 2: CT Scan Parameters

Definitions and Abbreviations: **Detector** – UTCT uses three detector systems. These include the image intensifier (II) detector, the P250D detector, and the radiographic line scanner (RLS). The II detector is used for small specimens (10 cm maximum length), and the P250D and RLS detectors have a maximum size constraint of 30-40 cm. **Number of slices** – the number of slices obtained in the original slice plane (coronal slice plane unless otherwise noted). **Slice thickness** – thickness of slices, measured in mm. **Interslice spacing** – distance between consecutive slices, measured in mm. If the interslice spacing value is less than slice thickness for a particular scan, this indicates there is overlap between consecutive slices. Slice overlap may improve image quality in some instances. Field of reconstruction (**FR**) – dimensions of the CT slices, measured in mm. **File size** – 512 x 512 pixel slice or 1024 x 1024 pixel slice. Field of reconstruction divided by file size determines the in-plane resolution of the image. **A** = The *Pucadelphys* skull was scanned in horizontal plane. **B** = The *Thrinaxodon* skull was scanned in the horizontal plane at Scientific Measurement Systems (**SMS**), Inc. (Austin, TX) in 1992.

| Taxon | Specimen # | Detector | Number of slices | Slice Thickness | Interslice Spacing | FR | File size |
|---|---|---|---|---|---|---|---|
| *Canis lupus* | TMM M-1709 | RLS | 457 | 0.5 | 0.5 | 145 | 512 |
| *Dasypus novemcinctus* | TMM M-7417 | II | 711 | 0.123 | 0.123 | 38 | 1024 |
| *Dasyurus hallucatus* | TMM M-6921 | II | 781 | 0.0784 | 0.0784 | 35.75 | 1024 |
| *Diademodon* sp. | UCMP 42446 | P250D | 410 | 1.0 | 0.8 | 266 | 1024 |
| *Didelphis virginiana* | TMM M-2517 | II | 859 | 0.132 | 0.132 | 61 | 1024 |
| *Dromiciops australis* | FMNH 127463 | II | 711 | 0.0395 | 0.0395 | 16.5 | 1024 |
| *Felis silvestris catus* | TMM M-628 | II | 387 | 0.238 | 0.238 | 67 | 512 |
| *Hadrocodium wui* | IVPP 8275 | II | 735 | 0.0191 | 0.0191 | 9.0 | 1024 |
| *Kryptobaatar dashzevegi* | PSS-MAE 101 | II | 364 | 0.11 | 0.08 | 21.5 | 512 |
| *Manis tricuspis* | AMNH 53896 | II | 648 | 0.116 | 0.116 | 35.5 | 1024 |
| *Monodelphis domestica* | TMM M-7595 | II | 495 | 0.0371 | 0.0371 | 10.8 | 512 |
| *Monodelphis domestica* | TMM M-8265 | II | 570 | 0.0338 | 0.0338 | 13 | 1024 |
| *Monodelphis domestica* | TMM M-8261 | II | 345 | 0.0483 | 0.0483 | 16.5 | 1024 |
| *Monodelphis domestica* | TMM M-7536 | II | 381 | 0.0625 | 0.0625 | 14 | 512 |
| *Monodelphis domestica* | TMM M-8269 | II | 795 | 0.03549 | 0.03549 | 17 | 1024 |
| *Monodelphis domestica* | TMM M-8266 | II | 825 | 0.03549 | 0.03549 | 17 | 1024 |
| *Monodelphis domestica* | TMM M-7539 | II | 390 | 0.0676 | 0.0676 | 14.9 | 512 |
| *Monodelphis domestica* | TMM M-7542 | II | 481 | 0.0608 | 0.0608 | 17.9 | 512 |
| *Monodelphis domestica* | TMM M-8267 | II | 720 | 0.04802 | 0.04802 | 22 | 1024 |
| *Monodelphis domestica* | TMM M-7545 | II | 455 | 0.0682 | 0.0682 | 19 | 512 |
| *Monodelphis domestica* | TMM M-8268 | II | 780 | 0.04802 | 0.04802 | 22 | 1024 |

| Taxon | Specimen # | Detector | Number of slices | Slice Thickness | Interslice Spacing | FR | File size |
|---|---|---|---|---|---|---|---|
| *Monodelphis domestica* | TMM M-8273 | II | 248 | 0.117 | 0.117 | 55.65 | 1024 |
| *Monodelphis domestica* | TMM M-8271 | II | 465 | 0.105 | 0.105 | 40 | 1024 |
| *Monodelphis domestica* | TMM M-7599 | II | 450 | 0.095 | 0.09 | 23 | 512 |
| *Obdurodon dicksoni* | QM F20568 | II | 612 | 0.26 | 0.22 | 53 | 512 |
| *Ornithorhynchus anatinus* | AMNH 200255 | II | 438 | 0.21 | 0.21 | 53 | 512 |
| *Ornithorhynchus anatinus* | AMNH 252512 | II | 522 | 0.157 | 0.15 | 33 | 512 |
| *Orycteropus afer* | AMNH 51909 | II | 1237 | 0.202 | 0.202 | 95 | 1024 |
| *Phascolarctos cinereus* | TMM M-2946 | II | 599 | 0.238 | 0.238 | 107.5 | 1024 |
| *Procavia capensis* | TMM M-4351 | II | 975 | 0.07986 | 0.07986 | 70 | 1024 |
| *Pucadelphys andinus* | MHNC 8266 | II | 213[A] | 0.1 | 0.1 | 35.1 | 512 |
| *Tachyglossus aculeatus* | AMNH 154457 | II | 693 | 0.15 | 0.15 | 47 | 1024 |
| *Thrinaxodon liorhinus*[B] | UCMP 40466 | SMS | 153 | 0.2 | 0.2 | ? | 512 |
| *Trichechus senegalensis* | AMNH 53939 | P250D | 560 | 0.5 | 0.5 | 218 | 1024 |
| *Vincelestes neuquenianus* | MACN-N 04 | II | 315 | 0.21 | 0.2 | 49 | 512 |
| *Vombatus ursinus* | TMM M-2953 | P250D | 399 | 0.5 | 0.45 | 132 | 1024 |
| *Zaglossus bruijni* | AMNH 157072 | II | 909 | 0.175 | 0.175 | 55 | 1024 |

# Appendix 3: Relevant Web Addresses

| Description/Specimen | Web address |
|---|---|
| UTCT website | <www.ctlab.geo.utexas.edu/index.php> |
| Digimorph homepage | <www.digimorph.org> |
| *Canis lupus* | <www.digimorph.org/specimens/Canis_lupus_lycaon/> |
| *Dasypus novemcinctus* | <www.digimorph.org/specimens/Dasypus_novemcinctus/> |
| *Dasyurus hallucatus* | <www.digimorph.org/specimens/Dasyurus_hallucatus/> |
| *Diademodon* sp. | <www.digimorph.org/specimens/Diademodon_sp/> |
| *Didelphis virginiana* | <www.digimorph.org/specimens/Didelphis_virginiana/> |
| *Dromiciops australis* | <www.digimorph.org/specimens/Dromiciops_australis/> |
| *Felis silvestris catus* | <www.digimorph.org/specimens/Felis_silvestris_catus/> |
| *Hadrocodium wui* | <www.digimorph.org/specimens/Hadrocodium_wui/> |
| *Kryptobaatar dashzevegi* | <www.digimorph.org/specimens/Kryptobaatar_dashzevegi/> |
| *Monodelphis domestica* adult female (TMM M-7599) | <www.digimorph.org/specimens/Monodelphis_domestica/adult/> |
| *Monodelphis domestica* adult male (TMM M-8273) | <www.digimorph.org/specimens/Monodelphis_domestica/whole/> |
| *Monodelphis domestica* day 27 (TMM M-7595) | <www.digimorph.org/specimens/Monodelphis_domestica/day27/> |
| *Monodelphis domestica* day 48 (TMM M-7536) | <www.digimorph.org/specimens/Monodelphis_domestica/day48/> |
| *Monodelphis domestica* day 57 (TMM M-7539) | <www.digimorph.org/specimens/Monodelphis_domestica/day57/> |
| *Monodelphis domestica* day 75 (TMM M-7542) | <www.digimorph.org/specimens/Monodelphis_domestica/day75/> |

| **Description/Specimen** | **Web address** |
|---|---|
| *Monodelphis domestica* | <www.digimorph.org/specimens/Monodelphis_domestica/day90/> |
| day 90 (TMM M-7545) | |
| *Obdurodon dicksoni* | <www.digimorph.org/specimens/Obdurodon_dicksoni> |
| *Orycteropus afer* | <www.digimorph.org/specimens/Orycteropus_afer/> |
| adult *Ornithorhynchus anatinus* | <www.digimorph.org/specimens/Ornithorhynchus_anatinus/adult/> |
| juvenile *Ornithorhynchus anatinus* | <www.digimorph.org/specimens/Ornithorhynchus_anatinus/juvenile/> |
| *Phascolarctos cinereus* | <www.digimorph.org/specimens/Phascolarctos_cinereus/> |
| *Pucadelphys andinus* | <www.digimorph.org/specimens/Pucadelphys_andinus> |
| *Tachyglossus aculeatus* | <www.digimorph.org/specimens/Tachyglossus_aculeatus/skull/> |
| *Thrinaxodon liorhinus* | <www.digimorph.org/specimens/Thrinaxodon_liorhinus/> |
| *Trichechus senegalensis* | <www.digimorph.org/specimens/Trichechus_senegalensis/> |
| *Vincelestes neuquenianus* | <www.digimorph.org/specimens/Vincelestes_neuquenianus> |
| *Vombatus ursinus* | <www.digimorph.org/specimens/Vombatus_ursinus/> |
| *Zaglossus bruijni* | <www.digimorph.org/specimens/Zaglossus_bruijni/> |

# Appendix 4: Encephalization Quotients

Encephalization quotient values calculated from endocranial volumes including and excluding the olfactory bulbs using three different equations. Equation A = $EV/(0.12[Wt]^{0.67})$; from Jerison (1973). Equation B = $EV/(0.055[Wt]^{0.74})$; from Eisenberg (1981). Equation C = $EV/(0.047[Wt]^{0.79})$; from Hurlburt (1996) for extant mammals with body masses under 300 g. Abbreviations: **A** = adult; **EQ** = encephalization quotient; **Equat**. = equation; **EV** = endocranial volume; **J** = juvenile; **Reference 1** = Kielan-Jaworowska (1984); **Reference 2** = Kielan-Jaworowska (1983); **Reference 3** = Eisenberg and Wilson (1981); **Reference 4** = Quiroga (1980b); **Reference 5** = Novacek (1982); **Reference 6** = Krause and Kielan-Jaworowska (1993); **Reference 7** = Kielan-Jaworowska et al. (2004); **Reference 8** = Jerison (1973); **Wt** = weight or body mass; **1** = EQ calculated with olfactory bulbs; **2** = EQ calculated without olfactory bulbs. *Monodelphis domestica* range is based on EQs calculated from the three adult specimens listed in Appendix 1. *Hadrocodium wui* range is based on EQs calculated using two different estimates of body mass: 2 g and 3.5 g.

| Taxon | Equat. A | Equat. B | Equat. C | Data source |
|---|---|---|---|---|
| *Asioryctes nemegetensis*[1] | 0.33 | 0.56 | 0.54 | Reference 1 |
| *Asioryctes nemegetensis*[2] | 0.30 | 0.51 | 0.49 | Reference 1 |
| *Canis lupus*[1] | 1.13 | 1.18 | N/A | Appendix 1 |
| *Canis lupus*[2] | 1.05 | 1.10 | N/A | Appendix 1 |
| *Chulsanbaatar vulgaris*[1] | 0.30-0.35 | 0.54-0.64 | 0.56-0.67 | Reference 2 |
| *Chulsanbaatar vulgaris*[2] | ? | ? | ? | Reference 2 |
| *Dasypus novemcinctus*[1] | 0.34 | 0.41 | N/A | Appendix 1 |
| *Dasypus novemcinctus*[2] | 0.30 | 0.36 | N/A | Appendix 1 |
| *Dasyurus hallucatus*[1] | 0.50 | 0.72 | N/A | Appendix 1 |
| *Dasyurus hallucatus*[2] | 0.46 | 0.66 | N/A | Appendix 1 |
| *Diademodon* sp[1] | 0.16 | 0.16 | N/A | Appendix 1 |

| Taxon | Equat. A | Equat. B | Equat. C | Data source |
|---|---|---|---|---|
| *Diademodon* sp[2] | ? | ? | N/A | Appendix 1 |
| didelphids[1] | 0.38-0.72 | 0.50-1.09 | N/A | Reference 3 |
| didelphids[2] | ? | ? | ? | Reference 3 |
| *Didelphis virginiana*[1] | 0.27 | 0.34 | N/A | Appendix 1 |
| *Didelphis virginiana*[2] | 0.24 | 0.30 | N/A | Appendix 1 |
| *Dromiciops australis*[1] | 0.88 | 1.54 | 1.55 | Appendix 1 |
| *Dromiciops australis*[2] | 0.84 | 1.49 | 1.49 | Appendix 1 |
| *Exaeretodon* sp[1] | 0.11-0.15 | 0.11-0.16 | N/A | Reference 4 |
| *Exaeretodon* sp[2] | 0.08-0.12 | 0.09-0.13 | N/A | Reference 4 |
| *Felis silvestris catus*[1] | 0.84 | 1.02 | N/A | Appendix 1 |
| *Felis silvestris catus*[2] | 0.82 | 0.99 | N/A | Appendix 1 |
| *Hadrocodium wui*[1] | 0.16-0.24 | 0.32-0.49 | 0.36-0.55 | Appendix 1 |
| *Hadrocodium wui*[2] | 0.14-0.20 | 0.28-0.42 | 0.31-0.48 | Appendix 1 |
| *Kennalestes gobiensis*[1] | 0.21 | 0.36 | 0.35 | Reference 1 |
| *Kennalestes gobiensis*[2] | 0.19 | 0.33 | 0.32 | Reference 1 |
| *Kryptobaatar dashzevegi*[1] | 0.30 | 0.53 | 0.52 | Appendix 1 |
| *Kryptobaatar dashzevegi*[2] | 0.29 | 0.50 | 0.49 | Appendix 1 |
| *Leptictis dakotensis*[1] | 0.54-0.70 | 0.59-0.80 | N/A | Reference 5 |
| *Leptictis dakotensis*[2] | 0.45-0.58 | 0.47-0.64 | N/A | Reference 5 |
| *Manis tricuspis*[1] | 0.32 | 0.39 | N/A | Appendix 1 |
| *Manis tricuspis*[2] | 0.30 | 0.37 | N/A | Appendix 1 |
| *Massetognathus* sp[1] | 0.15-0.22 | 0.19-0.29 | N/A | Reference 4 |
| *Massetognathus* sp[2] | 0.14-0.21 | 0.18-0.21 | N/A | Reference 4 |

| Taxon | Equat. A | Equat. B | Equat. C | Data source |
|---|---|---|---|---|
| *Monodelphis domestica*[1] | 0.34–0.42 | 0.54–0.68 | 0.50–0.63 | Appendix 1 |
| *Monodelphis domestica*[2] | 0.31–0.39 | 0.49–0.62 | 0.45–0.58 | Appendix 1 |
| *Obdurodon dicksoni*[1] | 0.78 | 1.00 | N/A | Appendix 1 |
| *Obdurodon dicksoni*[2] | 0.77 | 0.98 | N/A | Appendix 1 |
| *Ornithorhynchus anatinus*[1A] | 0.64 | 0.84 | N/A | Appendix 1 |
| *Ornithorhynchus anatinus*[2A] | 0.63 | 0.83 | N/A | Appendix 1 |
| *Ornithorhynchus anatinus*[1J] | 0.39 | 0.53 | N/A | Appendix 1 |
| *Ornithorhynchus anatinus*[2J] | 0.38 | 0.52 | N/A | Appendix 1 |
| *Orycteropus afer*[1] | 0.54 | 0.55 | N/A | Appendix 1 |
| *Orycteropus afer*[2] | 0.49 | 0.50 | N/A | Appendix 1 |
| *Phascolarctos cinereus*[1] | 0.47 | 0.54 | N/A | Appendix 1 |
| *Phascolarctos cinereus*[2] | 0.46 | 0.53 | N/A | Appendix 1 |
| *Probainognathus jenseni*[1] | 0.12-0.17 | 0.16-0.24 | N/A | Reference 4 |
| *Probainognathus jenseni* [2] | 0.11-0.16 | 0.15-0.23 | N/A | Reference 4 |
| *Probelesodon* sp[1] | 0.13-0.18 | 0.15-0.22 | N/A | Reference 4 |
| *Probelesodon* sp[2] | 0.12-0.16 | 0.14-0.21 | N/A | Reference 4 |
| *Procavia capensis*[1] | 0.48 | 0.58 | N/A | Appendix 1 |
| *Procavia capensis*[2] | 0.46 | 0.57 | N/A | Appendix 1 |
| *Ptilodus* sp[1] | 0.41 | 0.62 | 0.56 | Reference 6 |
| *Ptilodus* sp[2] | 0.36 | 0.55 | 0.50 | Reference 6 |
| *Pucadelphys andinus*[1] | 0.19 | 0.32 | 0.31 | Appendix 1 |
| *Pucadelphys andinus*[2] | 0.17 | 0.28 | 0.27 | Appendix 1 |
| *Tachyglossus aculeatus*[1] | 0.62 | 0.75 | N/A | Appendix 1 |

| Taxon | Equat. A | Equat. B | Equat. C | Data source |
|---|---|---|---|---|
| *Tachyglossus aculeatus*[2] | 0.60 | 0.73 | N/A | Appendix 1 |
| tenricids[1] | ? | 0.4-1.03 | ? | Reference 7 |
| tenricids[2] | ? | ? | ? | Reference 7 |
| *Triconodon* sp[1] | 0.31 | 0.49 | 0.45 | Reference 8 |
| *Triconodon* sp[2] | 0.28 | 0.44 | 0.41 | Reference 8 |
| *Thrinaxodon liorhinus*[1] | 0.16 | 0.22 | N/A | Appendix 1 |
| *Thrinaxodon liorhinus*[2] | ? | ? | N/A | Appendix 1 |
| *Trichechus senegalensis*[1] | 1.11 | 1.06 | N/A | Appendix 1 |
| *Trichechus senegalensis*[2] | 1.11 | 1.06 | N/A | Appendix 1 |
| *Vincelestes neuquenianus*[1] | 0.21 | 0.28 | N/A | Appendix 1 |
| *Vincelestes neuquenianus*[2] | 0.18 | 0.25 | N/A | Appendix 1 |
| *Vombatus ursinus*[1] | 0.60 | 0.64 | N/A | Appendix 1 |
| *Vombatus ursinus*[2] | 0.58 | 0.62 | N/A | Appendix 1 |
| *Zaglossus bruijni*[1] | 0.76 | 0.89 | N/A | Appendix 1 |
| *Zaglossus bruijni*[2] | 0.74 | 0.86 | N/A | Appendix 1 |
| *Zalambdalestes lechei*[1] | 0.44 | 0.71 | 0.66 | Reference 1 |
| *Zalambdalestes lechei*[2] | 0.40 | 0.64 | 0.60 | Reference 1 |

# Appendix 5: Endocast Character Matrix

Abbreviations: **A-G** = character states 10-16; **N** = not applicable; **?** = missing data.

| **Taxon** | **1** | **2** | **3** | **4** | **5** | **6.1** | **6.2** | **7** | **8** | **9** | **10.1** | **10.2** | **11** | **12** | **13** |
|---|---|---|---|---|---|---|---|---|---|---|---|---|---|---|---|
| *Asioryctes nemegetensis* | 1 | 0 | 0 | 2 | ? | ? | ? | 0 | 1 | 1 | 9 | 0 | 1 | ? | 0 |
| *Canis lupus* | 2 | 0 | 0 | 0 | 0 | 3 | 1 | 0 | 1 | 0 | 6 | 0 | 1 | 0 | 1 |
| *Dasypus novemcinctus* | 2 | 0 | 0 | 1 | 1 | 5 | 1 | 0 | 1 | 0 | C | 0 | 1 | 0 | 1 |
| *Dasyurus hallucatus* | 1 | 0 | 0 | 2 | 1 | 6 | 1 | 0 | 1 | 0 | 7 | 0 | 1 | 0 | 0 |
| *Diademodon* sp. | 0 | 0 | 0 | 1 | 0 | ? | ? | 0 | 0 | ? | ? | ? | ? | ? | 0 |
| *Didelphis virginiana* | 1 | 0 | 0 | 1 | 1 | 7 | 0 | 0 | 1 | 0 | B | 0 | 1 | 1 | 0 |
| *Dromiciops australis* | 2 | 0 | 0 | 2 | 0 | 7 | 1 | 0 | 1 | 0 | 3 | 1 | 1 | 0 | 0 |
| *Felis silvestris catus* | 2 | 0 | 0 | 1 | 1 | 5 | 1 | 0 | 1 | 0 | 2 | 1 | 1 | 0 | 1 |
| *Hadrocodium wui* | 1 | 0 | 0 | 2 | 0 | 8 | 0 | 0 | ? | 0 | E | 0 | 0 | ? | 0 |
| *Kennalestes gobiensis* | ? | 0 | ? | ? | ? | ? | ? | 0 | ? | 2 | A | 0 | ? | ? | 0 |
| *Kryptobaatar dashzevegi* | 1 | 0 | 0 | 2 | 0 | 3 | 1 | 0 | 1 | 0 | 5 | 1 | 1 | 0 | 0 |
| *Leptictis dakotensis* | 1 | 0 | 0 | 2 | 0 | ? | ? | 0 | 1 | 1 | G | 0 | 1 | ? | 1 |
| *Manis tricuspis* | 2 | 0 | 0 | 2 | 0 | ? | ? | 0 | 1 | 1 | 4 | 1 | 1 | 0 | 1 |
| *Monodelphis domestica* | 1 | 0 | 0 | 2 | 0 | 7&9 | 0&1 | 0 | 1 | 0 | 8 | 0 | 1 | 0 | 0 |
| *Obdurodon dicksoni* | 2 | 0 | 0 | 2 | 0 | 7 | 0 | 0 | 1 | 0 | 1 | 1 | ? | 0 | 0 |
| *Ornithorhynchus anatinus* | 2 | 1 | 0 | 2 | 0 | A | 0 | 0 | 1 | 0 | 0 | 1 | 1 | 0 | 0 |
| *Orycteropus afer* | 1 | 0 | 0 | 2 | 1 | ? | ? | 0 | 1 | 0 | 9 | 0 | 1 | 1 | 1 |
| *Phascolarctos cinereus* | 1 | 0 | 0 | 2 | 0 | 4 | 1 | 0 | 1 | 0 | 2 | 1 | 0 | 0 | 0 |
| *Probainognathus* sp. | 0 | 0 | 0 | 2 | 0 | ? | ? | 0 | 0 | 0 | 6 | 0 | 0 | ? | 0 |
| *Procavia capensis* | 1 | 0 | 0 | 2 | 0 | ? | ? | 0 | 1 | 2 | 3 | 1 | 1 | 0 | 1 |
| *Pucadelphys andinus* | 1 | 0 | 0 | 2 | 0 | 5 | 1 | 0 | 1 | 0 | B | 0 | 1 | ? | 0 |
| *Tachyglossus aculeatus* | 1 | 0 | 0 | 2 | 0 | 8 | 0 | 0 | 1 | 1 | ? | ? | 0 | 0 | 1 |
| *Thrinaxodon liorhinus* | 0 | 0 | 0 | 0 | 0 | ? | ? | 0 | 0 | ? | ? | ? | ? | ? | 0 |
| *Trichechus senegalensis* | 2 | 0 | 0 | 2 | 1 | N | N | 1 | N | N | N | N | N | 0 | 1 |
| Triconodontidae | 1 | 0 | ? | ? | ? | ? | ? | 0 | 1 | 1 | B | 0 | 1 | ? | 0 |
| *Vincelestes neuquenianus* | 1 | 0 | 0 | 2 | 0 | 4 | 1 | 0 | 1 | 0 | A | 0 | 1 | ? | 0 |
| *Vombatus ursinus* | 2 | 0 | 0 | 0 | 0 | 7 | 1 | 0 | 1 | 2 | 3 | 1 | 0 | 0 | 1 |
| *Zaglossus bruijni* | 1 | 1 | 0 | 2 | 0 | 9 | 0 | 0 | 1 | 1 | ? | ? | 0 | 0 | 1 |
| *Zalambdalestes lechei* | 1 | 0 | 0 | 2 | ? | ? | ? | 0 | 1 | 1 | 8 | 0 | 1 | ? | 0 |

**Appendix 5 continued.**

| Taxon | 14 | 15 | 16 | 17 | 18 | 19.1 | 19.2 | 20 | 21 | 22 | 23 | 24 | 25 |
|---|---|---|---|---|---|---|---|---|---|---|---|---|---|
| *Asioryctes nemegetensis* | ? | ? | 1 | 1 | 0 | ? | ? | ? | ? | ? | ? | ? | 1 |
| *Canis lupus* | 1 | 1 | 0 | 0 | 0 | 0 | 1 | 1 | 1 | 0 | 0 | 0 | 1 |
| *Dasypus novemcinctus* | 1 | 0 | 1 | 0 | 1 | N | N | 1 | N | 1 | 0 | 0 | 1 |
| *Dasyurus hallucatus* | 1 | 0 | 1 | 0 | 0 | 2 | 0 | 1 | 1 | 1 | 0 | 0 | 1 |
| *Diademodon* sp. | 0 | N | 0 | 0 | 1 | N | N | 0 | N | 0 | 0 | 0 | 0 |
| *Didelphis virginiana* | 1 | 0 | 0 | 0 | 0 | 1 | 1 | 1 | 1 | 1 | 0 | 0 | 1 |
| *Dromiciops australis* | 1 | 0 | 1 | 0 | 0 | 2 | 0 | 1 | 1 | 1 | 0 | 0 | 1 |
| *Felis silvestris catus* | 1 | 1 | 0 | 0 | 1 | N | N | 1 | N | 1 | 0 | 0 | 1 |
| *Hadrocodium wui* | 0 | N | 1 | 0 | 0 | 0 | 1 | ? | ? | ? | 0 | 0 | ? |
| *Kennalestes gobiensis* | 0 | N | ? | 1 | ? | ? | ? | ? | ? | ? | ? | ? | 1 |
| *Kryptobaatar dashzevegi* | 0 | N | 1 | 0 | 0 | 8 | 0 | 1 | 0 | 0 | 0 | 0 | 1 |
| *Leptictis dakotensis* | 1 | 0 | 1 | 0 | 0 | ? | ? | 1 | 1 | 1 | 0 | 0 | 1 |
| *Manis tricuspis* | 1 | 1 | 1 | 0 | 1 | N | N | 1 | N | 1 | 1 | 0 | 0 |
| *Monodelphis domestica* | 0 | N | 1 | 0 | 0 | 2 | 0 | 1 | 1 | 1 | 0 | 0 | 1 |
| *Obdurodon dicksoni* | 1 | 1 | 1 | 0 | 0 | 1 | 1 | 1 | 1 | 1 | 0 | 0 | 0 |
| *Ornithorhynchus anatinus* | 1 | 1 | 1 | 0 | 0 | 1 | 1 | 1 | 1 | 1 | 0 | 0 | 0 |
| *Orycteropus afer* | ? | ? | 1 | ? | 1 | N | N | 1 | N | 1 | 0 | 0 | 0 |
| *Phascolarctos cinereus* | 1 | 0 | 1 | 0 | 0 | 0 | 1 | 1 | 0 | 1 | 0 | 0 | 1 |
| *Probainognathus* sp. | 0 | N | 1 | 1 | 0 | ? | ? | 0 | N | 1 | 0 | 0 | 0 |
| *Procavia capensis* | 1 | 1 | 0 | 0 | 0 | 0 | 1 | 1 | 1 | 1 | 0 | 0 | 1 |
| *Pucadelphys andinus* | 0 | N | 1 | 0 | 0 | 1 | 1 | 1 | 0 | 1 | 0 | 0 | 0 |
| *Tachyglossus aculeatus* | 1 | 1 | 1 | 0 | 1 | N | N | 1 | N | 1 | 0 | 0 | 0 |
| *Thrinaxodon liorhinus* | 0 | N | 0 | 0 | 0 | 3 | 0 | 0 | N | 0 | 0 | 0 | 0 |
| *Trichechus senegalensis* | 1 | 1 | 1 | 0 | 1 | N | N | 0 | N | 0 | 0 | 0 | 1 |
| Triconodontidae | ? | ? | 1 | 0 | 0 | ? | ? | 1 | 0 | ? | ? | ? | 1 |
| *Vincelestes neuquenianus* | 0 | N | 1 | 0 | 0 | 0 | 1 | 1 | 0 | 1 | 0 | 0 | 0 |
| *Vombatus ursinus* | 1 | 0 | 0 | 0 | 1 | N | N | 1 | N | 1 | 0 | 0 | 1 |
| *Zaglossus bruijni* | 1 | 1 | 1 | 0 | 1 | N | N | 1 | N | 1 | 0 | 0 | 0 |
| *Zalambdalestes lechei* | ? | ? | 1 | 1 | 0 | ? | ? | 1 | 1 | ? | 0 | 0 | 1 |

**Appendix 5 continued.**

| Taxon | 26 | 27 | 28 | 29 | 30 | 31.1 | 31.2 | 32 | 33 | 34 | 35 |
|---|---|---|---|---|---|---|---|---|---|---|---|
| *Asioryctes nemegetensis* | ? | ? | ? | ? | 1 | ? | ? | ? | ? | ? | ? |
| *Canis lupus* | 0 | 1 | 0 | 1 | 1 | 0 | 0 | 0 | 1 | 0 | 0 |
| *Dasypus novemcinctus* | 0 | 0 | 0 | 1 | 1 | 0 | 0 | 2 | 2 | 0 | 0 |
| *Dasyurus hallucatus* | 0 | 0 | 0 | 1 | 1 | 0 | 0 | 1 | 1 | 0 | 0 |
| *Diademodon* sp. | 0 | 0 | ? | ? | 0 | D | 1 | 0 | 0 | 0 | 1 |
| *Didelphis virginiana* | 1 | 1 | 0 | 1 | 1 | 4 | 1 | 1 | 1 | 0 | 0 |
| *Dromiciops australis* | 1 | 1 | 0 | 1 | 1 | 0 | 0 | 1 | 1 | 0 | 0 |
| *Felis silvestris catus* | 1 | 1 | 0 | 1 | 1 | 0 | 0 | 2 | 2 | 0 | 0 |
| *Hadrocodium wui* | ? | ? | ? | 1 | 1 | 2 | 1 | 0 | 0 | 0 | 2 |
| *Kennalestes gobiensis* | ? | ? | ? | ? | 1 | ? | ? | ? | ? | ? | ? |
| *Kryptobaatar dashzevegi* | ? | ? | ? | 1 | 1 | 7 | 1 | 0 | 0 | 0 | 0 |
| *Leptictis dakotensis* | 1 | 1 | ? | 1 | 1 | ? | ? | 0 | ? | 0 | 0 |
| *Manis tricuspis* | 1 | 1 | 0 | 1 | 1 | 1 | 0 | 2 | 2 | 0 | 0 |
| *Monodelphis domestica* | 0 | 1 | 0 | 1 | 1 | 2&5 | 1 | 1 | 1 | 0 | 0 |
| *Obdurodon dicksoni* | 0 | 0 | ? | 1 | 1 | 1 | 0 | 1 | 1 | 1 | 0 |
| *Ornithorhynchus anatinus* | 0 | 0 | 1 | 1 | 1 | 1 | 0 | 1 | 1 | 1 | 0 |
| *Orycteropus afer* | 0 | 0 | ? | 1 | 1 | 1 | 0 | 1 | 1 | 0 | 0 |
| *Phascolarctos cinereus* | 0 | 0 | 0 | 1 | 1 | 0 | 0 | 1 | 1 | 0 | 0 |
| *Probainognathus* sp. | 0 | 0 | ? | 1 | 1 | ? | ? | ? | ? | ? | ? |
| *Procavia capensis* | 0 | 0 | ? | 1 | 1 | 1 | 0 | 1 | 1 | 0 | 0 |
| *Pucadelphys andinus* | 0 | 0 | ? | 1 | 1 | 5 | 1 | 0 | 0 | 0 | 0 |
| *Tachyglossus aculeatus* | 0 | 0 | 1 | 1 | 1 | 1 | 0 | 1 | 1 | 0 | 0 |
| *Thrinaxodon liorhinus* | 0 | 0 | ? | 0 | 0 | 1 | 0 | 0 | 0 | 0 | 0 |
| *Trichechus senegalensis* | 0 | 0 | 0 | 1 | 1 | 0 | 0 | 0 | 0 | 0 | 1 |
| Triconodontidae | ? | ? | ? | 1 | 1 | ? | ? | ? | ? | ? | ? |
| *Vincelestes neuquenianus* | 0 | 0 | ? | 1 | 1 | 7 | 1 | 2 | 2 | 0 | 0 |
| *Vombatus ursinus* | 0 | 1 | 0 | 1 | 1 | 0 | 0 | 1 | 1 | 0 | 0 |
| *Zaglossus bruijni* | 0 | 0 | 1 | 1 | 1 | 0 | 0 | 1 | 1 | 0 | 0 |
| *Zalambdalestes lechei* | 1 | ? | ? | 1 | 1 | ? | ? | ? | ? | ? | ? |

**Appendix 5 continued.**

| Taxon | 36.1 | 36.2 | 37 | 38 | 39 |
|---|---|---|---|---|---|
| *Asioryctes nemegetensis* | ? | ? | 1 | ? | ? |
| *Canis lupus* | 7 | 0 | 1 | 0 | 0 |
| *Dasypus novemcinctus* | 0 | 1 | 1 | 0 | 1 |
| *Dasyurus hallucatus* | 3 | 1 | 1 | 0 | 1 |
| *Diademodon* sp. | ? | ? | ? | N | 1 |
| *Didelphis virginiana* | 5 | 0 | 1 | 0 | 1 |
| *Dromiciops australis* | 0 | 1 | 1 | 0 | 1 |
| *Felis silvestris catus* | 3 | 1 | 1 | 0 | 1 |
| *Hadrocodium wui* | 6 | 0 | 0 | 0 | ? |
| *Kennalestes gobiensis* | ? | ? | 1 | ? | ? |
| *Kryptobaatar dashzevegi* | C | 0 | 0 | ? | ? |
| *Leptictis dakotensis* | ? | ? | 1 | 0 | 0 |
| *Manis tricuspis* | ? | ? | 1 | 0 | 0 |
| *Monodelphis domestica* | 2&3 | 1 | 1 | 0 | 1 |
| *Obdurodon dicksoni* | C | 0 | 0 | 0 | 1 |
| *Ornithorhynchus anatinus* | 9 | 0 | 0 | 1 | 1 |
| *Orycteropus afer* | ? | ? | ? | 0 | 0 |
| *Phascolarctos cinereus* | 4 | 0 | 1 | 0 | 1 |
| *Probainognathus* sp. | ? | ? | 0 | ? | ? |
| *Procavia capensis* | ? | ? | ? | 0 | 0 |
| *Pucadelphys andinus* | 0 | 1 | 1 | 0 | 1 |
| *Tachyglossus aculeatus* | C | 0 | 1 | 0 | 0 |
| *Thrinaxodon liorhinus* | ? | ? | 0 | N | 1 |
| *Trichechus senegalensis* | ? | ? | ? | N | 0 |
| Triconodontidae | ? | ? | 1 | ? | ? |
| *Vincelestes neuquenianus* | 7 | 0 | 1 | 1 | 1 |
| *Vombatus ursinus* | 4 | 0 | 1 | 0 | 1 |
| *Zaglossus bruijni* | A | 0 | 1 | 0 | 0 |
| *Zalambdalestes lechei* | ? | ? | 1 | ? | 0 |

# Appendix 6: Distribution of Endocast Character States for Major Extant Mammalian Clades

Abbreviations: "+" indicates apomorphy, "-" indicates plesiomorphy, "*" indicates character state reversal, "/" indicates character is equivocal for that clade. Note that polarity for character 15 is uncertain.

| Character | Mammalia | Monotremata | Theria | Marsupialia | Placentalia |
|---|---|---|---|---|---|
| 1 | -1 | -1 | -1 | -1 | +2 |
| 2 | -0 | -0 | -0 | -0 | -0 |
| 3 | -0 | -0 | -0 | -0 | -0 |
| 4 | -2 | -2 | -2 | -2 | 0/1/2 |
| 5 | -0 | -0 | -0 | 0/1 | 0/1 |
| 6.1 | -8 | -8 | +5 | +7 | -5 |
| 6.2 | -0 | -0 | -1 | -1 | -1 |
| 7 | -0 | -0 | -0 | -0 | -0 |
| 8 | +1 | -1 | -1 | -1 | -1 |
| 9 | -0 | -0 | -0 | -0 | +0* |
| 10.1 | 0/1/2/5/6/A/B/E | 0/1/2/5/6/A/B/E | 2/6/A/B | +B | 2/6/8/9/A/B/C/G |
| 10.2 | -0 | 0/1 | -0 | -0 | -0 |
| 11 | 0/1 | 0/1 | -1 | -1 | -1 |
| 12 | -0 | -0 | -0 | -0 | -0 |
| 13 | -0 | -0 | -0 | -0 | -1 |
| 14 | -0 | +1 | -0 | +1 | -1 |
| 15 | 0/1 | 1 | 0 | 0 | 0 |
| 16 | -1 | -1 | -1 | -1 | -1 |
| 17 | -0 | -0 | -0 | -0 | -0 |
| 18 | -0 | -0 | -0 | -0 | 0/1 |
| 19.1 | -0 | 0/1 | -0 | -1 | -0 |
| 19.2 | -1 | -1 | -1 | -1 | -1 |
| 20 | +1 | -1 | -1 | -1 | -1 |
| 21 | 0/1 | 0/1 | 0/1 | +1 | -1 |
| 22 | -1 | -1 | -1 | -1 | -1 |
| 23 | -0 | -0 | -0 | -0 | -0 |
| 24 | -0 | -0 | -0 | -0 | -0 |
| 25 | -0 | -0 | -1 | -1 | -1 |
| 26 | -0 | -0 | -0 | -0 | 0/1 |
| 27 | -0 | -0 | 0/1 | 0/1 | 0/1 |
| 28 | -0 | +1 | -0 | -0 | -0 |
| 29 | -1 | -1 | -1 | -1 | -1 |
| 30 | -1 | -1 | -1 | -1 | -1 |
| 31.1 | -1 | -1 | +0 | -0 | -0 |
| 31.2 | -1 | +0* | -1 | -1 | +0* |

| Character | Mammalia | Monotremata | Theria | Marsupialia | Placentalia |
|---|---|---|---|---|---|
| 32 | -0 | +1 | -0 | +1 | 0/2 |
| 33 | -0 | +1 | 0/2 | +1 | +2 |
| 34 | -0 | -0 | -0 | -0 | -0 |
| 35 | -0 | -0 | -0 | -0 | -0 |
| 36.1 | +C | -C | 0/7 | -0 | 0/7 |
| 36.2 | -0 | -0 | +1 | -1 | -1 |
| 37 | 0/1 | -1 | -1 | -1 | -1 |
| 38 | -0 | -0 | -0 | -0 | -0 |
| 39 | -0 | -0 | -0 | -0 | 0/1 |

# References


Abbie, A. A. 1934. The brain-stem and cerebellum of *Echidna aculeata*. Philosophical Transactions of the Royal Society of London, Series B 224:1-74.

Aiello, L. C., and P. Wheeler. 1995. The expensive-tissue hypothesis: the brain and the digestive system in humans and primate evolution. Current Anthropology 36:199-221.

Aitkin, L., S. Cochran, S. Frost, A. Martsi-McClintock, and B. Masterton. 1997. Features of the auditory development of the short-tailed Brazilian opossum, *Monodelphis domestica*: evoked responses, neonatal vocalizations and synapses in the inferior colliculus. Hearing Research 113:69-75.

Alexander, R. M., A. S. Jayes, G. M. O. Maloiy, and E. M. Wathuta. 1979. Allometry of the limb bones of mammals from shrews (*Sorex*) to elephant (*Loxodonta*). Journal of Zoology (London) 189:305-314.

Andres, K. H., and M. von Düring. 1988. Comparative anatomy of vertebrate electroreceptors; pp. 113-131 in W. Hamann, and A. Iggo (eds.), Transduction and Cellular Mechanisms in Sensory Receptors. Progress in Brain Research, Vol. 74. Elsevier, New York, New York.

Archer, M., T. F. Flannery, A. Ritchie, and R. E. Molnar. 1985. First Mesozoic mammal from Australia—an early Cretaceous monotreme. Nature 318:363-363.

Archer, M., P. Murray, S. J. Hand, and H. Godthelp. 1993. Reconsideration of monotreme relationships based on the skull and dentition of the Miocene *Obdurodon dicksoni*; pp. 75-94 in F. S. Szalay, M. J. Novacek, and M. C. McKenna (eds.), Mammal Phylogeny. Volume 1: Mesozoic Differentiation, Multituberculates, Monotremes, Early Therians, and Marsupials. Springer-Verlag, New York, New York.

Archer, M., F. A. Jenkins, S. J. Hand, P. Murray, and H. Godthelp. 1992. Description of the skull and non-vestigial dentition of a Miocene platypus (*Obdurodon dicksoni* n. sp.) from Riversleigh, Australia, and the problem of monotreme origins; pp. 15-27 in M. L. Augee (ed.), Platypus and Echidnas. Royal Zoological Society of New South Wales, Mosman, New South Wales, Australia.

Armstrong, E. 1983. Relative brain size and metabolism in mammals. Science 220:1302-1304.

Augee, M. L., and B. A. Gooden. 1992. Evidence for electroreception from field studies of the echidna, *Tachyglossus aculeatus*; pp. 211-215 in M. L. Augee (ed.), Platypus and Echidnas. Royal Zoological Society of New South Wales, Mosman, New South Wales, Australia.

Ax, P. 1987. The phylogenetic system: the systematization of organisms on the basis of their phylogenesis. John Wiley and Sons, New York, New York, 340 pp.

Bohringer, R. C. 1992. The platypus bill receptors and their central connections; pp. 194-203 in M. L. Augee (ed.), Platypus and Echidnas. Royal Zoological Society of New South Wales, Mosman, New South Wales, Australia.

Bonaparte, J. F. 1966. Sobre las cavidades cerebral, nasal y otras estructuras del cráneo de *Exaeretodon* sp. (Cynodontia, Traversodontidae). Acta Geológica Lilloana 1966:5-29.

Brauer, K., and W. Schober. 1970. Katalog der Säugetiergehirne. Veb Gustav Fischer Verlag, Jena, Germany, 150 pp.

Brochu, C. A. 2000. A digitally-rendered endocast for *Tyrannosaurus rex*. Journal of Vertebrate Paleontology 20:1-6.

Brunjes, P. C., A. Jazaeri, and M. J. Sutherland. 1992. Olfactory bulb organization and development in *Monodelphis domestica* (grey short-tailed opossum). Journal of Comparative Neurology 320:544-554.

Buchholtz, E. A., and E.-A. Seyfarth. 1999. The gospel of the fossil brain: Tilly Edinger and the science of paleoneurology. Brain Research Bulletin 48:351-361.

Bullock, T. H., D. A. Bodznick, and R. G. Northcutt. 1983. The phylogenetic distribution of electroreception: evidence for convergent evolution of a primitive vertebrate sense modality. Brain Research Reviews 6:25-46.

Butler, A. B., and W. Hodos. 1996. Comparative Vertebrate Neuroanatomy. Evolution and Adaptation. Wiley-Liss, New York, New York, 514 pp.

Cheon, J.-E., J.-E. Kim, and H. J. Yang. 2002. CT and pathologic findings of a case of subdural osteoma. Korean Journal of Radiology 3:211-213.

Colbert, M. W., R. Racicot, and T. Rowe. 2005. Anatomy of the cranial endocast of the bottlenose dolphin *Tursiops truncatus*, based on HRXCT. Journal of Mammalian Evolution 12:195-207.

Cothran, E. G., M. J. Aivaliotis, and J. L. VandeBerg. 1985. The effects of diet on growth and reproduction in gray short-tailed opossums *Monodelphis domestica*. Journal of Experimental Zoology 236:103-114.

Damuth, J., and B. J. MacFadden (eds.). 1990. Body Size in Mammalian Paleobiology: Estimation and Biological Implications. Cambridge University Press, New York, New York, 397 pp.

Deacon, T. W. 1990. Rethinking mammalian brain evolution. American Zoologist 30:629-705.

Denison, C., W. D. Carlson, and R. A. Ketcham. 1997. Three-dimensional quantitative textural analysis of metamorphic rocks using high-resolution computed X-ray tomography: Part I. Methods and techniques. Journal of Metamorphic Geology 15:29-44.

Dunbar, R. I. M. 1995. Neocortex size and group size in primates: a test of the hypothesis. Journal of Human Evolution 28:287-296.

Edinger, T. 1941. The brains of three Pontian Ovibovidae from China. Bulletin of the Geological Institutions of Uppsala 28:133-140.

Edinger, T. 1942. The pituitary body in giant animals fossil and living: a survey and a suggestion. Quarterly Review of Biology 17:31-45.

Edinger, T. 1948. Evolution of the horse brain. Geological Society of America Memoir 25:1-177.

Edinger, T. 1949. Paleoneurology versus comparative brain anatomy. Confinia Neurologica 9:5-24.

Edinger, T. 1951. The brains of the Odontognathae. Evolution 5:6-24.

Edinger, T. 1955. Hearing and smell in cetacean history. Monatsschrift für Psychiatrie und Neurologie 129:37-58.

Edinger, T. 1964. Midbrain exposure and overlap in mammals. American Zoologist 4:5-19.

Edinger, T. 1975. Paleoneurology 1804-1966. An annotated bibliography. Advances in Anatomy, Embryology and Cell Biology (Ergebnisse der Anatomie und Entwicklungsgeschichte) 49:1-258.

Eisenberg, J. F. 1981. The Mammalian Radiations. University of Chicago Press, Chicago, Illinois, 610 pp.

Eisenberg, J. F., and D. E. Wilson. 1978. Relative brain size and feeding strategies in the Chiroptera. Evolution 32:740-751.

Eisenberg, J. F., and D. E. Wilson. 1981. Relative brain size and demographic strategies in didelphid marsupials. American Naturalist 118:1-15.

Elgar, M. A., and P. H. Harvey. 1987. Basal metabolic rates in mammals: allometry, phylogeny and ecology. Functional Ecology 1:25-36.

Farrand, W. R. 1961. Frozen mammoths and modern geology. Science 133:729-735.

Felsenstein, J. 1985. Phylogenies and the comparative method. American Naturalist 125:1-15.

Felsenstein, J. 2004. Inferring Phylogenies. Sinauer Associates, Sunderland, Massachusetts, 664 pp.

Feng, A. S. 1991. Electric organs and electroreceptors; pp. 317-334 in C. L. Prosser (ed.), Neural and Integrative Animal Physiology. Wiley-Liss, New York, New York.

Franzosa, J. W. 2004. Evolution of the Brain in Theropoda (Dinosauria). Ph.D. dissertation, University of Texas, Austin, Texas, 357 pp.

Franzosa, J. W., and T. Rowe. 2005. Cranial endocast of the Cretaceous theropod dinosaur *Acrocanthosaurus atokensis*. Journal of Vertebrate Paleontology 25:859-864.

Fritzsch, B., and H. Münz. 1986. Electroreception in amphibians; pp. 483-496 in T. H. Bullock, and W. Heiligenberg (eds.), Electroreception. John Wiley and Sons, New York, New York.

Gardner, A. L. 1973. The systematics of the genus *Didelphis* (Marsupialia: Didelphidae) in North and Middle America. Special Publications of the Museum, Texas Tech University 4:1-81.

Gauthier, J., A. G. Kluge, and T. Rowe. 1988. Amniote phylogeny and the importance of fossils. Cladistics 4:105-209.

Gregory, W. K. 1947. The monotremes and the palimpsest theory. Bulletin of the American Museum of Natural History 88:1-52.

Griffiths, M. 1968. Echidnas. Pergamon Press, New York, New York, 282 pp.

Griffiths, M. 1978. The Biology of the Monotremes. Academic Press, New York, New York, 367 pp.

Guthrie, R. D. 1990. Frozen Fauna of the Mammoth Steppe: the Story of Blue Babe. University of Chicago Press, Chicago, Illinois, 323 pp.

Harvey, P. H., and P. M. Bennett. 1983. Brain size, energetics, ecology and life history patterns. Nature 306:314-315.

Harvey, P. H., and J. R. Krebs. 1990. Comparing brains. Science 249:140-146.

Harvey, P. H., and M. D. Pagel. 1991. The Comparative Method in Evolutionary Biology. Oxford University Press, New York, New York, 239 pp.

Hofer, H. O., and J. A. Wilson. 1967. An endocranial cast of an early Oligocene primate. Folia Primatologica 5:148-152.

Hopson, J. A. 1979. Paleoneurology; pp. 39-146 in C. Gans, R. G. Northcutt, and P. Ulinski (eds.), Biology of the Reptilia, Volume 9, Neurology A. Academic Press, London, England.

Hopson, J. A. 1991. Systematics of nonmammalian Synapsida and implications for patterns of evolution in synapsids; pp. 635-693 in H.-P. Schultze, and L. Trueb (eds.), Origins of the Higher Groups of Tetrapods: Controversy and Consensus. Comstock Publishing Associates (Cornell University Press), Ithaca, New York.

Hopson, J. A., and R. Barghusen. 1986. An analysis of therapsid relationships; pp. 83-106 in N. Hotton III, P. D. MacLean, J. J. Roth, and E. C. Roth (eds.), The Ecology and Biology of Mammal-like Reptiles. Smithsonian Institution Press, Washington, D.C.

Hopson, J. A., and J. W. Kitching. 2001. A probainognathian cynodont from South Africa and the phylogeny of nonmammalian cynodonts. Bulletin of the Museum of Comparative Zoology 156:5-35.

Hopson, J. A., and G. W. Rougier. 1993. Braincase structures in the oldest known skull of a therian mammal: implications for mammalian systematics and cranial evolution. American Journal of Science 293-A-A:268-299.

Horovitz, I., and M. R. Sánchez-Villagra. 2003. A morphological analysis of marsupial mammal higher-level phylogenetic relationships. Cladistics 19:181-212.

Hu, Y., Y. Wang, Z. Luo, and C. Li. 1997. A new symmetrodont mammal from China and its implications for mammalian evolution. Nature 390:137-142.

Huber, E. 1930. Evolution of facial musculature and cutaneous field of trigeminus. Part I. Quarterly Review of Biology 5:133-188.

Hurlburt, G. R. 1996. Relative Brain Size in Recent and Fossil Amniotes: Determination and Interpretation. Ph.D. dissertation, University of Toronto, Toronto, Ontario, Canada, 250 pp.

Hurum, J. H., Z.-X. Luo, and Z. Kielan-Jaworowska. 2006. Were mammals originally venomous? Acta Palaeontologica Polonica 51:1-11.

Jansa, S. A., and R. S. Voss. 2000. Phylogenetic studies on didelphid marsupials I. Introduction and preliminary results from nuclear IRBP gene sequences. Journal of Mammalian Evolution 7:43-77.

Jerison, H. J. 1955. Brain to body ratios and the evolution of intelligence. Science 121:447-449.

Jerison, H. J. 1961. Quantitative analysis of evolution of the brain in mammals. Science 133:1012-1014.

Jerison, H. J. 1973. Evolution of the Brain and Intelligence. Academic Press, New York, New York, 482 pp.

Jerison, H. J. 1991. Fossil brains and the evolution of the neocortex; pp. 5-19 in B. L. Finlay, G. Innocenti, and H. Scheich (eds.), The Neocortex: Ontogeny and Phylogeny. NATO Advanced Science Institutes Series A: Life Sciences Vol. 200, Plenum Press, New York, New York.

Jerison, H. J. 2001. The evolution of neural and behavioral complexity; pp. 523-553 in G. Roth, and M. F. Wullimann (eds.), Brain Evolution and Cognition. John Wiley and Sons, New York, New York.

Ji, Q., Z. Luo, and S. Ji. 1999. A Chinese triconodont mammal and mosaic evolution of the mammalian skeleton. Nature 398:326-330.

Ji, Q., Z.-X. Luo, C.-X. Yuan, and A. R. Tabrum. 2006. A swimming mammaliaform from the Middle Jurassic and ecomorphological diversification of early mammals. Science 311:1123-1127.

Johnson, J. I., R. C. Switzer, and J. A. W. Kirsch. 1982a. Phylogeny through brain traits: fifteen characters which adumbrate mammalian genealogy. Brain, Behavior and Evolution 20:72-83.

Johnson, J. I., R. C. Switzer, and J. A. W. Kirsch. 1982b. Phylogeny through brain traits: the distribution of categorizing characters in contemporary mammals. Brain, Behavior and Evolution 20:97-117.

Johnson, J. I., J. A. W. Kirsch, R. L. Reep, and R. C. Switzer. 1994. Phylogeny through brain traits: more characters for the analysis of mammalian evolution. Brain, Behavior and Evolution 43:319-347.

Kemp, T. S. 1982. Mammal-like Reptiles and the Origin of Mammals. Academic Press, New York, New York, 363 pp.

Kemp, T. S. 1983. The relationships of mammals. Zoological Journal of the Linnean Society 77:353-384.

Kemp, T. S. 1988. Interrelationships of the Synapsida; pp. 1-22 in M. J. Benton (ed.), The Phylogeny and Classification of the Tetrapods. Volume 2: Mammals. The Systematics Association Special Volume No. 35B. Clarendon Press, Oxford, England.

Kermack, D. M., and K. A. Kermack. 1984. The Evolution of Mammalian Characters. Kapitan Szabo Publishers, Washington, D.C., 149 pp.

Kermack, K. A. 1963. The cranial structure of the triconodonts. Philosophical Transactions of the Royal Society of London, Series B 246:83-103.

Kielan-Jaworowska, Z. 1983. Multituberculate endocranial casts. Palaeovertebrata 13:1-12.

Kielan-Jaworowska, Z. 1984. Evolution of the therian mammals in the late Cretaceous of Asia. Part VI. Endocranial casts of eutherian mammals. Palaeontologia Polonica 46:157-171.

Kielan-Jaworowska, Z. 1986. Brain evolution in Mesozoic mammals; pp. 21-34 in K. M. Flanagan, and J. A. Lillegraven (eds.), Vertebrates, Phylogeny, and Philosophy. Contributions to Geology, University of Wyoming, Special Paper 3.

Kielan-Jaworowska, Z. 1997. Characters of multituberculates neglected in phylogenetic analyses of early mammals. Lethaia 29:249-266.

Kielan-Jaworowska, Z., and T. E. Lancaster. 2004. A new reconstruction of multituberculate endocranial casts and encephalization quotient of *Kryptobaatar*. Acta Palaeontologica Polonica 49:177-188.

Kielan-Jaworowska, Z., R. L. Cifelli, and Z.-X. Luo. 2004. Mammals from the Age of Dinosaurs: Origin, Evolution, and Structure. Columbia University Press, New York, New York, 630 pp.

Kielan-Jaworowska, Z., R. Presley, and C. Poplin. 1986. The cranial vascular system in taeniolabidoid multituberculate mammals. Philosophical Transactions of the Royal Society of London, Series B 313:525-602.

Kirsch, J. A. W. 1983. Phylogeny through brain traits: objectives and method. Brain, Behavior and Evolution 22:53-59.

Kirsch, J. A. W., and J. I. Johnson. 1983. Phylogeny through brain traits: trees generated by neural characters. Brain, Behavior and Evolution 22:60-69.

Kirsch, J. A. W., J. I. Johnson, and R. C. Switzer. 1983. Phylogeny through brain traits: the mammalian family tree. Brain, Behavior and Evolution 22:70-74.

Krabbe, K. H. 1942. Studies on the morphogenesis of the brain in lower mammals. Morphogenesis of the Vertebrate Brain II. Einar Munksgaard, Copenhagen, Denmark, 123 pp.

Kraus, D. H., and B. H. Fadem. 1987. Reproduction, development, and physiology of the gray short-tailed opossum (*Monodelphis domestica*). Laboratory Animal Science 37:478-482.

Krause, D. W., and Z. Kielan-Jaworowska. 1993. The endocranial cast and encephalization quotient of *Ptilodus* (Multituberculata, Mammalia). Palaeovertebrata 22:99-112.

Kuhn, H.-J. 1971. Die Entwicklung und Morphologie des Schädels von *Tachyglossus aculeatus*. Abhandlungen der Senckenbergischen Naturforschenden Gesellschaft 528:1-224.

Lande, R. 1979. Quantitative genetic analysis of multivariate evolution, applied to brain: body size allometry. Evolution 33:402-416.

Larsell, O. 1936. The development and morphology of the cerebellum in the opossum. Journal of Comparative Neurology 63:251-291.

Larsson, H. C. E., P. C. Sereno, and J. A. Wilson. 2000. Forebrain enlargement among nonavian dinosaurs. Journal of Vertebrate Paleontology 20:615-618.

Lewy, Z., A. C. Milner, and C. Patterson. 1992. Remarkably preserved natural endocranial casts of pterosaur and fish from the Late Cretaceous of Israel. Geological Survey of Israel Current Research 7:31-35.

Loo, Y. T. 1930. The forebrain of the opossum, *Didelphis virginiana*. Journal of Comparative Neurology 51:13-64.

Luo, Z. 1994. Sister-group relationships of mammals and transformations of diagnostic mammalian characters; pp. 98-128 in N. C. Fraser, and H. D. Sues (eds.), In the Shadow of the Dinosaurs: Early Mesozoic Tetrapods. Cambridge University Press, New York, New York.

Luo, Z.-X., and J. R. Wible. 2005. A late Jurassic digging mammal and early mammalian diversity. Science 308:103-107.

Luo, Z.-X., R. L. Cifelli, and Z. Kielan-Jaworowska. 2001a. Dual origin of tribosphenic mammals. Nature 409:53-57.

Luo, Z.-X., A. W. Crompton, and A.-L. Sun. 2001b. A new mammaliaform from the early Jurassic and evolution of mammalian characteristics. Science 292:1535-1540.

Luo, Z.-X., Z. Kielan-Jaworowska, and R. L. Cifelli. 2002. In quest for a phylogeny of Mesozoic mammals. Acta Palaeontologica Polonica 47:1-78.

Luo, Z.-X., Q. Ji, J. R. Wible, and C.-X. Yuan. 2003. An early Cretaceous tribosphenic mammal and metatherian evolution. Science 302:1934-1940.

Macrini, T. E. 2000. High Resolution X-ray Computed Tomography (CT) of the Skull of an Extant Opossum (*Monodelphis domestica*) and a Comparison of its Ontogeny to Synapsid Phylogeny. M.S. thesis, University of Texas, Austin, Texas, 158 pp.

Macrini, T. E. 2004. Monodelphis domestica. Mammalian Species 760:1-8.

Macrini, T. E., and T. B. Rowe. 2002. Ontogenetic variation in endocasts of *Monodelphis domestica* and implications for the fossil record. Journal of Vertebrate Paleontology 22(3, Supplement):81A.

Macrini, T. E., and T. B. Rowe. 2004. Cranial endocasts of monotremes. Journal of Vertebrate Paleontology 24(3, Supplement):87A.

Macrini, T. E., and T. B. Rowe. 2005. Preliminary comparison of cranial endocasts of marsupials. Society for Integrative and Comparative Biology 2005 Annual Meeting Final Program and Abstracts, San Diego, California, p. 182.

Maisey, J. G. 2004. Endocranial morphology in fossil and recent chondrichthyans; pp. 139-170 in G. Arriata, M. V. H. Wilson, and R. Cloutier (eds.), Recent Advances

in the Origin and Radiation of the Vertebrates. Verlag Dr. Friedrich Pfeil, Munich, Germany.

Maisey, J. G. 2005. Braincase of the Upper Devonian shark *Cladoides wildungensis* (Chondrichthyes, Elasmobranchii), with observations on the braincase in early chondrichthyans. Bulletin of the American Museum of Natural History 288:1-103.

Manger, P. R., R. Collins, and J. D. Pettigrew. 1997. Histological observations on presumed electroreceptors and mechanoreceptors in the beak of the long-beaked echidna, *Zaglossus bruijnii*. Proceedings of the Royal Society of London B 264:165-172.

Marino, L. 1998. A comparison of encephalization between odontocete cetaceans and anthropoid primates. Brain, Behavior and Evolution 51:230-238.

Marino, L., M. D. Uhen, N. D. Pyenson, and B. Frohlich. 2003. Reconstructing cetacean brain evolution using computed tomography. Anatomical Record (Part B) 272B:107-117.

Marino, L., M. D. Uhen, B. Frohlich, J. M. Aldag, C. Blane, D. Bohaska, and F. C. Whitmore, Jr. 2000. Endocranial volume of mid-late Eocene Archaeocetes (Order: Cetacea) revealed by computed tomography: implications for cetacean brain evolution. Journal of Mammalian Evolution 7:81-94.

Marsh, O. C. 1884. Dinocerata. A monograph of an extinct order of gigantic mammals. United States Geological Survey 10:1-237.

Marshall, L. G. 1978. Dromiciops australis. Mammalian Species 99:1-5.

Marshall, L. G., and C. de Muizon. 1988. The dawn of the age of mammals in South America. National Geographic Research 4:23-55.

Marshall, L. G., and C. de Muizon. 1995. Part II. The skull; pp. 21-90 in L. G. Marshall, C. de Muizon, and D. Signogneau-Russell (eds.), *Pucadelphys andinus* (Marsupialia, Mammalia) from the early Paleocene of Bolivia. Mémoires du Muséum national d'Histoire naturelle 165, Paris.

Marshall, L. G., and D. Sigogneau-Russell. 1995. Part III. Postcranial skeleton; pp. 91-164 in L. G. Marshall, C. de Muizon, and D. Signogneau-Russell (eds.), *Pucadelphys andinus* (Marsupialia, Mammalia) from the early Paleocene of Bolivia. Mémoires du Muséum national d'Histoire naturelle 165, Paris.

Marshall, L. G., C. de Muizon, and D. Sigogneau-Russell. 1995. Part I. The locality of Tiupampa: age, taphonomy and mammalian fauna; pp. 11-20 in L. G. Marshall,

C. de Muizon, and D. Signogneau-Russell (eds.), *Pucadelphys andinus* (Marsupialia, Mammalia) from the early Paleocene of Bolivia. Mémoires du Muséum national d'Histoire naturelle 165, Paris.

Martin, R. D. 1981. Relative brain size and basal metabolic rate in terrestrial vertebrates. Nature 293:57-60.

Martin, R. D. 1996. Scaling of the mammalian brain: the maternal enery hypothesis. News in Physiological Sciences 11:149-156.

Martinez, R. N., C. L. May, and C. A. Forster. 1996. A new carnivorous cynodont from the Ischigualasto Formation (Late Triassic, Argentina), with comments on eucynodont phylogeny. Journal of Vertebrate Paleontology 16:271-284.

McBee, K., and R. J. Baker. 1982. Dasypus novemcinctus. Mammalian Species 162:1-9.

McManus, J. J. 1974. Didelphis virginiana. Mammalian Species 40:1-6.

Mech, L. D. 1974. Canis lupus. Mammalian Species 37:1-6.

Meisami, E., and K. P. Bhatnagar. 1998. Structure and diversity in mammalian accessory olfactory bulb. Microscopy Research and Technique 43:476-499.

Menkhorst, P., and F. Knight. 2001. A Field Guide to the Mammals of Australia. Oxford University Press, South Melbourne, Australia, 269 pp.

Messer, M., A. S. Weiss, D. C. Shaw, and M. Westerman. 1998. Evolution of the monotremes: phylogenetic relationship to marsupials and eutherians, and estimation of divergence dates based on ά-lactalbumin amino acid sequences. Journal of Mammalian Evolution 5:95-105.

Miao, D. 1988. Skull morphology of *Lambdopsalis bulla* (Mammalia, Multituberculata) and its implications to mammalian evolution. Contributions to Geology, University of Wyoming, Special Paper 4:1-104.

Muizon, C. de. 1998. *Mayulestes ferox*, a borhyaenoid (Metatheria, Mammalia) from the early Paleocene of Bolivia. Phylogenetic and palaeobiologic implications. Géodiversitas 20:19-142.

Musser, A. M. 2003. Review of the monotreme fossil record and comparison of palaeontological and molecular data. Comparative Biochemistry and Physiology Part A 136:927-942.

Musser, A. M., and M. Archer. 1998. New information about the skull and dentary of the Miocene platypus *Obdurodon dicksoni*, and a discussion of ornithorhynchid

relationships. Philosophical Transactions of the Royal Society of London, Series B 353:1063-1079.

Northcutt, R. G. 1984. Evolution of the vertebrate central nervous system: patterns and processes. American Zoologist 24:701-716.

Northcutt, R. G. 1985. The brain and sense organs of the earliest vertebrates: reconstruction of a morphotype; pp. 81-112 in R. E. Foreman, A. Gorbman, J. M. Dodd, and R. Olsson (eds.), Evolutionary Biology of Primitive Fishes. Plenum Press, New York, New York.

Novacek, M. J. 1982. The brain of *Leptictis dakotensis*, an Oligocene leptictid (Eutheria: Mammalia) from North America. Journal of Paleontology 56:1177-1186.

Novacek, M. J. 1986. The skull of leptictid insectivorans and the higher-level classification of eutherian mammals. Bulletin of the American Museum of Natural History 183:1-112.

Novacek, M. J. 1992. Fossils, topologies, missing data, and the higher level phylogeny of eutherian mammals. Systematic Biology 41:58-73.

Novacek, M. J., A. R. Wyss, and M. C. McKenna. 1988. The major groups of eutherian mammals; pp. 31-71 in M. J. Benton (ed.), The Phylogeny and Classification of the Tetrapods. Volume 2: Mammals. The Systematics Association Special Volume No. 35B. Clarendon Press, Oxford, England.

Novacek, M. J., G. W. Rougier, J. R. Wible, M. C. McKenna, D. Dashzeveg, and I. Horovitz. 1997. Epipubic bones in eutherian mammals from the Late Cretaceous of Mongolia. Nature 389:483-486.

Nowak, R. M. 1991. Walker's Mammals of the World. Volume 1. Fifth edition. The Johns Hopkins University Press, Baltimore, Maryland, 642 pp.

Olds, N., and J. Shoshani. 1982. Procavia capensis. Mammalian Species 171:1-7.

Pagel, M. D., and P. H. Harvey. 1988. The taxon-level problem in the evolution of mammalian brain size: facts and artifacts. American Naturalist 132:344-359.

Pagel, M. D., and P. H. Harvey. 1989. Taxonomic differences in the scaling of brain on body weight among mammals. Science 244:1589-1593.

Pascual, R., M. Archer, E. O. Jaureguizar, J. L. Prado, H. Godthelp, and S. J. Hand. 1992. First discovery of monotremes in South America. Nature 356:704-706.

Pasitschniak-Arts, M., and L. Marinelli. 1998. Ornithorhynchus anatinus. Mammalian Species 585:1-9.

Paulli, S. 1900. Über die Pneumacität des Schädels bei den Säugetieren. I. Über den Bau des Siebbeins. Über die Morphologie des Siebbeins und die Pneumacität bei den Monotremen und den Marsupialiern. Gegenbaurs Morphologisches Jahrbuch 28:147-178.

Pirlot, P., and J. Nelson. 1978. Volumetric analysis of monotreme brains. Australian Zoologist 20:171-179.

Pitnick, S., K. E. Jones, and G. S. Wilkinson. 2006. Mating system and brain size in bats. Proceedings of the Royal Society B: Biological Sciences 273:719-724.

Proske, U., J. E. Gregory, and A. Iggo. 1998. Sensory receptors in monotremes. Philosophical Transactions of the Royal Society of London, Series B 353:1187-1198.

Quiroga, J. C. 1979. The brain of two mammal-like reptiles (Cynodontia- Therapsida). Journal für Hirnforschung 20:341-350.

Quiroga, J. C. 1980a. Sobre un molde endocraneano del cinodonte *Probainognathus jenseni* Romer, 1970 (Reptilia, Therapsida), de la Formación Ischichuca (Triasico Medio), La Rioja, Argentina. Ameghiniana 17:181-190.

Quiroga, J. C. 1980b. The brain of the mammal-like reptile *Probainognathus jenseni* (Therapsida, Cynodontia). A correlative paleo-neoneurological approach to the neocortex at the reptile-mammal transition. Journal für Hirnforschung 21:299-336.

Quiroga, J. C. 1984. The endocranial cast of the advanced mammal-like reptile *Therioherpeton cargnini* (Therapsida- Cynodontia) from the Middle Triassic of Brazil. Journal für Hirnforschung 25:285-290.

Radinsky, L. 1967. Relative brain size: a new measure. Science 155:836-838.

Radinsky, L. 1968a. A new approach to mammalian cranial analysis, illustrated by examples of prosimian primates. Journal of Morphology 124:167-180.

Radinsky, L. 1968b. Evolution of somatic sensory specialization in otter brains. Journal of Comparative Neurology 134:495-505.

Radinsky, L. 1973a. Are stink badgers skunks? Implications of neuroanatomy for mustelid phylogeny. Journal of Mammalogy 54:585-593.

Radinsky, L. 1973b. Evolution of the canid brain. Brain, Behavior and Evolution 7:169-202.

Radinsky, L. 1975. Viverrid neuroanatomy: phylogenetic and behavioral implications. Journal of Mammalogy 56:130-150.

Radinsky, L. 1976. The brain of *Mesonyx*, a middle Eocene mesonychid condylarth. Fieldiana Geology 33:323-337.

Radinsky, L. 1977. Brains of early carnivores. Paleobiology 3:333-349.

Radinsky, L. 1978. Evolution of brain size in carnivores and ungulates. American Naturalist 112:815-831.

Radinsky, L. 1981. Brain evolution in extinct South American ungulates. Brain, Behavior and Evolution 18:169-187.

Rauhut, O. W. M., T. Martin, E. Ortiz-Jaureguizar, and P. Puerta. 2002. A Jurassic mammal from South America. Nature 416:165-168.

Reimer, K. 1996. Ontogeny of hearing in the marsupial *Monodelphis domestica*, as revealed by brainstem auditory evoked potentials. Hearing Research 92:143-150.

Rich, T. H., P. Vickers-Rich, A. Constantine, T. F. Flannery, L. Kool, and N. van Klaveren. 1999. Early Cretaceous mammals from Flat Rocks, Victoria, Australia. Records of the Queen Victoria Museum 106:1-35.

Rich, T. H., P. Vickers-Rich, P. Trusler, T. F. Flannery, R. Cifelli, A. Constantine, L. Kool, and N. van Klaveren. 2001. Monotreme nature of the Australian Cretaceous mammal *Teinolophos*. Acta Palaeontologica Polonica 46:113-118.

Riska, B., and W. R. Atchley. 1985. Genetics of growth predict patterns of brain-size evolution. Science 229:668-671.

Romer, A. S., and L. I. Price. 1940. Review of the Pelycosauria. Geological Society of America Special Papers Number 28:1-538 (reprinted in 1980 by Arno Press, New York, New York).

Ross, C. F., M. Henneberg, M. J. Ravosa, and S. Richard. 2004. Curvilinear, geometric and phylogenetic modeling of basicranial flexion: is it adaptive, is it constrained? Journal of Human Evolution 46:185-213.

Roth, G., and M. F. Wullimann (eds.). 2001. Brain Evolution and Cognition. John Wiley and Sons, New York, New York, 597 pp.

Roth, J. J., E. C. Roth, and N. Hotton. 1986. The parietal foramen and eye: their function and fate in therapsids; pp. 173-184 in N. Hotton III, P. D. MacLean, J. J. Roth, and E. C. Roth (eds.), The Ecology and Biology of Mammal-like Reptiles. Smithsonian Institution Press, Washington, D.C.

Rougier, G. W. 1993. *Vincelestes neuquenianus* Bonaparte (Mammalia, Theria), un Primitivo Mamífero del Cretácico Inferior de la Cuenca Neuquina. Ph.D. dissertation, University of Buenos Aires, Buenos Aires, Argentina, 3 volumes, 720 pp.

Rougier, G. W., J. R. Wible, and J. A. Hopson. 1992. Reconstruction of the cranial vessels in the early Cretaceous mammal *Vincelestes neuquenianus*: implications for the evolution of the mammalian cranial vascular system. Journal of Vertebrate Paleontology 12:188-216.

Rougier, G. W., J. R. Wible, and J. A. Hopson. 1996a. Basicranial anatomy of *Priacodon fruitaensis* (Triconodontidae, Mammalia) from the late Jurassic of Colorado, and a reappraisal of mammaliaform interrelationships. American Museum Novitates 3183:1-38.

Rougier, G. W., J. R. Wible, and M. J. Novacek. 1996b. Middle-ear ossicles of the multituberculate *Kryptobaatar* from the Mongolian late Cretaceous: implications for mammaliamorph relationships and the evolution of the auditory apparatus. American Museum Novitates 3187:1-43.

Rougier, G. W., J. R. Wible, and M. J. Novacek. 1998. Implications of *Deltatheridium* specimens for early marsupial history. Nature 396:459-463.

Rowe, T. 1986. Osteological Diagnosis of Mammalia, L. 1758, and its Relationship to Extinct Synapsida. Ph.D. dissertation, University of California, Berkeley, California, 446 pp.

Rowe, T. 1988. Definition, diagnosis, and origin of Mammalia. Journal of Vertebrate Paleontology 8:241-264.

Rowe, T. 1993. Phylogenetic systematics and the early history of mammals; pp. 129-145 in F. S. Szalay, M. J. Novacek, and M. C. McKenna (eds.), Mammal Phylogeny. Volume 1: Mesozoic Differentiation, Multituberculates, Monotremes, Early Therians, and Marsupials. Springer-Verlag, New York, New York.

Rowe, T. 1996a. Brain heterochrony and origin of the mammalian middle ear; pp. 71-95 in M. Ghiselin, and G. Pinna (eds.), New perspectives on the history of Life. California Academy of Sciences, Memoir 20, San Francisco, California.

Rowe, T. 1996b. Coevolution of the mammalian middle ear and neocortex. Science 273:651-654.

Rowe, T., C. A. Brochu, and K. Kishi. 1999. Cranial morphology of *Alligator mississippiensis* and phylogeny of Alligatoroidea. Society of Vertebrate Paleontology, Memoir 6, 19:1-100 + CD-ROM.

Rowe, T., W. Carlson, and W. Bottorff. 1995. *Thrinaxodon*: Digital Atlas of the Skull. CD-ROM (Second Edition, for Windows and Macintosh platforms), University of Texas Press, Austin, Texas.

Rowe, T. B., T. P. Eiting, T. E. Macrini, and R. A. Ketcham. 2005. Organization of the olfactory and respiratory skeleton in the nose of the gray short-tailed opossum *Monodelphis domestica*. Journal of Mammalian Evolution 12:303-336.

Sánchez-Villagra, M. R. 2001. Ontogenetic and phylogenetic transformations of the vomeronasal complex and nasal floor elements in marsupial mammals. Zoological Journal of the Linnean Society 131:459-479.

Sánchez-Villagra, M. R. 2002. The cerebellar paraflocculus and the subarcuate fossa in *Monodelphis domestica* and other marsupial mammals: ontogeny and phylogeny of a brain-skull interaction. Acta Theriologica 47:1-14.

Sánchez-Villagra, M. R., and F. Sultan. 2002. The cerebellum at birth in therian mammals, with special reference to rodents. Brain, Behavior and Evolution 59:101-113.

Scheich, H., G. Langner, C. Tidemann, R. B. Coles, and A. Guppy. 1986. Electroreception and electrolocation in platypus. Nature 319:401-402.

Schlosser, G. 2002. Development and evolution of lateral line placodes in amphibians. II. Evolutionary diversification. Zoology 105:177-193.

Senn, D. G. 1979. Embryonic development of the central nervous system; pp. 173-244 in C. Gans, R. G. Northcutt, and P. Ulinski (eds.), Biology of the Reptilia, Volume 9, Neurology A. Academic Press, London, England.

Shoshani, J., C. A. Goldman, and J. G. M. Thewissen. 1988. Orycteropus afer. Mammalian Species 300:1-8.

Sidor, C. A., and J. A. Hopson. 1998. Ghost lineages and "mammalness": assessing the temporal pattern of character acquisition in the Synapsida. Paleobiology 24:254-273.

Simpson, G. G. 1927. Mesozoic Mammalia. IX. The brain of Jurassic mammals. American Journal of Science 214:259-268.

Simpson, G. G. 1928. A Catalogue of the Mesozoic Mammalia in the Geological Department of the British Museum. William Cloves and Sons, London, England, 215 pp.

Simpson, G. G. 1937. Skull structure of the Multituberculata. Bulletin of the American Museum of Natural History 73:727-763.

Smith, R. J. 2005. Relative size versus controlling for size. Interpretation of ratios in research on sexual dimorphism in the human corpus callosum. Current Anthropology 46:249-273.

Sokal, R. R., and F. J. Rohlf. 1998. Biometry: the Principles and Practice of Statistics in Biological Research. W. H. Freeman and Company, New York, New York, 887 pp.

Sollas, W. J. 1904. A method for the investigation of fossils by serial sections. Philosophical Transactions of the Royal Society of London, Series B 196:259-265.

Striedter, G. F. 2005. Principles of Brain Evolution. Sinauer Associates, Sunderland, Massachusetts, 436 pp.

Sunderland, S. 1941. The vascular pattern in the central nervous system of the monotremes and Australian marsupials. Journal of Comparative Neurology 75:123-129.

Swofford, D. L. 1998. PAUP*: Phylogenetic Analysis Using Parsimony (* and Other Methods). Version 4. Sinauer Associates, Sunderland, Massachusetts.

Szalay, F. S., and B. A. Trofimov. 1996. The Mongolian late Cretaceous *Asiatherium*, and the early phylogeny and paleobiogeography of Metatheria. Journal of Vertebrate Paleontology 16:474-509.

Thiele, K. 1993. The holy grail of the perfect character: the cladistic treatment of morphometric data. Cladistics 9:275-304.

Tykoski, R. S., T. B. Rowe, R. A. Ketcham, and M. W. Colbert. 2002. *Calsoyasuchus valliceps*, a new crocodyliform from the early Jurassic Kayenta Formation of Arizona. Journal of Vertebrate Paleontology 22:593-611.

Ulinski, P. S. 1986. Neurobiology of the therapsid-mammal transition; pp. 149-171 in N. Hotton III, P. D. MacLean, J. J. Roth, and E. C. Roth (eds.), The Ecology and

Biology of Mammal-like Reptiles. Smithsonian Institution Press, Washington, D.C.

VandeBerg, J. L. 1990. The gray short-tailed opossum (*Monodelphis domestica*) as a model didelphid species for genetic research. Australian Journal of Zoology 37:235-247.

Van Valkenburgh, B., J. Theodor, A. Friscia, A. Pollack, and T. Rowe. 2004. Respiratory turbinates of canids and felids: a quantitative comparison. Journal of Zoology (London) 264:281-293.

Voris, H. C. 1928. The arterial supply of the brain and spinal cord of the Virginian opossum (*Didelphis virginiana*). Journal of Comparative Neurology 44:403-423.

Voris, H. C., and N. L. Hoerr. 1932. The hindbrain of the opossum, *Didelphis virginiana*. Journal of Comparative Neurology 54:277-355.

Voss, R. S., and S. A. Jansa. 2003. Phylogenetic studies on didelphid marsupials II. Nonmolecular data and new IRBP sequences: separate and combined analyses of didelphine relationships with denser taxon sampling. Bulletin of the American Museum of Natural History 276:1-82.

Wang, Y., Y. Hu, J. Meng, and C. Li. 2001. An ossified Meckel's cartilage in two Cretaceous mammals and the origin of the mammalian middle ear. Science 294:357-361.

Watson, D. M. S. 1911. The skull of *Diademodon*, with notes on those of some other cynodonts. The Annals and Magazine of Natural History, Series 8 8:293-330.

Watson, D. M. S. 1913. Further notes on the skull, brain, and organs of special sense of *Diademodon*. The Annals and Magazine of Natural History, Series 8 12:217-228.

Wible, J. R. 1991. Origin of Mammalia: the craniodental evidence reexamined. Journal of Vertebrate Paleontology 11:1-28.

Wible, J. R. 2003. On the cranial osteology of the short-tailed opossum *Monodelphis brevicaudata* (Didelphidae, Marsupialia). Annals of the Carnegie Museum 72:137-202.

Wible, J. R., and G. W. Rougier. 2000. Cranial anatomy of *Kryptobaatar dashzevegi* (Mammalia, Multituberculata), and its bearing on the evolution of mammalian characters. Bulletin of the American Museum of Natural History 247:1-120.

Wible, J. R., G. W. Rougier, M. J. Novacek, M. C. McKenna, and D. Dashzeveg. 1995. A mammalian petrosal from the early Cretaceous of Mongolia: implications for the

evolution of the ear region and mammaliamorph interrelationships. American Museum Novitates 3149:1-19.

Wiens, J. 1995. Polymorphic characters in phylogenetic systematics. Systematic Biology 44:482-500.

Wiens, J. 1998. Testing phylogenetic methods with tree congruence: phylogenetic analysis of polymorphic morphological characters in phrynosomatid lizards. Systematic Biology 47:427-444.

Wiens, J. 1999. Polymorphism in systematics and comparative biology. Annual Review of Ecology and Systematics 30:327-362.

Williams, S. L., R. Laubach, and H. H. Genoways. 1977. Guide to the management of Recent mammal collections. Carnegie Museum of Natural History Special Publication 4:1-105.

Wilson, J. A. 1971. Early Tertiary vertebrate faunas, Vieja Group, Trans-Pecos, Texas: Agriochoeridae and Merycoidodontidae. Bulletin of the Texas Memorial Museum 18:1-83.

Wislocki, G. B., and A. C. P. Campbell. 1937. The unusual manner of vascularization of the brain of the opossum (*Didelphys virginiana*). Anatomical Record 67:177-191.

Witmer, L. M., S. Chatterjee, J. Franzosa, and T. Rowe. 2003. Neuroanatomy of flying reptiles and implications for flight, posture and behaviour. Nature 425:950-953.

Zeller, U. 1988. The lamina cribrosa of *Ornithorhynchus* (Monotremata, Mammalia). Anatomy and Embryology 178:513-519.

Zeller, U. 1989a. Die Entwicklung und Morphologie des Schädels von *Ornithorhynchus anatinus* (Mammalia: Prototheria: Monotremata). Abhandlungen der Senckenbergischen Naturforschenden Gesellschaft 545:1-188.

Zeller, U. 1989b. The braincase of *Ornithorhynchus*. Fortschritte der Zoologie 35:386-391.

# Vita

Thomas Edward (Ted) Macrini was born in Birmingham, Alabama on January 21, 1975, the son of Thomas Gene and Nancy Jean Macrini. At the age of six months, Ted moved to Houston, Texas where he grew up and attended high school. After graduating from Memorial High School in May, 1993, he entered Washington University in Saint Louis, Missouri in August, 1993. As an undergraduate student, he began his research career under the guidance of Jonathan Losos and Duncan Irschick of the Department of Biology at Washington University. He worked on three projects examining the evolutionary ecology of *Anolis* lizards. Ted received the degree of Bachelor of Arts in Biology from Washington University in May, 1997. He entered into the Department of Geological Sciences at The University of Texas at Austin as a graduate student in vertebrate paleontology in August, 1997. Ted received the degree of Master of Science in August, 2000 for a thesis examining aspects of the cranial osteology of a South American opossum, *Monodelphis domestica*. He began his doctoral studies in the Department of Geological Sciences in August, 2000 and became a doctoral candidate in the summer of 2002. Ted is an author on eight peer-reviewed journal articles (seven published and one in press). Ted will begin a postdoctoral position in the Department of Mammalogy at the American Museum of Natural History in New York, New York upon completion of his dissertation.

Permanent address: 8607 Stable Crest Blvd., Houston, Texas 77024

This dissertation was typed by the author.